Seismic History Matching Using Proxy Models

CHONG GENG

Thesis presented for the degree of Doctor of Philosophy

Heriot-Watt University
Institute of Petroleum Engineering
School of Energy, Geoscience, Infrastructure and Society

June 2018

Abstract

Generally, reservoir simulation is used to predict field performance and analyse uncertainties for assistance in decision making, while history matching is a key step in reservoir simulation, which is a process of model adjustment and simulation runs with different reservoir parameter settings until the differences between simulated data and historical data reach minima. An efficient reservoir simulation model must be the one that can predict reservoir performance and update history matching results continuously by modifying the reservoir model as long as new data become available. However, reservoir simulation can be very time consuming, depending on the complexity of the reservoir model, and history matching is even more computationally expensive, since it requires many simulation runs. Recently, intelligent technology advances in the oil and gas industry, have initiated a new era of big data. As different varieties of data have been integrated to make better decisions, together with the generation of high frequency data streams, a major concern for petroleum engineers is how reservoir simulation should be calibrated in line with the real time data without compromising the simulation time. In the seismic history matching (SHM) workflow this may be a more obvious issue than in the conventional well production history matching.

In order to address this problem, many studies have been undertaken. Besides increasing computational power, various types of research have focused on speeding up the reservoir simulation process, especially history matching, by either implementing optimisation algorithms or generating efficient proxy models. Nevertheless, there has not yet been a standard method recognized in reservoir simulation.

In this study, a novel method has been proposed as an attempt to investigate the possibility of achieving efficient seismic history matching by data-driven proxy models. This thesis essentially involves detailing background motivations, proxy model building, followed by its testing and application in SHM. Comparisons of proxy models with conventional simulators have been made from different aspects. The objective is mainly focused on examining the capability of the proxy models as a simplification of the conventional physics-based simulators in SHM. According to the simulation results, the feasibility of the combination of proxy models has been proven to be successful and efficient. Importantly, huge amounts of time and effort have been saved in the reservoir simulation process. In addition, it is suggested that other challenges of SHM, such as multi-domain comparison and multi-field communication, could be tackled by using the proxy method.

This thesis is dedicated to my late grandmother,

赵爱英.

Even though she did not have any formal education,

she never stopped sharing her compassion, kindheartedness and wisdom.

Acknowledgements

I remember that day, 8th October 2013, like it was yesterday, when I was offered the chance of joining ETLP.

I am very grateful to Prof. Colin MacBeth for taking a chance on a fresh bachelor graduate for doing a PhD in a joint domain of applied geophysics and reservoir engineering. Colin's knowledge, experience, and patience has been a great inspiration to me. I am extremely lucky to have a supervisor who cared so much about the work of his students. Before meeting Colin, I cannot imagine how it would be that a supervisor spends one to two days weekly to talk with his students one by one. I am also grateful to him for helping me to understand how to do the research work. My journey was not perfectly smooth, however, I did enjoy studying as student of Colin.

I would also like to thank Dr. Romain Chassagne for being my supervisor. Romain sets a perfect example of taking the balance between work and life, and between science and art. Thank you for your scientific vision and research strategy, without which I would not finish this work. Thank you for teaching me how to manage the working schedule as a young researcher, I did learn from each of our meetings. In addition, I enjoyed browsing your album on Flickr, hopefully I can become a professional photographer like you in the future.

In addition, many thanks to my examiners Dr. Mickaele Le Ravalec and Prof. Eric Mackay, for taking the time to read through this thesis and their constructive suggestions.

Acknowledgments go to all the Edinburgh Time Lapse Project (ETLP) sponsors of Phase V and VI, for their support and for providing the datasets used in my research (BG Group, BP, Chevron, CGG, ConocoPhillips, ENI, ExxonMobil, Hess, Ikon Science, Landmark, Maersk, Nexen, Norsar, RSI, OMV, Petoro, Petrobras, Shell, Statoil, Suncor, TAQA, TGS and Total). Thanks to Schlumberger for provision of the Petrel and Eclipse software. I am also grateful to the Society of Exploration Geophysicists (SEG) for awarding me the prestigious SEG/Leon Thomsen Award scholarship for academic excellence in the Reservoir Geophysics domain in 2016. I am also grateful for the opportunities to present my research at the EUROPEC conference.

To my ETLP colleagues, thank you for the mental support, technical discussions, lunch and learn sessions, the positive outlook and the ability to talk at any time. I will like to

show my appreciation to all ETLP colleagues I came in contact with during my PhD: Colin MacBeth, Romain Chassagne, Maria-Daphne Mangriotis, Hamed Amini, Ming Yi Wong, Nkechi Obiwulu, Dennis Obidegwu, Ilya Fursov, Zhen Yin, Sean Shuzhe Tian, Veronica Omofoma, Lu Ji, Ricardo Rangel, Angel Briceno, Phung Nguyen, Qi Zhang, Miguel Alfonzo, Gustavo Corte, Alejandro Jaramillo, Lee Jean Wong and Ambuj Tyagi.

Most importantly, my deepest gratitude goes to my dear parents, 刘振兰 and 耿华, for their unconditional love and support. They, and my beloved big family, have always been with me during all good and bad times.

My PhD and this thesis are about to come to an end. It is certain that the date of today, 18th May 2018, when I pass my viva, will be another memorial day of my life.

Chong Geng, May 2018

Declaration Statement

ACADEMIC REGISTRY
Research Thesis Submission

Name*:*	Chong Geng		
School/PGI:	EGIS / IPE		
Version: *(i.e. First, Resubmission, Final)*	Final	Degree Sought	PhD

Declaration

In accordance with the appropriate regulations I hereby submit my thesis and I declare that:

1) the thesis embodies the results of my own work and has been composed by myself
2) where appropriate, I have made acknowledgement of the work of others and have made reference to work carried out in collaboration with other persons
3) the thesis is the correct version of the thesis for submission and is the same version as any electronic versions submitted*.
4) my thesis for the award referred to, deposited in the Heriot-Watt University Library, should be made available for loan or photocopying and be available via the Institutional Repository, subject to such conditions as the Librarian may require
5) I understand that as a student of the University I am required to abide by the Regulations of the University and to conform to its discipline.
6) I confirm that the thesis has been verified against plagiarism via an approved plagiarism detection application e.g. Turnitin.

* *Please note that it is the responsibility of the candidate to ensure that the correct version of the thesis is submitted.*

Signature of Candidate*:*		Date:	

Submission

Submitted By *(name in capitals):*	CHONG GENG
Signature of Individual Submitting:	
Date Submitted:	

For Completion in the Student Service Centre (SSC)

Received in the SSC by *(name in capitals):*			
Method of Submission (Handed in to SSC; posted through internal/external mail):			
E-thesis Submitted (mandatory for final theses)			
Signature:		Date:	

Contents

List of Figures

List of Tables

Nomenclature

ΔA	*4D seismic*
ΔP	*4D changes of pressure*
ΔR	*Effect of fluid saturation and pressure changes in the reservoir*
ΔSg	*4D changes of gas saturation*
ΔSw	*4D changes of water saturation*
0D	*Dimensionless*
1D	*One dimentional*
2D	*Two dimentional*
3D	*Three dimentional*
4D	*Time lapse3D seismic*
4DRMS	*4D root mean square map*
A_0	*Baseline seismic*
BHP	*Bottom hole pressures*
CV	*Coefficients of variation*
C_{res}	*Proportion of fluid retained in the tank*
E_k	*Excess compliance present in the rock*
EnKF	*Ensemble kalman filter*
EWT	*Extended well test*
FGPR	*Field gas production rate*
FOPR	*Field oil production rate*
FWCT	*Field water production*
G	*Reservoir geology*
GOR	*Gas oil ratio*
h	*Reservoir thickness*
I_p	*P-wave impedance*
HM	*History matching*
K	*Absolute permeability of the rock*
k_r	*Relative permeability of the fluid*
K_{sat}	*bulk modulus of the saturated rock*
K_{dry}	*bulk modulus of the porous rock frame*
K_f	*bulk modulus of the pore-filling fluids*
K_{gr}	*bulk modulus of the mineral matrix*
K_w	*Water modulus*
K_o	*Oil modulus*
K_g	*Gas modulus*
K_{inf}	*Dry bulk modulus at standard temperature and pressure*
MA4D	*4D amplitude change*
MTM	*Multiple tank model*
M_s	*Mismatch of mapped seismic*
M_w	*Mismatch of BHP curves*
n	*Noise*
NRMS	*Normalised root mean square*
NTG	*Net to gross*

O.F.	*Objective function*
OWC	*Oil water contact*
P	*Pressure*
P/S	*Pressure and saturation*
PEM	*Petro elastic model*
P_{eff}	*Effective pressure,*
PMR	*Percentage mismatch ratio*
POD	*Proper orthogonal decomposition*
PRM	*Permanent reservoir monitoring*
PSO	*Particle swarm optimisation*
r	*Pearson correlation coefficient*
r_1	*Reflectivity between layer 1 and 2*
$s(t)$	*Seismic trace as a function of time*
S_w	*Water saturation*
S_o	*Oil saturation*
S_g	*Gas saturation*
SAGD	*Steam assisted gravity drainage*
Seis2sim	*Inversion: from 4D seismic to fluid flow simulation domain*
SHM	*Seismic history matching*
Sim2seis	*Forward modelling: from fluid flow simulation domain to 4D seismic*
SNA	*Sum of negative amplitude*
STOIIP	*Stock tank oil-initially-in-place*
SVD	*Singular value decomposition*
T_{ai}	*Transmissibility multiplier between tanks*
TVDSS	*Sub-sea TVD: True Vertical Depth measured from Mean Sea Level*
Vapex	*Vapour extraction*
V_p	*P-wave velocity*
V_s	*S-wave velocity*
W_s	*Weight of mapped seismic*
W_w	*Weight of BHP curves*
ρ	*Spearman's rank correlation coefficient*
μ	*Fluid viscosity*
μ_{sat}	*Shear modulus of the saturated rock*
μ_{dry}	*Shear modulus of the dry rock frame*
φ	*Porosity*
λ	*two phase mobility*
ρ_{sat}	*Density of the saturated rock*
ρ_f	*Density of the fluid*
ρ_m	*Rock matrix density*
ρ_w	*Water density*
ρ_o	*Oil density*
ρ_g	*Gas density*
$\omega(t)$	*Wavelet as a function of time*

Chapter 1

Introduction – 4D Seismic and Seismic History Matching (SHM)

This chapter presents the background of this research project and sets the structure for this thesis. A brief introduction to reservoir history matching (HM), 4D seismic and seismic history matching (SHM) is firstly given. I then review the history and state of the art technologies applied in HM and SHM, and the numerous challenges are acknowledged. The objectives of this research, its challenges and the contribution of this work are then discussed. The chapter concludes with an outline of the subsequent chapters of this thesis.

1.1 Reservoir History Matching and 4D Seismic

1.1.1 Reservoir History Matching

One of the major goals of any oil company is to optimise production and maximise profit. To achieve this, it is required to obtain the most accurate reservoir model. This plays a major role in field management and development. In many oil and gas assets, model based predictions are used to help with field management and can provide a large number of feasible production profiles. Thus, the field development decisions can be made based on reliable reservoir-simulation models.

Reservoir simulation is an efficient method for helping engineers estimate the oil and gas reserves; practically all major reservoir development disciplines utilise simulation results to some extent. In fact, reservoir development comprises geological and reservoir model building, history matching, in the case of mature fields, and forecasting. Data assimilation stems from the requirement to improve the output of the model. In particular, there is a need to reduce the parameter uncertainty and increase prediction accuracy by incorporating production and 4D seismic data. The available data for constructing a reliable and useful reservoir model are of different natures, which can be classified as static or dynamic; the latter being data which may vary during reservoir production, whilst the former does not. Data that have originated from geology, electrical logs, core analysis, fluid properties and pre-production seismic surveys can be generally classified as static, whereas the information originating from well testing, repeat formation tests, production logs, production history, bottomhole pressure from permanent gauges, water cut, and gas-oil ratio can be classified as dynamic (Landa and Horne, 1997).

The data assimilation process of tuning unknown parameters in a reservoir simulation is known as history matching and has been studied extensively over the last four decades. The objective of history matching is to validate the reservoir simulation model by matching the historical data in order to better understand the fluid flow behaviour, enable reliable prediction of future performance to support production optimisations and detect operational issues during the reservoir management process.

The general procedure for history matching can be summarized as:

i) Decide the targets of the history matching process, such as production, pressure or saturation, which must be matched with the actual data;

ii) Determine the history matching method, which is affected by the history matching targets, available data and resources, and also the history matching time;

iii) Determine the reservoir's uncertain parameters that can be modified during history matching and the confidence range for those properties. Those parameters must have most significant impact on reservoir behaviour but have less accuracy in the field;

iv) Perform the simulation run with the initial input parameters;

v) Compare the simulation result with the historical data selected for history matching;

vi) Modify the reservoir parameters within the range of confidence until a criteria of objective function has been met.

The oil industry hopes to benefit from history-matched reservoir models that are accurate predictors of future performance. However, the history matching is not only mathematically and computationally challenging, but also non-unique in nature: it is an ill-posed problem. This means that multiple models can generate the same response as the real data, where none of them could be perfectly reliable. Therefore, the prediction profiles of the reservoir performance based on these matched model predictions would have huge variance, weakening the prediction ability of the reservoir model. In the last few decades, the industry has laboured to generate accurate history matched reservoir models, but these attempts have been hindered by the lack of information between wells (Walker and Lane, 2007). In those early works of history matching, only the well-based data used to be matched. However, in the last decade, time-lapse (4D) seismic has been involved in the history matching workflow. 4D seismic surveys have the potential to identify changes between wells and provide advanced warning of events, such as water breakthrough, before a production signal is observed at a well. More details of 4D seismic data will be given in the following section.

1.1.2 4D Seismic

As mentioned in the last section, a model simply being matched to well production data is not a sufficient condition for it to make improved predictions. All the available data, especially the 4D seismic data which contain the spatial information, need to be integrated in order to provide the most representative reservoir model or models (Landa and Horne, 1997). A bank of 4D seismic data has become a powerful ingredient in the history matching of reservoir models, due to its spatially high coverage, which complements the spatially sparse and distributed nature of well data; conversely, the rapid time sampling of well data compensates for the coarser time sampling of the seismic data (Nielsen et al., 2010, Jin et al., 2012). For instance, the need to monitor fluid displacement is a great challenge that has been successfully overcome with the use of 4D seismic technology (Hatchell et al., 2005, Lygren et al., 2002).

The integration of 4D seismic data into the reservoir simulation model began on a qualitative basis to reduce uncertainties (Lumley and Behrens, 1999, Elde et al., 2000, Pannett et al., 2004), mainly by identifying saturation fronts, which resulted in improved reservoir characterisation and consequently good history matching. For example, in the study of Alsos et al. (2013) on the Norne field (Figure 1-1), it is observed that the oil water contact (OWC) could be directly interpreted from the 4D seismic. More applications of 4D seismic in reservoir engineering and management are listed in Table 1-1.

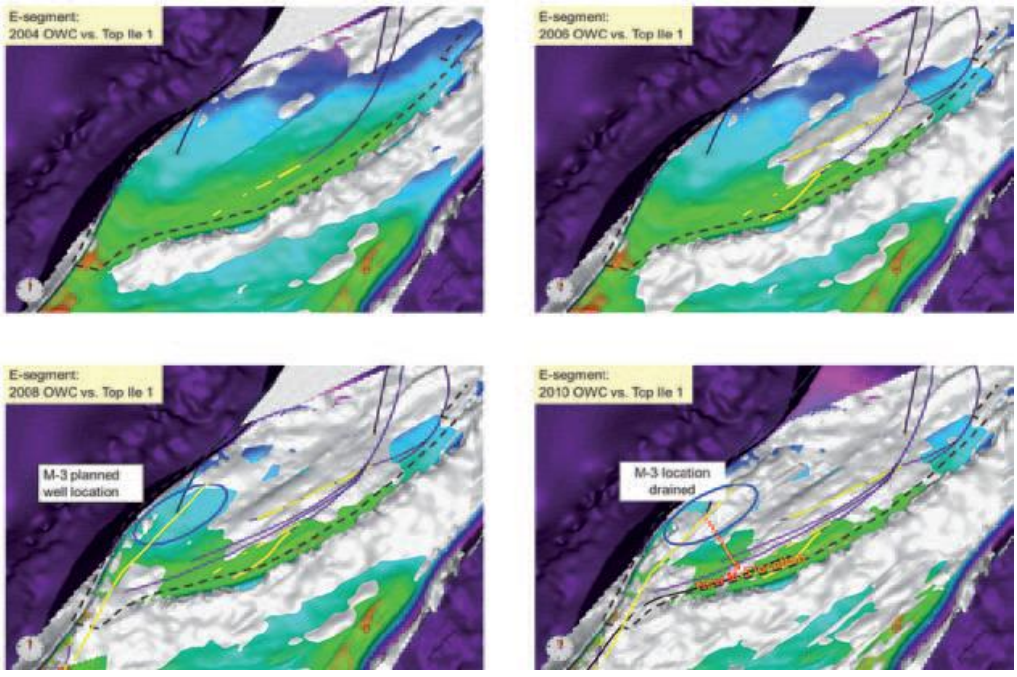

Figure 1-1 *Top Ile 1 horizon (coloured) overlaid with the OWC (grey), interpreted on 4D difference data from (a) 2004–2001, (b)2006–2001, (c)2008–2001, and (d) 2010–2001 (Alsos et al., 2013).*

Table 1-1 *A summary of the application of 4D seismic interpretation in the reservoir engineering and management domain.*

Field	Geology	Oil type	Country	Onshore/ offshore	Surveys	Uses of 4D seismic
Scarborough	Deltaic - Turbidites (Triassic - Jurassic)	Gas	Australia	offshore	1996, 2004, 2007, 2012	Gas monitoring
Midgard	Fluvial - Shallow marine (Jurassic)	Gas	Norway	offshore	2001, 2006, 2009	Gas monitoring
Magnus	Turbidites (Jurassic)	39° API	UK	offshore	1992, 2001	Gas injection monitoring
Njord	Shallow marine (Jurassic)	47° API & gas	Norway	offshore	2001, 2004, 2007, 2011	Gas injection monitoring
Kristin	Shoreface - Shallow marine (middle Jurassic)	Gas & condensate	Norway	offshore	2003, 2007	HPHT reservoir. Pressure depletion monitoring
Elgin	Fluvial - Shallow marine (Jurassic)	40° API & gas & condensate	UK	offshore	1989, 1996, 2005	HPHT reservoir. Pressure depletion monitoring
Shearwater	Shallow marine (Jurassic)	40° API & condensate	UK	offshore	1992, 1996, 2002, 2004, 2013	HPHT reservoir. Pressure depletion monitoring
Franklin	Fluvial - Shallow marine (Jurassic)	40° API & gas & condensate	UK	offshore	1987, 1996, 2005	HPHT reservoir. Pressure depletion monitoring
Gullfaks	Fluvial - deltaic (Middle Jurassic) Brent Group	37° API	Norway	offshore	1985, 1995, 1996, 1999	Water and gas injection monitoring
Snorre	Fluvial (Late Triassic - Lower Jurassic)	40 - 42° API	Norway	offshore	1997, 2001, 2006, 2009	Water and gas injection monitoring
Erha	Turbidites (Tertiary)	32.8° API	Nigeria	offshore	2000, 2005, 2009	Water and gas injection monitoring
Hibernia	Fluvial (braided) Early Cretaceous	32 - 34° API	Canada	offshore	1981, 1991, 2001	Water and gas injection monitoring
Jasmin	Turbidites (Oligocene)	30° API	Angola	offshore	1999, 2012	Water injection monitoring
Dikanza	Turbidites (Miocene)	25 - 29° API	Angola	offshore	1997, 2002, 2008	Water injection monitoring
Moho Bilondo	Turbidites (Upper Miocene)	22 - 29° API	Congo	offshore	2001, 2012	water injection monitoring
Veslefrikk	Fluvial - Shallow marine (Jurassic)	38° API	Norway	offshore	2003, 2005, 2010	Water injection monitoring
Edvard Grieg	Fluvial and Eolian (Triassic)	34° API	Norway	offshore	2008, 2009, 2010, 2012, 2013, 2014	Water injection monitoring
Grane	Turbidites (Palaeocene)	18.7° API	Norway	offshore	2005, 2007, 2009	Water injection monitoring.
Alba	Turbidites (Middle Eocene)	19° API	UK	offshore	1989, 1998, 2008	Water injection monitoring.
Ketzin	Fluvial -Transitional (Upper Triassic)	Gas	Germany	onshore	2005, 2009, 2012	CO2 storage monitoring
Salah	Shallow marine (Devonian - Carboniferous)	Dry gas	Algeria	onshore	2003, 2005, 2006, 2008, 2009, 2010	CO2 storage monitoring
Liaohe	Deltaic (Plio - Pleistocene)	10 - 26° API	China	onshore	1992, 1993, 1994, 2009, 2011	Steam injection monitoring
Peace River	Fluvial sands (Cretaceous)	7 - 41° API (bitumen)	Canada	onshore	2002, 2009, 2010, 2014	Steam injection monitoring
Steepbank	Fluvial (lower Cretaceous)	6 - 8° API	Canada	onshore	1985, 1991, 1992	Steam injection monitoring

Despite the success, there was still need to utilise the information available in a more efficient and quantitative manner in order to achieve improved results. This led to the birth of the integration of 4D seismic data into the reservoir model in a quantitative manner. The seismic history matching procedure is the commonly used workflow where 4D seismic data can be used quantitatively together with the well production data. This workflow will be introduced and discussed in the next section.

1.1.3 Seismic History Matching

In the fields where 4D seismic has proved to be a successful monitoring technology, acquiring more frequent repeat seismic surveys can be accommodated in the reservoir management plan. In this case, the high lateral resolution 4D seismic data (compared to the well spacing) is very appealing to be incorporated into the conventional (production) history matching (HM) process. The underlying motivation of this process is to use the 4D signal as a high resolution spatial constraint to guide the updating algorithm in the history matching workflow.

In the seismic history matching (SHM) workflow (Figure 1-2), in addition to the evaluation of the match quality to the well production data, at each iteration, the loop between the simulation model and seismic is closed and the simulation model is assessed against the observed 4D data in the desired domain. As presented in the Figure 1-2, the common used domain to close the loop is 4D seismic (amplitude), impedance or dynamic domain (pressure and saturation). The misfit function in this workflow is a combination of the match to the production data and the match to the 4D data (or only seismic). The outcome of this workflow is a simulation model with a performance consistent with both the production data at wells and the 4D seismic. To close the loop in the seismic domain, forward simulation models from flow simulation to seismic response (sim2seis) or its inversion (seis2sim) should be involved to compare the information in different domains.

Compared with the conventional production history matching, the SHM workflow has new challenges. Before introducing these challenges and the methods, it is essential to review the development history of HM and SHM. After reviewing the HM and SHM in the next section, I will then point out the challenges of SHM and introduce the potential methods to solve these problems in the following section.

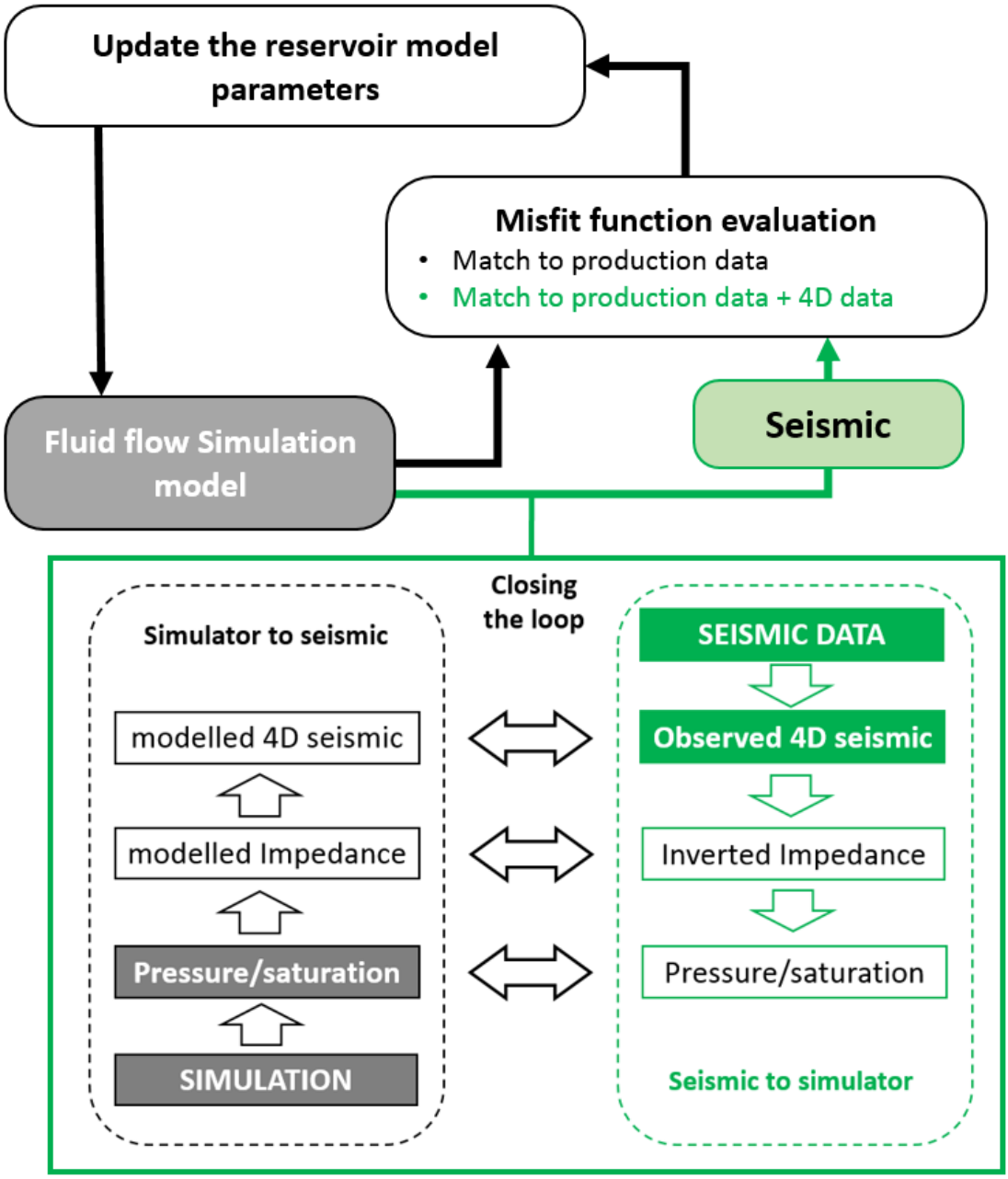

Figure 1-2 *The seismic history matching (SHM) workflow. The black arrows show the conventional (production) history matching (HM) workflow. The misfit function in SHM is a combination of match to the production data and the match to the 4D data. Closing the loop and 4D data evaluation can be performed across different domains.*

1.2 Review of HM and SHM

The reservoir history matching (HM) technique was developed from the 1960's when only well production data were available. In the 1990's, after the 4D seismic data appeared in the industry, the research studies on seismic history matching began to come to the front of the stage. Therefore, SHM can be regarded as a side branch of HM because they share the same parameter perturbation techniques, optimisation algorithms and other processes. Thus, in this section I will first review the development history of HM, then that of SHM.

1.2.1 Reservoir History Matching (HM)

One of the first studies on history matching was carried out in 1961 by Kruger, who computed the areal permeability distribution of a reservoir (Kruger, 1961), while Jacquard and Jain (1965) was the first to implement a perturbation technique to the problem of history matching, using a steepest descent based method to calculate permeabilities in a one-dimensional model. Jacquard and Jain (1965) later extended the method to a two-dimensional case. They also introduced the idea of zonation (subdividing the reservoir model into a limited number of constant parameter zones) to reduce the number of unknowns. Jahns (1966) used the Gauss-Newton method to solve for the updated parameters at each iteration, while Coats et al. (1970) used least squares and linear programming to solve for reservoir parameters using zonation. Wasserman et al. (1974) were among the first to use optimal control theory as a mathematical optimisation method in history matching multiphase simulator models. An optimal control is a set of differential equations describing the paths of the control variables that minimize the objective function (Chen et al., 1974). However, instead of using a multi-phase optimal control theory, they used an adjoint equation only for the pressure equation. Hirasaki (1975) used sensitivity analysis to graphically display the effects that variations in certain parameters had on recovery efficiency and cumulative oil production, while Dougherty and Khairkhah (1975) used optimal control theory for history matching of a gas reservoir. Gavalas et al. (1976) used nonlinear regression and Bayesian estimation theory as a substitute for zonation in calculating porosity and permeability; however, this technique is only viable when sufficient statistics are available concerning the parameter to be calculated. Watson et al. (1979) studied history matching in two-phase petroleum reservoirs. Later, Fasanino et al. (1986) investigated single-phase history matching of 2D gas reservoirs by means of the adjoint method in combination with geostatistical information and the pilot point method. Anterion et al. (1989) computed the gradients

analytically using a commercial simulator and demonstrated how they could be used to aid in history matching.

Significant work has also been done using nonlinear programming to automate the process of history matching simulators to field data by varying formation properties, such as porosity, permeability and relative permeability. For example, Bi et al. (2000) studied the conditioning of three-dimensional stochastic channels to pressure data in single-phase reservoirs. Li et al. (2003) studied a three-dimensional history matching case using three-phase flow production data. The aim was to minimize the misfit in flowing wellbore pressure, water oil ratio (WOR) and producing gas oil ratio (GOR).

In terms of the optimisation algorithms, a number of pioneering global optimisation methods have gained popularity in the research amongst oil and gas companies for tackling history-matching problems. These include an ensemble Kalman filter, evolutionary algorithms, neighbourhood algorithm, swarm intelligence techniques and others. Stochastic techniques have also been used in the petroleum engineering, including Genetic algorithms (Goldberg, 1989; Romero et al., 2000; Carter and Ballester, 2004; Erbas and Christie, 2007; Stephen and Arwini, 2010), Ant Colony Optimisation (Hajizadeh et al.,2009; Selvi, and Umarani, 2010; Hajizadeh, 2010), Particle Swarm Optimisation (Eberhart and Kennedy 1995; Shi and Eberhart 2001; Mohamed et al. 2010; Rwechungura et al. 2011, Geng et al., 2017), Ensemble Kalman Filter Methods (EnKF) (Van Leeuwen, 1999; Evensen, 2003; Haugen et al., 2006; Zhang and Oliver 2009; Aanonsen et al., 2009) and the Neighbourhood Algorithm (Christie et al., 2002; Subbey et al., 2004; Rotondi et al., 2006; Stephen et al., 2006).

Great progress has been made in the last decade in the development of history matching technology. In particular, the optimisation algorithms have been developed from gradient-based methods and Newton-like methods to EnKF and its variants. Despite the rapid progress in algorithms; however, there is no single best method for every history matching scenario (Wolpert and Macready 1997). To determine the proper algorithm for a certain case depends on the model size, objective function, uncertain parameter selection and so on, which is a case-dependent decision. With regard to the observation data aspect, different types of observation data, such as 4D seismic and electromagnetic data, have been included in the history matching workflow. Their joint synergy effects have proved to lead to considerable improvements in history matching. In the next section, the development history of seismic history matching will be reviewed.

1.2.2 Seismic History Matching (SHM)

A number of publications in the literature have discussed the problem of using real time-lapse seismic data in the history matching of reservoir simulation models to improve the characterization of permeability and porosity heterogeneity. Landa and Horne (1997) estimated reservoir parameters assuming that water saturation changes could be derived from the time lapse seismic and compared with the simulation results while Huang et al. (1997) utilised 4D seismic amplitude data and a finite perturbation method to compute the required derivatives. Gosselin et al. (2001) suggested a gradient based optimisation method to minimise the mismatch of all types of measured data simultaneously, including 4D seismic data. Waggoner et al. (2002) used acoustic impedance differences derived from time-lapse seismic data to perform SHM. Mezghani et al. (2004) used time-lapse acoustic impedance derived from pre-stack data to predict petrophysical properties using non-linear optimisation based on derivatives with respect to the parameterization. Dong and Oliver (2005) matched both seismic impedance change data and production data in a medium scale problem. Stephen et al. (2006) applied a multiple-model history matching workflow based on simultaneous comparison of spatial data offered by seismic and production data for the UKCS Schiehallion reservoir using the Neighbourhood Algorithm in the context of 4D seismic history matching. Dong et al. (2006) used the ensemble Kalman filter (EnKF) to match production and time-lapse seismic impedance data and to improve estimation of the porosity field. Andersen et al. (2006) used 4D inverted elastic data to condition geological models in order to reduce the uncertainty in the facies distribution for the fluvial Ness formation in the Oseberg field. Roggero et al. (2007) studied advanced parameterization methods to constrain fine scale geo-statistical models using a gradual deformation method in the framework of time lapse seismic history matching of the Girassol field. Dong and Oliver (2008) applied an adjoint method to calculate the gradient of the data mismatch and a quasi-Newton method to estimate the search direction in the context of automatic history, with the aim of incorporating 4D seismic data to a reservoir in the Gulf of Mexico. Leeuwenburgh et al. (2010) showed the distribution of reservoir fluids and rock properties (porosity and permeability) can be better extracted from seismic amplitude data to be compared with the simulation results in the SHM. Sedighi and Stephen (2010) used the ‘divide and conquer’ approach to spatial decomposition of the SHM misfit function. Arwini and Stephen (2010) applied proxy derived methods to aid stochastic sampling in the SHM workflow. Le Ravalec et al. (2012) developed a meta-model to integrate the well production data with 4D seismic data, and used it in the seismic history matching. Rukavishnikov (2015) updated the

reservoir simulation model using dynamic clusters extracted from 4D seismic data in the SHM workflow. Fursov (2015) tested the possibility of using 4D seismic to update thin-reservoir simulation models by the SHM loop. Obidegwu (2015) used binary maps extracted from 4D seismic to carry out SHM on a North Sea turbidites reservoir. Yin (2016) applied the 'well2seis' technique to update the reservoir connectivity parameters embedded in the simulation model.

In summary, there is a growing interest and need to incorporate 4D seismic data quantitatively into the SHM workflow for reservoir management. As illustrated in Figure 1-2, the SHM loop needs to be closed at one particular domain: the engineering (pressure and saturation) domain, the impedance domain or the seismic amplitude domain. Thus, Table 1-2 presents the 'closing-loop' domain selected to perform the SHM and the optimisation algorithms used in those cases.

Table 1-2 *The 'closing-loop' domain and optimisation algorithms used in Selected SHM cases.*

Data set (field)	Authors	Closing-loop domain	SHM algorithm
Synthetic data	Davolio et al. 2011	Pressure and saturation	Gradient-based algorithm
Schiehallion	Fursov 2015	Pressure and saturation	CMA-ES
Synthetic data	Souza et al. 2010	Pressure and Saturation	Conjugate-Gradient method
Namorado	Souza et al. 2011	Impedance	Global objective function
Schiehallion	Sedighi and Stephen 2009	Impedance	Neighbourhood algorithm
Gullfaks	Fahimuddin et al. 2010	Impedance	EnKF
North Sea field data	Gervais et al. 2010	Impedance	Gradient-based algorithm
Turbidite reservoir (Campos basin)	Emerick and Reynolds 2013	Impedance	Ensemble smoother with multiple data assimilation (ES-MDA)
Brugge	Luo et al. 2016	Amplitude	Iterative ensemble smoother
Norne	Geng et al. 2017	Amplitude	Particle Swarm Optimisation (PSO)
Valhall	van Gestel et al. 2011	Time-shift	Genetic algorithm Match quality factor
Ekofisk	Tolstukhin et al. 2012	Time-shift	Evolutionary algorithm

1.3 SHM: challenges and opportunities

Section 1.2 outlined the development history of conventional history matching (HM) and seismic history matching (SHM). It is widely acknowledged that after introducing 4D seismic as an extra constraint, the reservoir simulation model would be more representative after the history matching process. However, every advantage has its counterpart disadvantage: to conduct a successful and efficient SHM is a more challenging task than conducting HM. In this section, I will summarise four main challenges associated with SHM.

1.3.1 Speed

One of the main problems of seismic history matching (SHM) is the speed of convergence of the misfit between observed and predicted data. The SHM workflow is an iteration process, and each iteration needs to run two forward models: the fluid flow simulation model and the sim2seis model. In the conventional HM workflow, where only the fluid flow simulation model is involved, it is still a problem that the HM will take hours, even days, to converge to the final optimal solution. If a stochastic optimisation algorithm is applied, which needs more iteration runs, the total computation time for the SHM to converge could be weeks.

On the other hand, to enhance the data quality and seismic repeatability, and also to obtain more frequently shot seismic monitors cost effectively over the long term, seabed permanent reservoir monitoring (PRM) has become popular to provide life-of-field 4D seismic surveys. It appears that PRM is gradually becoming used in quite a sizable subset of the offshore oil fields. For these fields, the permanently installed seismic acquisition system delivers clean, well-resolvable 4D seismic data with a significantly low non-repeatability level within a rapid-turn-around processing time. If the frequently acquired 4D seismic data are used to conduct SHM, then the computation cost of SHM has to be reduced to support the real-time model updating. This fact places a major emphasis on the efficient use of 4D seismic data to carry out SHM.

1.3.2 4D seismic: acquisition and interpretation

If we want to speed up the SHM workflow, one of the essential steps is to deal with the 4D seismic data: from data acquisition to interpretation. Unlike the well production data, for which there are robust ways to obtain and process these data, 4D seismic acquisition is still challenging (Harris and Henry, 1998; Vauthrin et al., 1999; Marsh et al., 2003; Johnston 2013): even when utilising the same techniques for seismic acquisition of the base and the monitor surveys, one needs to decide whether to work with the surveys separately or use the differences. The latter may need special reprocessing anyway, to ensure the surveys can be denoised properly and compared to each other.

Furthermore, even if the 4D seismic data set was 'perfectly' acquired and processed, the very nature of 4D seismic means that the 4D seismic response in general is a combination of two effects (pressure and fluid saturation changes). The fluid substitution that occurs during the production of hydrocarbon reservoirs changes the compressibility of the pore fluids and rocks, thus changing the bulk velocity. However, the magnitude of the changes depends on the petrophysical properties of the dry rock frame and the filling pore fluids. These changes could have opposite effects on the seismic velocities. Therefore, the polarity of the response depends on the increasing-decreasing trends of pressure change and the difference between the fluid properties at the beginning and the end of the survey (in some cases such as SAGD the temperature should also be considered as an important parameter on the 4D seismic response). This feature of 4D seismic increases the uncertainty of the SHM results, because different scenarios of simulation model (with different pressure and saturation changes) may lead to the same 4D response.

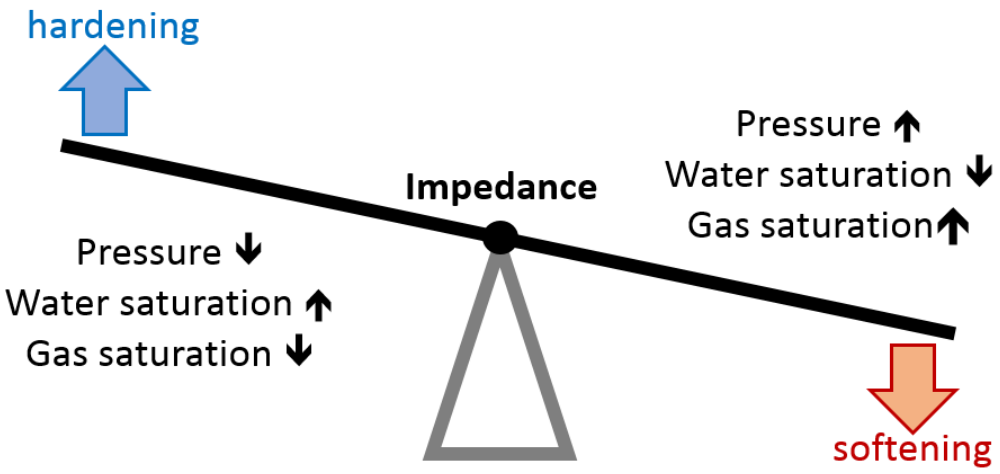

Figure 1-3 *Change in acoustic impedance in response to production and injection (after Marsh et al., 2003).*

1.3.3 Which domain to compare

Apart from the extra computation cost and the nature of 4D seismic, the other challenge may face a reservoir engineer conducting SHM is to decide in which domain to compare the simulation with observation. Unlike production simulation, which can be directly compared with observation, the 4D seismic is not a direct output of the reservoir simulator (Amini, 2014). In order to be history matched, the simulation domain and observation domain have to be at a comparable attribute, so a simulator to seismic (sim2seis) modelling procedure is indispensable. In most cases, this procedure includes the calibration of a petro-elastic model to obtain impedance, based on the results of the reservoir simulator, and seismic wave propagation modelling. This multidisciplinary process is case dependent, contains high uncertainty and can be the most challenging task facing a reservoir engineer engaged in SHM (MacBeth et al., 2016; Santos et al., 2016).

Figure 1-4 illustrates the different domains of comparison between seismic and simulation. Specifically, if the comparison is performed in the seismic domain, then petro-elastic and seismic modelling will be applied to generate the simulated 4D seismic data. A main drawback of this forward modelling procedure is the associated uncertainty of the model parameters. It could be a huge challenge for the cases where a reliable petro-elastic model is hard to build. Moreover, forward modelling requires intensive computation, which can be unaffordable for large sized models.

In another way, when bringing the seismic into the saturation and pressure domain to bypass forward modelling in SHM, the petro-elastic model is still necessary for the inversion, which is a non-unique procedure. The literature examples of SHM in this domain are often conducted on a synthetic model (Landa and Horne, 1997; Davolio et al., 2011), and the non-uniqueness is usually treated inappropriately, or not treated at all (Jin et al., 2011; Osdal, 2012).

Furthermore, the intermediate domain of seismic impedance can also be used to compare simulation and real data. This approach appears to be the most popular choice in SHM studies (Gosselin et al., 2003; Haverl et al., 2005; Emerick et al., 2007; Roggero et al., 2012); however, it has the disadvantages of the previous two: although the seismic modelling can be avoided, an extra suitable rock physics model is still needed to convert the seismic into impedance (Fursov, 2015; MacBeth et al., 2016).

None of the above approaches can totally avoid the petro-elastic modelling or seismic modelling route and all carry considerable uncertainty. Perturbing and calibrating these models makes it difficult for a reservoir engineer to undertake a rapid and effective SHM, and this fact can bring one more challenge, which is explained in the next section.

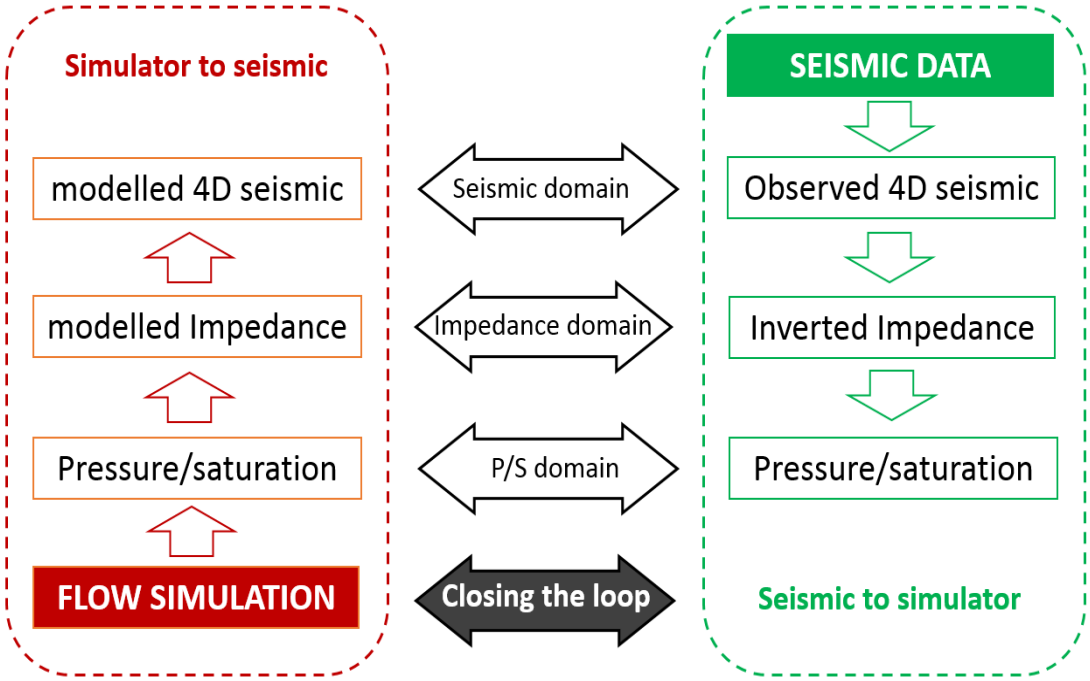

Figure 1-4 *Different domains of closing the loop between the simulation model and the seismic data (Geng et al., 2017).*

1.3.4 Communication between multidisciplinary experts

The use of multi-source data requires teamwork and mutual technical understanding. The preferred scheme for work would be to have a development team with proper communication skills. Another problem is that the technical languages also differ. Geophysicists, geologists, petrophysicists and reservoir engineers have their own terminologies and share different views on the static and dynamic reservoir behaviour. Even within these main subject areas there are specialisms. This denotes that successful projects require team members to be able to understand and express the value and uncertainty of their own and others' data. Normally, it is the reservoir engineers that have the responsibility to conduct the SHM process, but it will be a challenge for them to perturb the conventional sim2seis model which contains a large number of uncertain parameters. Although this is the last challenge I have listed in this section, complaints the reservoir engineers about the tricky sim2seis model are very common in the real practice of SHM jobs.

1.3.5 Potential Opportunities

In the development history of the SHM technique, many efforts have been devoted to conquering the challenges mentioned above. For instance, in order to deal with the high computational cost issue of SHM, the computer power has been upgraded step by step, and distributed computation techniques (Yadav et al., 2005; Guo et al., 2016) and cloud computing (Eldred et al., 2014; Wilson, 2016) techniques were applied to speed up the SHM workflow. These IT and computing techniques did improve the computing power and will continue in that direction. However, with the usage of uncertainty analysis and ensemble based algorithms in the SHM workflow, the computational need of SHM has also increased significantly (Chen and Oliver, 2013; Vasconcellos and Soares, 2017). The proxy model based methods have been developed in order to reduce the number of iteration runs or decrease the computing time of each iteration run. A detailed review of the proxy model based methods will be carried out in Chapter 2.

Apart from reducing the computation cost, in order to deal with the discrimination of the pressure and saturation effects, some proxy model based pressure-saturation inversion methods have been developed (Omofoma, 2017; Wong, 2017). These methods are trying to circumvent the conventional sim2seis model and build a direct link between pressure and saturation changes with 4D seismic responses (time-shift, amplitude, etc.). These methods used in 4D seismic inversion may also give insights into potential strategies for SHM: by applying the proxy model, the 4D seismic response could be simulated based on the fluid flow simulation model outputs and the 'loop' could be closed without using the conventional forward modelling process. Applying this kind of proxy model to conduct SHM is one of the motivations of this project and will also be discussed in next chapter.

In terms of multidisciplinary communication, little, if any, attention has been paid to this practical challenge. It is believed that the level of understanding of reservoir engineers regarding the sim2seis model, and of the geophysicists regarding the fluid flow model will finally determine whether a particular SHM job can be done successfully and efficiently. Therefore, this research will also consider how to make a more straightforward 'bridge' between these two disciplines.

1.4 The work of this thesis

1.4.1 Research Objectives

After introducing the current challenges associated with the SHM workflow, and analysing the potential opportunities to solve the problems, the targets of my research are summarised in this section. The main objective and challenge of this thesis is to quantitatively integrate 4D seismic data and production data into a history matching workflow on the basis of previous research outputs. The main task is to utilise a proxy model based approach as a technique to significantly reduce the times of forward simulation model (fluid flow simulation and 4D seismic modelling) running times. This will be achieved by following these main targets:

1. An extensive study of the conventional petro-elastic model, seismic modelling procedure, and fluid flow simulation models.

2. An in-depth analysis of the currently used proxy models. Searching for new types of proxy models which can offer insights into solving the challenges listed previously.

3. Developing proxy models for sim2seis and the 3D fluid flow simulation model independently, validating them in the SHM workflows, and examining its potential, as well as contrasting it to the conventional approach to further underscore its usefulness.

4. Exploring the SHM workflow of combining the two proxy models together, and developing a method to evaluate the proxy performance in SHM.

The main value of this work arises from the ability to integrate 4D seismic data and production data into a history matching workflow in a fast, efficient and reliable manner.

1.4.2 Thesis structure

Chapter 2 provides a review of the physics based fluid flow simulators and 4D seismic simulation models of which the proxy models will be built in later chapters. In this chapter the currently used proxy models and methods, such as response surface models, reduced order models and reduced physics models, will also be reviewed. After reviewing the simulation models and proxy models, the types of proxy models that I will build are determined.

Chapter 3 presents the first proxy model I build in this thesis: the linear superposition sim2seis proxy model. This proxy model is developed to generate a 4D seismic map, using only the original baseline seismic data and dynamic pressure and saturation predictions from reservoir flow simulation. The building of this proxy is a data training procedure, the accuracy of the proxy will be quantified by metrics in a blind test. Finally, the effects of seismic attributes and coefficient sensitivities on the performance of the proxy model will also be analysed.

Chapter 4 describes the building of the areal model, which is the second proxy model that will be developed in this thesis, as the proxy for fluid flow simulation model. The motivation for building this proxy will be introduced and the proxy will also be tested in a blind test and its robustness will be analysed at the end.

Chapter 5 presents the last proxy, the multiple tank model, which will be used to replace the 3D fluid flow simulation model in the SHM workflow. The field development history will be firstly reviewed, in which the material balance tank model played an important role in the early life of the field. I will then build the multiple tank model based on a reference 3D model and quantify the simplification error. The model is built through a data training step; thus, its quality will also be tested in a blind test.

Chapter 6 shows how the three proxy models which have been built in the previous three chapters will be used in the SHM workflows. Before applying them in the SHM, I will review the method of utilising proxies in the HM workflow and develop a new way to evaluate the proxy models and 4D seismic as an HM constraint. Subsequently, the proxy model based SHM will be conducted on Norne and Schiehallion fields. The value of 4D seismic will be evaluated and the proxy driven SHM solutions will be compared with the conventional SHM solutions.

Chapter 7 provides a summary of this thesis. The results of the proxy model based SHM will be discussed and the final conclusions will be drawn. Moreover, recommendations will be given on how to refine this work and go further in this direction.

1.4.3 Publications

MacBeth, C., Geng, C. and Chassagne, R., 2016, January. A fast-track simulator to seismic proxy for quantitative 4D seismic analysis. In 2016 SEG International Exposition and Annual Meeting. Society of Exploration Geophysicists.

MacBeth, C., Geng, C. and Chassagne, R., 2016, December. A Practical Fast-track Solution for Seismic History Matching. In Third EAGE Integrated Reservoir Modelling Conference.

Geng, C., MacBeth, C. and Chassagne, R., 2017, June. Seismic History Matching Using a Fast-Track Simulator to Seismic Proxy. In SPE Europec featured at 79th EAGE Conference and Exhibition. Society of Petroleum Engineers.

Geng, C., MacBeth, C. and Chassagne, R., Fast Translation from Fluid Flow Simulation to 4D Seismic for History Matching. Journal of Geophysics and Engineering, submitted.

Chapter 2

Review of the simulation models and proxy models

In this chapter, firstly the conventional physics based simulation models used in the SHM workflow, the fluid flow simulator and sim2seis model, will be reviewed, followed by a review of the proxy model method used in the literature to conduct history matching. The fluid flow simulation models are classified by the model dimension, and the suitable application cases of each model will be briefly introduced. The petro-elastic model and a fast track seismic modelling method, the 1D convolution model, will be introduced as the sim2seis model. Three main kinds of proxy model methods will be summarised: the response surface model, the reduced-order model and the reduced physics model. The last model is the type of proxy I will apply in this thesis. After reviewing the simulation models and proxy models, the exact proxy models will be built on real fields as reported in the next chapter.

2.1 Numerical reservoir flow simulator

Simulation of petroleum reservoir performance refers to the construction and operation of a model whose behaviour assumes the appearance of actual reservoir behaviour. A model itself is either physical (for example, a laboratory sand-pack) or mathematical. A mathematical model is a set of equations that, subject to certain assumptions, describes the physical processes active in the reservoir. In this work I only focused on the mathematical simulation model, or numerical reservoir simulator. Numerical reservoir simulators are used widely, primarily because they can solve problems that cannot be solved by any other analysis methods, such as well testing. Simulation is the only way to describe quantitatively the flow of multiple phases in a heterogeneous reservoir, having a production schedule determined not only by the properties of the reservoir, but also by market demand and investment strategy.

The potential of simulation was recognized in the late 1940's and early 1950's by a number of companies. Their commitment of effort both to fundamental research on numerical analysis and to development of practical methods for using available computers resulted in crude, but nonetheless useful, simulators by the mid 1950's. The principal application of early simulators was in studies of reservoirs that were large enough to justify costly studies. The need at that time was for detailed performance predictions to be used in intermediate- and long-term planning. Reservoir simulation successfully met that need in most cases and, as a result, became established as an important management tool for most large reservoirs.

Nowadays, the reliability of modern simulators and the power of computers suggest that simulation is practical for use on all sizes of reservoirs for day-to-day decision-making, as well as for planning. Specifically, the 3D multi-phase reservoir simulator has been commonly used by reservoir engineers for almost every reservoir. As mentioned earlier, reservoir simulators are used primarily because they can solve problems that cannot be solved in any other way. However, this is not to say, of course, that complex 3D numerical simulation is always the best method for a particular reservoir engineering problem. Such problems should be solved by the simplest and least costly method that will yield an adequate answer. Reservoir engineers should always first determine the proper level of simplification and then select the appropriate model, to avoid technical 'over-complexity'.

Considering the challenges of the SHM workflow listed in Chapter 1, the complexity of the simulators should be optimised in order to conduct an efficient and effective SHM. From the development history of the reservoir simulator, different dimensional models have been developed:

1) tank models (zero dimension)

2) 1D models

3) 2D areal models

4) 2D cross-sectional models

5) multilayer models, and

6) 3D models

It has to be pointed out that there are different ways to classify the reservoir simulators: by the reservoir geometry, by the way in which the flow equations are discretised or by the number and nature of the mobile phases. A general review of each aspect of the reservoir simulation models is beyond the scope of this thesis; my focus is on the dimensions of the simulation models. Given choices to build different models, one of the first steps in choosing a model is to decide on the number of space dimensions needed to represent the geometry of the physical system and, simultaneously, to determine which simplifications are justified. Both external and internal reservoir geological properties must be considered. External geometry includes the field or aquifer limits and the top and bottom of the reservoir or aquifer. Internal geometry comprises the areal and vertical variance of the permeability and properties of the faults. In this section, the reservoir simulators will be introduced by their dimension order, from 0D tank model to 3D model.

2.1.1 Tank models

The tank model is useful when rapid answers are needed and average reservoir pressure behaviour is deemed the only important factor in making operating or investment decisions (Mattax and Dalton, 1990). Especially, this model will be built in the early stage of the life cycle of a field. In order to regard the whole reservoir as a tank, its pressure gradient over the reservoir should be small or their impact should not be considered significant (Dobbyn and Marsh, 2001). The key function of the tank model is the material balance equation, so this method is also called the 'material balance model'.

$$Mass\ of\ fluids\ originally\ in\ place\ =\ fluids\ produced\ +\ remaining\ reserves \quad (2.1)$$

This equation was first presented by Schilthuis (1936) and is one of the basic tools in reservoir engineering (Pletcher, 2000). Practically all reservoir engineering techniques involve some application of material balance (Mattax and Dalton, 1990). Since the equation is a volumetric balance, relating volumes to pressures, it is limited in its application, because of any time dependent terms. The equation provides a relationship with a reservoir's cumulative production and its average pressure. However, when combined with fluid flow terms, we have a basis to carry out predictive reservoir modelling, for example to put a time scale to production figures. This is limited in the tank model.

Over recent years, as increasingly powerful computers have enabled the application of large numerical 3D reservoir simulators, some have looked down on the simple material balance equation and the tank model of the reservoir (Zangl and Hermann, 2004; Idogun et al., 2015; Molokwu and Onyekonwu, 2017). However, reservoir simulators are still using the material balance approach within each of their multi-dimensional cells (Mattax and Dalton, 1990). The value of this classical tool is that it enables the engineer to get a 'feel', of the reservoir and the contribution of the various processes in fluid production (Archer and Wall, 1986). A danger of blind application of reservoir simulators is that the awareness of the various components responsible for production might be lost to the engineer using the simulation output in predictive forecasting.

2.1.2 1D models

The 1D model is also known as the ‘core model’, based on which the Darcy’s Law was developed. Apart from being applied at core scale, this model was also used as a simplification to analyse the fluid flow between wells in a reservoir (Mattax and Dalton, 1990). Although the 1D core model cannot model the areal and vertical sweep, it still can be used effectively to investigate the sensitivity of reservoir performance to variations in reservoir parameters. These sensitivity studies can provide valuable insights when the engineer is history matching large reservoirs using more complex models. For instance, Hirasaki (1975) used a 1D model to study the sensitivity of oil recovery to changes in displaceable oil volume, mobility ratio, and relative permeability curves.

At the present time, although the 1D model can seldom be used for field-wide reservoir studies, in some studies on the modification of the fluid flow equation, the 1D model is still effective as a testing model. For instance, Wang (2013) developed non-Darcy flow equations for shales by modifying Darcy’s Law, and tested the new equation on a 1D core model to analyse the effects of capillary and compaction. Moreover, in order to enable the 1D model to simulate the fluid flow through the whole reservoir, a new version was built as ‘streamline model’ (LeBlanc and Caudle, 1971). Streamlines represent a snapshot of the instantaneous flow field and thereby produce data such as flow rate allocation between injector/producer pairs that are not easily determined by other simulation techniques.

The 1D streamline model differentiates itself from any other cell-based 2D or 3D simulation models: in the 1D streamline model, the phase saturations and components are transported along a flow-based grid defined by streamlines, rather than moved from cell-to-cell. This difference allows streamlines to be extremely efficient in solving large, heterogeneous models if key assumptions in the formulation are met by the physical system being simulated (Mattax and Dalton, 1990). The computational speed and novel solution data available have made streamlines an important approach to the popular 3D simulation models to (Thiele, 2001):

- Perform sensitivity runs
- Visualize the flow field
- Evaluate the efficiency of injectors and producers
- Reduce turnaround time in history matching

2.1.3 2D models

The 2D areal model used to be the most commonly used model in reservoir studies before computer modelling became common, in which the 3D aspects of a waterflood evaluation were simplified so that the technical problem could be treated as either a 2D areal problem or a 2D vertical problem. In essence, the 2D model is a variant of Darcy's Law (Mattax and Dalton, 1990). Many currently used well-testing models are derived from the 2D areal model (also named the 'pancake model') (Buchert et al., 1993). To simplify a 3D reservoir to a 2D areal model, either the reservoir must be assumed to be vertically a thin and homogeneous rock interval, or one of the published techniques to handle the vertical heterogeneity must be used.

The primary areal considerations for a waterflood involve the choices of the pattern style and the well spacing (Shirer et al., 1974). Maximizing the ultimate oil recovery and economic return from waterflooding requires making many pattern- and spacing-related decisions when secondary recovery is evaluated. This has been particularly true for onshore oil fields in the US, in which a significant number of wells were drilled for primary production (Chappelear and Hirasaki, 1976).

The areal models normally use Cartesian (x,y) coordinate systems, but there are some applications for which a radial (r,θ) coordinate system is more suitable, because it can provide better definition near well than do x-y areal models, or may reduce the number of gridblocks needed in the areal model (Cottrell, 1983). For a thick field, if it contains several independent reservoirs, each one should be modelled in a separate areal model; then the whole field can be presented by a 'multilayer model' (Fetkovich et al., 1994). However, a 3D model must be used if production from one reservoir influences that from another, or significant crossflow occurs between layers (Hunt and Rester, 2003).

Beside 2D areal models, 2D cross-sectional models are also used primarily 1) to develop well functions or pseudofunctions for use in 2D areal or 3D models (Jacks et al., 1973); 2) to simulate peripheral water injection, crestal gas injection, or other processes in which frontal velocities toward producers are largely uniform (DesBrisay et al., 1975); and 3) to evaluate well behaviour when vertical effects dominate performance, as in gas or water coning (Miller et al., 1973).

2.1.4 3D models

The 3D finite difference simulator is the most versatile tool in the current practice of reservoir engineering and management. Over the decades of use it has been improved to account for variety of physical and chemical processes that can occur in reservoirs. This allows us to work with a range of 3D models from very detailed to very coarse resolutions. At its extremes, the finite difference simulator can work with models at geological scale and models that contain just a few cells and closely resemble material balance models and their functionality. It all depends on the resolution we need, the data we have to construct the model, and the objectives we are trying to achieve (Aziz and Settari, 1979; Mattax, and Dalton, 1990; Ertekin and Abou-Kassem, 2001; Fanchi, 2006; Mustafiz and Islam, 2008; Islam and Moussavizadegan, 2010). The construction of the simulation model is the most important and time-consuming process. The quality of the constructed model is critical, since it directly defines the accuracy and applicability of the simulated results. Typically, the process of building a 3D model begins by generating a base model with initial parameter settings, which consists of three main parts (Lie and Mallison, 2013):

(i) a 3D high resolution geo-cellular model with different physical properties (e.g., porosity, permeability, thickness, rock compressibility) that describe the given porous rock formation;

(ii) a flow model that describes how fluids interact within a porous medium (e.g. relative permeability curve, fluid components) by solving a set of partial differential equations (e.g. Darcy's Law, conservation of mass, equation of state);

(iii) a well model that describes how the fluids flow in and out of the reservoir, including a model for flow within the wellbore and any coupling to flow control devices or surface facilities.

Once a 3D simulation model is created, it is then sent to the simulator for processing. A finite difference simulator is a computer program that has the ability to solve a set of partial differential equations replaced with finite differences. The following example shows a simplified isothermal simulator workflow, where the finite differences are derived from Taylor's series (Fanchi, 2005):

1. The two-phase fluid flow equations (saturation equation and pressure equation) are formulated as:

$$\frac{\partial}{\partial x}\left[\frac{Kk_r}{\mu}\left(\frac{\partial P}{\partial x}\right)\right] = \varphi\frac{\partial S}{\partial t} \tag{2.2}$$

$$\frac{\partial}{\partial x}\left[\lambda\left(\frac{\partial P}{\partial x}\right)\right] = 0 \tag{2.3}$$

where: K – absolute permeability of the rock; k_r – relative permeability of the fluid (oil or water); μ - fluid viscosity (oil or water); P – pressure; φ – porosity; S – fluid saturation (oil or water); x – coordinate along x-axis; t – time coordinate; λ – two phase mobility, $\lambda = \frac{KK_{ro}}{\mu_o} + \frac{KK_{rw}}{\mu_w}$.

2. Derivatives are approximated with finite differences:

a. Discretise region into grid blocks Δx:

$$\frac{\partial P}{\partial x} \approx \frac{P_{i+1}-P_i}{x_{i+1}-x_i} \equiv \frac{\Delta P}{\Delta x} \tag{2.4}$$

b. Discretise time into time steps Δt:

$$\frac{\partial S}{\partial t} \approx \frac{S_{n+1}-S_n}{t_{n+1}-t_n} \equiv \frac{\Delta S}{\Delta t} \tag{2.5}$$

where: i – index labelling grid location along x-axis; n – index labeling the present time level, so that $n+1$ represents the next time level.

3. Numerically solve the resulting set of linear algebraic equations.

Once the finite difference analogues (2.4) and (2.5) of the partial differential equations are obtained, they can be substituted into the flow equations (2.2) and (2.3). Further, the full set of flow equations is rearranged algebraically and solved using numerical methods. As a result of computation, the unknown primary variables, pressure and saturation, are calculated in spatiotemporal coordinates, which allows updating of the pressure-dependent parameters of the model.

This process can be repeated iteratively, many times. The results of the 3D simulation represent the reservoir behaviour in a time perspective under particular conditions. The model should then be validated by implementation of a history-matching procedure, where observed or historical pressure, saturation, and productivity measurements are

sequentially matched with simulated ones. In the case where there is no sufficient deviation observed, the simulation model can be further used for the reservoir performance prediction, including all life stages from exploration to abandonment. Otherwise, some key parameters should be revised and adjusted.

2.1.5 Overview

In this section, reservoir simulation models at different physics complexity levels have been reviewed. It has been seen that the control function of the 0D tank model is the material balance equation; in the 1D and 2D models, Darcy's Law acts as the main control function. In the 3D simulation model, the material balance equation and Darcy's Law are still the control function, but having the 3D high resolution grid model, the flow equation can be solved using the finite difference method.

There is no doubt that, compared with the 0D, 1D and 2D simulation models, 3D reservoir simulation is more powerful in the current petroleum industry. It can assist in resolving most of the problems related to reservoir management, field development strategy design, performance prediction, primary and enhanced hydrocarbon recovery evaluation, and many other activities. However, computational speed is an issue, especially for highly heterogeneous models consisting of more than one million grid blocks: despite the recent huge progress in computing speed, history matching assimilating more and more data, we still face a computational issue in the optimisation process. Although speed is not the only criterion for model selection, reservoir engineers are constantly looking for a method to deal with this issue, as explained in Chapter 1. One of the proxy methods that which will be introduced later in this chapter is to use the reduced physics model as a proxy. In Chapter 5, it is explained how the 0D tank model will work as the reduced physics proxy model for the fluid flow simulator.

2.2 Sim2seis model

2.2.1 PEM

A Petro Elastic Model (PEM) is sometimes known as the rock physics model. The petro-elastic model is often composed of empirical laws calibrated to laboratory measurements and analytical formulas. A PEM is used to convert changes in fluid saturations and pressures from the simulation into predicted impedance or other elastic properties for each simulation cell. A PEM is derived based on some laboratory work on core data, and ultimately it may be tested and calibrated by using petrophysical data from the logs. The output of the petro-elastic model will be the elastic properties of the reservoir, which will be used to generate the seismic data in the impedance domain or in the amplitude domain. For a PEM to be reliable within a 4D workflow it must be able to respond to changes due to the combined effect of pressure and saturation changes in the reservoir. Figure 2-1 shows the Petro-elastic modelling scheme for seismic comparison.

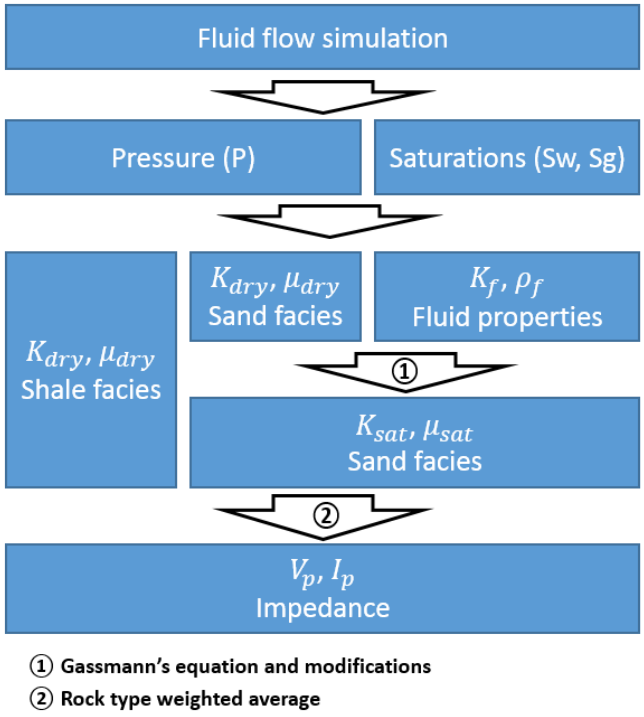

Figure 2-1 *Petro-elastic modelling scheme for seismic comparison (adapted from Soldo, 2005).*

The aim in this section is to develop an understanding of rock and fluid physics to relate seismic changes to changes in reservoir rock properties due to production. Usually the PEM represents a combination of equations and different parameters consisting of two parts: one representing the shaly part of the reservoir and the other one representing the sandy part. The formulae for these basic seismic properties are (Mavko et al., 1998):

$$I_{p_{sat}} = \rho_{sat} V_{p_{sat}} \tag{2.6}$$

$$V_{p_{sat}} = \sqrt{\frac{1}{\rho_{sat}}\left(K_{sat} + \frac{4}{3}\mu_{sat}\right)} \tag{2.7}$$

$$V_{s_{sat}} = \sqrt{\frac{\mu_{sat}}{\rho_{sat}}} \tag{2.8}$$

where the subscript sat indicates the fluid-saturated case, V_p is the P-wave velocity, V_s is the S-wave velocity, I_p is the P-wave impedance, ρ is the density, μ is the shear modulus and K is the bulk modulus.

Consequently, the saturated moduli and bulk density need to be calculated. Because the fluids do not affect the estimated shear modulus; thus, the shear modulus remains the same regardless of the fluid filling the rock pores:

$$\mu_{sat} = \mu_{dry} \tag{2.9}$$

The density of saturated rock is given by:

$$\rho_{sat} = \rho_f \varphi + (1 - \varphi)\rho_m \tag{2.10}$$

where $(1 - \varphi)\rho_m$ is the density of the dry rock frame, φ is porosity of the medium, and ρ_m is the matrix density, and ρ_f is the fluid density, which is a volume average of the individual fluids:

$$\rho_f = \rho_w S_w + \rho_o S_o + \rho_g S_g \tag{2.11}$$

where S_w, S_o and S_g are the water, oil and gas saturations respectively, and ρ_w, ρ_o and ρ_g are the densities of the water, oil and gas phases respectively.

Gassmann (1951) derived an equation to compute the bulk modulus of a fluid-saturated porous medium. The Gassmann equations divide the bulk modulus of a fluid saturated rock into three elements:

− bulk modulus of the porous rock frame

− bulk modulus of the pore-filling fluids, and

− bulk modulus of the mineral matrix

The Gassmann formulation is based on several assumptions: i) the rock's properties are homogeneous and isotropic, ii) pores in the rocks are well connected, iii) Pore pressure has enough time to reach equilibrium, thus the fluid saturations are homogeneously distributed, iv) viscosities of the fluids are negligible, and v) no chemical effects occur between the fluids and rock (Smith et al., 2003, Wang, 2001). Gassmann equations can be written as the following formula:

$$k_{sat}^{r} = k_{dry}^{r} + \frac{(1-\alpha)^2}{\frac{\varphi}{K_f} + \frac{\alpha-\varphi}{K_{gr}}} \tag{2.12}$$

where the superscript r indicates rock type (sand/shale), and φ is the porosity, K_{gr} is the bulk modulus of the mineral, $\alpha = (1 - \frac{k_{dry}^{r}}{K_{gr}})$. K_f is the fluid modulus, which is given by the saturation weighted harmonic average of the individual phase bulk moduli:

$$\frac{1}{K_f} = \frac{S_w}{K_w} + \frac{S_o}{K_o} + \frac{S_g}{K_g} \tag{2.13}$$

where K_w, K_o and K_g are the water, oil and gas moduli respectively which can be obtained using Batzle and Wang (1992) or from lab data for the specific sample.

Stress-dependency of k_{dry}

Gassmann's formulation requires the dry bulk modulus k_{dry}^{r}. Typically, dry rock properties are measured in the laboratory from core samples as a function of porosity, pressure and temperature. In this study, the stress dependency of the sandstone is captured in an empirical relationship (MacBeth, 2004):

$$k_{dry}^{r} = \frac{k_{inf}^{r}}{1 + E_k^{r} \exp(-\frac{P_{eff}}{P_k^{r}})} \tag{2.14}$$

where the superscript r identifies rock type (sand or shale), and the parameters K_{inf}, represent the dry bulk modulus at Standard Temperature and Pressure, and E_k is the excess compliance present in the rock as a result of geological or mechanical processes, and P_k is the stress sensitivity. P_{eff} is the effective pressure, which is the difference between the overburden pressure and the pore pressure. The overburden pressure is calculated at the centre of each grid cell using an average overburden pressure gradient of 1 psi/ft.

2.2.2 Seismic modelling

Having obtained the elastic properties, the following step is to model the seismic amplitude (seismic traces) based on the interlayer elastic property difference. Seismic forward modelling is one of the most well-established areas in exploration geophysics and reservoir geophysics, with a wide range of applications to seismic processing, seismic interpretation and special seismic studies such as seismic inversion. The most widely used method for seismic modelling is 1D convolution (Amini, 2014), which is illustrated in Figure 2-2.

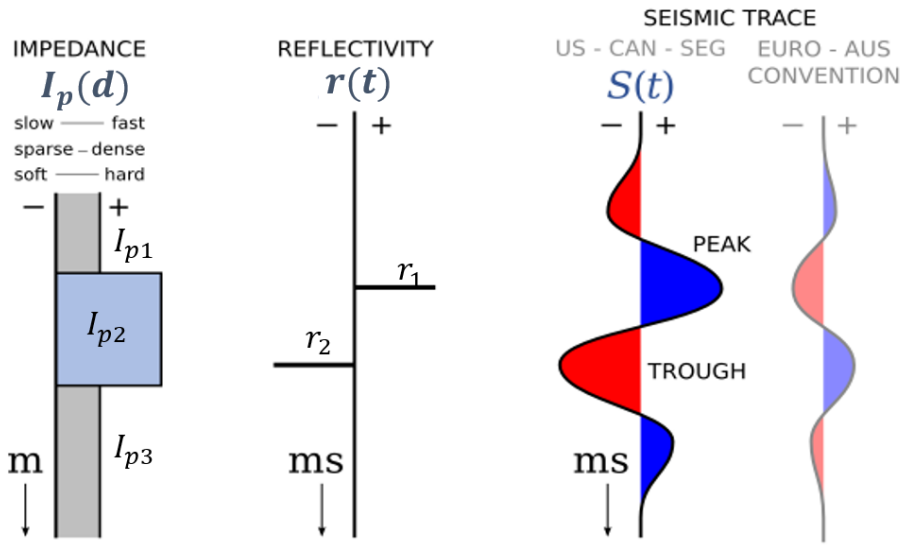

Figure 2-2 *Seismic modelling procedure: from impedance (left) to reflectivity (middle) then to amplitude (right two). (Adopted from http://subsurfwiki.org)*

$$r_1 = \frac{I_{p2} - I_{p1}}{I_{p2} + I_{p1}} \tag{2.15}$$

$$s(t) = \omega(t) * r(t) + n \tag{2.16}$$

where r_1 is the reflectivity between layers 1 and 2, $s(t)$ is the seismic trace as a function of time, *t*. ω is the wavelet vector and n is noise. In Figure 2-2, the reservoir geology is plotted on the left: one hard (high value of I_p) reservoir layer, surrounded by two softer layers. This is transformed to the time domain, and represented by only the impedance contrasts. The reflectivity of the interface is calculated, by which a wavelet $\omega(t)$ can be convoluted to produce the synthetic seismic trace, $s(t)$. The output traces at the rightmost side shows the peak and trough at interfaces. (There are two traces to illustrate that American geophysicists generally display the seismic with opposite polarity, compared to their European cousins.)

2.2.3 Overview

The aim in this section has been to develop an understanding of the petro-elastic model that relates reservoir rock elastic properties to pressure and fluid saturation changes due to production and also the model that further simulates the seismic traces based on the rock physical properties. The sim2seis workflow combines these two parts: the petro-elastic model and the seismic modelling procedure. Using the sim2seis workflow, the loop between the reservoir fluid flow simulation model and seismic data (normally the seismic amplitude data) could be closed, as shown in Figure 1-4. The models introduced in this section are all carrying out forward modelling, but can also be used in inversion problems, such as inversion from amplitude to impedance, or from impedance to the pressure and saturation domain. In terms of the computation cost, the petro-elastic model consists of linear equations only, thus is cheap to run. But the convolution process is time-consuming compared with petro-elastic modelling. Thus, in the SHM workflow, if the loop is closed at amplitude domain, the 1D convolution procedure will be used in each iteration, which is expensive for computing. This could be one of the reasons why impedance is more popularly used to perform SHM: the observed seismic amplitude data are inversed to the impedance domain; then, in each iteration only the fast petro-elastic model needs to be run. In the following chapters, the data-driven proxy model for sim2seis will directly relate the pressure and saturation domain with the amplitude domain, which is an attempt to shorten the time consumption and also reduce the number of required parameters.

2.3 Proxy models

A proxy model, also known as a surrogate model or meta-model, is a simplified model representation to resemble the full dynamic behaviour of a numerical simulation model (Sacks et al., 1989; Forrester et al., 2009; Zubarev, 2009 and Mohaghegh and Abdulla, 2014). It becomes advantageous when a direct evaluation of a system is either impossible or too expensive to simulate. An efficient proxy model must enable the reservoir behaviour to be replicated with high accuracy at minimum computational cost; in addition, it must be cheap to operate.

Many proxy models have been studied for the petroleum industry, including least squares (Pan and Horne, 1998; Zubarev 2009), kriging (Pan and Horne, 1998; Guyaguler et al., 2002; Zubarev 2009; Thenon et al., 2016), neural networks (Sampaio et al., 2009; Mohaghegh 2000) and statistical proxies (Artus et al., 2006; Onwunalu 2006) for purposes such as reservoir optimisation, history matching, uncertainty analysis and risk assessment. Generally, the proxy models that have been studied in the petroleum engineering field can be classified into three main types:

i) Response Surface Methodology

ii) Reduced Order Models

iii) Reduced Physics Models

An extensive description of the theoretical background and applications of these proxy models in reservoir engineering will be introduced in the following three sections, and their capabilities and limitations will be summarised in section 2.3.4.

2.3.1 Response surface model

In a response surface model, a sequence of training simulations is first performed using input parameters determined by an experimental design technique, such as a Plackett-Burman design (Yeten et al., 2005) or Latin Hypercube design (Zubarev, 2009). The simulated responses are then used to fit some predefined parameterized functions (called response surfaces), such as polynomials, kriging models or artificial neural networks, which will be used in place of the simulator to estimate the output for new input.

The main idea of a response surface model is to explore the relationships between several variables (x_1, x_2, …) and one or more response variables (y_1, y_2, ...). For example, where there are only two independents, the relationship between the variables and the response can be expressed as (Gunst, 1996):

$$y = f(x_1 + x_2) + \varepsilon \tag{2.16}$$

The variables x_1 and x_2 are independent variables that produce a response with y value, and the experimental error term is denoted as ε, which represents any measurement error on the response, as well as other type of variations not counted in the function f. If a polynomial model is selected as this function, depending on the approximation of the unknown response, either a first-order or second-order polynomial can be employed. If a linear function is enough to describe the relationship between the response and independent variables, then a first-order model will be firstly used to approximately define the function, which is expressed as (Gunst 1996):

$$y = \beta_0 + \beta_1 x_1 + \beta_2 x_2 + \varepsilon \tag{2.17}$$

The value of coefficients β_0, β_1 and β_2 can be obtained by a least square linear regression approach (Zubarev 2009). A higher degree polynomial model should be used if a curvature exists in the response surface. The approximating function with two variables is expressed as:

$$y = \beta_0 + \beta_1 x_1 + \beta_2 x_2 + \beta_{11} {x_1}^2 + \beta_{22} {x_2}^2 + \beta_{12} x_1 x_2 + \varepsilon \tag{2.18}$$

Box and Wilson (1951) suggested using a first-degree polynomial model to approximate the response variable. They claimed that, although this model is only an approximation, and not accurate, it is easy to estimate and apply, even without very much information about the process. Response surface models have been used in reservoir engineering, especially in the history matching procedure. Zubarev (2009) applied a polynomial regression model, a multivariate kriging model, a thin-plate splines model and an artificial neural network model as the response function f. He reported that all the proxies had shown a strong dependence on the model complexity, dimension of the design space and quality of the input dataset. The type of proxy model was found to have no major impact on proxy model performance. Amudo (2008), Slotte and Smorgrav (2008), Jawwad Ahmed et al. (2013), Shahkarami et al. (2014) and Wantawin et al. (2017) also used the response surface models in the history matching and uncertainty quantification.

2.3.2 Reduced order models

The reduced order model, as another type of proxy model, is considered as a simplified approximation of a given mathematical model of a system or process, which only captures the key characteristics of the original system or process (He, 2013). Due to the complexity and large size or dimensions of a system, many modern mathematical models have encountered challenges when used in numerical simulations, therefore, a reduced order model is used to replace a given mathematical model of a system or process by a much "smaller" model than the original model, but which still approximately describes the main behaviours of the system or process (Bai et al., 2005). By a reduction of the model's associated state space dimension or degrees of freedom, an approximation to the original model is computed, which can be evaluated with lower accuracy but in significantly less time. The grid-based and snapshot-based reduced order models are commonly used in the literature.

Grid-based reduced order model

In grid-based methods, the dimension of the problem is reduced by constructing a coarser grid and then computing properties for this grid. The original problem is then solved on the coarser grid. Upscaling is one of the most straightforward methods for dimension reduction. Upscaling provides a reduced-order model because it reduces the dimension of the problem by decreasing the number of grid blocks. Given a fine-grid model containing a large number of grid blocks, the main idea of upscaling is to define a coarser grid covering the same space, compute the coarse-scale (upscaled) parameters or functions (e.g., transmissibility or relative permeability), and then solve the reservoir equations on the coarse grid. Durlofsky (2005) and Chen (2005) have provided comprehensive reviews that describe a variety of upscaling methods. In application, the reservoir simulation model can be upscaled and solved by a commercial reservoir simulator (Eclipse Manual 2017 and CMG Manual 2017). This convenience makes upscaling a popular reduced-order method in the field of reservoir simulation (He, 2013).

Snapshot-based reduced order model

The second group of reduced-order models are derived from system control theory. These techniques are derived by considering a linear time invariant (LTI) system of the form:

$$\frac{dx}{dt} = Ax + Bu\ , y = Cx \tag{2.19}$$

where x ∈ R^n, u ∈ R^p and y ∈ R^q are state, input and output vectors respectively, and A ∈ $R^{n\times n}$, B ∈ $R^{n\times p}$ and C ∈ $R^{n\times q}$ are the so-called system matrices. A basis matrix, Φ ∈ $R^{n\times l}$, is defined such that x = Φξ. This means that an *n*-dimensional state, *x*, is reduced into an *l*-dimensional state, ξ. In addition, the constraint reduction matrix, Ψ ∈ $R^{n\times l}$, is defined to reduce the number of equations from *n* to *l*. The reduced linear time invariant system is thus of the form:

$$\Psi^T\Phi\frac{d\xi}{dt} = \Psi^T A\Phi\xi + \Psi^T Bu \quad , \quad y = C\Phi\xi \tag{2.20}$$

The introduction of Φ and Ψ converts the full-order (n-dimensional) linear time invariant system into a reduced-order (l-dimensional) system, which can be solved much more efficiently, since $l \ll n$. Snapshot-based methods derive the basis matrices, Φ and Ψ, from "snapshots," which are the states at each time step of training simulations. Almost all of the methods to derive the basis matrices are based on Proper Orthogonal Decomposition (POD) or its variants.

Proper Orthogonal Decomposition (POD) reduces the dimension of the problem by projecting the high-dimensional states (e.g. pressure and saturation at each grid block in an oil-water problem) into an optimal lower-dimensional subspace. The basis of this subspace is obtained by performing singular value decomposition (SVD) of a matrix containing, as its columns, the solution states (snapshots) computed from previous simulations. The simulations used to provide these snapshots are the training runs; new (prediction) runs are referred to as "test" cases. POD has been applied for model reduction in many application areas (Bui-Thanh et al., 2004; Vermeulen et al., 2006; Cai et al., 2009 and Liberge et al., 2010). Within the context of reservoir simulation, van Doren et al. (2006) applied POD to reduce the dimensions of both the forward model and the adjoint model, with the goal of accelerating the optimisation of a waterflood process. A 35% reduction in computing time was reported in that work. Cardoso et al. (2009) proposed a snapshot clustering procedure and a missing point estimation technique to further accelerate a POD-based reduced-order reservoir simulation model. They achieved speedups of about a factor of 6 to 10. Thenon et al. (2016) extended the reduced order model approach to the multi-fidelity context to model the vectorial outputs. They compared the reduced order model with kriging in history matching, found that the performances of the two models were similar for large simulation times.

2.3.3 Reduced physics models

The reduced-physics model is another method of performing the approximation of the real process by simplifying the full physics model. Traditionally, a full-physics simulation involves steps including gridding and discretization, fluid properties collection, rock-fluid interaction and well modelling. It is built based on a set of finite difference equations or finite element discretization, and contains hundreds of thousands of unknown variables (Yang et al., 2009). Considering that running a full-physics model is a computationally intensive task and that it may take days or even weeks for a large model to be computed, a reduced-physics model as a proxy model has been worked out as an alternative to full-physics simulation, by simplifying the physics.

In the reservoir engineering field, streamline methods, for example, (Batycky et al., 1997; Datta-Gupta and King, 2007) fall into this category. Streamline methods decouple the flow and transport equations and then solve the transport equations as a series of one-dimensional problems along each streamline. This simplification can lead to substantial speedups relative to traditional simulation, for some problems. The reduced-physics models are also used for simulation cases of thermal recovery processes, such as Steam Assisted Gravity Drainage (SAGD) and Vapour extraction (Vapex), and shale gas production. Azad and Chalaturnyk (2010) discussed an analytical physics-based proxy model for the purpose of reservoir characterization. Vanegas et al. (2008) developed a reduced-physics proxy model for predicting oil flow rate, cumulative oil production, and cumulative steam injection for a reservoir model with uncertain parameters of porosity, horizontal permeability, vertical permeability, and rock type. Leung and Shi (2013) built a physics-based proxy model for a vapour extraction process in a heterogeneous reservoir, which was used for prediction of total drainage rate, drainage rate change with time, and the change of the solvent chamber boundary position during the spreading chamber period. Wilson and Durlofsky (2012) presented an example of a reduced-physics model to simulate the matrix flow, flow through fractures (primary and secondary) of diverse sizes, gas desorption, non-Darcy effects and stress-dependent permeability. Instead of including all physics, the reduced-physics model simplified the physics; for example, single porosity replaced dual-porosity, and stimulated reservoir volume was used instead of explicitly describing the fractures by local grid refinement. They reported that the reduced-physics model provided predictions in close agreement with results from the full-physics model.

2.3.4 Overview

Following the previous three sections in which the theoretical backgrounds and applications of the three kinds of proxy model were described, this section summarises their capabilities and limitations.

Response surface models use the reservoir simulator as a black box and are thus easy to implement (He, 2013). However, to generate a reasonably accurate response surface requires a large number of training simulations, and this number grows very quickly as the number of parameters increases. Therefore, response surface methods are commonly applied for cases with relatively few parameters (no more than 20) (Yeten et al., 2005)

The reduced-order models can speed up the simulation running by about a factor of 6 to 10 in some cases (Cardoso et al., 2009). The main challenge of reduced-order modelling is how to extract a reduced basis of lower-dimension, which at the same time contains all the essential information of the original model with large dimensions (Burkardt et al., 2003). Therefore, to build a successful reduced-order model requires good communication between reservoir engineers and mathematicians.

The physics-reduced model has been successfully used as an efficient way to model very complex reservoir conditions, and this simplification can lead to substantial speedups relative to traditional simulation models (Wilson and Durlofsky, 2012). However, a great deal of simplification of the fluid flow process has been carried out, using this approach, which may result in a very unrealistic system representation (He, 2016).

In summary, each proxy model has its capabilities and limitations; thus, to determine the best proxy for the conventional simulation model is a case-dependent issue. No decision could be made before running the simulation model of the field and considering the data type of outputs, number of uncertain parameters and the complexity of the model itself.

2.4 Summary

This chapter has provided a review of fluid flow simulators and 4D seismic simulation models, together with proxy models. The fluid flow simulation models were classified by the model dimension (or by physics complexity), of which the control functions are the material balance equation, Darcy's Law and multiphase flow equations. In the development history of reservoir models, from the 0D tank model to the 3D model, the physics complexity was also increased. The sim2seis model contains two parts, a petro-elastic model and convolutional seismic modelling, using which the seismic response can be produced based on the output properties of the fluid flow simulation model, such as pressure and saturation. These two simulators are inevitable components of the seismic history matching workflow. The proxy models were then introduced as potential alternatives to these two simulators. The theoretical background and applications of the response surface model, reduced-order model (model upscaling and POD) and reduced-physics model were discussed. Finally, the advantages of each type of proxy model and their drawbacks were summarised.

The three proxy models that will be built in the following three chapters are based on the review in this chapter. The sim2seis proxy model (Chapter 3) is a response surface model; the first proxy for the reservoir simulation model (Chapter 4) is a reduced order model (upscaled model); and the second flow simulation proxy (Chapter 5) is a reduced -physics model: the conventional 3D fluid flow simulation model is 'reduced' to a 0D tank model.

Chapter 3

Seismic modelling proxy: linear superposition model

This chapter presents a proxy model for seismic modelling, and analyses its quality and robustness. The proxy model is developed to generate a 4D seismic map, using only the original baseline seismic data and dynamic pressure and saturation predictions from reservoir flow simulation. Based on a linear simplification, this method can significantly reduce the required running times of the seismic modelling simulator (sim2seis). The accuracy of the proxy is quantified by two metrics in a blind test, following the validation of the linear superposition assumption. Additionally, a different seismic attribute and an 'adaptive proxy' are analysed to test the robustness of the proxy. The seismic proxy model established here will be applied in the SHM workflow in a later chapter.

3.1 Introduction

In modern reservoir management practice, simulation of the hydrocarbon reservoirs is an essential, but complex and multi-disciplinary tool. Reservoir engineers always need a satisfactorily built simulation model (or models) to forecast various data under different operational plans or development scenarios such as exploring different locations for infill wells (Watkins et al. 1992). The accuracy of a simulation model is limited, at best, by the quality of the geological and reservoir data used as inputs in its construction. If the historical data such as production profiles, well bottom pressure, or time-lapse (4D) seismic data is available, then the simulation model input parameters can be calibrated by a history matching procedure.

Because the well-based production data is the dynamic consequence of subsurface flow and provides limited information on spatial changes in the reservoir, accordingly, in many cases time-lapse (4D) seismic data has been used to keep track of spatial changes due to production (Lumley 2001, Dadashpour et al. 2007, Geng et al. 2017). Compared with the production history matching (PHM) workflow, as introduced in Chapter 2, the seismic history matching (SHM) loop involves two forward simulators: a fluid flow simulator and sim2seis modelling (Figure 3-1). One of the main challenges of SHM is that the computation cost of simulation runs can be very high, particularly in cases where a single run of simulation is heavy or where thousands (even millions) of iteration runs are needed to analyse the model uncertainty (He et al. 2016). Moreover, from a practical perspective, sim2seis modelling, which is a multidisciplinary process, contains high uncertainty and can be the most difficult task facing a reservoir engineer engaged in SHM (MacBeth et al. 2016, Santos 2017).

The method I propose in this chapter is to make an assumption for the second simulator, sim2seis modelling (green box in Figure 3-1, below), by introducing a linear superposition proxy to model the 4D seismic response, directly from the output of fluid flow simulator: changes of pressure and saturation (Figure 3-2). That way, the computation cost of the SHM loop becomes more affordable for some huge reservoirs and for the analysis of prediction uncertainty. Moreover, compared with the complex petro-elastic model and convolution model, this proxy only consists of three coefficients which indicate the contribution of saturation and pressure changes to 4D seismic. By applying this proxy method, the seismic modelling procedure could appear less tedious to a reservoir engineer and facilitate interdisciplinary exchanges within an asset team.

This method is developed based on the data of a Norwegian Sea turbidite field. A description of this field, proxy building steps, proxy quality quantification and the proxy model robustness will be introduced in detail in following sections of this chapter.

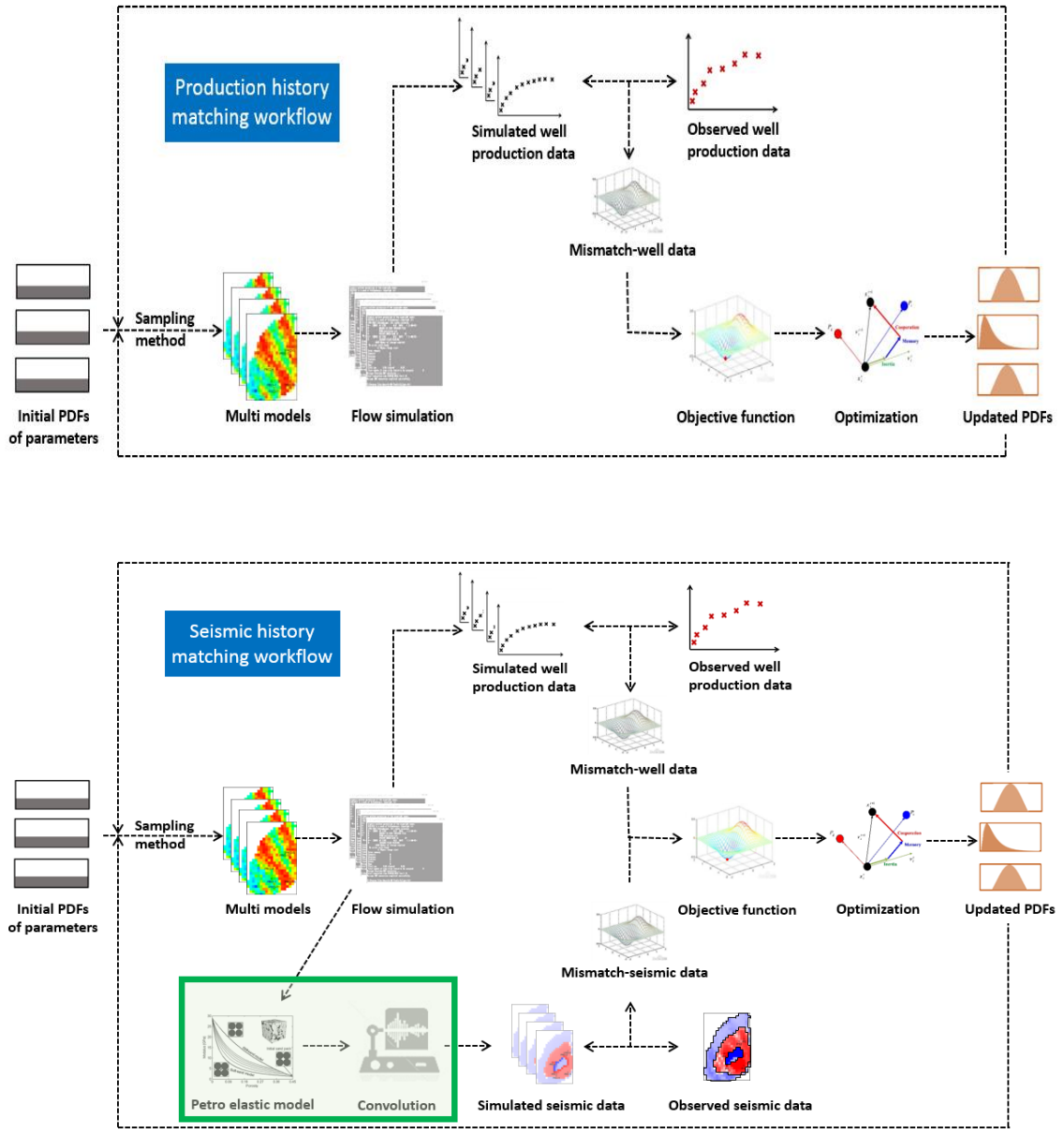

Figure 3-1 *Conventional workflows for production history matching (PHM, above) and seismic history matching ('SHM', below). In the green box is the conventional seismic modelling part: petro-elastic model and convolution model. In this chapter my target is to build a proxy for this part.*

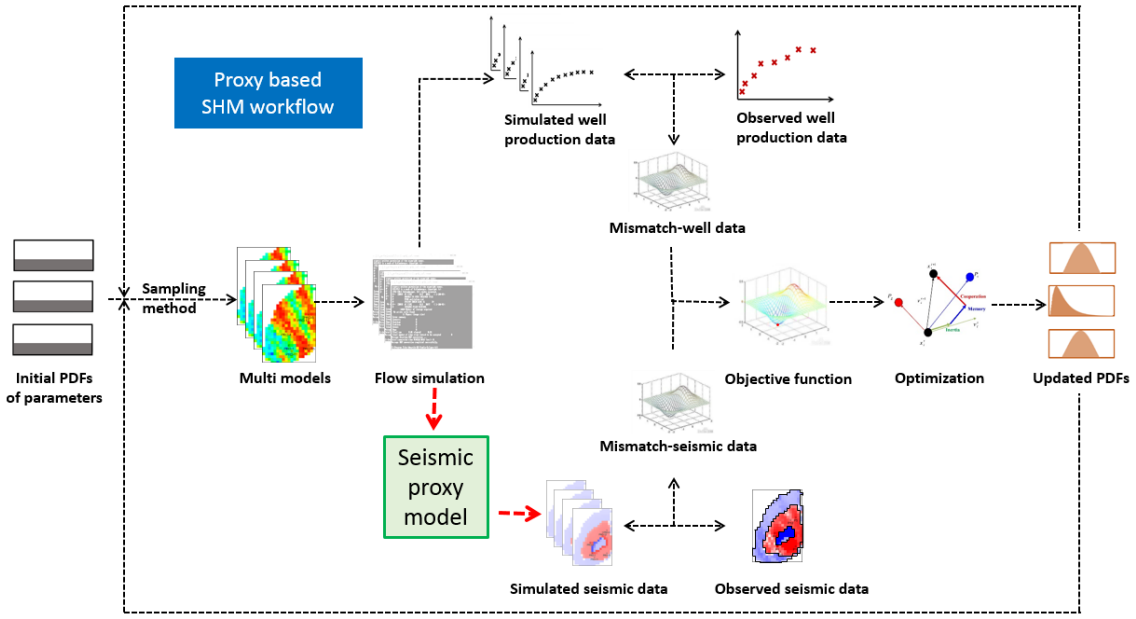

Figure 3-2 *Proxy model based seismic history matching workflow, with seismic modelling proxy only.*

3.2 Field description and data sources

Norne is a rotated fault block turbidite field which is located in the Norwegian Sea; it covers approximately an area of 9×3 km^2 and is an oil and gas field with average water depth of 380 metres. Discovered in 1992 and developed from 1997, Norne had produced 86.42 million Sm^3 oil by May 2012 under the drainage strategy. The expected ultimate oil recovery is more than 60%; probably the highest recovery of all subsea oil reservoirs, worldwide. From the early to the late life of the Norne field, 4D seismic has played a critical role in monitoring fluid contacts (Osdal et al., 2006), evaluation of in-fill wells and mapping flooding (Huang et al. 2013). Until 2012, 4D seismic surveys have contributed to the drilling of 21 wells with an estimated added value of 4.5 billion NOK (Huang et al. 2013).

The *Norne benchmark case* is a unique set of real oil field data which is currently being organized by the Norwegian University of Science and Technology (NTNU). The operator Statoil and partners (ENI and Petoro) of Norne Field have agreed with NTNU to release large amounts of subsurface data from the Norne field for research and educational purposes. My research is also based on these available historical data and reference models (a flow simulation model which has already been matched to production data only and a reference petro-elastic model) offered by NTNU.

In June 2011, an applied technology workshop, 'Use of 4D Seismic and Production Data for History Matching and Optimisation – Application to Norne (Norway)', was held by the Society of Petroleum Engineer (SPE). Participants from universities and other research organizations were asked to test different mathematical methods in order to extract extra value from production and seismic data through history matching (Rwechungura et al. 2012). Rather than exploring different forward models and optimisation algorithms, as was done in this workshop, the target of my research is to build a proxy model as an approximation of the full physical seismic modelling procedure, as introduced in Chapter 1.

3.2.1 Field geology

The trap type of Norne Field is a rotated fault block of Jurassic age in a horst and graben terrane with complex fault blocks within the major faults zone. The source rock, Spekk Formation, formed during the rifting in the Late Jurassic. Coal beds of the Åre Formation were deposited in the Early Jurassic and may be the source of the gas in the formation (Clayton et al., 1990). A schematic illustration of the Norne field is shown in Figure 3-3. The reservoir is horizontally divided into 4 segments bounded by major tectonic faults and segments C, D and E contain over 97% of the initial oil in place (Statoil, 2001).

Figure 3-3 *The Norne Field location (left) and four main segments (right, Statoil, 2001).*

Vertically, the Early to Middle Jurassic rocks host the main reservoirs of the field. There are four main sandstone formations within this area namely: Tilje, Tofte, Ile and Garn formations. The details of the key characteristics of each formation are listed in Table 3-1. The reservoir sands within the Ile and Tofte formations are of good quality with porosities in the range of 25 – 30% and permeability in the range of 50 – 3000mD. These

two formations contain over 90% of the initial oil in place. The laterally extended carbonate layers are partially sealing and dominate the vertical communication of the Ile and Tofte formations (Statoil, 2006).

Table 3-1 *Key characteristics of five formations of the Norne Field (after Statoil, 2001).*

Formation	Key characteristics
Garn	• near shore sands of about 30m thickness • porosity range from 18 – 29% • gas filled • vertically overlaid by the Melke and Spekk formation which act as seals for the whole reservoir
Not	• a very effective sealed shale formation • breaks the communication between the reservoirs above and below it
Ile	• composed of mostly thick sands and channelized sands • has an average porosity of 25% and a total thickness of about 45m • contains flow barriers such as faults and carbonate layers • main reservoir of oil in place • separated from the Garn formation by Not shale formation • vertical communication with Tofte formation below
Tofte	• a laterally uniform formation with channelized sands • there is a set of lateral extended carbonate layers which are partially sealing • main reservoir of oil in place • porosity range from 22 – 28% and a total thickness of 47m
Tilje	• tidally influenced deposits • porosity varies from 16 – 25% and a total thickness of about 90m • main aquifer • separated from the Tofte formation by an unconformity

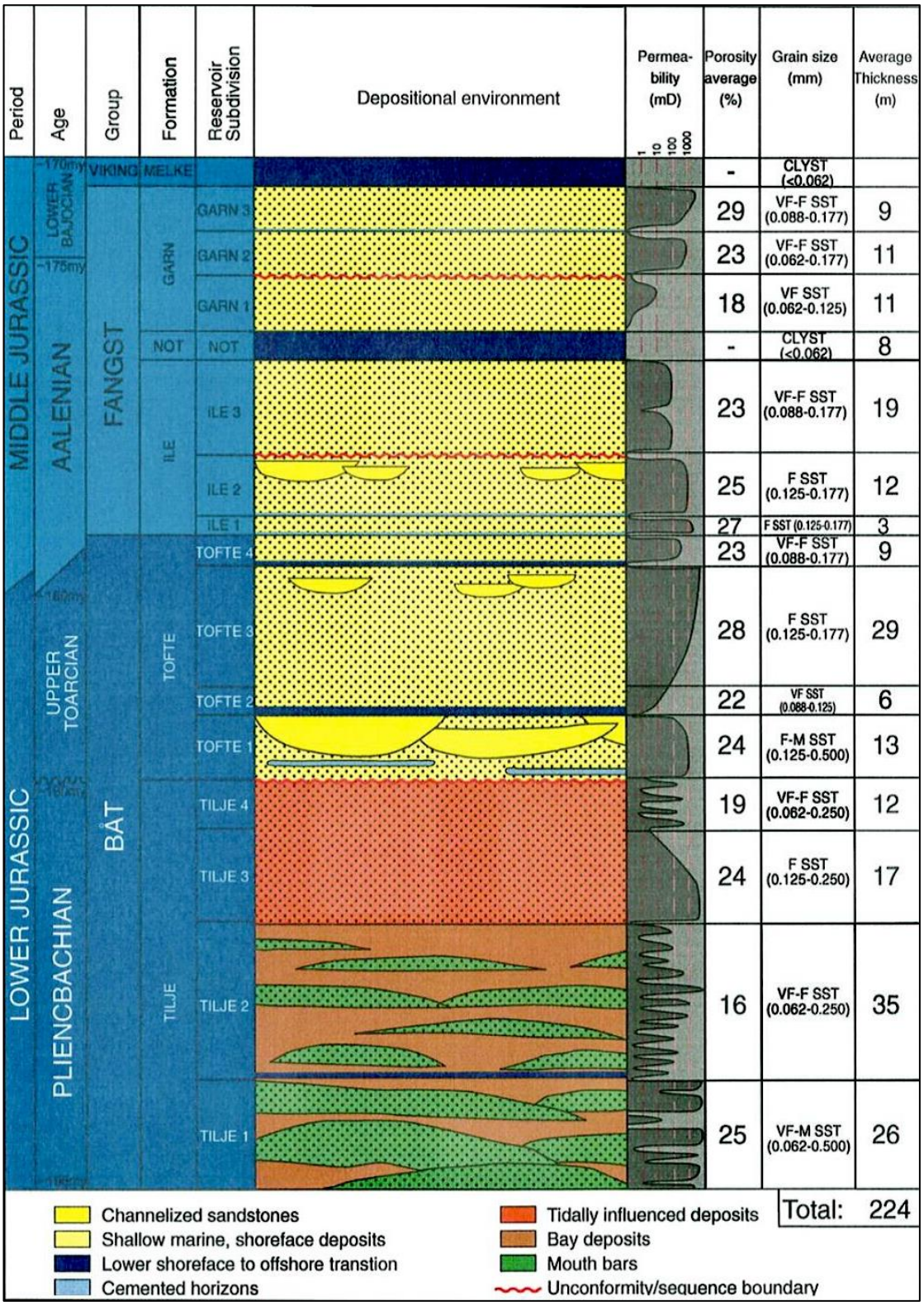

Figure 3-4 *Stratigraphic sub-division of the Norne reservoir (Statoil, 2001).*

3.2.2 Field development history and challenges

Oil is mainly found in the Ile and Tofte formations. To maximize drainage, a water injection strategy has been applied to maintain the reservoir pressure; more than 50 wells have been drilled at Norne, including the sidetracks from main boreholes and multi-lateral wells drilled to obtain a co-mingled flow from multiple targets. So far, the production has mainly come from the Ile and Tofte formations with bottom and side water injection as the primary driving mechanisms.

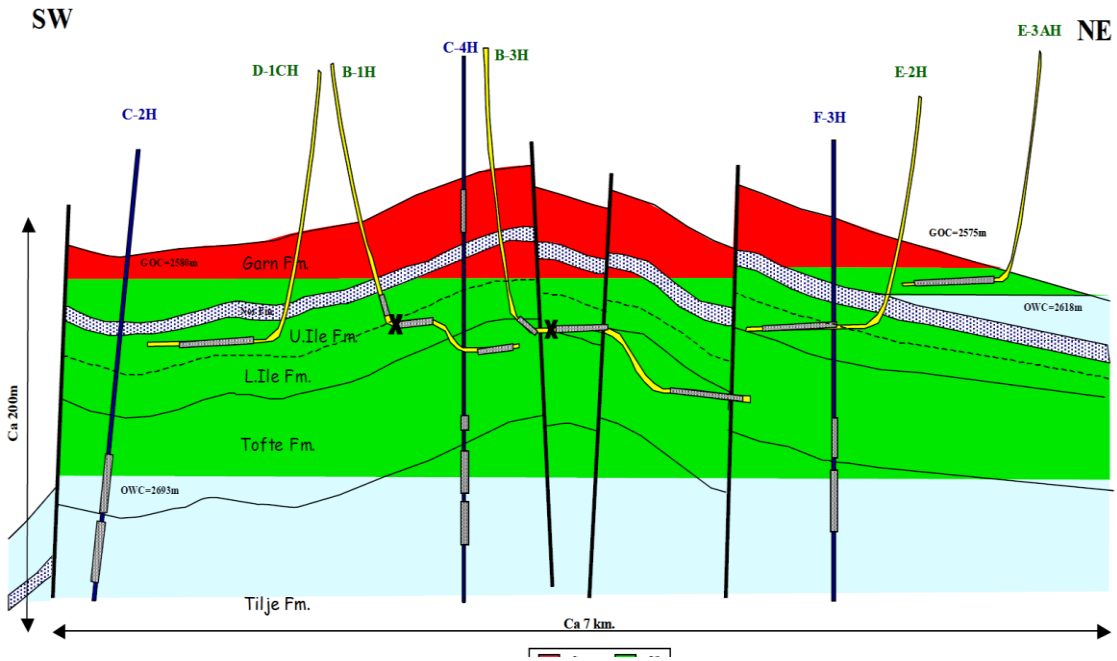

Figure 3-5 *NE-SW running structural cross section through the Norne Field with initial fluid contacts and current drainage strategy (Statoil, 2004).*

The development history of the Norne Field from discovery to production has been described by Steffensen and Karstad (1996), while the development of horizontal wells and methods to control gas lift were described by Al-Kasim (2002) and Selle et al. (2008), Husby et al. (2005) also described the use of natural geochemical tracers in the Norne Field to improve reservoir simulation models. Koalewski et al. (2006) reported an experimental study for testing the possibility of using microbial improved oil recovery in the Norne Field.

The main goal is to develop the Norne Field such that the economic optimum production profile is obtained. However, in the whole life cycle of the development, the Norne Team faced various challenges (Huang et al., 2013):

In the main reservoir Ile and Tofte formations, there are carbonate-cemented layers up to ~1 m thick, which commonly act as barriers to the vertical flow. The discontinuous nature and distribution of these stringers create complex drainage patterns in the main reservoir and lead to uneven movement of oil-water contact (OWC). Monitoring the OWC was one of the main challenges that faced the reservoir engineers in the early stage of production of Norne. In the later life of Norne, with around 50 wells drilled in the field, it has been a challenge to find new infill targets that satisfy the economic requirements. A target area located between segments C and G of the field has been evaluated. The complex fault system and lack of information about the drainage pattern in this area represent the main risks for drilling this well. Thus studies need to be carried out to reduce these risks.

The Norne team has, during the whole field life, been very actively using time lapse seismic in reservoir monitoring. From the monitoring of OWC to the evaluation of infill well planning, 4D seismic has played a major role in helping the reservoir engineers to respond to the challenges and solve the problems: the seismic data has been interpreted to map the fluid contacts and to analyse the transmissibility of faults and barriers. This information was then used to calibrate the reservoir model. In order to extract more value from 4D seismic, the reservoir simulation model should be history-matched using both seismic and production data as constraints (Rwechungura et al. 2012). In next section, I will present the simulation model and observed 4D seismic and production data and then develop a fast-track proxy method to run the SHM workflow.

3.2.3 Simulation models

3.2.3.1 3D fluid flow simulation model

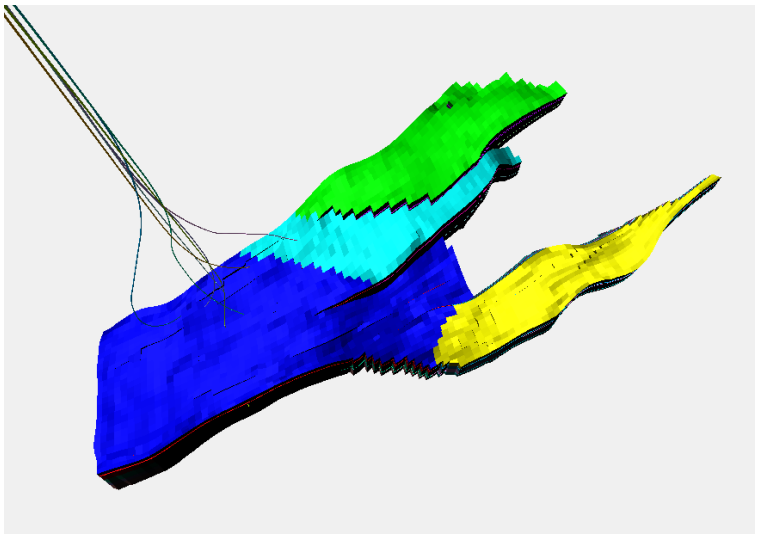

Figure 3-6 *3D simulation model of Norne Field (each colour stands for a segment).*

The Norne reservoir simulation model has been built as a three phase three dimensional black oil model (ECLIPSE 100). The reservoir has 46 cells by 112 cells by 22 cells in the X, Y and Z direction respectively, with 44,431 active cells in total. The model is physically divided into two sections by a sealed shale layer (the Not formation). The upper and lower sections consist of 3 and 18 layers respectively. The simulation model layers and corresponding formations are listed in Table 3-2.

Table 3-2 *Simulation model layers and corresponding reservoir formations.*

Layers in simulation model	Formation	Simulated formation average thickness/m	Simulation layers average thickness/m
1-3	Garn	31	10.3
4	Not shale	8	8.0
5-11	Ile	43	6.14
12-18	Tofte	48	6.86
19-22	Tilje	90	22.5

According to the geology of the field, formation Ile and Tofte contain over 90% of the STOOIP (stock tank original oil-in-place) in Norne and there is a set of flow barriers within these two formations; therefore, these formations are presented with a finer vertical scale (6-7 m/layer) in the simulation model compared to the upper or lower formations.

3.2.3.2 Petro-elastic model

A petro-elastic model (PEM) is a set of parameters and equations which relates reservoir properties (such as pore volume, pore fluid, fluid saturation, reservoir pressures and rock composition) to seismic elastic parameters (such as P-wave and S-wave velocities, Vp and Vs, respectively, and density). Forward seismic modelling produces seismic amplitudes from these elastic properties. A PEM can be used both in inversion and forward seismic modelling, and for the interpretation of seismic data in terms of lithology (Falcone et al. 2004).

The PEM used for the Norne field has been given in Chapter 2; Table 3-3 presents the input parameters for this PEM (Dadashpour, 2009).

Table 3-3 *Model of input parameters for the petro elastic model (Dadashpour, 2009).*

Shale properties			
Shale Type1 (Not Formation)	P-wave Velocity S-wave Velocity Shale Density	V_{PSH1} V_{PSH1} ρ_{PSH1}	3200 m/s 1600 m/s 2300 kg/m^3
Shale Type 2 (Overburden)	P-wave Velocity S-wave Velocity Shale Density	V_{PSH1} V_{PSH1} ρ_{PSH1}	3350 m/s 1800 m/s 2450 kg/m^3
Shale Type 3 (Under reservoir)	P-wave Velocity S-wave Velocity Shale Density	V_{PSH1} V_{PSH1} ρ_{PSH1}	3500 m/s 1900 m/s 2450 kg/m^3
Rock (sand) properties			
Garn formation	Frame bulk modulus Frame shear modulus Matrix bulk modulus Matrix Density	k_{fr} μ_{fr} k_{ma} ρ_{ma}	18.8-36.8φ 11.8-21.4φ 37 GPa 2650 kg/m^3
Ile, Tilje, and Tofte Formations	Frame bulk modulus Frame shear modulus Matrix bulk modulus Matrix Density	k_{fr} μ_{fr} k_{ma} ρ_{ma}	18.5-27.4φ 10.9-13.0φ 37 GPa 2650 kg/m^3
Fluid properties (Reservoir Temperature 98.3 ℃)			
Fluid bulk modulus Oil density Water density Water salinity Gas density		K_o, K_w, K_g ρ_o ρ_w SAL ρ_g	Batzle and Wang (1992) 860 kg/m^3 1000 kg/m^3 0.05 kg/m^3 190 kg/m^3

3.2.4 Production and seismic data

3.2.4.1 Production data

Monthly production and injection rates are available for all wells for the period from November 1997 to December 2006. The producers are under reservoir volume constraint and the injectors are under water or gas injection rate constraint (both rates are provided by the operator). The oil, water and gas production rates are normally used as the data to be matched. The initial simulation model was reviewed in the previous section; it has been matched with the production data by the operator. However, a simulation model can never be perfectly matched, so here I will show how well the initial simulation model matches the data. Figure 3-7 (a, b and c) displays the matching of the field water production (FWCT), field oil production rate (FOPR) and field gas production rate (FGPR). Such field production profiles can help to generate an overall evaluation of the simulation model. In order to quantify the matching quality, I introduce a metric percentage mismatch ratio (PMR), as follows:

$$\mathrm{PMR}_i = \frac{|S_i - D_i|}{|D_i|} \times 100\% \tag{3.1}$$

where PMR_i denotes the percentage mismatch at the ith data point, S_i and D_i represents the simulation value and observer data values respectively. With this metric, I plot the mismatch over the 9 years, in Figure 3-7 (d).

According to the field production rate matching, it is found that the field oil and gas production rate were pretty well-matched (with average PMR=16.2% and 8.8% over 9 years). The field water cut, however, was not well-matched, especially between 2002 and 2005. With the average PMR=112.1%, the simulated water cut is obviously over-predicted. From the point of reservoir reality, the complex flow barriers may not be fully represented in the simulation model; therefore the flow resistance was under-simulated and the injected water arrived at the producer too fast.

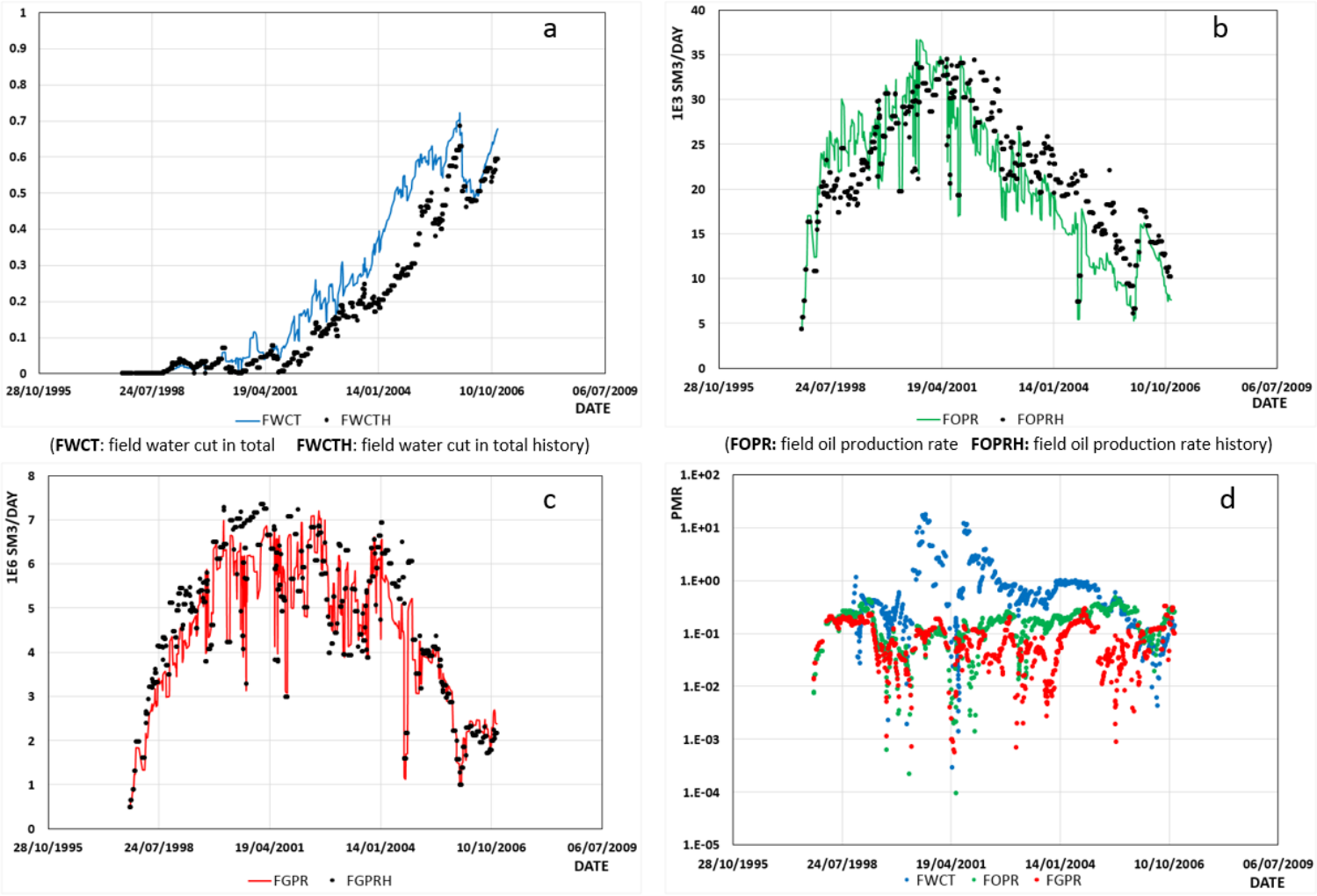

(**FWCT**: field water cut in total **FWCTH**: field water cut in total history)

(**FOPR:** field oil production rate **FOPRH:** field oil production rate history)

(**FGPR:** field gas production rate **FGPRH:** field gas production rate history)

Figure 3-7 *Matching of FWCT (a), FOPR (b), FGPR (c) and PMR (d) over the 9 years of the initial simulation model.*

To be specific, I also analysed the wells which have perforation in the main reservoir (Ile formation and Tofte formation, Figure 3-8).

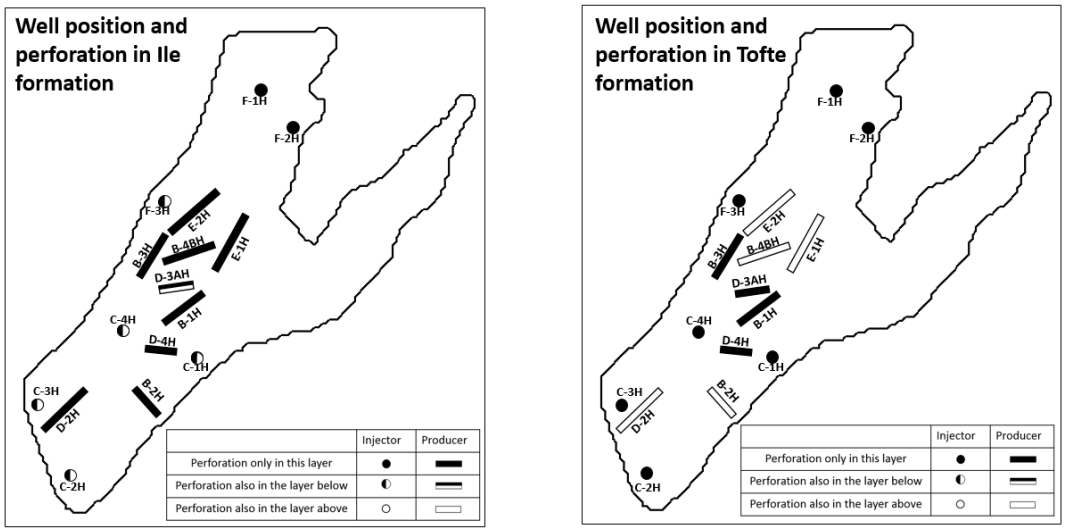

Figure 3-8 *Horizontal well injections and perforations set in Ile and Tofte formations*

There are seven injectors and nine producers which have perforations in the main reservoir. According to the cumulative oil production, I ranked all the nine producers which have perforations in the Ile formation and analysed their history matching quality (Table 3-4).

Table 3-4 *History matching quality of the nine producers which have perforations in Ile and Tofte formations.*

Well	Cumulative oil production /1E6 SM3	Oil production	Gas production	Water production	Segment
B-2H	8.4	well matched	well matched	over simulated	C
E-1H	7.1	well matched	well matched	over simulated	D
E-2H	6.9	well matched	well matched	over simulated	E
B-1H	4.7	under simulated	under simulated	under simulated	C
B-3H	4.5	well matched	well matched	over simulated	D
D-3AH	3.9	well matched	well matched	well matched	C
D-2H	3.6	well matched	well matched	over simulated	C
D-4H	3.4	well matched	well matched	well matched	C
B-4BH	1.2	well matched	well matched	well matched	D

Figure 3-9 illustrates the simulation and observation data for producers E-1H and E-2H. It can be seen that the oil and gas production rates were well-matched, but the water cuts were both over-predicted. According to Statoil (2006), injectors F-1H, F-2H and F-3H provided the main support to the two producers, so the fluid flow barriers such as local faults and low-permeability layers between injectors and producers are the main sources of uncertainty and will thus be selected as the parameters for later history matching.

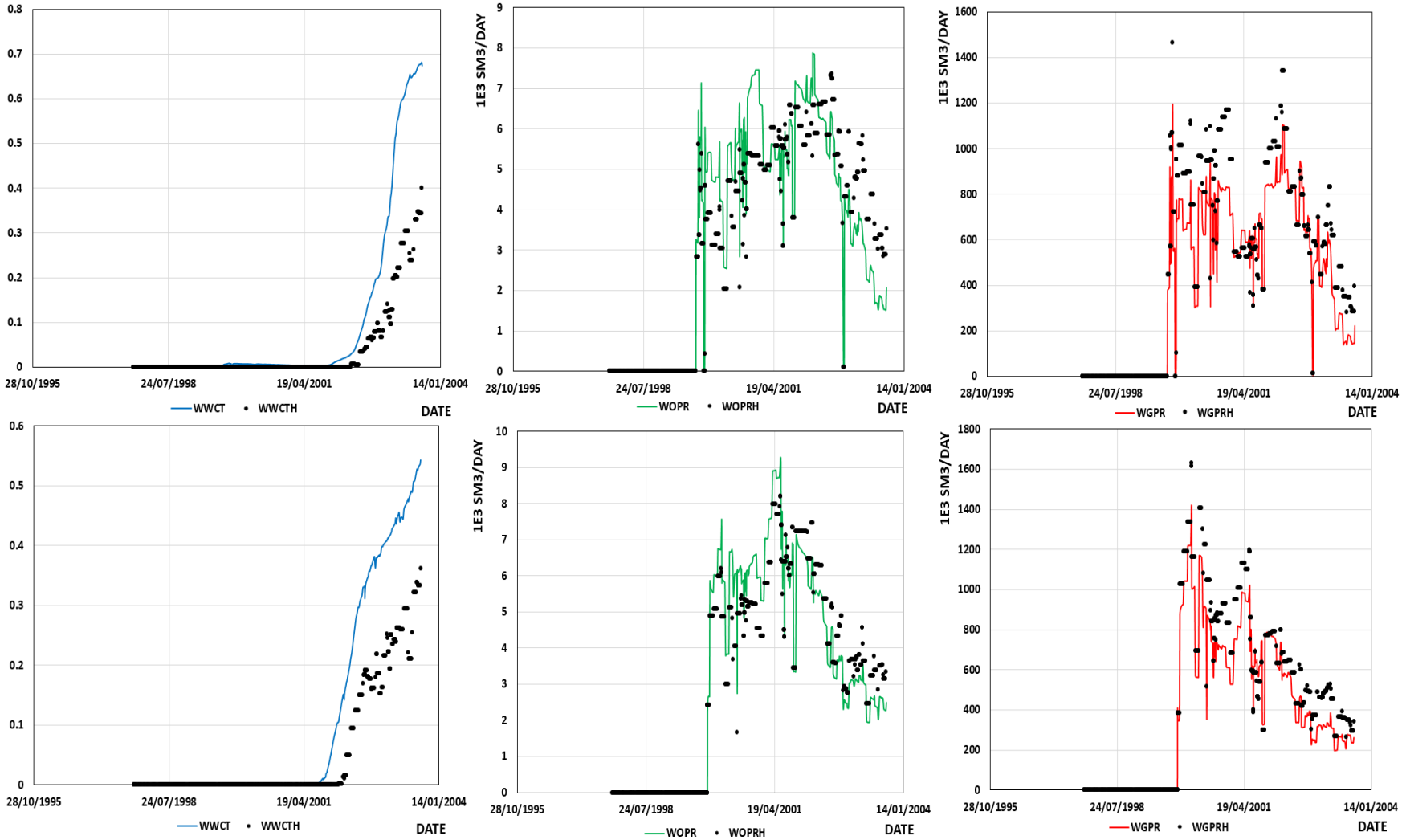

Figure 3-9 *Matching of WWCT (well water cut in total), WOPR (well oil production rate), and WGPR (well gas production rate) of producer E-1H (top) and E-2H (below).*

3.2.4.2 4D seismic data

A total of 5 seismic surveys have been carried out on the Norne Field, starting with the first conventional base survey in 1992. The next four surveys were undertaken with a Q-marine vessel in 2001, 2003, 2004 and 2006 (Statoil, 2006). Osdal et al., 2006 provided a detailed description of the seismic acquisition and processing of each survey. They analysed the movement of the OWC then mapped the water flooding pattern in this field, concluding that the value of 4D could be estimated at approximately USD $240 million in helping to optimise new drilling targets at Norne.

In terms of the repeatability of 4D data, in the main field area, an average NRMS of around 20% was measured for the 4D seismic in 2003-2001 and 2004-2003 (Osdal et al., 2006).

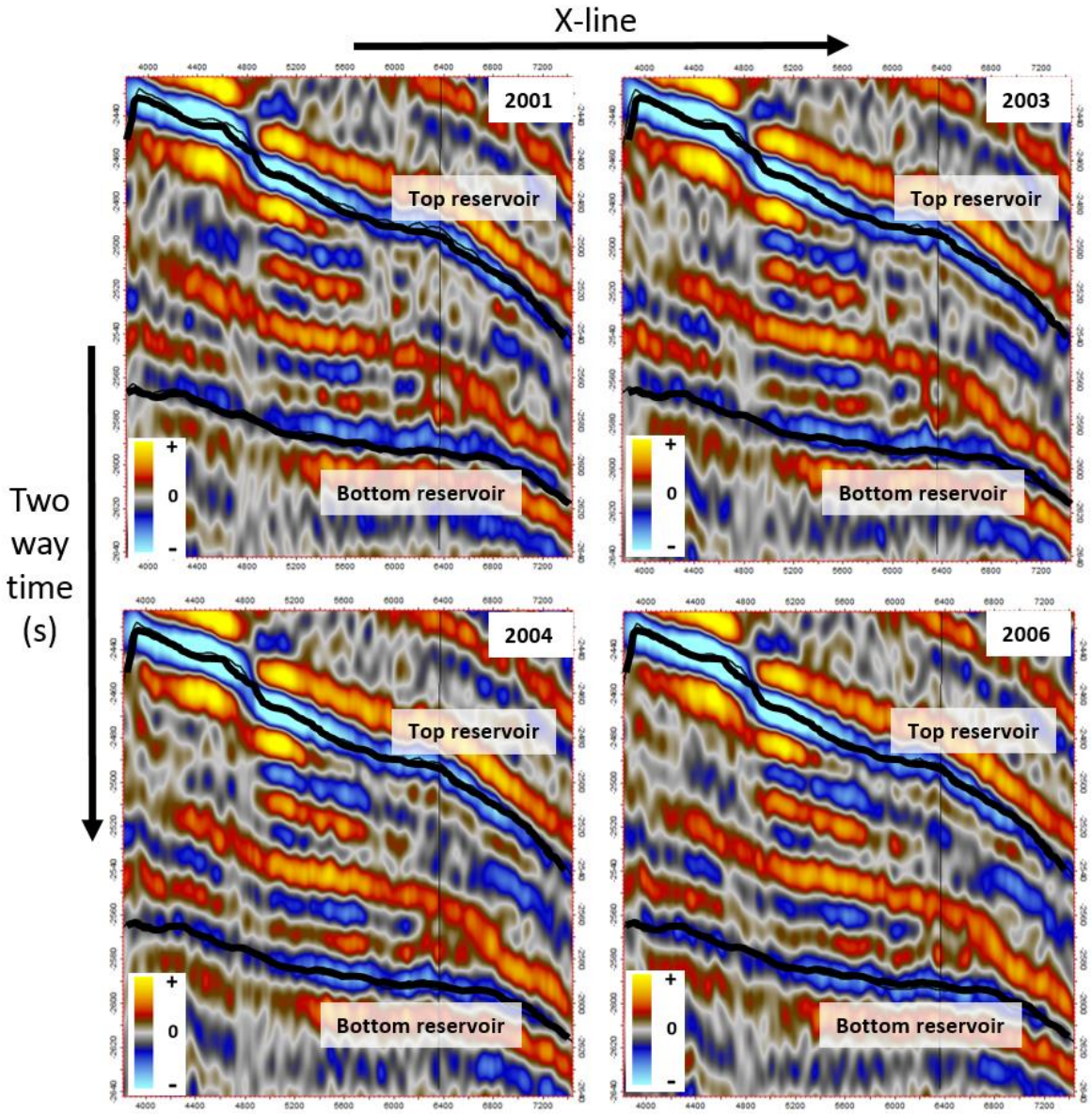

Figure 3-10 *Observed 3D seismic (amplitude) datasets in the years 2001, 2003, 2004 and 2006.*

According to the reservoir geology and the matching quality of the initial simulation model, segments D and E and formation Ile were selected to conduct a regional seismic history matching. For this purpose, survey 2001 was selected as baseline seismic and survey 2003 as the monitor. Survey 2004 would be used for prediction analysis in later chapters. With regard to the seismic attribute, I have selected the mean value of the 4D amplitude change (MA4D) as a representation of the 4D data. Using one 3D seismic survey (2003) and subtracting the former 3D survey (2001), then the arithmetic mean value is evaluated inside a window between top and bottom horizon of the Ile formation. The observed MA4D seismic map of the Ile formation (segment E and D) is plotted in Figure 3-11 (left).

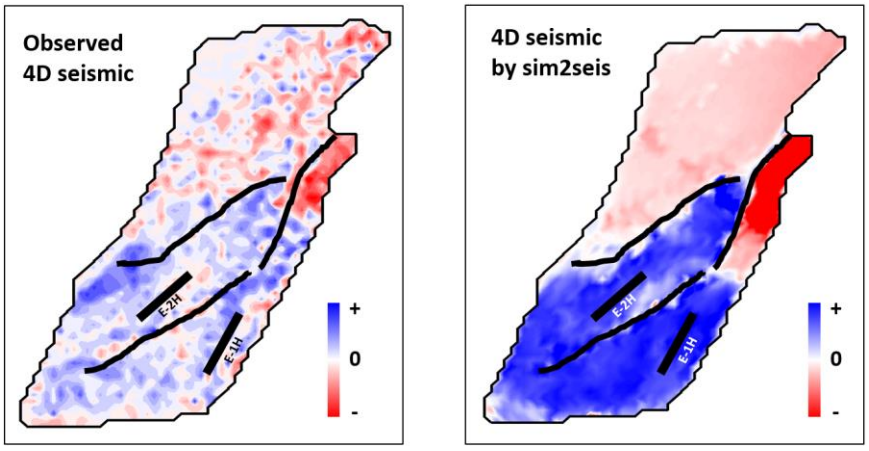

Figure 3-11 *4D seismic (MA4D) of segments E and D: observation (left) and simulation result (right) of sim2seis model.*

The synthetic seismic was modelled based on the sim2seis model (Figure 3-11, right). The two producers E-1H and E-2H were also plotted in both the observed and synthetic 4D seismic maps. As a general interpretation of the seismic map, the softening anomaly is mainly due to pressure depletion; the hardening signal denotes the saturation change (increased Sw and decreased Sg). By comparing the two maps, it can be seen that the hardening signal is stronger in the synthetic map than in the observed map. This indicates that probably the water supplement to the two producers was too fast, therefore the water saturation increment was over-predicted. It also needs to be pointed out that the scales of simulation and observation are different, so the comparison should be validated through quantitative analysis: SHM. The improvement of matching of synthetic and observed 4D seismic (2003-2001) will be the objective of the later SHM.

3.3 Proxy model

3.3.1 Derivation of the proxy model

Commonly, 4D seismic is created by differencing the monitor seismic survey from the baseline survey, in theory it can be through a 3D cube or 2D maps. Considering the relatively lower vertical resolution, it is more common to use mapped seismic attributes (Landa et al., 2015, Obidegwu et al. 2015, MacBeth et al. 2004), where the attribute has been evaluated with respect to a clear, stable and interpretable seismic horizon, such as the top of the producing reservoir that has been clearly identified in the seismic volume. For thin sheet-like reservoirs which are generally thinner than a fraction of a seismic wavelength, the top and bottom reservoir horizons can be used as the window to generalise seismic map (Obidegwu 2016); for thick reservoirs or ones containing major shale layers, multiple maps can be generated separately for each formation (Yin 2016).

In order to build the proxy model, I have limited this research to mapped 4D seismic, and the role of the proxy model is to calculate the time-lapse seismic maps from the depth-averaged pressure and saturation maps obtained from reservoir flow simulation.

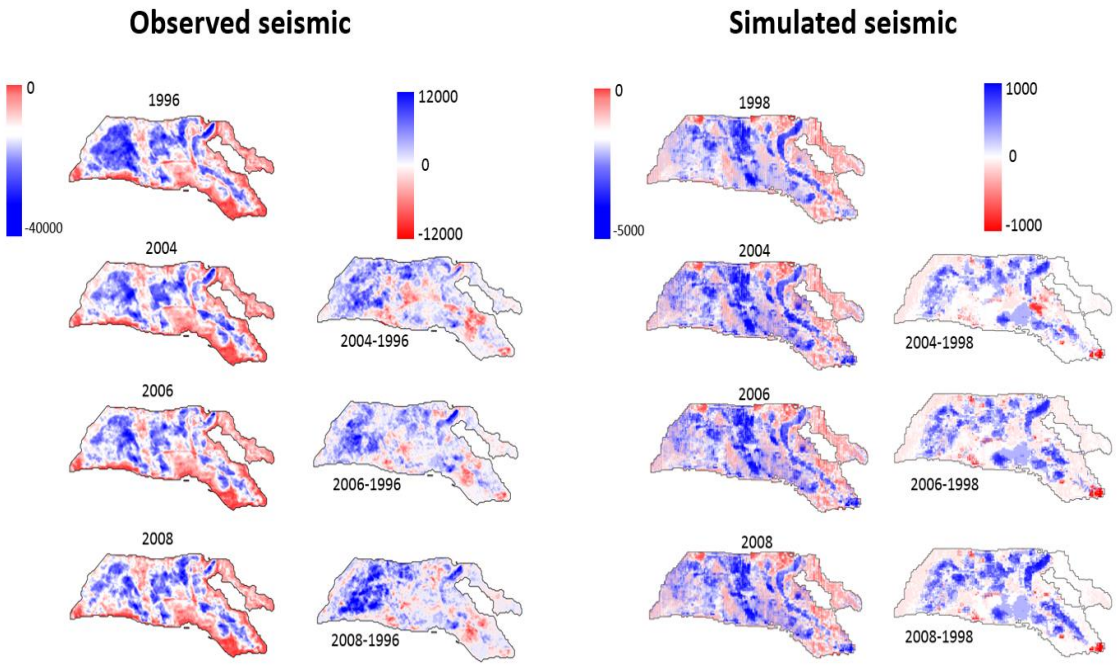

Figure 3-12 *Comparison between the observed mapped seismic amplitudes for multiple 3D seismic surveys (the first column); and the corresponding mapped 4D seismic responses (the second column); Comparison between the simulated mapped seismic amplitudes for multiple 3D seismic surveys (the third column); and the corresponding mapped 4D seismic responses (the last column).*

A previous study on such map based seismic was done on Schiehallion, a North Sea clastic field (MacBeth et al., 2016). Figure 3-12 (a) shows observed maps of the root mean square (RMS) amplitude of the top reservoir event for Schiehallion, Figure 3-12 (b) shows an identical sequence of maps, but all are derived from sim2seis using a well-log calibrated petro-elastic model (see Amini et al., 2011 for details of the modelling). Both the observed and synthetic data indicates that baseline and monitor images look visually similar. This is because the baseline map reflects the geological imprint of the reservoir's depositional architecture, together with the initial fluid saturations and pressure. The monitors represent the same geology but with the fluid saturation and pressure changed due to well production and injection (MacBeth et al., 2016). These saturation and pressure signals only modify the seismic amplitudes in the regions bounded by the reservoir and, thus, the regions defined by the initial amplitude distribution (a similar concept is described by Stephen et al. 2009).

Analysis of the above modelling and data suggests that the time-lapse seismic map $\Delta A(x, y)$ can be constructed as the product

$$\Delta A(x, y) = f(\Delta R, G) * A_0(x, y) \tag{3.2}$$

where $A_0(x, y)$ represents the seismic response (any particular seismic attribute such as impedance, RMS amplitude, instantaneous frequency, time-shift) at the pre-production baseline time and $\Delta R(x, y)$ represents the effect of subsequent fluid saturation and pressure changes in the reservoir. f is a function of the production-related changes and the geology, G, which depends on the petro-elastic and seismic modelling. By involving the baseline map $A_0(x, y)$ in the 4D seismic (ΔA) calculation, I account for variations of the static reservoir properties such as thickness, porosity and net-to-gross. Although the 'proxy' relationship in Equation 3.2 is empirical in origin, the utility of the dynamic part of this equation has been established in past inversion studies (for example, Alvarez and MacBeth 2014).

In this case, as I am dealing with relatively small changes, one obvious form for $f(\Delta R, G)$ can be obtained by a linear polynomial (Falahat et al. 2013)

$$f(\Delta R, G) = (c_1 \cdot \Delta P + c_2 \cdot \Delta S_w + c_3 \cdot \Delta S_g) \tag{3.3}$$

The relationship in Equation 3.3 amplifies or diminishes the baseline seismic response according to the depth-averaged pressure ΔP and water and gas saturation changes

$(\Delta S_w, \Delta S_g)$ obtained from the fluid flow simulator. The coefficients c_i with $i = 1{:}3$ are derivatives of the seismic attribute with respect to the individual pressure and saturation changes. The coefficients are functions of the reservoir geology, rock properties and fluid properties (Alvarez and MacBeth, 2014). As the main reservoir variability is supplied by the baseline amplitude, the weighting coefficients c_i can be assumed as fixed across the reservoir (Falahat et al. 2013).

This equation is valid in practice, provided the seismic survey configurations are reasonably repeatable (Fursov, 2015), and it should be noted that in the literature some debate has arisen as to whether the polynomial in (2) should be expanded as a quadratic (MacBeth et al. 2006). Arguments in favour of quadratic terms for pressure and saturation change have been put forward by Meadows (2001) and Cole (2002). At a practical level, the linear version of this proxy is found to be useful for the purposes of directly inverting to pressure and saturation changes (Landrø 2001, Falahat et al. 2013; Floricich et al. 2006, MacBeth et al., 2006). In this study I will apply the linear version; the validation of this linearity assumption and test of the accuracy and robustness of this proxy for history matching purposes will be described in the following sections.

3.3.2 Linearity assumptions and validation

The base case simulation model and sim2seis were utilised to validate the two linearity assumptions mentioned above. The flow simulation was run first, after which the pressure, water and gas saturation changes in the Ile formation during 2001-2003 were represented as pore volume weighted 2D maps (Figure 3-13), as recommended by Falahat (2013).

Two steps were then taken to validate the assumptions:

1) The first assumption behind Equation 3.3 is that the modelled seismic response might be decomposed linearly into effects of pressure (P) and saturation (Sw, Sg) changes. Although it is a data-driven approach as compared to a modelling (physical description of processes) type of approach, it has been proven in the literature (Falahat et al., 2013, Fursov, 2015) to be successful on synthetic or real field data. However, considering the complexity of the seismic attributes and reservoir geometry, the linear proxy (Equation 3.3) would have a different performance based on specific cases. In order to qualitatively validate this linear assumption, I decomposed the 4D seismic signature linearly, as follows:

$$\Delta A\left(\Delta P, \Delta S_w, \Delta S_g\right) \approx \Delta A(\Delta P, 0,0) + \Delta A(0, \Delta S_w, 0) + \Delta A\left(0,0, \Delta S_g\right) \quad (3.4)$$

where ΔA represents the simulated seismic change from sim2seis, which is a function of $\Delta P, \Delta S_w$ and ΔS_g (changes in pressure, water saturation and gas saturation, as shown in Figure 3-13, top left three figures). On the right side of the equation, the respective impacts of pressure and saturation on the seismic change are simulated individually through sim2seis process, then the three terms ('individual 4D seismic', Figure 3-13, bottom left three figures) are linearly added as a 'mixed 4D seismic'(Figure 3-13, bottom right). On the left side is the simulated 4D seismic ('full 4D seismic', Figure 3-13, top right) which considers all the contributions of pressure and saturation changes. Subsequently, the 'mixed 4D seismic' (right side of the equation) and the 'full 4D seismic' (left of the equation) are cross-plotted in Figure 3-13 and a correlation coefficient r is evaluated to quantify the approximation.

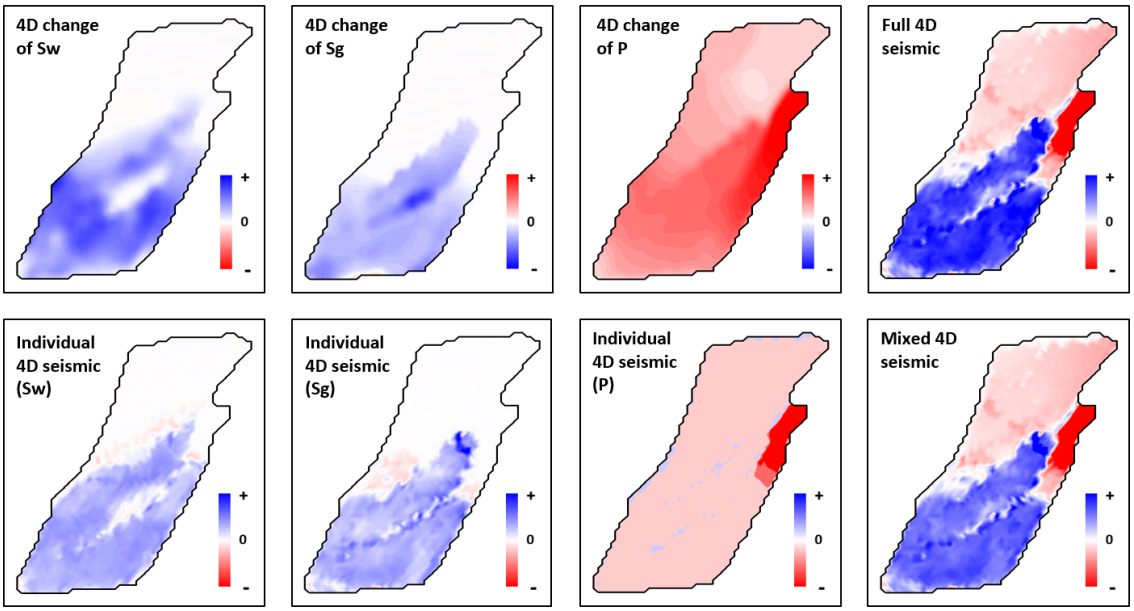

Figure 3-13 *Comparison between the observed mapped seismic amplitudes for multiple 3D seismic surveys (the first column); and the corresponding mapped 4D seismic responses (the second column); Comparison between the simulated mapped seismic amplitudes for multiple 3D seismic surveys (the third column); and the corresponding mapped 4D seismic responses (the last column).*

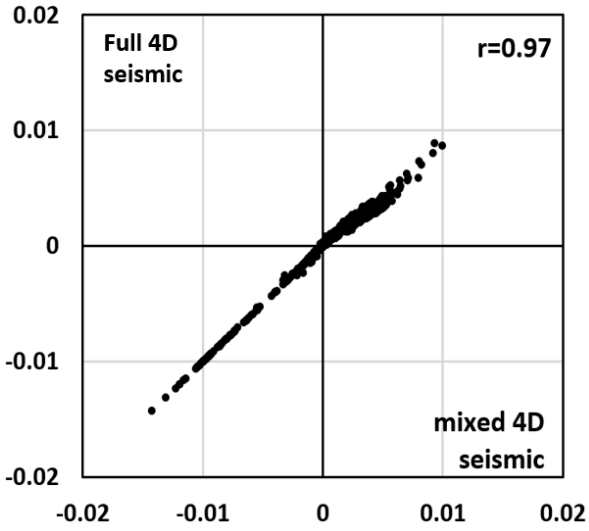

Figure 3-14 *Cross-plot of mixed 4D seismic and full 4D seismic.*

According to Figure 3-13 and 3.14, the linear superposition of the individual 4D seismic responses (mixed 4D seismic) is very close to the real simulated 4D seismic, a value 0.97 of *r* also indicates significant correlation. Based on this cross-plot (Figure 3-14), it can be concluded that the assumption of linearity in superposition of pressure and saturation effects to approximate the simulated 4D seismic is validated.

2) As mentioned in last section, a linear polynomial is also applied to model the individual effects of ΔP, ΔS_w, and ΔS_g (see equation below). Therefore, apart from the linear superposition assumption (Equation 3.4), the equation defined below is the second linear assumption which needs to be validated.

$$\begin{cases} \Delta A(\Delta P, 0,0) = c_1 \cdot \Delta P \\ \Delta A(\Delta S_w, 0,0) = c_2 \cdot \Delta Sw \\ \Delta A\left(\Delta S_g, 0,0\right) = c_3 \cdot \Delta S_g \end{cases} \tag{3.5}$$

As with the validation method utilised previously, I firstly plotted the paired maps of seismic with pressure or saturation changes ($\Delta A(\Delta S_w, 0,0) \sim \Delta S_w$, $\Delta A\left(\Delta S_g, 0,0\right) \sim \Delta S_g$ and $\Delta A(\Delta P, 0,0) \sim \Delta P$), as shown in Figure 3-15. Equation set 3.5 is an overdetermined problem, and coefficients c_1, c_2 and c_3 were then calculated for each cell of the map, afterwards the distributions of the coefficients are shown below each paired maps (Figure 3-15). It is found that the values of c_1, c_2 and c_3 show significant unimodal distribution, which means for each of the coefficients, a single value could be selected to stand for the whole distribution. Accordingly, the linear equation to model the effect of individual pressure or saturation change on seismic change (Equation 3.5) can be validated.

In this section, the linearity assumption of this superposition model has been validated by two steps. Firstly, the 4D seismic change was linearly decomposed into effects of pressure, water saturation and gas saturation. Secondly, the individual 4D seismic modelled through sim2seis was approximated as a product of the pressure or saturation change and a single coefficient. After this validation, a case study of how the proxy model is developed on Norne field will be shown in next part.

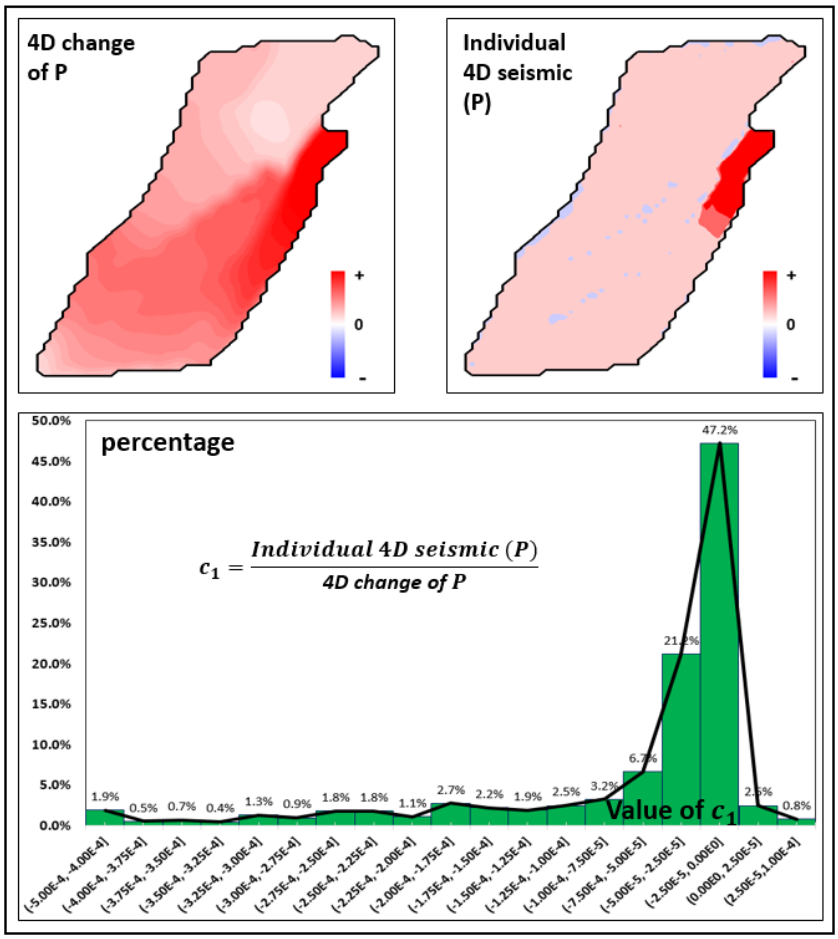
4D change of P
Individual 4D seismic (P)
+
0
-
percentage
$c_1 = \frac{Individual\ 4D\ seismic\ (P)}{4D\ change\ of\ P}$
Value of c_1
50.0%
45.0%
40.0%
35.0%
30.0%
25.0%
20.0%
15.0%
10.0%
5.0%
0.0%
47.2%
21.2%
6.7%
3.2%
2.5%
2.7%
2.2%
1.9%
2.5%
1.9%
1.1%
1.8%
1.8%
0.9%
1.3%
0.4%
0.7%
0.5%
1.9%
0.8%
(-5.00E-4, -4.00E-4]
(-4.00E-4, -3.75E-4]
(-3.75E-4, -3.50E-4]
(-3.50E-4, -3.25E-4]
(-3.25E-4, -3.00E-4]
(-3.00E-4, -2.75E-4]
(-2.75E-4, -2.50E-4]
(-2.50E-4, -2.25E-4]
(-2.25E-4, -2.00E-4]
(-2.00E-4, -1.75E-4]
(-1.75E-4, -1.50E-4]
(-1.50E-4, -1.25E-4]
(-1.25E-4, -1.00E-4]
(-1.00E-4, -7.50E-5]
(-7.50E-4, -5.00E-5]
(-5.00E-5, -2.50E-5]
(-2.50E-5, 0.00E0]
(0.00E0, 2.50E-5]
(2.50E-5,1.00E-4]

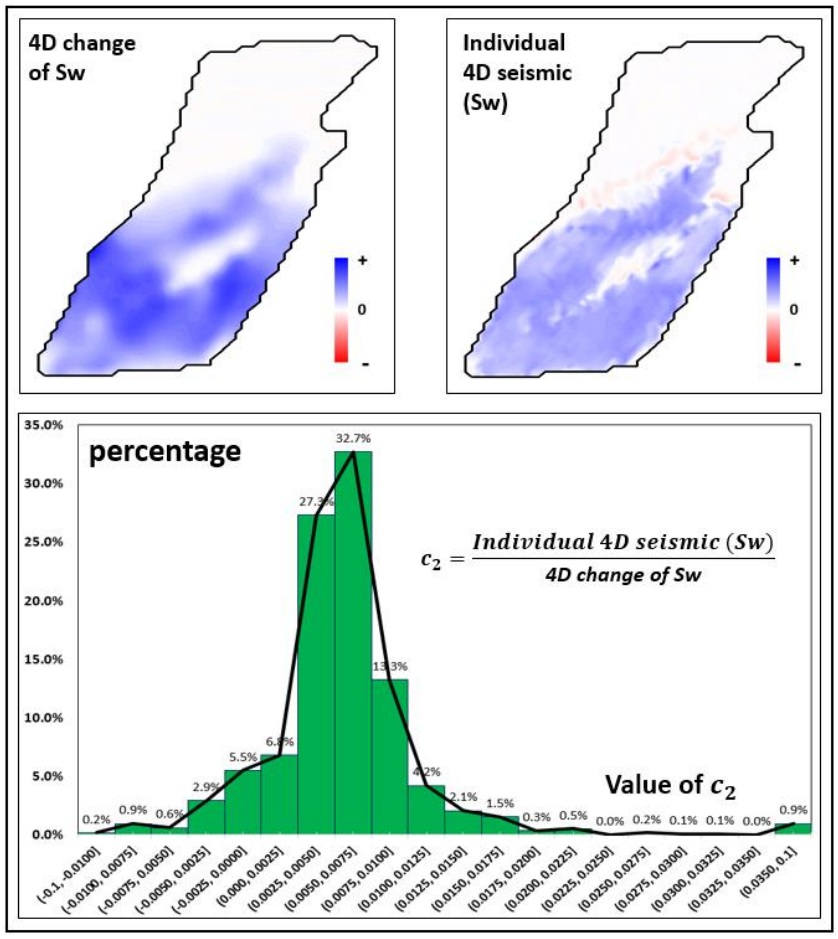
4D change of Sw
Individual 4D seismic (Sw)
+
0
-
percentage
$c_2 = \frac{Individual\ 4D\ seismic\ (Sw)}{4D\ change\ of\ Sw}$
Value of c_2
35.0%
30.0%
25.0%
20.0%
15.0%
10.0%
5.0%
0.0%
32.7%
27.3%
13.3%
6.8%
5.5%
4.2%
2.9%
2.1%
1.5%
0.9%
0.6%
0.9%
0.2%
0.3%
0.5%
0.0%
0.2%
0.1%
0.1%
0.0%
0.9%
(-0.1, -0.0100]
(-0.0100, 0.0075]
(-0.0075, 0.0050]
(-0.0050, 0.0025]
(-0.0025, 0.0000]
(0.000, 0.0025]
(0.0025, 0.0050]
(0.0050, 0.0075]
(0.0075, 0.0100]
(0.0100, 0.0125]
(0.0125, 0.0150]
(0.0150, 0.0175]
(0.0175, 0.0200]
(0.0200, 0.0225]
(0.0225, 0.0250]
(0.0250, 0.0275]
(0.0275, 0.0300]
(0.0300, 0.0325]
(0.0325, 0.0350]
(0.0350, 0.1]

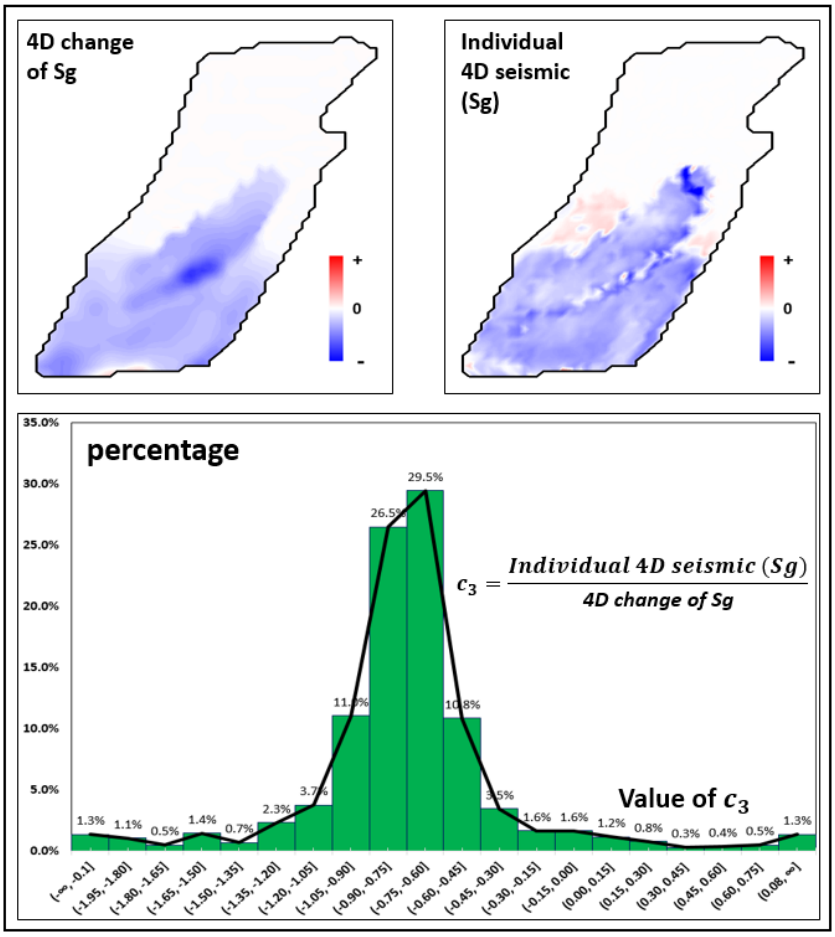

Figure 3-15 *From top left to right: paired 4D change maps of dynamic properties (Sw, Sg and P) and correlated individually simulated seismic (by sim2seis); below: distribution of the quotients (c1, c2 and c3) of individual 4D seismic and related dynamic properties (P, Sw and Sg).*

3.3.3 Building the proxy model

As introduced in section 3.2.3, a 3D simulation model and sim2seis model are available before building the proxy. Based on those models, the 4D map of dynamic properties (ΔP, ΔS_w, ΔS_g), 4D synthetic seismic and baseline seismic map are firstly produced. Then the 2D maps (matrix of data points) are reconstructed into vectors, and a least-square linear regression (Chatterjee et al. 1986) is conducted on the vectors to determine the coefficients in this proxy equation:

$$\Delta A(\Delta P, \Delta S_w, \Delta S_g) = (c_1 \cdot \Delta P + c_2 \cdot \Delta S_w + c_3 \cdot \Delta S_g) \cdot A_0 \quad (3.6)$$

where A_0 denotes the baseline seismic which contains the geology imprint from the static reservoir properties such as reservoir thickness (h), porosity (∅), and net to gross (NTG). Falahat et al. (2013) gave an equation to determine A_0 for a thin turbidite reservoir:

$$A_0 = h \cdot \emptyset \cdot NTG \quad (3.7)$$

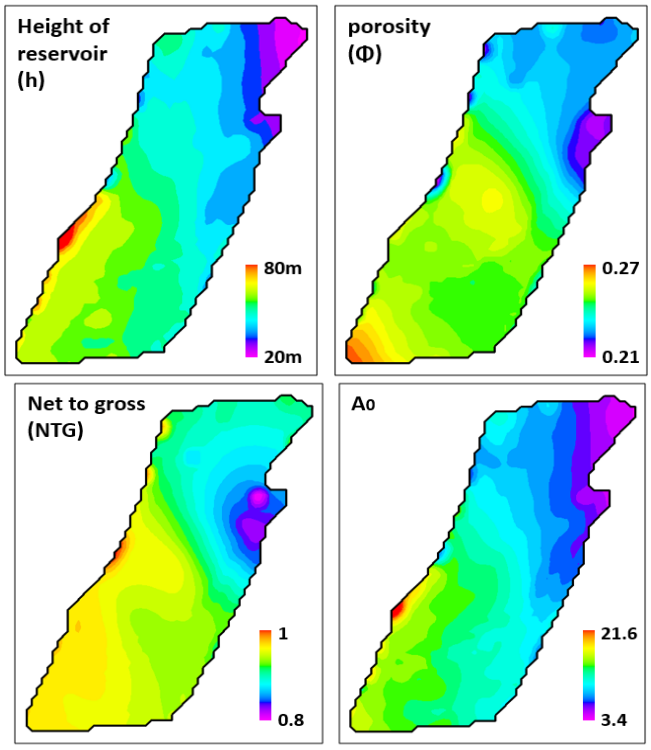

Figure 3-16 *Maps of h, ∅, NTG and A_0 from the initial simulation model.*

The above maps (Figure 3-16) are generated from the initial flow simulation model. As in the traditional history matching workflow, such static properties were not selected as the perturbing parameter, therefore the scaling item A_0 remains constant during the history matching. After running a least-square linear regression (Chatterjee et al. 1986), the coefficients were calculated and then used (shown in Table 3-5):

Table 3-5 *Value of three coefficients: results of linear regression.*

c_1	c_2	c_3
-6.3228 E-4	3.9756 E-2	-6.0869 E-2

After this step, I cross plot the 4D seismic maps generated by sim2seis and the proxy model in Figure 3-17.

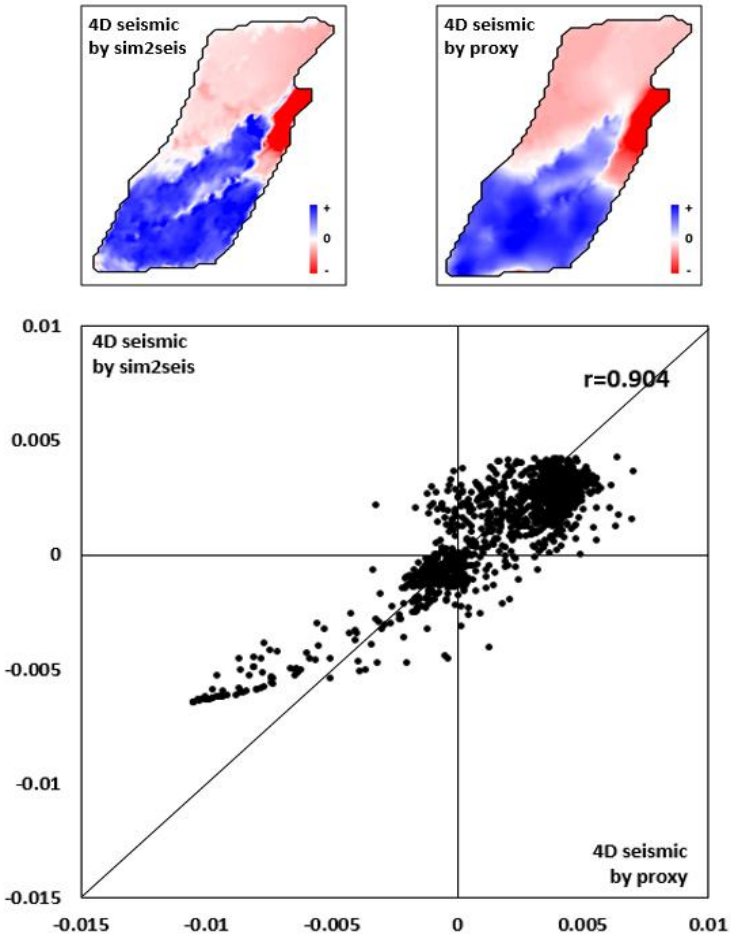

Figure 3-17 *Upper: sim2seis- and proxy-seismic maps based on the base case simulation model; lower: cross plot of the two maps with correlation coefficient r=0.904*

As expected, sim2seis shows more detail as compared to the proxy, however the main features can be very well reproduced with the proxy (see top two maps in Figure 3-17). The correlation coefficient, r, was measured to be 0.904, indicating an obvious correlation between proxy 4D seismic and sim2seis 4D seismic. As mentioned above, the scaling item A_0 is a constant during the history matching; one could ask if a dynamic update of the coefficients could lead to a better history matched model. In other words, is a 'fixed' proxy model enough for history matching purposes? In section 3.5.2 a fixed proxy will be applied to conduct SHM, and in section 3.7 both a fixed and an adaptive proxy will be tested to explore this question.

3.4 Proxy quality

3.4.1 Metrics to quantify the proxy quality

The function of a proxy model is to replace the initial time consuming model or system, therefore the inputs-outputs of the proxy should correlate to this relationship of the initial model or system. As mentioned in chapter 2, after being trained on a training dataset, the proxy model's quality can be quantified through a blind test, in which a new dataset is used to test the correlation between the results of the proxy model and the initial model.

In this study the blind test (Figure 3-18) is set up as follows: firstly, there is an initial simulation model which is not well matched with the observation data, this model is used as the reference model. A number of n simulations with randomly assigned input values are then launched by the sim2seis and proxy model independently. Finally the mismatch of each scenario with the reference case is then evaluated for both methods (sim2seis and proxy) and represented as two mismatch vectors. Generally, the correlation of these two vectors can be quantified by Pearson correlation coefficient r:

$$r = \frac{\sum_{i=1}^{n}(x_i-\bar{x})(y_i-\bar{y})}{\sqrt{\sum_{i=1}^{n}(x_i-\bar{x})^2}\sqrt{\sum_{i=1}^{n}(y_i-\bar{y})^2}} \tag{3.8}$$

x_i, y_i are the mismatched values of the i^{th} model evaluated by the sim2seis and proxy model. The arithmetic mean $\bar{x} = \frac{1}{n}\sum_{i=1}^{n} x_i$ and $\bar{y} = \frac{1}{n}\sum_{i=1}^{n} y_i$.

I also apply Spearman's rank correlation coefficient, ρ, to quantify the quality of proxy model (Daniel, 1978).

$$\rho = 1 - \frac{6\sum_{i=1}^{n}(p_i-q_i)^2}{n(n^2-1)} \tag{3.9}$$

where p_i and q_i are the rankings of the true mismatch values x_i and y_i. The benefit of introducing this metric is that ρ can demonstrate the monotonic relationship between two datasets. Considering the purpose of history matching is to find out the best simulation(s) from the rank of all candidate models (He et al. 2016); this metric brings useful quantitative information about the quality of the proxy and will also be applied.

Intuitively, a higher r or ρ indicates higher similarity between sim2seis and the proxy model, therefore either can be used to quantify the quality of the proxy model. Statistically, a value of r or ρ above 0.7 indicates a significant correlation between two

variables; this threshold will be used to test the quality of the proxy model in later sections. (Freedman, 2009).

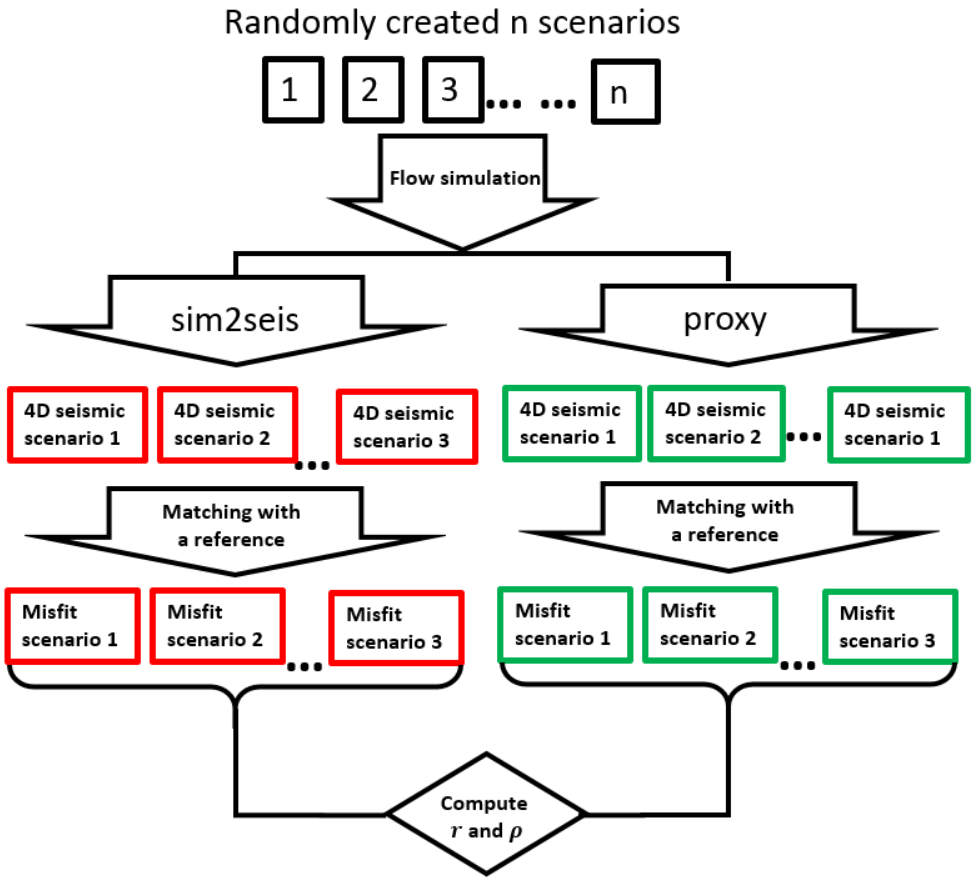

Figure 3-18 *The whole workflow of the blind test: a number of n simulation models with different input values are randomly created; based on the results of fluid flow simulation, the sim2seis and proxy model are applied independently to produce the 4D seismic outputs.*

3.4.2 Blind test

In order to quantify the proxy quality, I set up a quasi-history matching procedure as a blind test to calculate the correlation coefficient r and ranking correlation coefficient ρ. As illustrated in Figure 3-18, 30 scenarios were created by applying Latin Hypercube Sampling (Iman, 2008) method at the beginning of the test (more details about the selection of uncertain parameters and their value ranges will be given in chapter 6).

In Figure 3-18, the variance shown in the 4D seismic maps is a result of the variance of the S_w, S_g and P maps, which are effected by the input parameters. The purpose of this plot is to check whether the randomly created 30 scenarios are 'different enough' from each other. According to the variance shown in 4D seismic maps, it could be qualitatively assumed that the 30 scenarios are indeed 'different enough' from each other.

Firstly, a reference simulation model was launched to obtain dynamic outputs such as $\Delta S_w, \Delta S_g$ and ΔP. Based on these, seismic data $(\Delta A, A_0)$ were then modelled by sim2seis and used later as synthetic history data for quasi-history matching. With the data $(\Delta S_w, \Delta S_g, \Delta P, \Delta A, A_0)$, a linear regression of Equation 3.3 lead to the first set of coefficients from which the proxy model can be created.

$$misfit = \frac{\sum(sim_i - ref_i)^2}{\sum(ref_i)^2} \times 100\% \tag{3.10}$$

A misfit function (Equation 3.10) was defined to evaluate the distance between each of the 30 scenarios and the reference model. sim_i stands for the i^{th} cell of simulated (by sim2seis or proxy) seismic map of each scenario (plotted in Figure 3-20), and ref_i is the seismic value at the corresponding cell in the reference model. In this procedure, *misfit* of all 30 scenarios were evaluated by sim2seis and proxy model independently, then the data sequences misfit_sim2seis and misfit_proxy were cross-plotted, as shown in Figure 3-19.

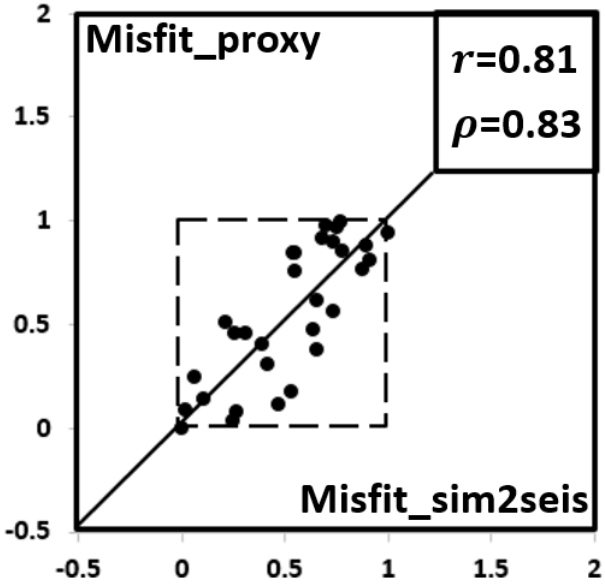

Figure 3-19 *Cross-plot of misfit_sim2seis and misfit_proxy: sim2seis and proxy model were used to produce the seismic data then evaluated by Equation 3.10.*

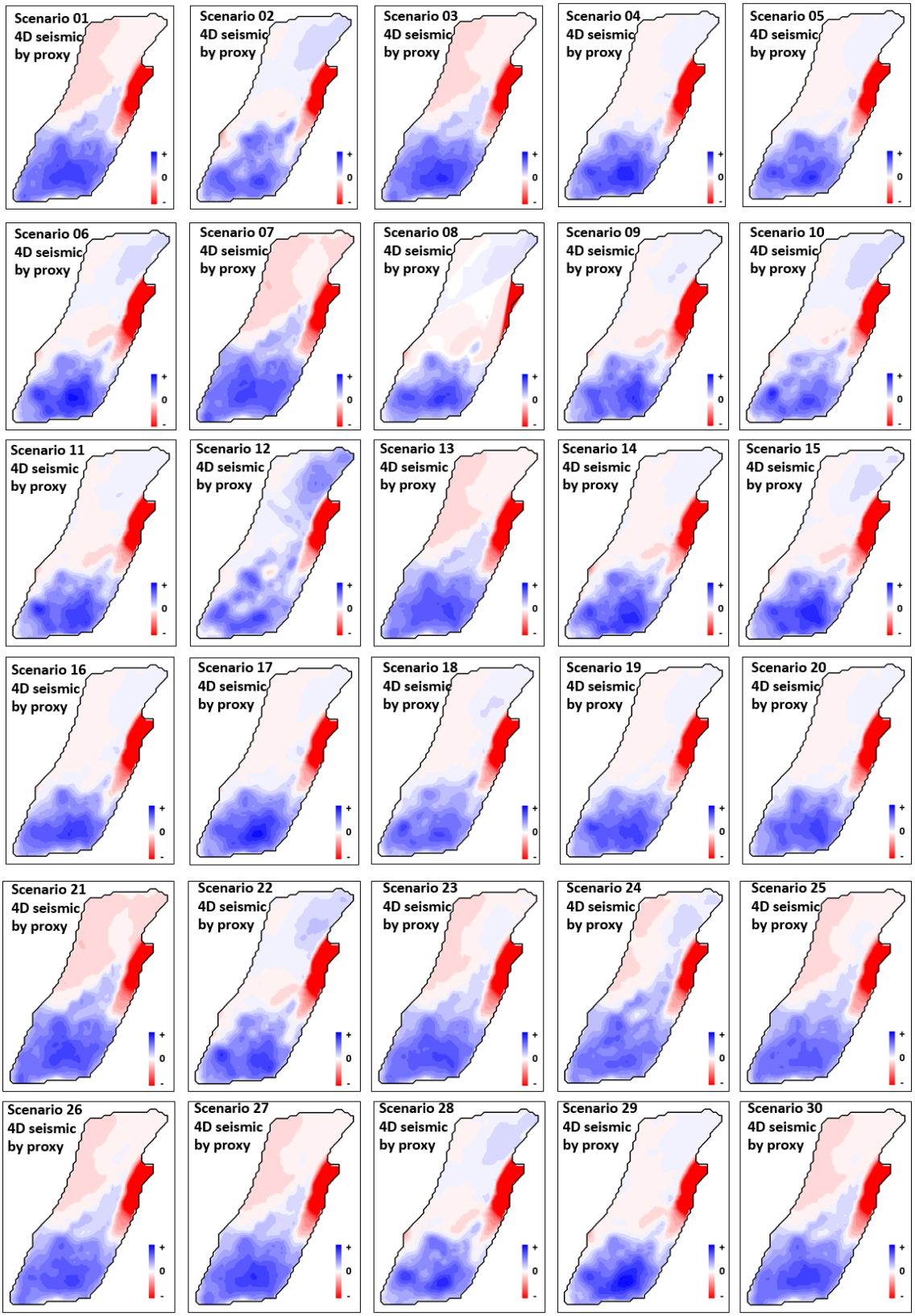

Figure 3-20 *Simulated 4D seismic by proxy model over all of 30 scenarios.*

3.5 Proxy robustness analysis

3.5.1 Seismic attribute

In this part, I intend to test the robustness of the proxy model in terms of seismic attribute, to analyse if a different seismic attribute was selected on Norne, whether it would affect the performance of the proxy model. When the proxy model was built in section 3.3.3, a mean value of 4D amplitude change (MA4D) was selected as the seismic attribute. However, this is not a general choice in any case. For each individual field, which attribute should be selected to generate the map and be used for interpretation purpose is always a question. This will have effect on the proxy building as well. Here I selected another commonly used attribute, 4D root mean square map (4DRMS), to set up a control experiment to analyse the robustness of the linear superposition proxy model.

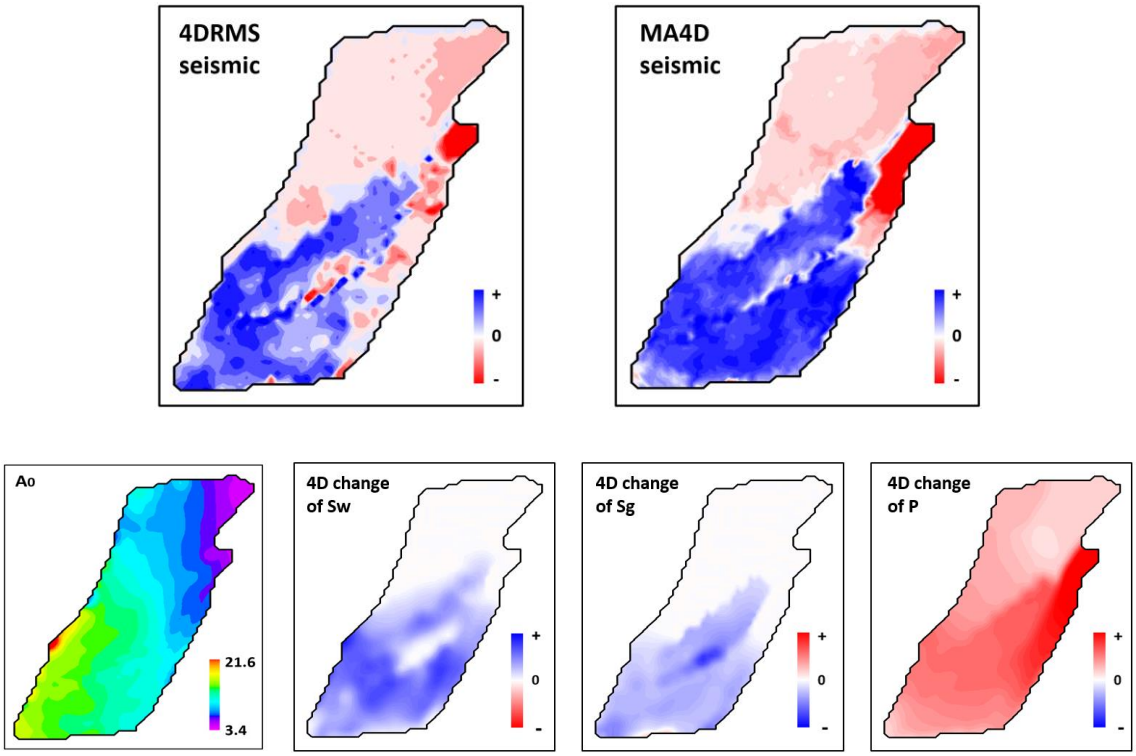

Figure 3-21 *Upper left: 4D Root Mean Square (4DRMS) seismic map; upper right: 4D amplitude change (MA4D) seismic map; lower: static A_0 and dynamic properties (pore volume weighted averaging) maps based on the initial simulation model.*

Figure 3-21 shows the MA4D and 4DRMS maps and the pressure and saturation changes of the same reservoir (Ile formation). Following the same method introduced in section 3.3.3, a least-square linear regression was conducted to obtain the coefficients of the proxy model. Based on this set of coefficients (Table 3-5), the proxy seismic map was generated (Figure 3-22, top left) and cross-plotted with the 4DRMS map (Figure 3-22, below). According to the value of the correlation coefficient, 0.667, a conclusion is drawn

than this proxy is less effective than the proxy for MA4D (r=0.904), that is, the attribute MA4D is a better selection in this case. More widely, the seismic attribute would have effect on the performance of the proxy model on different fields based on its unique feature, therefore a geophysical analysis should be done prior to the proxy building.

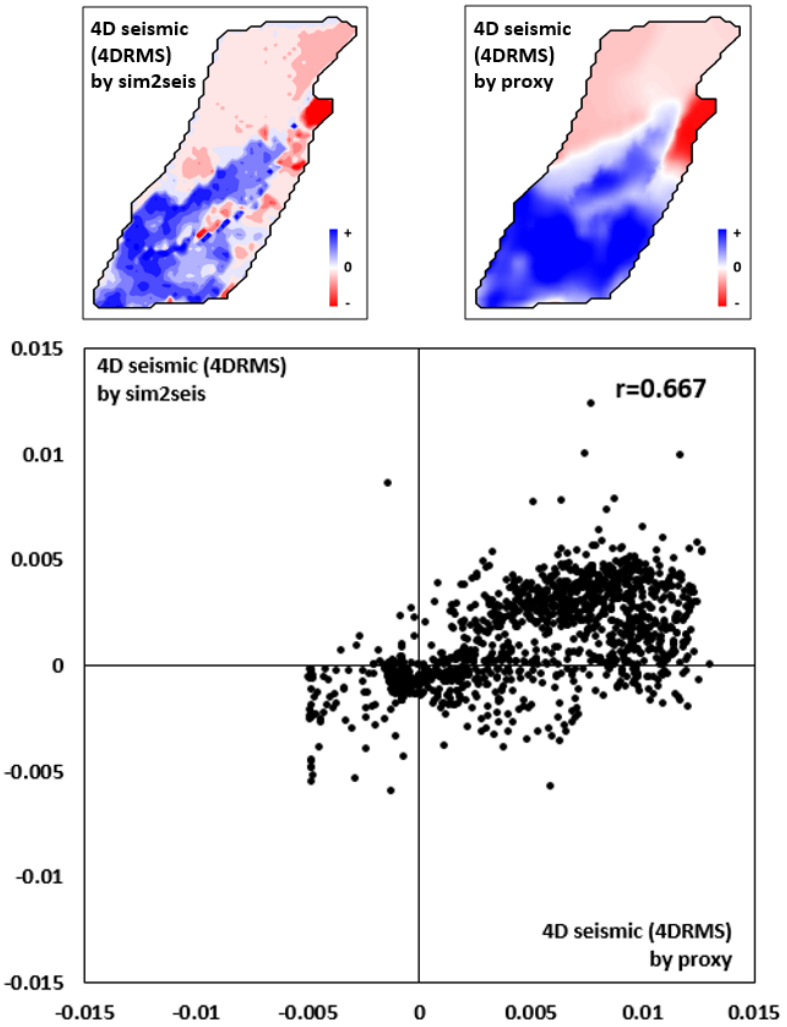

Figure 3-22 *Upper: sim2seis- and proxy-seismic maps based on the initial simulation model; lower: cross plot of the two maps with correlation coefficient r=0.667.*

3.5.2 Adaptive versus fixed proxy

On the basis of the derivation of the proxy model (section 3.3.1), the three coefficients indicate the effect of ΔP, ΔSw, and ΔSg on 4D seismic. Their values are determined by a linear regression. Because they are data-driven coefficients, so the value of different models should vary with different training data. One may argue that in order to be a better approximation of the simulator, the coefficients need to be updated for each simulation model (this is named as 'adaptive proxy'). In contrast, if the coefficients are kept same for different simulation models, this is a 'fixed proxy'.

In the SHM workflow, a fixed proxy has to be applied, because, if the coefficients need to be updated for each model, then the sim2seis needs to be run for each model, making the proxy-driven SHM even heavier than the conventional loop. However, before accepting the fixed proxy, a comparison needs to be made between the adaptive and fixed proxy model. In section 3.4.2, in which a blind test was conducted to quantify the proxy quality, 30 simulation models were generated randomly. Based on this group of models, I calculated the coefficients for each and quantified their variability to test the robustness of the proxy model. The values of c1, c2 and c3 are plotted in Figure 3-23.

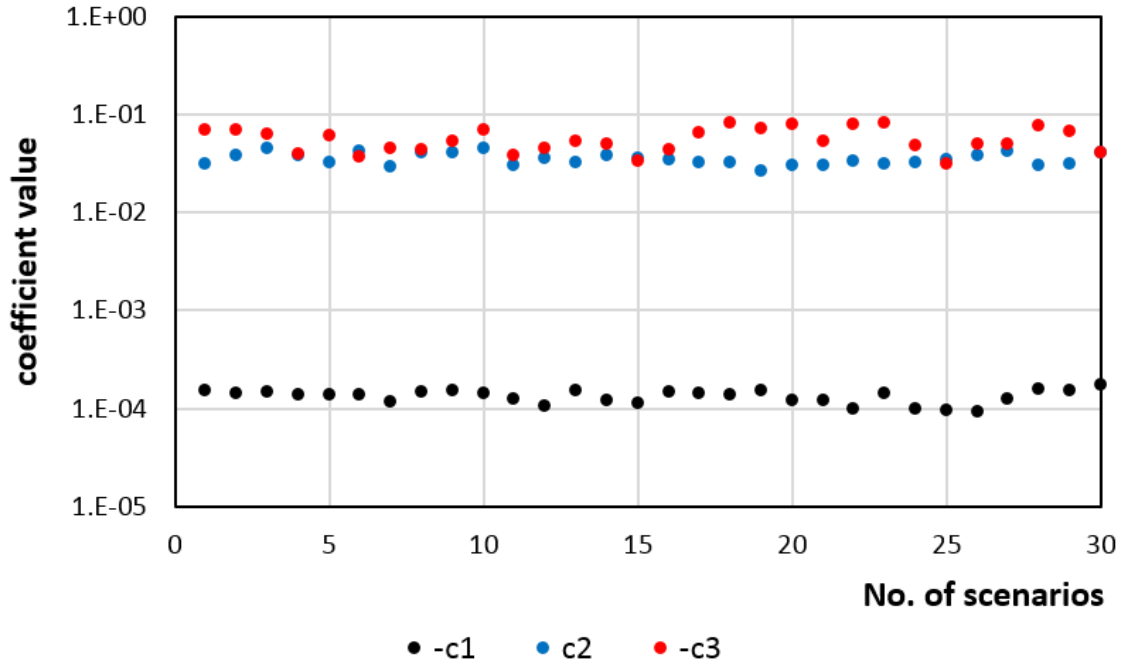

Figure 3-23 *Value of coefficients $-c_1, c_2$ and $-c_3$ over all 30 scenarios.*

The coefficients of variation ($\mathrm{CV} = \frac{\text{standard deviation}}{|mean|} \cdot 100\%$) of the coefficients are calculated to be 15.5%, 14.4% and 27.6%, which are considered as 'low-variance' (Freitag et al. 2007). Furthermore, still based on the same 30 simulation scenarios, a sim2seis model, a fixed proxy and an adaptive proxy were independently applied to evaluate the misfit values. The results were then normalized to [0, 1] and plotted in Figure 3-24.

The metrics r and ρ were measured as (r=0.81, ρ=0.83) for the fixed proxy, and (r=0.92, ρ=0.87) for the adaptive proxy respectively. They were all above 0.7, indicating that the results of both adaptive and fixed proxy were significantly correlated with the sim2seis result. Although the adaptive proxy has higher values, the fixed proxy is sufficient in this case. This helps to confirm that the proxy coefficients do not have to be updated for each simulation model so the fixed proxy can be utilised in the SHM, thus the fixed proxy is a robust approximation of the sim2seis model in further history matching workflow.

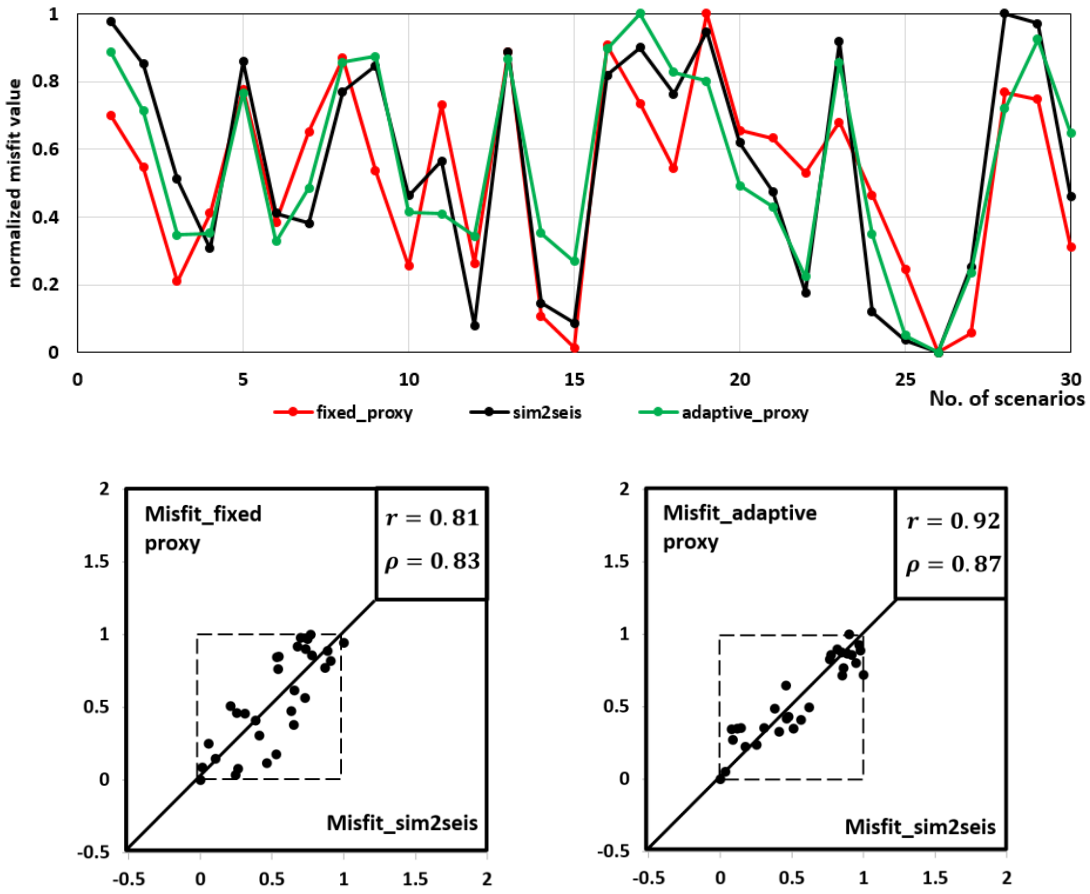

Figure 3-24 *Upper: normalized objective function evaluated by sim2seis, adaptive proxy and fixed proxy model over the 30 scenarios. It is observed that both green line (by adaptive proxy) and red line (by static proxy) are close to the black line (by sim2seis). Lower: cross plot of sim2seis versus fixed proxy (left) and adaptive proxy (right).*

3.6 Summary

In this chapter I have developed a proxy model to simplify the seismic modelling and to offer a more direct way of communication between reservoir engineers and geophysicists. This method relies on a data-driven relationship between the 4D seismic data and the reservoir dynamic properties. It has been studied in three ways from different perspectives: firstly I validated the linearity assumption, then I performed a blind test to quantify the proxy quality and finally I analysed the robustness of this proxy. All of these studies were conducted on a Norwegian Sea field. The following results, conclusions and further recommendations can be drawn from this study:

1. The proxy model has three coefficients (Equation 3.3), indicating the effects of pressure and saturation changes on 4D seismic, respectively. Such a concise and clear 'engineering' representation, is a real strength, as it makes the multi-disciplinary SHM task easier by offering a convenient interface between geophysics and reservoir engineering.
2. The linear relationship assumption between the 4D seismic map and 4D pressure and saturation maps has been confirmed, and the results of the blind test indicate the possibility of utilising a fixed proxy to evaluate the objective function.
3. The robustness of the proxy model has been analysed from two aspects: it was observed that 1) the seismic attribute would dramatically affect the proxy quality and 2) the values of the proxy coefficients did not show significant variation over different scenarios; thus, a fixed proxy is sufficient in the history matching workflow.
4. In order to utilise the proxy model, mapped seismic, pressure and saturation data are prerequisites. Therefore, this method can only be successfully applied in cases where the reservoir is significantly vertically-homogeneous to generate such mapped properties.

Chapter 4

Flow simulation proxy model I: areal model

Following the last chapter in which a seismic modelling proxy model was developed, this chapter presents a 2D areal model as a proxy for the 3D fluid flow simulation model. It is built based on an initial 3D model: each reservoir property in the 2D areal model is a vertical average of that in the 3D model. It is observed that the areal model can generate dynamic property change maps (ΔP, ΔS_w and ΔS_g) that are comparable with the 3D model results. These outputs will then be utilised by a linear seismic proxy to simulate the 4D seismic change. This method is tested on the Schiehallion field in which the areal flow patterns dominate reservoir production profiles. The proxy quality is first tested through visualization, then by quantitative metrics in a blind test. Additionally, the 2D areal model is further refined in the lateral direction, which is an attempt to keep resolution as high as in the seismic data. However, results show that the laterally refined areal model fails to bring significant improvement, but requires higher computation cost. The final conclusion is that, considering the trade-off between upscaling errors and computing time, the 2D areal model, without laterally refinement, is a better choice in this case.

4.1 Introduction

The SHM workflow requires two simulators, the fluid flow simulator and the sim2seis model. The inputs and outputs of each simulator are listed in Table 4-1. The outputs (fluid and pressure distributions) of the fluid flow simulator are the inputs of the sim2seis model. In Chapter 3, I developed a proxy model to increase the efficiency of the seismic modelling step only. Here I address the flow simulation model, by proposing a 2D areal model as a simplification of the 3D flow simulator for a certain specific reservoir.

Table 4-1 *Inputs and outputs of fluid flow simulation model and sim2seis model.*

	Inputs	Outputs
Fluid flow simulator	• static reservoir properties • prior- production distribution of fluid and pressure • development strategies	• Post-production distribution of fluid and pressure • Well production data
Sim2seis simulator	• Prior- and post- production distribution of fluid and pressure • petro-elastic properties • seismic wavelet	• 4D seismic data • (Impedance, amplitude, etc.)

A literature review of conventional fluid flow simulation models was provided in Chapter 2. One of the main motivations in developing this areal model came from the need to accelerate the model run. In the history matching workflow, thousands or even millions of simulation model runs are needed; thus, a minor improvement of model running speed will lead to huge computation cost saving. On the other hand, in many cases, the features shown in seismic resolution suggest the use of mapped seismic for SHM (MacBeth et al. 2004, Landa et al. 2015 and Obidegwu et al. 2015). This is also a source of motivation which will be discussed in detail later.

A UKCS offshore field, Schiehallion, was selected to test this method in this chapter. I will first introduce the field background, then build the 2D areal model based on a 3D model and couple it with a sim2seis proxy (Figure 4-1). The proxy model quality will then be quantified visually and quantitatively. Finally, the areal model will be refined laterally, to explore the possibility of improving the proxy model accuracy.

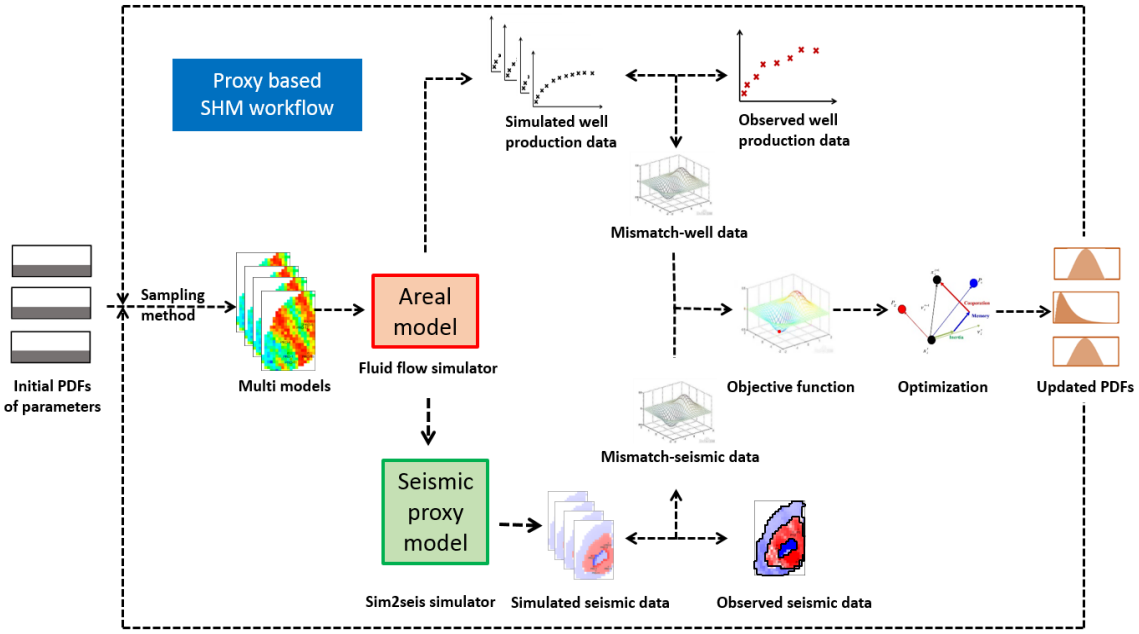

Figure 4-1 *Proxy model based seismic history matching workflow: coupling the areal model with linear sim2seis proxy in SHM workflow.*

4.2 Field Description and data sources

Located on the Atlantic margin of the UKCS (Figure 4-2), the Schiehallion field is a deepwater turbidite reservoir. The field consists of four segments separated by east-west trending normal faults and water injection has been used as the main development strategy so far. Reservoir connectivity is the main reservoir uncertainty facing the engineers (Govan et al., 2005). In the production history of Schiehallion, 4D seismic has been extensively used as a description of dynamic reservoir behaviour for management and decision-making purpose (Parr et al., 2000, Altan et al., 2001). Based on the appraisal well data, seismic data, well production profiles and other data sources, a 3D flow simulator and a sim2seis simulator have been built by the operator, and will be used as reference models in this work.

Figure 4-2 *Location of Schiehallion field in the North Sea.*

4.2.1 Field geology

The Schiehallion field is a deepwater turbidite reservoir of Tertiary age with water depth~400 m. The field is contained in a combination structural-stratigraphic trap formed during the Late Palaocene reservoir deposition and rifting. The reservoir intervals consist of several sand geobodies interlayered with shales. It shows varying degrees of channelisation in different parts of the field (Figure 4-3)

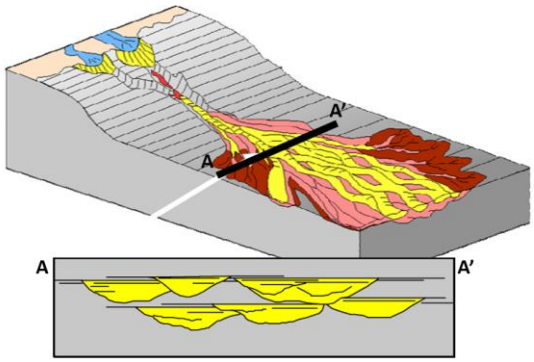

Figure 4-3 *Generic scheme of turbidite deposits adopted from Schiehallion field (adopted from Govan et al., 2005).*

Horizontally, the reservoir covers 35 km^2 and is divided into four main fault blocks or "segments" (Figure 4-4). Southernmost segments, segment 1 and 4, contain the majority of the original oil in place. This study is focused on segment 4, which is separated from the northern segment 1 by a mostly sealed fault, as suggested by the extended well test (see below). Segment 4 is sealed from the south by a fault with a large throw exceeding the reservoir thickness. The seal from the east is provided by the pinch-out of the reservoir sands. In the west, the structural dip works as the trapping mechanism (Gainski et al., 2010).

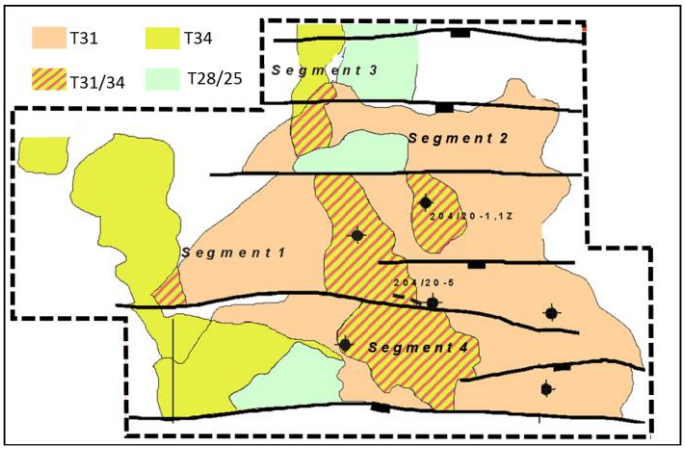

Figure 4-4 *Four segments of Schiehallion field, with main turbidite sand layers (adopted from Govan et al., 2005).*

Vertically, the field consists of a range of Tertiary age turbidites from the "T-sequence": T25, T28, T31a, T31b, T34, T35, with T31 (a and b) being the main reservoir (Martin and Macdonald, 2010, Figure 4-5). The productive sands range from channels to sheet-like sands with different patterns of overlap and connectivity.

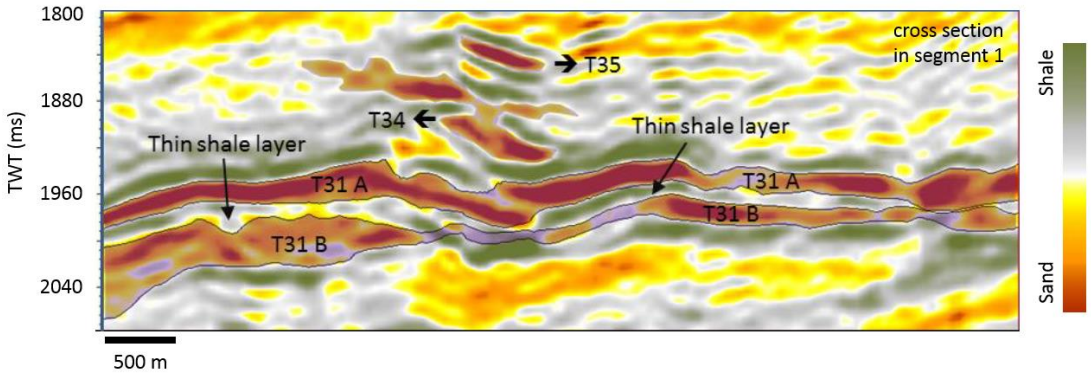

Figure 4-5 *Vertical section from the coloured inversion seismic data (1996 preproduction data), showing the distribution of the turbidite sequences T31A and T31B of the Schiehallion field. The top and base horizons of the sand layers are picked as zero crossing by the data provider (BP) (adopted from Amini 2014).*

The reservoir porosity (~0.27) and permeability (~600mD) are good, with initial reservoir pressure P_{init} = 2907 psi (at depth 1940 m TVDSS). A limited aquifer provides little natural support from the western part of the field. Inside the main reservoir, connectivity between sand geobodies is the main uncertainty for fluid flow. The complex connectivity pattern between the sand geobodies imposes the challenge of appropriate placement of the producing and injecting wells for good pressure support.

4.2.2 Field development history and challenges

Before the first oil, seven wells were used to appraise the field, revealing that the net oil sand could be accurately predicted from the seismic data. The field was then put into production in 1998, following an extended well test (EWT) which was conducted to evaluate the reservoir connectivity. After production, it was found that the field connectivity is much poorer than was anticipated initially, because many producers did not receive adequate pressure support and the field pressure depleted quickly, leading to the producing gas oil ratio (GOR) increased rapidly.

Since the field reached its mature stage, water production has increased continually. Consequently, the reservoir management focus has shifted to managing water injection by expanding the sweep area and controlling the water cut. Optimising water injection

distribution has become a principal approach to achieve the goal. As in other water injection fields, because of reservoir heterogeneity, the connection links between injectors and producers are highly uncertain. Considering that all the injectors support more than one producer, and vice versa, it is clear that the sweep pattern is quite complicated.

As a summary of the development challenges, it can be said that regardless of whether it was in the early or late field life, the reservoir connectivity was one of the key issues in the field development as it controlled the operator's decisions on the optimal well placement. Normally, each sand body has good interior connectivity but the exterior connectivity between the stacked channels or sheet-like sands are poor. However, even with sand body boundaries which were well interpreted from the seismic, the dynamic connectivity is still needed to be determined from the flow simulation (Figure 4-6).

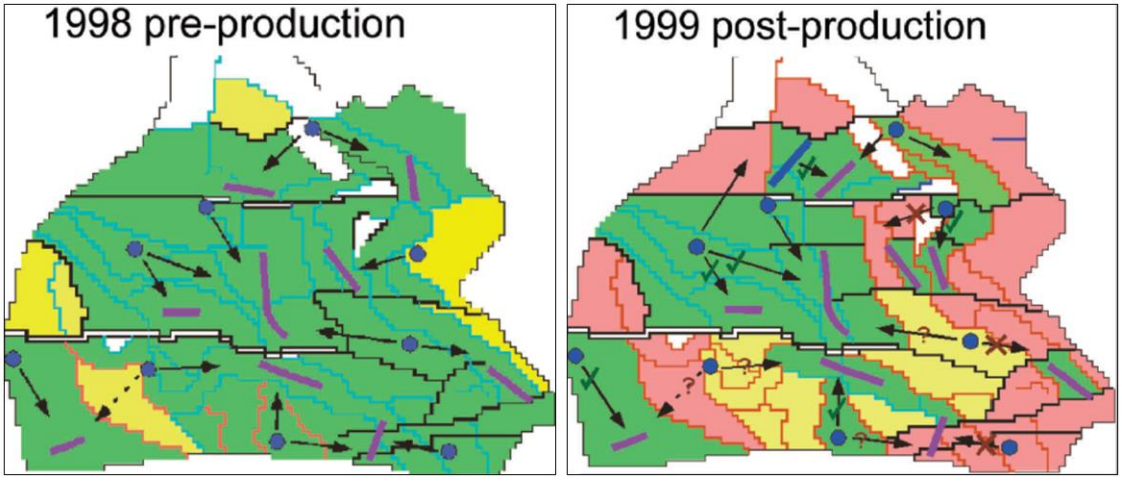

Figure 4-6 *Reservoir connectivity estimation before (left) and after (right) production. Green-connected, red-unconnected, yellow-uncertain (adopted from Govan et al., 2005).*

In the early stage, when only limited data was available, a material balance multiple tank model was built as a simulator to analyse the connectivity between sand geobodies and between wells. This method helped to obtain rapid indicative results as a fast-track method of connectivity analysis.

As the field matured, more types and volume of data became available. A 3D reservoir simulation model was built by the operator and consisted of more than 500 sand geobodies. In this model the reservoir connectivity was described in great detail: permeability and transmissibility multipliers have been applied as a quantitative control parameter. In the history matching procedure of the 3D simulation model, such multipliers are the main uncertain perturbation parameters. In next section, a history-matched 3D flow simulation model and a calibrated sim2seis model will be introduced.

4.2.3 Simulation models

4.2.3.1 3D fluid flow simulation model

As explained in last section, the Schiehallion field consists of four separated segments. The operator has built four individual simulation models for each of the segments. In this study, the simulation model of segment 4 (Eclipse 100 black oil model) is selected to test the method.

The model has dimensions of approximately 8000 × 1800 ×700 metres, and has 209 ×57×120 cells in the X, Y and Z directions respectively. It contains 359,035 defined cells out of total number of 1,429,560 cells. The full-history simulation model running from 1998 to 2008 on a standard computer workstation (Intel CPU i7-3770 @ 3.40GHz with 8 processors) takes approximately 24,000 seconds. Three Tertiary age turbidites, T34/35, T31 and T25/28 were modelled in this segment, where T31 is the main reservoir (Figure 4-7).

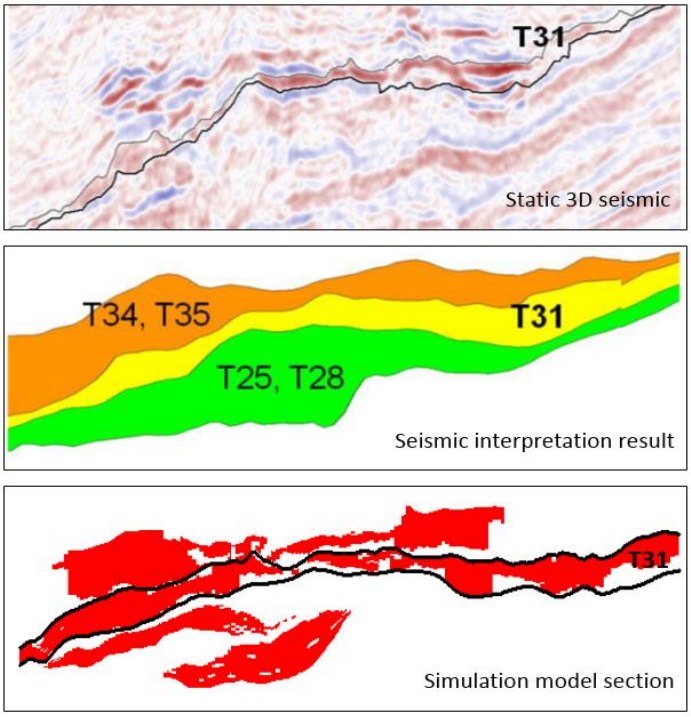

Figure 4-7 *Main reservoir T31 in observed static seismic (above), interpreted model (middle) and in 3D flow simulation model (below, red-defined grid blocks; white-undefined).*

The oil sands are sheet-like geobodies which can be interpreted from the seismic data. In the simulation model there are 400 groups of cells, each of which is labelled with a MULTNUM value, to simulate the geobodies (Figure 4-8). In total there are 16 wells

located in this segment, including eight producers and eight injectors. The perforation details of each well are listed in Table 4-2.

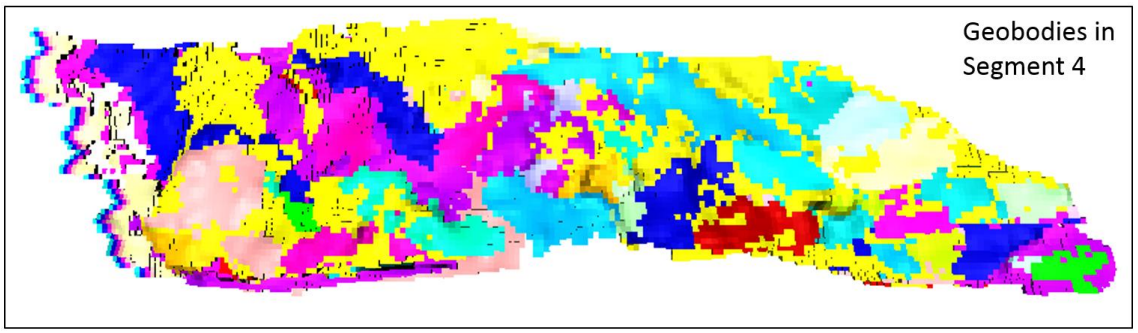

Figure 4-8 *The fine 3D grid with seismically-mapped geobodies, showing the top of T31 reservoir.*

Table 4-2 *Completion of the segment 4 wells: above T31 reservoir, in T31 reservoir and below T31 reservoir (percentage is calculated by counting the perforation layers over the whole reservoir).*

Well	Perforation percentage (%)		
	Above T31	In T31	Below T31
P1	0	100	0
P2	0	100	0
P3	100	0	0
P4	0	100	0
P5	25	50	25
P6	0	100	0
P7	100	0	0
P8	0	0	100
I1	0	100	0
I2	66.7	33.3	0
I3	0	100	0
I4	50	41.7	8.3
I5	0	100	0
I6	46	37	17
I7	0	100	0
I8	0	0	100

4.2.3.2 Petro-elastic model

For Schiehallion, a petro-elastic model (PEM) developed by Amini (2014) was applied (Equations 4.1, 4.2 and 4.3). By applying this model, each cell in the 3D flow simulator, which has been assigned a specific V_{shale} and porosity ($\emptyset$), together with saturation and pressure changes, can be transformed into a corresponding elastic property (V_p, V_s and ρ).

$$K_{dry} = K_{min}\left(\frac{1-\emptyset}{1+\alpha\emptyset}\right) \tag{4.1}$$

$$\mu_{dry} = \mu_{min}\left(\frac{1-\emptyset}{1+\alpha\emptyset}\right) \tag{4.2}$$

$$\alpha = a.V_{sand} + b.V_{shale} + c.\emptyset \tag{4.3}$$

Instead of using a single value for the consolidation factor, a multiple linear regression was engaged to create a consolidation factor that is aware of the lithology, which varies with shale and sand volume and porosity. The coefficients a, b and c are related to the dependency on lithology and porosity of the consolidation factor used for this specific paradigm. This PEM was designed for a sand-shale system in the petro-elastic domain and was calibrated by the use of well-logs and laboratory measurements. Together with a Gassmann modelling for sand-clay mixtures, the PEM can generate the elastic properties based on the static (V_{shale}, $\emptyset$, etc.) and dynamic (saturation and pressure) properties. By calibrating to the log data of seven wells, the calibrated parameters of the above petro-elastic model were given by Briceño (2017) (Table 4-3).

After obtaining the PEM results, a fast seismic modelling approach, 1D convolution, was then used to generate the seismic wiggles on each trace. A wavelet (Figure 4-9, a) from a seismic-to-well tie procedure was used for seismic modelling. The observed and simulated 3D and 4D seismic are plotted in Figure 4-9 (b, c, d, e).

Table 4-3 *Calibrated parameters, obtained from model fit to the logs using PEM for Schiehallion Field. The coefficients a, b and c are related to the dependency on lithology and porosity of the consolidation factor used for this specific paradigm (see Equations 4.1, 4.2 and 4.3).*

	well	Ksand (GPa)	Kshale (GPa)	μsand (GPa)	μshale (GPa)	ρsand (g/cc)	ρshale (g/cc)	a	b	c
Mixing before fluid substitution	1	24	15	20	4	2.72	2.40	2.11	1.73	4.42
	2	30	16	29	4	2.72	2.41	10.95	3.91	-9.94
	3	28	19	19	6	2.69	2.58	5.41	2.97	0.52
	4	24	19	16	6	2.67	2.58	4.83	3.06	-3.41
	5	27	15	21	4	2.68	2.39	4.99	3.17	0.88
	6	26	15	16	5	2.66	2.42	0.59	2.82	7.39
	7	36	16	28	5	2.62	2.40	14.00	5.38	-12.64
Mixing before fluid substitution	1	28	12	22	3	2.72	2.40	-9.35	11.82	33.80
	2	29	13	25	3	2.72	2.41	2.63	12.58	10.63
	3	32	13	22	3	2.69	2.58	-7.09	6.26	33.43
	4	31	13	17	4	2.67	2.58	-3.14	12.97	15.68
	5	27	13	19	3	2.68	2.39	-6.68	12.62	28.47
	6	29	13	18	4	2.66	2.42	-0.69	13.70	14.35
	7	26	14	14	5	2.62	2.40	-3.88	13.48	14.72
Backus averaging	1	24	12	26	3	2.72	2.40	-9.00	9.38	36.49
	2	27	12	23	4	2.72	2.41	5.55	13.27	1.42
	3	28	13	27	3	2.69	2.58	-7.12	5.51	36.95
	4	30	13	18	4	2.67	2.58	-3.92	12.25	18.03
	5	23	13	16	4	2.68	2.39	-3.47	16.13	15.59
	6	28	13	17	5	2.66	2.42	-1.28	16.79	13.19
	7	25	14	14	5	2.62	2.40	-1.05	13.10	7.80

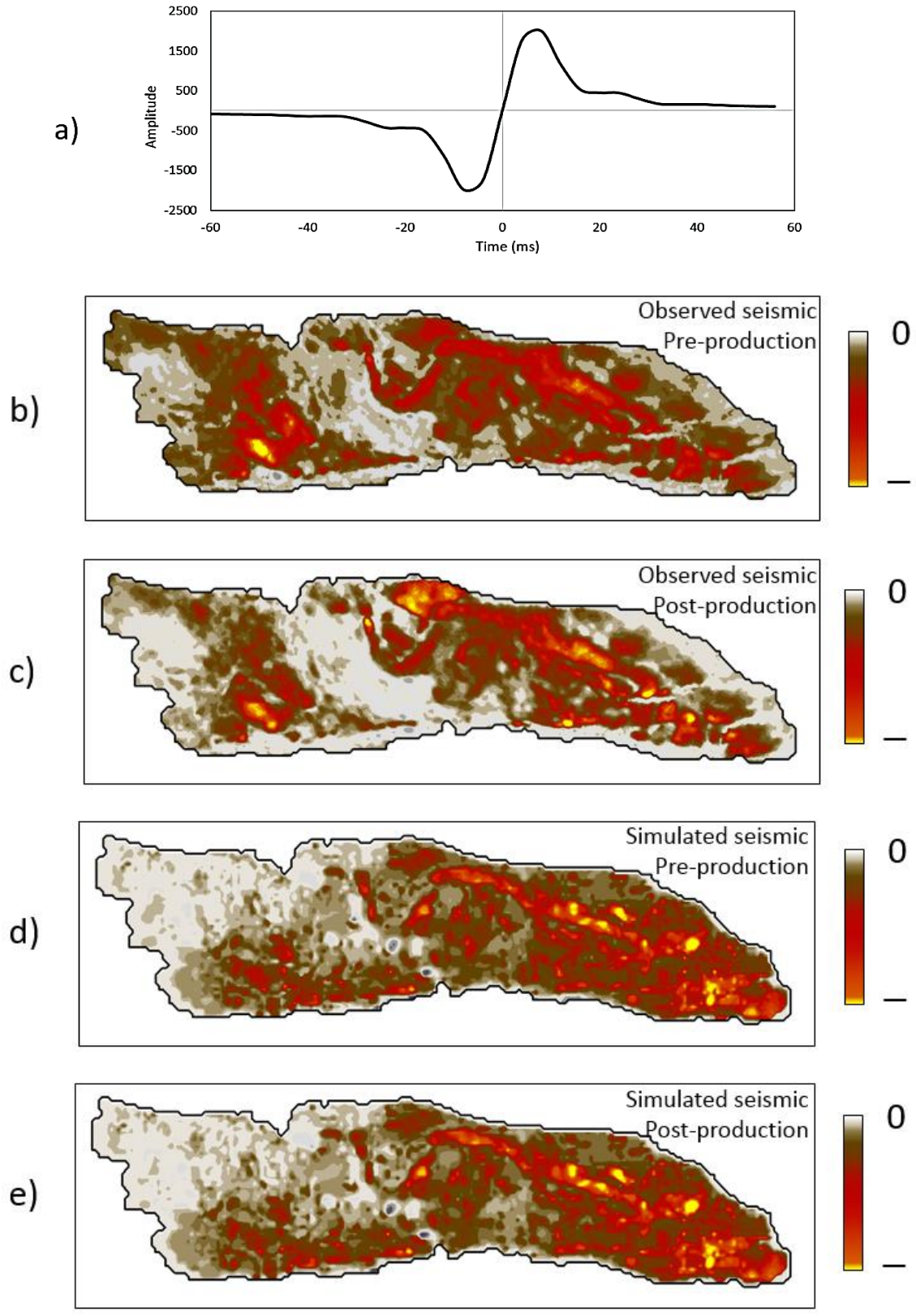

Figure 4-9 *a) The wavelet used for 1D convolution; b), c): observed seismic data (sum of negative amplitude of the reservoir); pre- and post-production) and d), e): synthetic seismic (sum of negative amplitude of the reservoir; pre- and post-production) by the history matched fluid flow simulation model and the calibrated sim2seis model.*

4.2.4 Production and seismic data

4.2.4.1 Production data

Historic well production data is available from 16/07/1998 (start of production) to 20/02/2008, including production and injection rates, water cuts, gas/oil ratios and well bottom hole pressures (BHP). The historical production rates for the entire segment can be seen in Figure 4-10. As explained earlier, seven producers and five injectors which have perforations in the main reservoir T31 were working during this period; the bottom hole pressure profiles of six producers (except P4) are available and are presented in Figure 4-11.

There are two flow simulation models available; one is upscaled from the geological model without matching to the observation data and the other has already been matched with well production data and seismic data by Fursov (2015). Production profiles of the six producers, which are simulated by these two models, are shown in Figure 4-11, with historical data as reference.

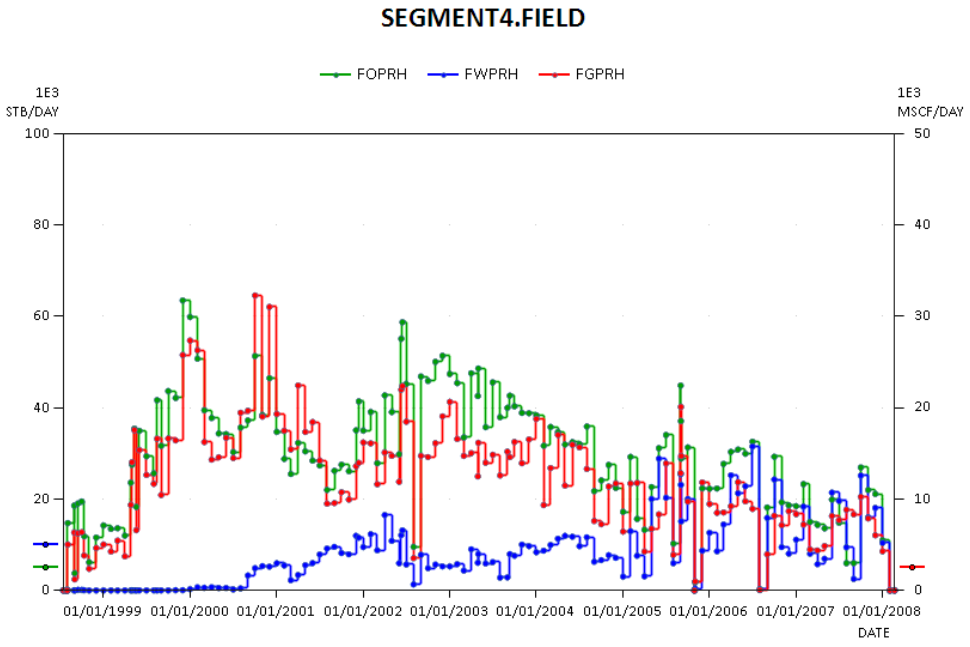

Figure 4-10 *History data of oil production rate (FOPTH), water production rate (FWPRH) and gas production rate (FGPRH) for segment 4.*

It is observed from Figure 4-12 that the second simulation model was well matched with the BHP data of five producers (P2, P3, P6, P7 and P8), whereas for producer P1 the pressure was still over simulated. These six producers will be used to quantify the proxy model quality and will be involved in the objective function (as the production data part) of the seismic history matching in later sections.

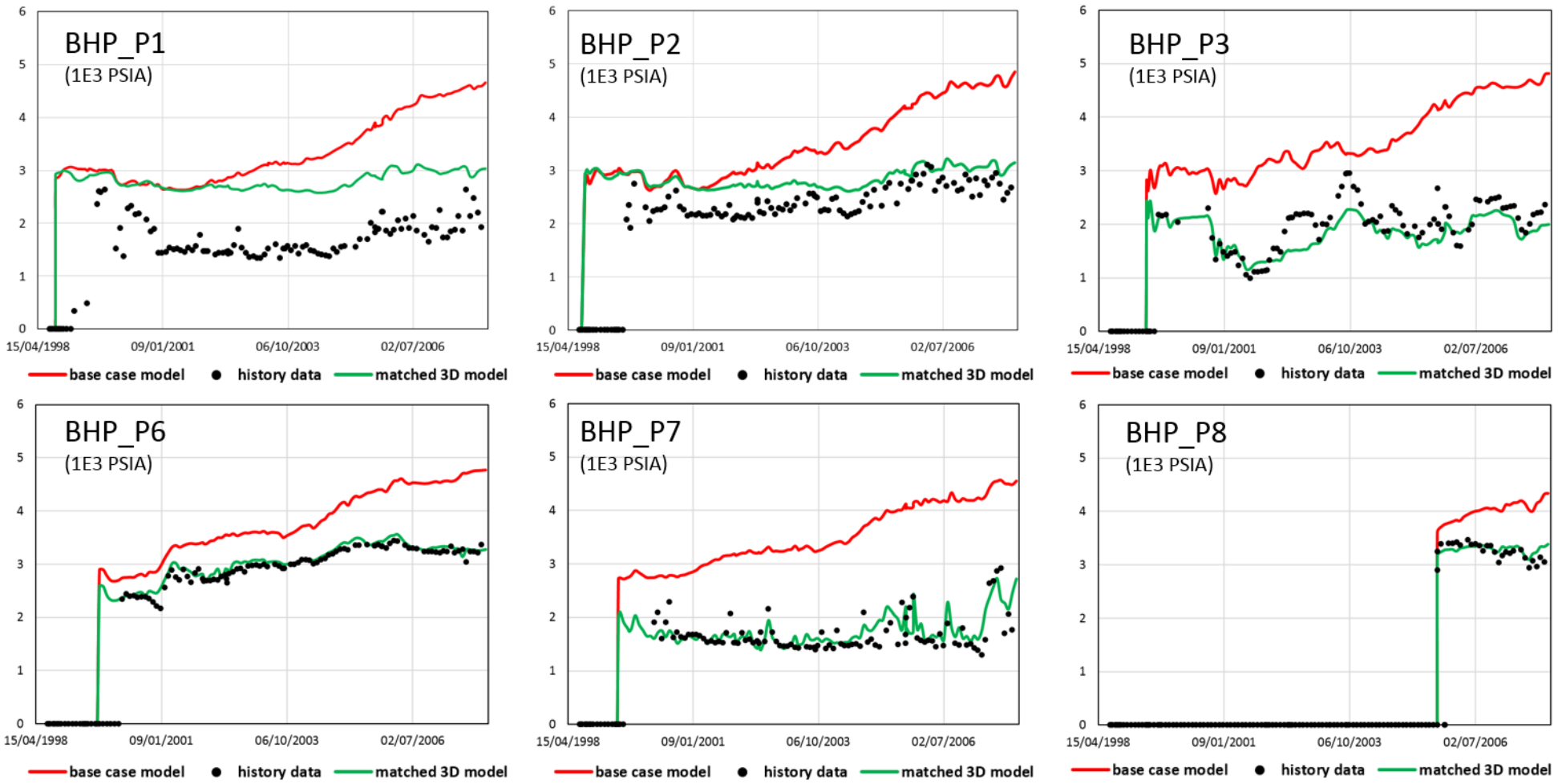

Figure 4-11 *History and simulation results of well bottom hole pressure (BHP) for the available 6 producers located in segment 4. The red line stands for the results of the initial upscaled model which has not been history matched; the green line stands for the results of a history matched model.*

4.2.4.2 4D seismic data

Five 3D seismic cubes were acquired at 1996, 2002, 2004, 2006 and 2008. These surveys were acquired and fast-track processed through a colour inversion (Stephen and MacBeth, 2006). The 1996 survey is the pre-production one and will be used as a baseline; the 2004 seismic will be used as the monitor for the time-lapse studies. Seismic horizons for the top and base of T31 are available, therefore I will use the attributes calculated for T31 in seismic history matching. In terms of the seismic attribute, I use the Sum of Negative Amplitude (SNA) attribute to present the 4D seismic data, which is recommended by the field operator, because the reservoir T31 has a whole negative half-wiggle (Figure 4-12).

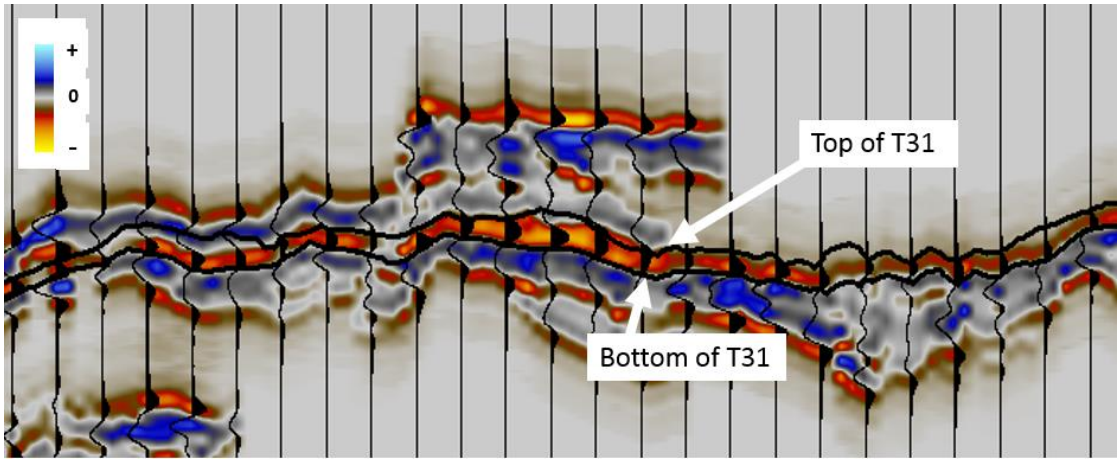

Figure 4-12 *Seismic amplitude (cross-section) data of Schiehallion segment 4, with reference horizons of top and bottom of formation T31.*

The '4D seismic' used in this case is the difference of SNA maps between the monitor and baseline surveys. Before applying the 4D signature in history matching, the noise level should be analysed. The common way of estimating 4D seismic signal to noise ratio is to calculate the normalised RMS (NRMS) for the overburden in the 4D difference seismic cube (monitor subtracts baseline). A high NRMS value means a high level of noise and, thus, that the 4D signature is less likely to be a result of the dynamic reservoir property changes.

To assess the 4D seismic non-repeatability of Schiehallion, NRMS was calculated in the overburden for the difference between the 1996 (baseline) and 2004 (monitor) surveys (Figure 4-13). The mean NRMS is 0.31, as reported by Falahat et al. (2013), indicating a low noise level and that the 4D seismic signature is mainly caused by the dynamic reservoir property changes.

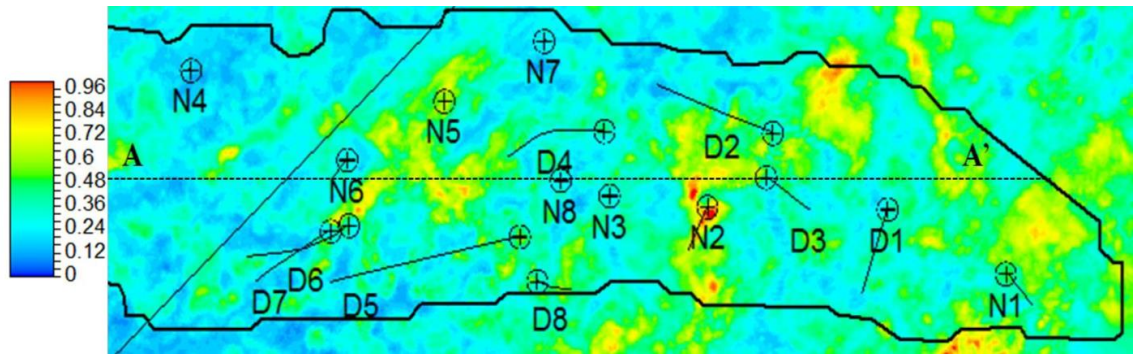

Figure 4-13 *Overburden NRMS map for the difference between seismic cubes 1996 and 2004. The black contour line shows the boundary of segment 4. The inclined black line shows the direction of the seismic in-lines (adopted from Fursov, 2015).*

As mentioned before, there is an available history matched 3D simulation model which has been matched with well production data and seismic data (Fursov, 2015). Figure 4-14 illustrates the simulated seismic data versus the observed seismic data, which have comparable patterns of anomalies. In order to omit the effect of seismic noise on the test of the proxy model's quality, the simulated seismic will be used as 'synthetic history' in my later study.

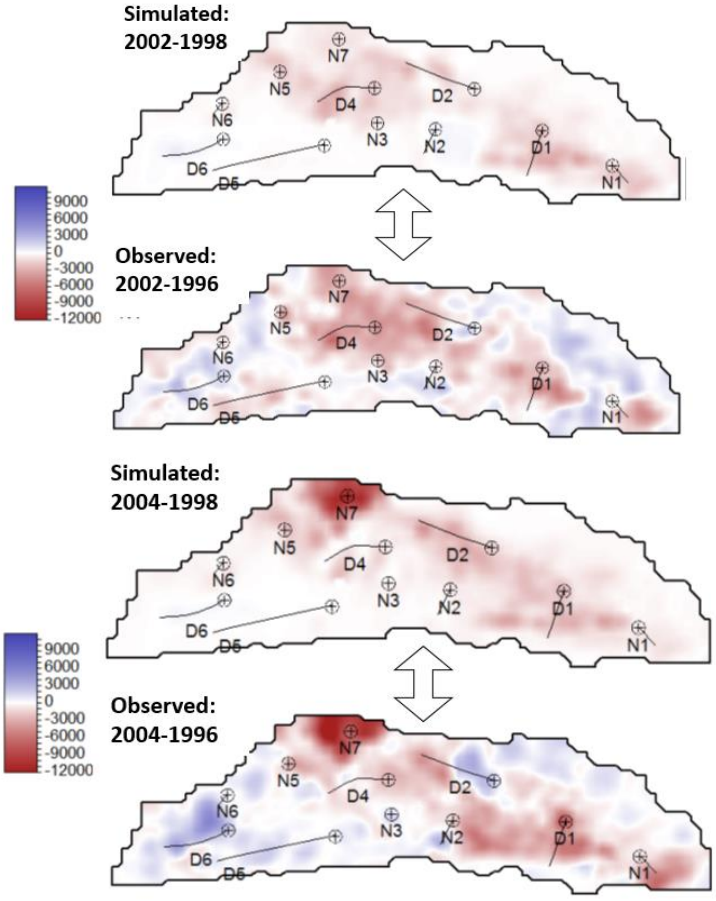

Figure 4-14 *Modelled and observed time-lapse seismic attributes (adopted from Fursov, 2015).*

4.3 Proxy models

4.3.1 Seismic proxy model

In the Chapter 3 a linear superposition seismic modelling proxy was introduced. As the final target is to use two proxy models to replace the two simulators in the SHM, the seismic proxy and the flow simulation proxy should work together. In this chapter, the 2D areal model is introduced as the flow simulation proxy. In order to further use it with the seismic proxy (see Figure 4-1), I firstly build and validate the linear seismic proxy for Schiehallion field in this section.

Based on these results of flow simulation (pressure and saturation distributions), the sim2seis model was used to calculate the 4D seismic, which is shown in Figure 4-15. Following the procedure applied in Chapter 3, the assumption of linear superposition is firstly validated. Synthetic 4D seismic maps generated by sim2seis on each of three parameters are summed up and compared with the 'real' 4D seismic maps, as shown in Figure 4-16.

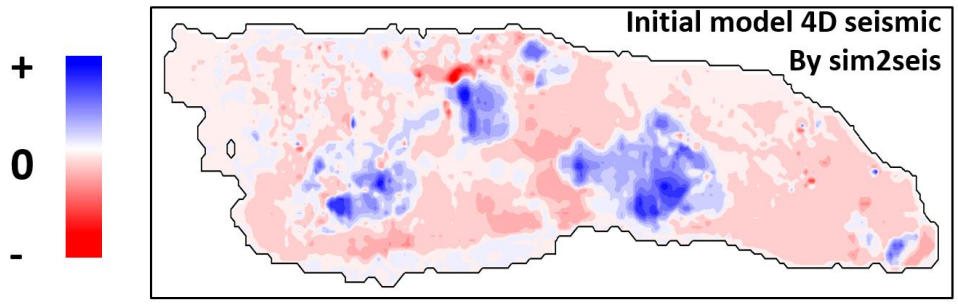

Figure 4-15 *Synthetic 4D seismic simulated by sim2seis model, based on the flow simulation results of initial 3D model.*

It is observed from Figure 4-16 that 1) the maps of three variables (ΔSw, ΔSg and ΔP) and their corresponding 'individual 4D seismic' maps are clearly correlated: hardening and softening anomalies have similar patterns in both sides. 2) The arithmetic sum of three 'individual 4D seismic' maps are visually similar to the 'full 4D seismic' map which is simulated by considering all of the three variables. Following the validation procedure introduced in Chapter 3, the linearity assumption can be qualitatively validated. In order to validate it in a more quantitative way, the 'full 4D seismic' and 'mixed 4D seismic' were cross-plotted in Figure 4-17 and the correlation coefficient, *r*, was measured to be 0.99. Based on this analysis, similar to that of Norne, the linearity assumption of seismic proxy was also validated on Schiehallion field.

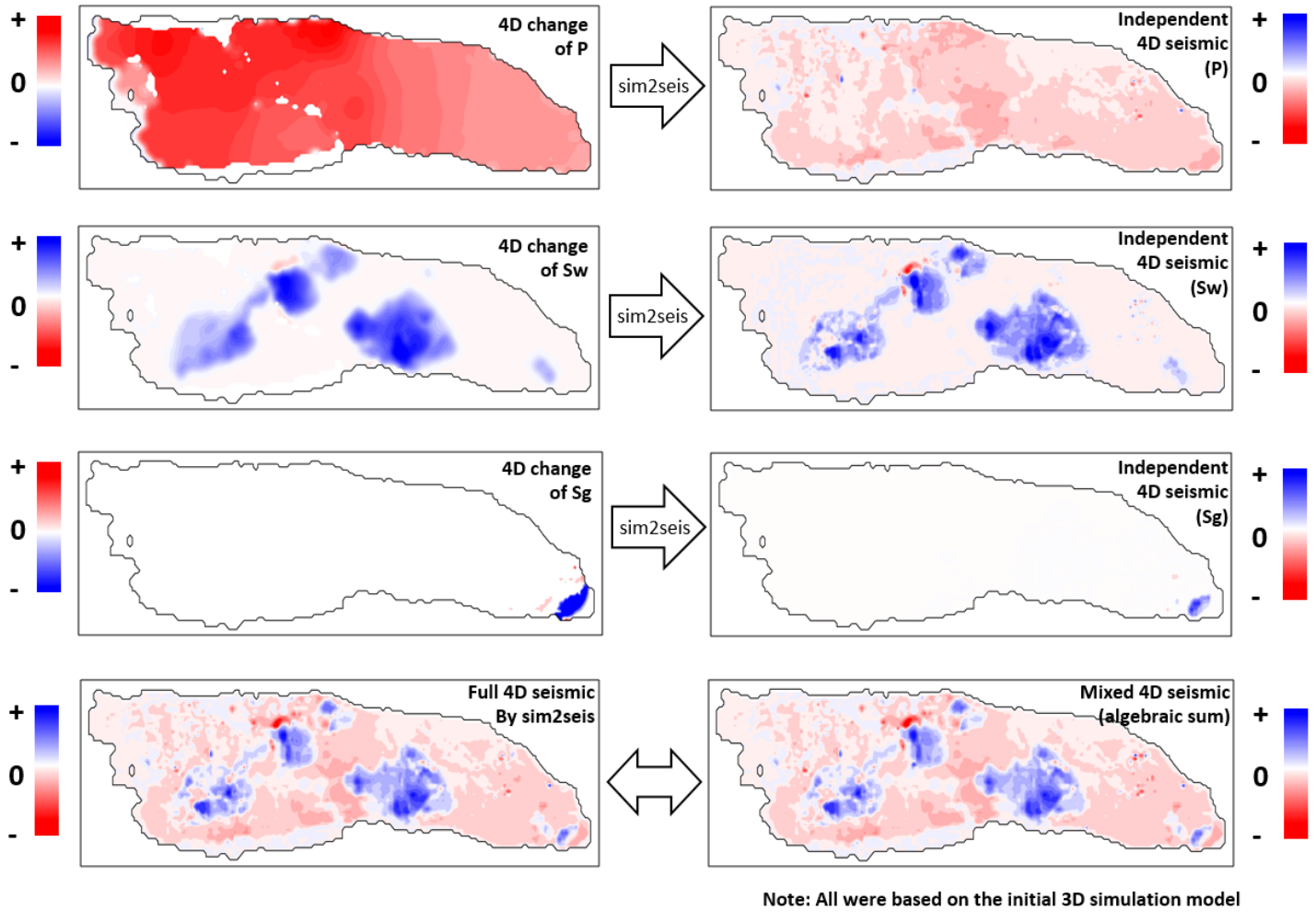

Figure 4-16 *From top left to third left: pressure, water saturation and gas saturation changes of T31 from initial simulation model, bottom left: 4D seismic modelled by sim2seis by taking all three variables into consideration; From top right to third right: modelled 4D seismic signatures considering each individual variable, bottom right: 'mixed 4D seismic' map, which is a superposition of all three left hand individual 4D seismic maps.*

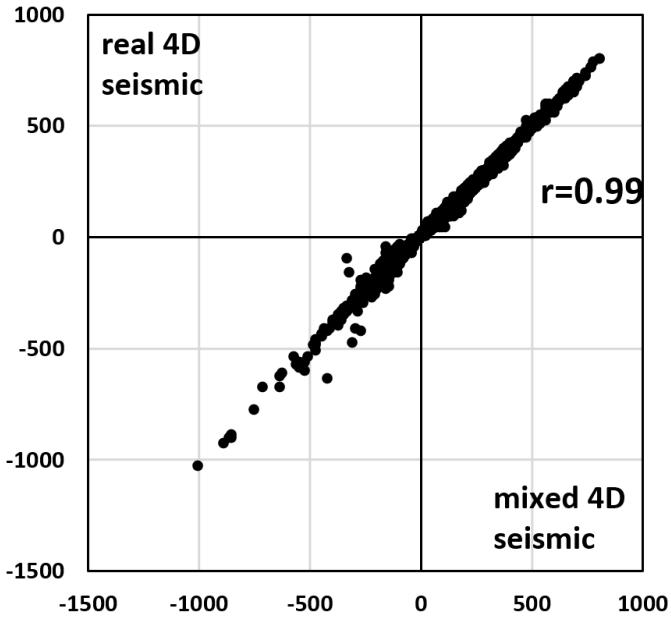

Figure 4-17 *Cross plot of mixed 4D seismic and real 4D seismic.*

Having validated the linearity assumption, the next step is to build the proxy on this specific field. Details on how to build the seismic proxy model were presented in section 3.3.3; the four required input properties are: 4D changes of pressure (ΔP), water saturation (ΔS_w), gas saturation (ΔS_g) and static seismic scalar (A_0). After running the 3D simulation model, four maps were generated, as shown in Figure 4-18.

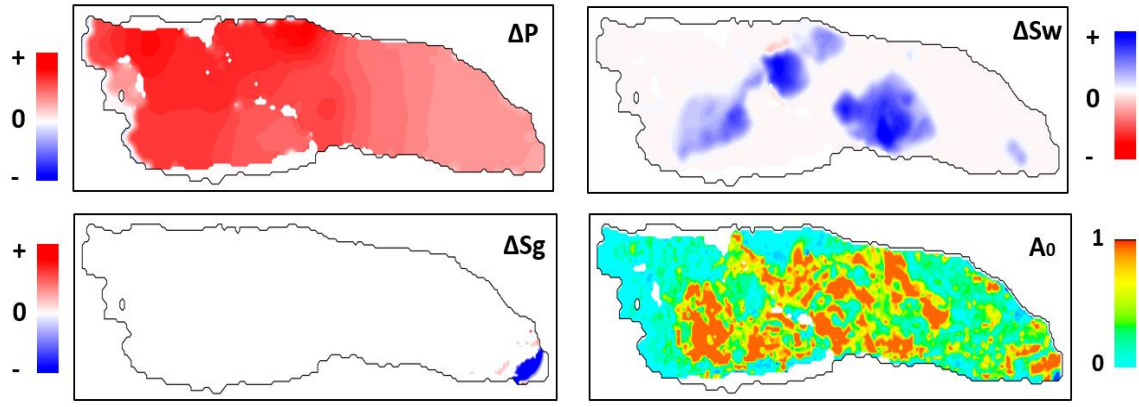

Figure 4-18 *Simulation result of the reference model: 4D changes of pressure (ΔP), water saturation (ΔS_w), gas saturation (ΔS_g) and static seismic scalar (A_0). All are pore volume weighted maps.*

As explained in Chapter 3, having obtained the four input maps and 4D seismic map (sim2seis), a least-square linear regression can be conducted to calculate the three coefficients in the seismic proxy equation:

$$\Delta A = \left(c_1 \cdot \Delta P + c_2 \cdot \Delta S_w + c_3 \cdot \Delta S_g\right) \cdot A_0 \qquad (4.4)$$

Table 4-4 *Value of three coefficients: results of linear regression.*

c_1	c_2	c_3
-3.27	1654.93	-2584.63

It should be pointed out that the absolute values of the three coefficients are related to the pressure unit and the wavelet amplitude used in the seismic modelling procedure. The coefficients for different fields are not comparable, but positive or negative values indicate the effect of the three parameters on 4D seismic hardening and softening. For one field, in order to keep consistency between the baseline and monitor seismic, the same wavelet should be applied so that the 4D seismic can be obtained directly by differencing the monitor from the baseline. Similarly, the amplitude of observed and simulated seismic are also on different scales. Thus, in order to match the simulation result with observation data, the seismic maps need to be normalized (normally [-1, 1] scale).

Having the linear sim2seis proxy (Equation 4.4), I then generated the 4D seismic map using this proxy and compared it with the sim2seis result in Figure 4-19. It is observed that the main features in sim2seis result (upper map) can be very well reproduced with the proxy (lower map); so in the Schiehallion field, the sim2seis model can also be approximated by the linear superposition model that was introduced in Chapter 3.

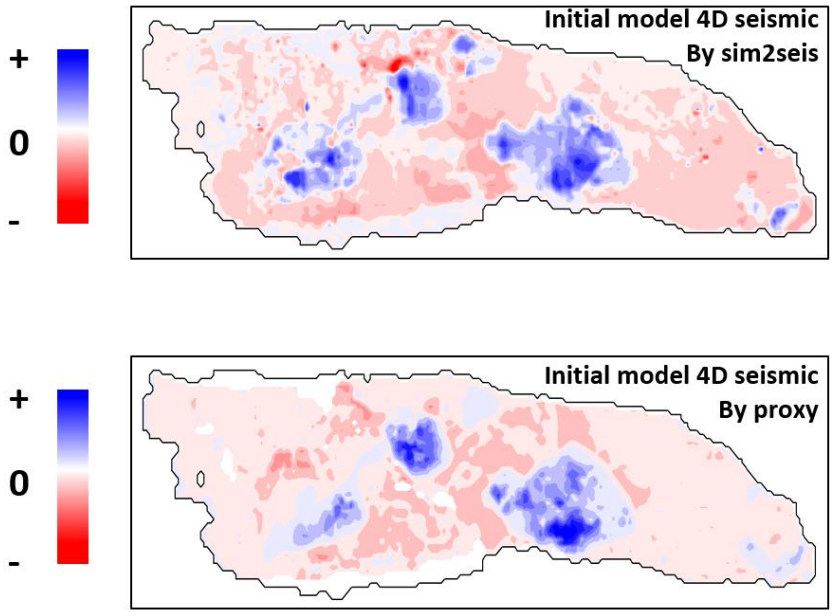

Figure 4-19 *4D seismic maps generated by sim2seis (upper) and proxy model (lower).*

4.3.2 Areal model: motivation

The first drive of developing a 2D areal simulation model for Schiehallion is the need to speed up the 3D simulation model in SHM. With high frequency of data acquisition and the need to analyse model uncertainty, a huge number of simulation model runs are indispensable. In order to accelerate model running, a common method is to make simplified version of the model. According to the field geology, T31 is the main reservoir which consists of many sheet-like (thin and laterally extended) turbidite sands; thus the idea emerged to simplify the 3D model by using a 2D areal model.

In the review of reservoir flow simulators (Chapter 2), I introduced the 3D model, 2D areal model, 1D streamline model and 0D tank model, in sequence. In order to build a simulation model for a specific field, the first step is to decide on the number of spatial dimensions to represent the geometry of the physical system and, simultaneously, to determine which simplifications are justified. For this decision and justification, internal and external geometries must be considered. The internal geometry mainly composes of the areal and vertical extent of individual permeability units and shale layers that are important to the results of the simulation. External geometry includes the overburden, underburden and sideburden of the target reservoir, such as aquifers (Mattax and Dalton, 1990).

Nowadays the 3D model is the most commonly used model in reservoir simulation, which needs to be built and run on a high performance computer or computer clusters. If one was asked why the 3D model should be selected, but not the other lower-dimension choices, one may argue that the 3D model has the capability to simulate complex reservoir geometry and fluid mechanisms. This is true, indeed, but the question is whether every field needs such a detailed model to simulate the reservoir structure and internal fluid flow? Moreover, can the more complex 3D model could produce more accurate information than a low-dimension model? Not only the model accuracy, but the computational cost should be taken into account when making the decision. More required input data may also lead to higher model uncertainty.

To deal with the trade-off of ‘accuracy versus computational cost’ and ‘model complexity versus uncertainty’, the reservoir engineers engaged in the simulation model building should consider to what extent the model structure can be simplified or the dimensionality can be reduced: without losing too much information and the results are still relevant.

In addition, how much benefit could be gained through structural simplification and reduction of dimensionality? Is the principle suitable for the case of the reservoir simulation domain: bearing in mind the Pareto principle, which states that roughly 80% of the effects come from 20% of the causes? In the reservoir engineering domain, could we find a simplified model which keeps only 20% of the model complexity and computational cost, but could produce 80% similar results with the conventional complexed model?

In order to reply all the above questions, I intend to build a 2D areal model as a proxy for the 3D simulator in the Schiehallion field. I will try to quantify both sides of the trade-off: model accuracy and computational cost, and give recommendations for the purpose of model selection (a complex one or a simplified one).

The second source of motivation came from the nature of seismic resolution. Resolution is the ability to distinguish between objects, that is, to see a second object in the presence of another (Badley, 1985). Concerning a set of seismic data, its vertical resolution relates to how far apart two interfaces must be to distinguish separate reflections from them or how thick a bed must be to allow distinguishable reflections from the top and bottom of the bed (Puryear and Castagna, 2008). In the ideal case, the length (in time) of the source wavelet should be short and with a distinctive, sharp peak and no side lobes (Figure 4-20) for true reflection interpretation. However, in practice, the wavelet frequency is not too high due to attenuation. Moreover, the seismic source, no matter whether it is dynamite or an air gun, can never avoid producing side lobes, which adds to the uncertainty of the seismic interpretation. So in general, the vertical seismic resolution is a limitation of seismic data when it comes to thin reservoirs or those that possess strong vertical heterogeneity.

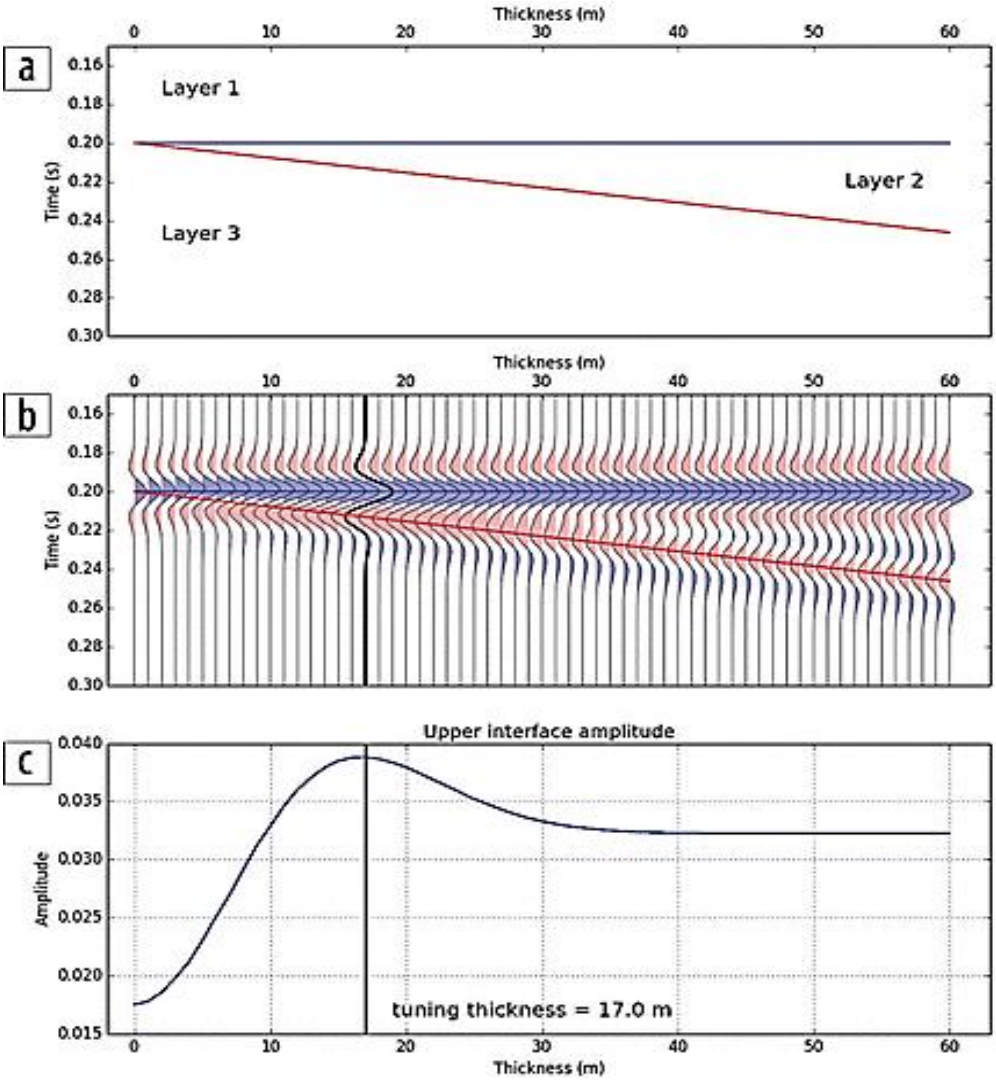

Figure 4-20 *(a) A three-layer wedge model. (b) Zero-offset synthetic seismogram displayed in normal polarity. (c) Amplitude of the synthetic extracted along the top of layer 2 (Hamlyn, 2014).*

In the case of Schiehallion, the vertical seismic resolution is one eighth of the wave-length (Widess 1973, Chopra et al. 2006, Hanneing and Paton, 2012), which is ~ 15.9 metres on average. As a reference, there are 12 simulation layers to model T31 (thickness ~ 62.3 metres) in the upscaled 3D flow simulation model, which means the vertical resolution of the 3D simulator is 5.2 metres. The simulation model has roughly three times greater vertical resolution; for a finer model this number would be higher.

Although the vertical resolution of seismic data is rather coarse compared with the 3D simulation model, its lateral resolution is a strength. Taking Schiehallion again, for instance, the initial simulation model (upscaled from the geological model) has 50 metres by 50 metre cell size, and the cells in the history matched model have been upscaled to 200 metres by 200 metres for a faster history matching, whereas the lateral post-migration

seismic resolution is one quarter of the wave length (Sheriff, 1980; Brown, 2011), which is ~31.8m. The lateral resolution is higher than in the 3D simulation model.

To summarize the above description of seismic and simulation resolutions, we can say that: the 3D simulation model has higher vertical resolution but lower lateral resolution compared with the seismic data. That is why, in practice, mapped seismic is most likely to be utilised in the visualization and calculation of seismic data. In SHM, the simulated and observed seismic need to be matched at the same scale, and the normal way to do the matching, is by calculating a vertical average of the simulated seismic to produce seismic maps; then upscaling the observed seismic map into the simulation model scale (Figure 4-21).

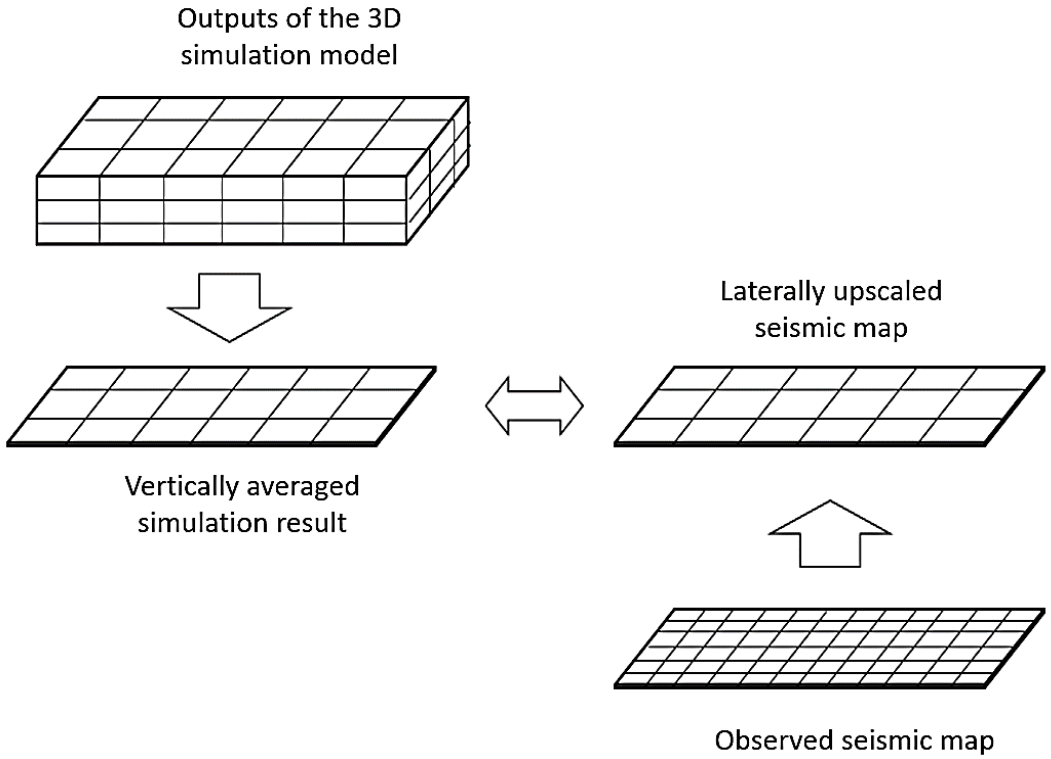

Figure 4-21 *Illustration of the common used way of comparing the simulated seismic with observed data.*

In this way, the vertical resolution of simulation model and lateral resolution of seismic data are partially sacrificed. If we only look at the simulation side, firstly the flow simulation is conducted on the 3D model, then the simulation results are averaged into 2D maps. In SHM this process will be repeated by iteration. Based on this analysis, a question could be: what if we vertically averaged the 3D model first, to get a 2D areal model, then used the 2D model in SHM to directly generate mapped results? In both approaches, the vertical resolution of the simulator needs to be sacrificed but the new approach could speed up the simulation procedure.

Furthermore, while vertically upscaling the simulation model, there is another option to perform lateral refinement at same time to enhance its horizontal resolution. In this way, the accuracy of simulation would be increased and become closer to that of the seismic domain. Considering the extra computation effort, the trade-off between accuracy and computation cost of this option has to be analysed carefully before making a decision.

All the above possibilities are the motivations for the areal model method. In the following sections, an explanation of how to build such an areal model for the Schiehallion Field will be presented. The upscaling error will then be formulated and the areal model results will be validated through a comparison with the 3D simulation outputs. The model upscaling technique is not the innovative point of this method; but, linking the 2D areal model with the seismic proxy and using them in the SHM is the main innovation of this work. My exploration is focused on the test of the accuracy and computation cost trade-off in the later parts of this chapter.

4.3.3 Building the areal model on Schiehallion

In this chapter an averaging method is applied to carry out vertical upscaling, which is the common method to perform model upscaling in petroleum industry (Christie et al., 1996; Fursov 2015). Upscaling of the continuous reservoir properties (NTG and porosity) is achieved by 'arithmetic mean' averaging with pore volume weighting (Equation 4.5). Upscaling of the discrete properties (geobody indices, equilibration regions) is realized using the 'mode' averaging (Equation 4.6).

$$P_{2D(x,y)} = [\sum_{z=1}^{n}(P_{3D(x,y,z)} \cdot V_{3D(x,y,z)})] \cdot [\sum_{z=1}^{n} V_{3D(x,y,z)}]^{-1} \quad (4.5)$$

$$P_{2D(x,y)} = mode(P_{3D(x,y,z)}, z = 1{:}n) \quad (4.6)$$

where $P_{2D(x,y)}$ denotes the property of the cell at (x, y) location in the 2D model; $P_{3D(x,y,z)}$ and $V_{3D(x,y,z)}$ denote the property and pore volume of the cell at (x, y, z) in the 3D model. For each 2D location (x, y), n represents the number of defined cells in the z-direction.

The dimension and computation cost of the history matched 3D model and corresponding 2D areal model are listed in Table 4-5. The visualisation of simulation results from the 3D and 2D models will be presented in the next section.

Table 4-5 *Comparison of 3D and 2D simulation models: model size and computational cost.*

	3D model	2D model
Dimension	$52 \times 14 \times 12$	$52 \times 14 \times 1$
Average cell size (in metre)	$200 \times 200 \times 5.2$	$200 \times 200 \times 62.3$
Total number of grid cells	8736	728
Total number of defined cells	7332	624
Computation cost (s)	607	476

4.3.4 Areal model: results

Having validated the linear assumption and built the proxy model, in this section I will qualitatively compare the simulation results of the 2D model with the 3D model from three aspects: the static reservoir property distribution, the dynamic mapped property distribution and well production profile.

After building the 2D areal model, it has to be checked: to what degree the reservoir characteristic has been changed from 3D model to 2D model. A first check was made on the distribution of the model parameters such as porosity, net-to-gross (NTG), permeability, etc. These static reservoir properties are often correlated to each other; for instance, in reservoir simulation the permeability could be approximately modelled through a linear quadratic function of porosity. Figure 4-22 shows the distribution of the NTG property which is important for seismic signal and fluid flow.

On the left are the lateral distributions of the NTG in the 3D (top) and 2D (bottom) models, and on the right are cross section plots. In the visual comparison, the 2D and 3D results are comparable, which is due to the fact that the reservoir is quite vertically homogeneous and confirms the assumption that the 2D model is sufficient for this field.

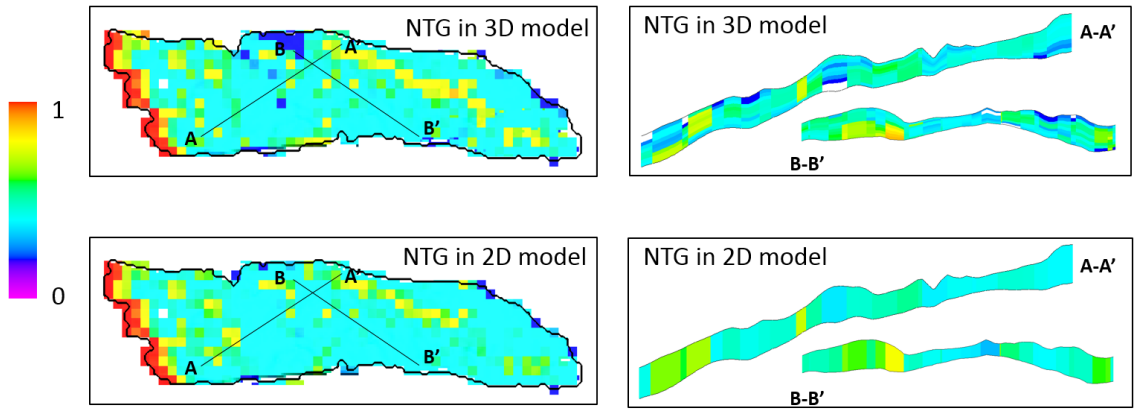

Figure 4-22 *of net-to-gross (NTG) of top reservoir: simulated by 3D model (upper) and by 2D model (lower). Left-hand column shows the lateral distribution and right-hand column shows the cross-section details.*

After running the flow simulation, I plotted the distribution of water saturation (ΔSw), as a dynamic simulation results of the two models (Figure 4-23). As with the previous comparison of the static property NTG, this comparison indicates that, after vertical upscaling, the 2D areal model and the reference 3D model generate very close dynamic results.

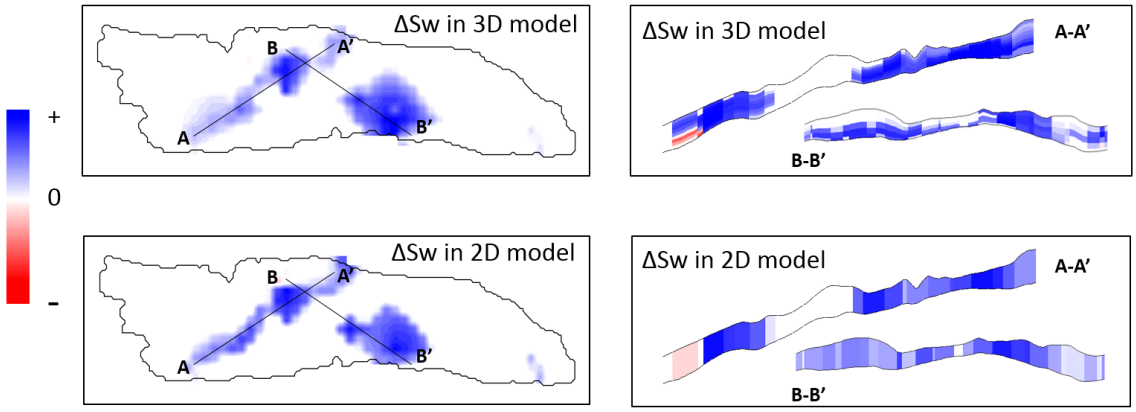

Figure 4-23 *Distribution of water saturation change (ΔSw): simulated by 3D model (upper) and by 2D model (lower). Left-hand column shows the lateral distribution and right-hand column shows the cross-section details.*

As well as the distribution of dynamic properties, another output of the flow simulation model is the well production profile. As introduced earlier, the bottom hole pressures (BHPs) of six producers are considered as the production data to match in SHM; therefore, the simulation results of these six producers are plotted in Figure 4-24. There is still no clear deviation between the results of the 2D and 3D models.

According to the above visual comparisons of the models, a conclusion can be made that the areal model is an effective approximation of the complex 3D model. From a more quantitative point of view, the upscaling error of the areal model needs to be formulated, and this will be done in section 4.4.

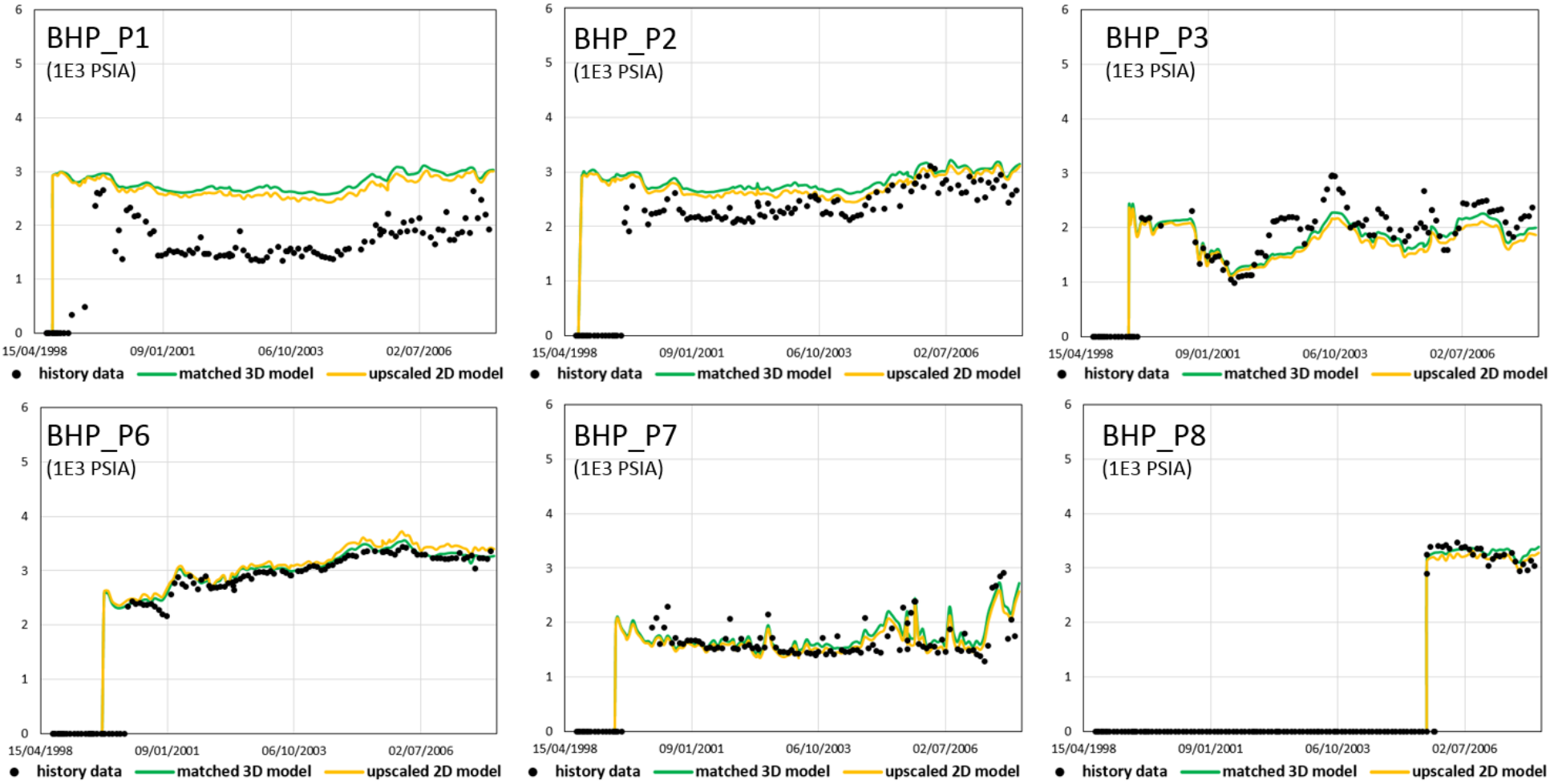

Figure 4-24 *History and simulation results of well bottom hole pressure (BHP) for the available 6 producers located in segment 4. The green line represents the results of a 3D simulation model, the yellow line represents the results of the areal proxy model.*

4.3.5 Coupling the areal model with the seismic proxy

Having the areal model as a proxy for the fluid flow simulator, one further question is how to couple this proxy with the seismic proxy model. Because in the SHM loop (Figure 4-1), the two simulators should work together to provide the simulation results in the well production domain and in the seismic domain (Figure 4-1). Section 4.3.1 described how a linear superposition model was built and validated for the Schiehallion field, but in that case a 3D grid-based flow simulation model was applied. In the case of the 2D model, a linear superposition proxy model will also be employed to simulate the synthetic seismic using the outputs of a 2D model. In other words, the linear equation will be used to calculate the mapped 4D seismic, based on the saturation and pressure change maps that are the direct outputs of the 2D model.

In the Figure 4-25, the saturation and pressure maps shown are the results of the 3D and 2D models, based on which a seismic proxy model was then used to produce the 4D seismic response. Qualitatively, the hardening and softening 4D anomalies in both 4D seismic maps (bottom two) are significantly correlated with each other. This because the input dynamic maps from the 2D and 3D simulation models are similar and the main patterns of property changes are preserved properly. The correlation coefficient of the two seismic maps (bottom two plots in Figure 4-25) is measured as r=0.78, indicating that the two procedures, '3D simulation + seismic proxy' and '2D simulation + seismic proxy', can work equally well in this case.

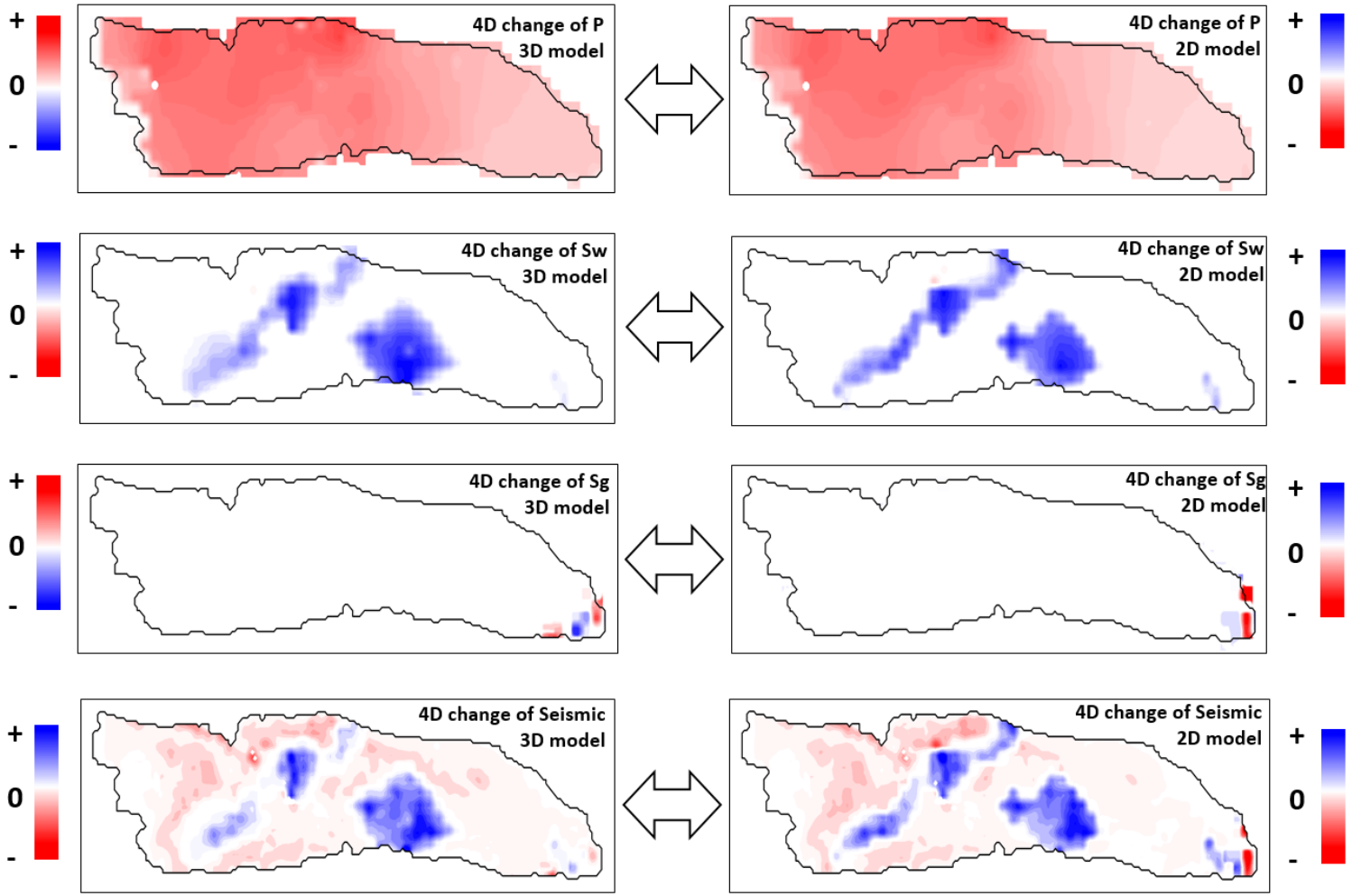

Figure 4-25 *Left column: pressure, water saturation and gas saturation changes and 4D seismic, simulated by using the 3D model; right column: pressure, water saturation and gas saturation changes and 4D seismic, simulated by using the 2D areal model.*

4.4 Proxy model quality

4.4.1 Metrics to quantify the proxy quality

To quantify errors which arise from vertical coarsening, I chose to compute the relative error in the 4D pressure, water and gas saturation change $(\Delta P, \Delta S_w, \Delta S_g)$ maps, and in the BHP profiles of the six producers. The definition of the error in the production profiles is based on the 'normalized absolute error' formulation (Equation 4.8), whilst the error in the mapped properties is based on the 'normalized square error' formulation (Equation 4.7) (Willmott and Matsuura 2005).

$$ERROR_{maps} = \frac{\sum(M_{3d,i} - M_{2d,i})^2}{\sum(M_{3d,i})^2} \times 100\% \tag{4.7}$$

$$ERROR_{curves} = \frac{\sum|M_{3d,i} - M_{2d,i}|}{\sum|M_{3d,i}|} \times 100\% \tag{4.8}$$

The $M_{3d,i}$ stands for the i^{th} data point (a point on the BHP curve or a cell value in the pressure map, etc.) of the 3D model simulation results, and $M_{2d,i}$ stands for the corresponding i^{th} data point of the 2D model outputs. The proxy quality has been quantified by the upscaling error metric in Table 4-6. These absolute values quantitatively indicate the errors resulting from the vertical upscaling. However, there is no well-accepted threshold in literature to define a 'huge error' or 'minor error'. Thus, the quality of the areal model needs to be further tested. Considering the target of developing this proxy is to assist the SHM procedure, in next section, the quality of the proxy will be tested in a blind test (quasi-SHM) on the Schiehallion field.

Table 4-6 *Upscaling error: from 3D model to 2D areal model.*

Property	Error type	Error (%)
ΔP	Map	7.85
ΔS_w	Map	9.10
ΔS_g	Map	11.15
$\Delta Seismic$	Map	8.79
BHP-P1	Curve	3.51
BHP-P2	Curve	3.18
BHP-P3	Curve	4.71
BHP-P6	Curve	2.57
BHP-P7	Curve	4.47
BHP-P8	Curve	3.33

4.4.2 Blind test

As aforementioned in Chapter 3, the blind test is a quasi-SHM workflow in which a reference model is first used to obtain the 'synthetic history data', then an ensemble of 30 scenarios are created by applying Latin Hypercube Sampling method (Iman, 2008). In Figure 4-26, the variance shown in the 4D seismic maps of all 30 models is a result of the variance of the S_w, S_g and P maps, which are initially affected by the input parameters. According to the variance shown in 4D seismic maps (Figure 4-26), it could be qualitatively assumed that the 30 scenarios are indeed 'different enough' with each other, thus can be used to conduct the blind test.

For each scenario, 3D model and 2D model are independently run and their outputs are then matched with the 'synthetic history data'. Thus, for each scenario, two sets of Objective Function (O.F.) value will be measured by Equation 4.9: one is calculated based on the 3D model results and the other on 2D model results. The effect of maps ($ERROR_{4\ maps}$) and curves ($ERROR_{6\ curves}$) are integrated into the Objective Function, so that the production data (BHP curves) and seismic data (in map) can be considered at the same time.

$$O.F. = (\sum ERROR_{4\ maps} + \sum ERROR_{6\ curves})/10 \tag{4.9}$$

Subsequently, the two set of objective function values were normalized to [0, 1], and plotted in Figure 4-27 (left). It is found that over all thirty scenarios, the normalised objective function values evaluated by the 3D and 2D models were close. To be quantitative, the two data-sets were then cross-plotted in Figure 4-27 (right). A correlation coefficient was measured as r=0.92; Spearman's rank correlation coefficient ρ=0.87; thus, both metrics are above 0.7, indicating significant correlation between the combination of '2D model + seismic proxy' with '3D model + seismic proxy'. It means that the 2D model and 3D model had 'equal' performance in the model ranking procedure. Based on the result of this blind test, the combination of '2D model + seismic proxy' will be further used in SHM in place of the '3D model + seismic proxy' sequence.

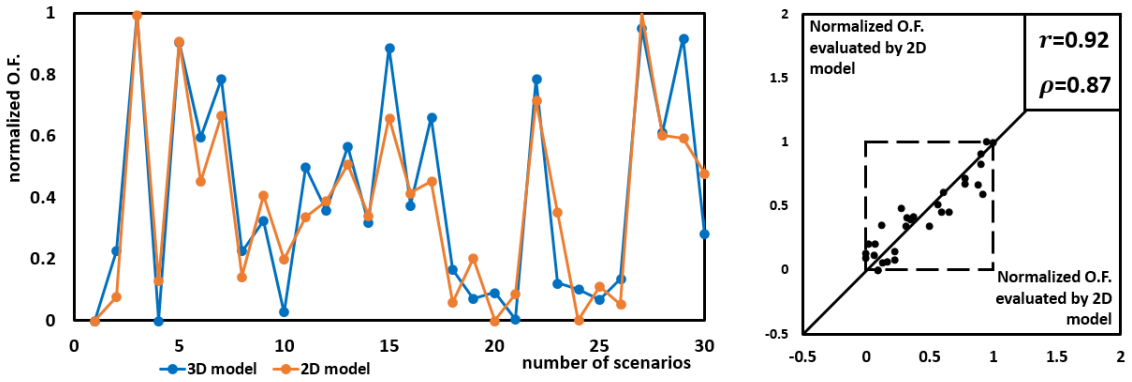

Figure 4-26 *Left: results of blind test, the objective function (misfit) evaluated by 3D model and 2D areal model; right: cross-plot of the misfit value ('2D model + seismic proxy' versus '3D model + seismic proxy').*

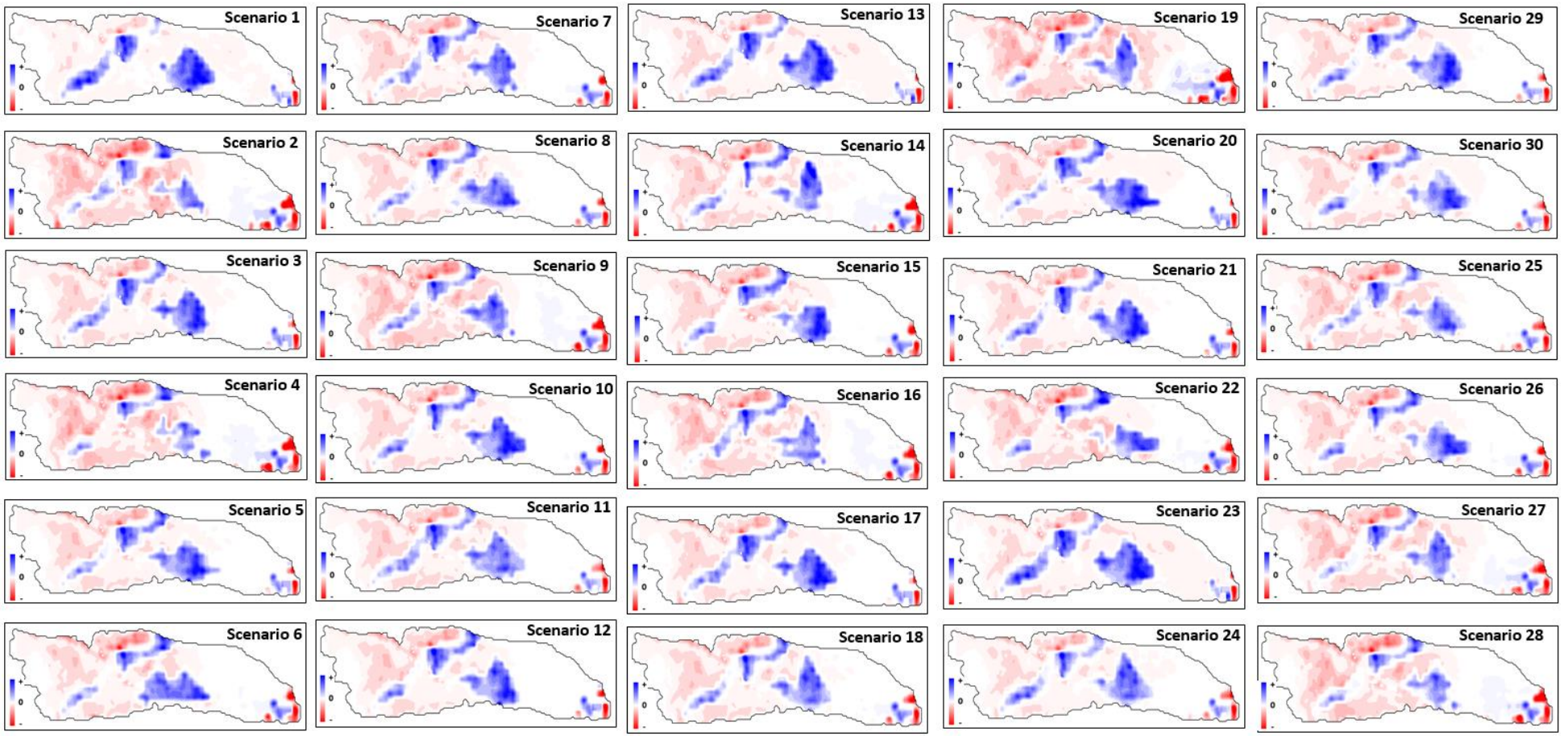

Figure 4-27 *Simulated 4D seismic from the proxy model of all 30 scenarios.*

4.5 Horizontal refinement of the areal model

In former sections, a vertical averaged areal model has been successfully built and tested. In section 4.3.2 I also came up with an option to build a vertically upscaled and horizontally refined areal mode. By increasing the lateral resolution, such a laterally refined areal model could remain consistent with seismic data resolution and could enhance the simulation results. In this section I will evaluate this option by comparing it with a vertically averaged areal model: how much is the difference between these two options and how much extra computational cost does the second option need.

The model is built based on the vertically averaged model: each cell is further refined into 4×4 cells. The dimension and computation cost of the two models are compared in Table 4-7.

Table 4-7 *Comparison of the first 2D areal model and XY-refined 2D areal model: model size and computation cost.*

	Vertically averaged areal model	Vertically averaged areal model with lateral refinement
Dimension	$52 \times 14 \times 1$	$208 \times 56 \times 1$
Average cell size (in metre)	$200 \times 200 \times 62.3$	$50 \times 50 \times 62.3$
Total number of grid cells	728	11648
Total number of defined cells	624	9984
Computation cost (s)	476	1239

When it comes to the model accuracy, as with the procedure introduced in section 4.3.2, it needs to be checked that to what degree the reservoir characteristic has been changed. Visualizations of the static and dynamic properties (NTG and ΔSw) are plotted in Figure 4-28. It can be observed from this figure that the lateral distributions of static and dynamic properties in the two models have no clear difference, and similar with the vertical sections. Thus it can be concluded that the laterally refinement did not provide more accurate reservoir characteristics when compared with the 2D model without lateral refinement.

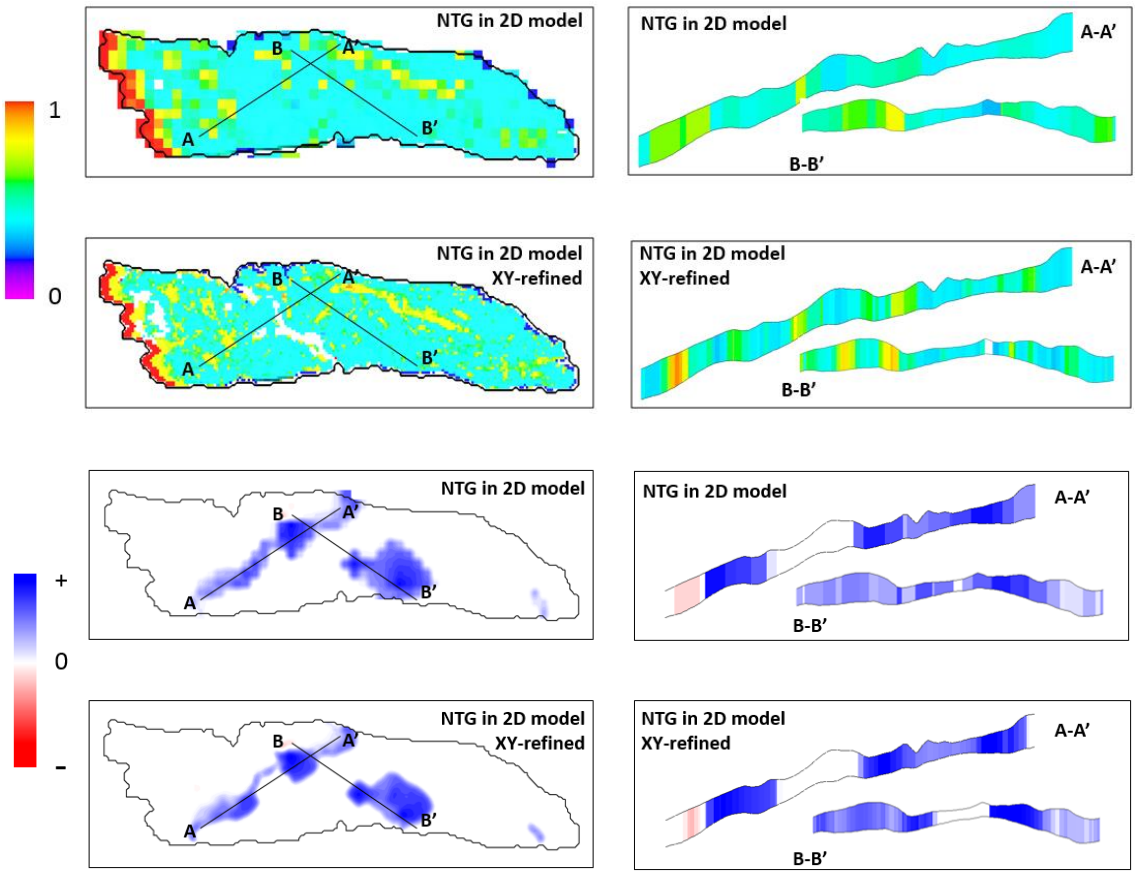

Figure 4-28 *Upper four plots: distribution of net-to-gross (NTG): simulated by the previous 2D model without XY-refinement (upper) and by the XY-refined 2D model (lower). Left column shows the lateral distribution and right column shows the cross-section details. Lower four plots: distribution of water saturation change (ΔSw): simulated by the previous 2D model without XY-refinement (upper) and by the XY-refined 2D model (lower). Left column shows the lateral distribution and right column shows the cross-section details.*

Along with the mapped properties, the well BHP profiles comparison was presented in Figure 4-29. The seismic proxy was then coupled with the areal model to produce the 4D seismic maps, the comparison between the 2D models with and without lateral refinement was made in Figure 4-30. Similar results could be found in both figures as in the property distributions comparison: these two 2D models generated very similar results. To be more quantitative, the differences between two areal models were quantified by the metrics which were used to check the proxy quality (Table 4-8). These visual comparisons (in Figure 4-28 and 4.29) and measured metric values imply that, after lateral refinement, the areal model has similar pattern with no significant difference: at least the main features presented in the 3D/2D model results are very comparable.

Table 4-8 *Error between the 2D areal models with and without XY-refinement..*

Property*	Property type	Difference (%)
ΔP	Map	5.21
ΔS_w	Map	7.99
ΔS_g	Map	9.10
$\Delta Seis$	Map	7.71
BHP-P1	Curve	2.09
BHP-P2	Curve	1.92
BHP-P3	Curve	2.17
BHP-P6	Curve	1.55
BHP-P7	Curve	2.64
BHP-P8	Curve	1.89

**Note: the mapped results from the reference 2D model were downscaled to keep same cell number with the refined areal model.*

As a summary, taking the trade-off between model accuracy and computation cost into consideration, the lateral refinement model brings marginal improvement of model accuracy, but requires higher cost. Thus, the lateral refinement method is not recommended to do SHM in this field, rather, the previous 2D model which was built by vertical averaging is a more suitable option.

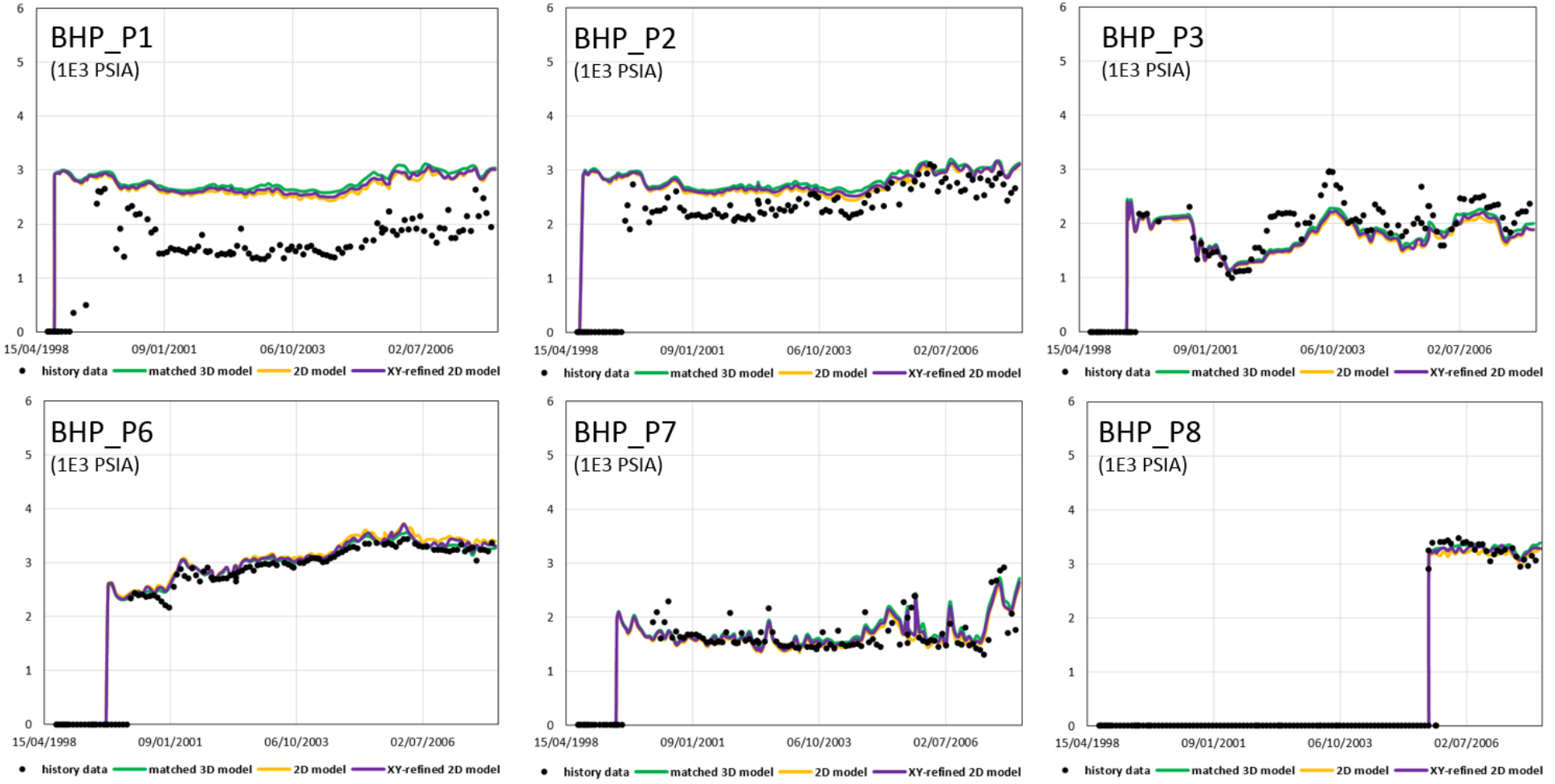

Figure 4-29 *History and simulation results of well bottom hole pressure (BHP) for the available 6 producers located in segment 4. The green line represents the results of a 3D simulation model, the yellow line represents the results of the areal proxy model, and the purple line represents the XY-refined areal model.*

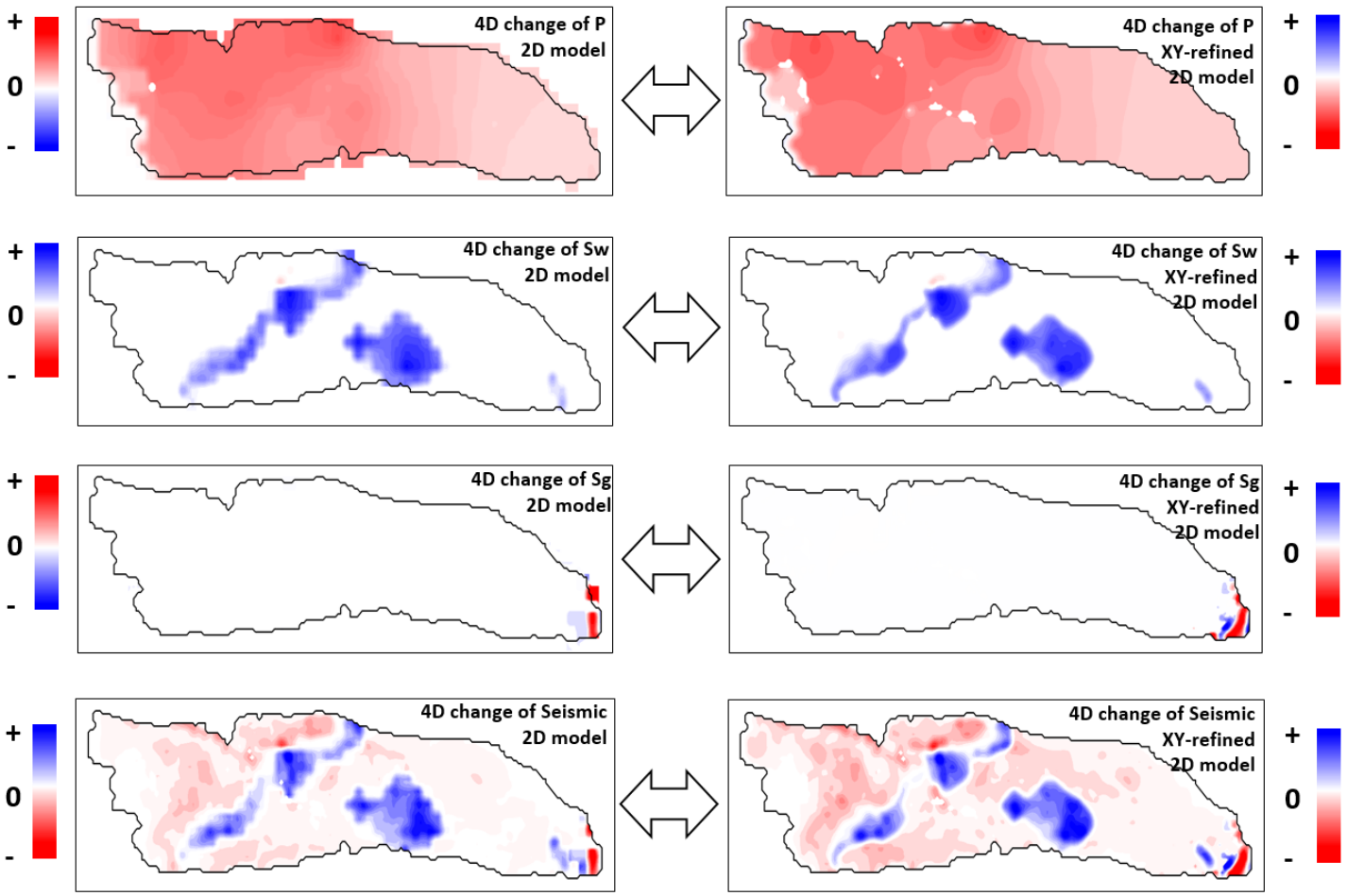

Figure 4-30 *Left column: pressure, water saturation and gas saturation changes and 4D seismic, simulated by the first 2D areal model; right column: pressure, water saturation and gas saturation changes and 4D seismic, simulated by the XY-refined 2D areal model..*

4.6 Summary

In this chapter an areal model was developed as a proxy for the 3D flow simulator used in SHM. It is a vertical average of the 3D model, designed to speed up the simulation and retain certain simulation accuracy. The geology of thin reservoirs and nature of seismic resolutions are the main motivations of this method. The areal model has been compared visually and by upscaling error quantification. Qualitatively and quantitatively, the areal model has been proven to be a good simplification of the base case 3D model, with lower computation cost. The quality of the areal model was then tested in a blind test on Schiehallion. It was observed that the 3D model and areal model work almost identically in ranking the candidate models. Finally, the vertically averaged areal model was refined laterally (in XY direction). The results show that the further laterally refinement of the areal model brings marginal improvement in accuracy but consumes more time; thus is not recommended for future SHM usage.

Additional benefit of the linear seismic proxy found through this procedure is that it can be applied to volumes and maps. However, the physics-based sim2seis model can only be applied to the 3D model. This also forms the main thread of this thesis: the seismic proxy is first introduced in 3D application, and is then applied together with the 2D areal flow simulation proxy and 0D tank model, which will be introduced in the next chapter.

Chapter 5

Flow simulation proxy model II: tank model

In Chapter 4, a 2D areal model was built on the Schiehallion field as a proxy for the 3D fluid flow simulation model. In this chapter, that 2D areal model is further 'upscaled' to a 0D multiple tank model (MTM) with material balance as a key control. This MTM is the second model I have built in this thesis as a proxy for the reservoir fluid flow simulator which is used in the SHM workflow. It will work together with the seismic modelling proxy and this combination of 'MTM + seismic proxy' is the main innovation point of this method. This procedure will be compared with the '3D model + seismic proxy' workflow, following a similar workflow to that used in Chapter 4: from model building, qualitative comparison to blind test and robustness analysis. The main observation is that, for the Schiehallion field, the 'MTM + seismic proxy' can reproduce similar results to the '3D mode + seismic proxy'; however, considering the model's accuracy, complexity and computational cost, this proxy is not as powerful as the 2D areal model on the Schiehallion field. The potential use of this method in SHM will be further tested in Chapter 6.

5.1 Motivation

As introduced in Chapter 1, the motivation for developing the proxy model came from the need to speed up the HM process and to help facilitate the communication between experts. The test on the Schiehallion field indicates that the 2D areal model can work as an effective proxy for the 3D simulator. Going further in this direction, one possible question would be whether the proxy can consist of lower-dimension models. Recalling the issue discussed in Chapter 1 that to what extent the conventional model can be simplified to do a proper history matching, I selected the 0D multiple tank model (MTM) as a potential candidate to test in this chapter. The motivation to apply this MTM came from the fact that the material balance model was successfully used in the early life of the Schiehallion field. Based on that, a seismic proxy model was initially built and connected with the MTM to produce well production profiles and 4D seismic response in SHM workflow.

5.1.1 Review of the multiple tank model used in Schiehallion

The value of material balance models in understanding the field dynamic performance of Schiehallion has been demonstrated by Dobbyn and Marsh, 2001. In the early life of the field, when a more complex 3D flow simulation model was not built, engineers found that the reservoir did not perform in line with the predictions prior to development. The possible reason for this mismatch was considered to be that the degree of connectivity within the reservoir was over-predicted. Thus the prediction of the extent to which the injectors were supporting the producers might be much higher than the truth.

Material balance was used to explore the reasons for this mismatch, because of its simplicity and rapidity in obtaining indicative results: this method was developed in an attempt to come quickly to a better understanding of the connectivity within the field. The field was subdivided into ‘tanks’ based on the location of the wells (one well is located in one tank) and material balance models were constructed for each tank. Tank boundaries came from the interpretation results of static seismic and an extended well test (EWT). The configuration of each tank such as the STOIIP, was estimated based on the appraisal wells. Figure 5-1 shows the tank boundaries. The models were used to test possible interpretations of the dynamic performance and to provide inter-well connectivity analysis. In this workflow, 4D seismic data were also used to calibrate the MTM prediction results.

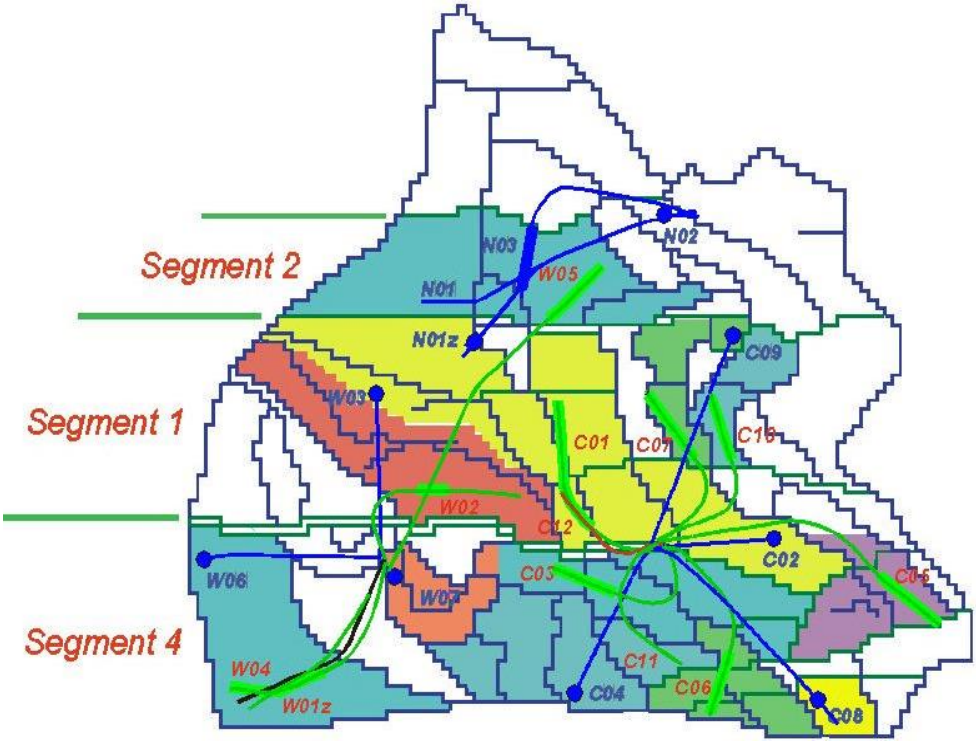

Figure 5-1 *Field layout and interpreted compartmentation of Schiehallion. The wells marked by green lines are producers and those marked by blue dots are injectors. Different colours indicate compartments and the dark blue lines are the tank boundaries (Dobbyn and Marsh, 2001).*

Specifically, the tanks were made to communicate with each other, controlled by a 'leakage factor' (or 'transmissibility multiplier'). The three main control parameters over the model are 1) the number, boundary, and configuration of the tanks; 2) the STOIIP of each tank; 3) the leakage factor applied to each pair of neighbouring tanks. The determination of the first two controls was introduced in the previous paragraph, and the final control, the leakage factor, needed to be determined through a history matching procedure: given a set of leakage factors, the MTM could make predictions of well production which would then be matched with the observations. After this history matching workflow, the 'best' solution for the leakage factor could be obtained. Considering the physical meaning of these factors, which was controlling the communication between two neighbouring tanks, the connectivity between an injector and a producer could be evaluated. However, because history matching is an inverse problem, plus the fact that tank boundaries could be interpreted in different ways, different history-matched scenarios could be obtained. In this case, 4D seismic could be used as an extra constraint to screen out the less possible scenarios.

A good example was given by Dobbyn and Marsh, 2001. In segment 4, the effect of injectors W07 and C04 on producer C03 was a key question to answer in order to understand the reservoir connectivity. Two multiple tank scenarios were built and both matched well with the C03 BHP profile (Figure 5-2). Scenario 1 indicated that 77% of the water supplement came from well W07; however, in scenario 2, this number was 86%. By analysing the 4D anomaly between C03 and W07 and C03 and C04, the results showed that a clear hardening 4D signal was found between C03 and W07, whereas there was no strong response around C04. The hardening signal was interpreted to be as a result of water flooding; thus scenario 2 was regarded as more reliable. In this study, 4D seismic helped to enhance the history matching results after the well production history matching. In the next section, I will present a new way of integrating well and seismic data in the SHM workflow.

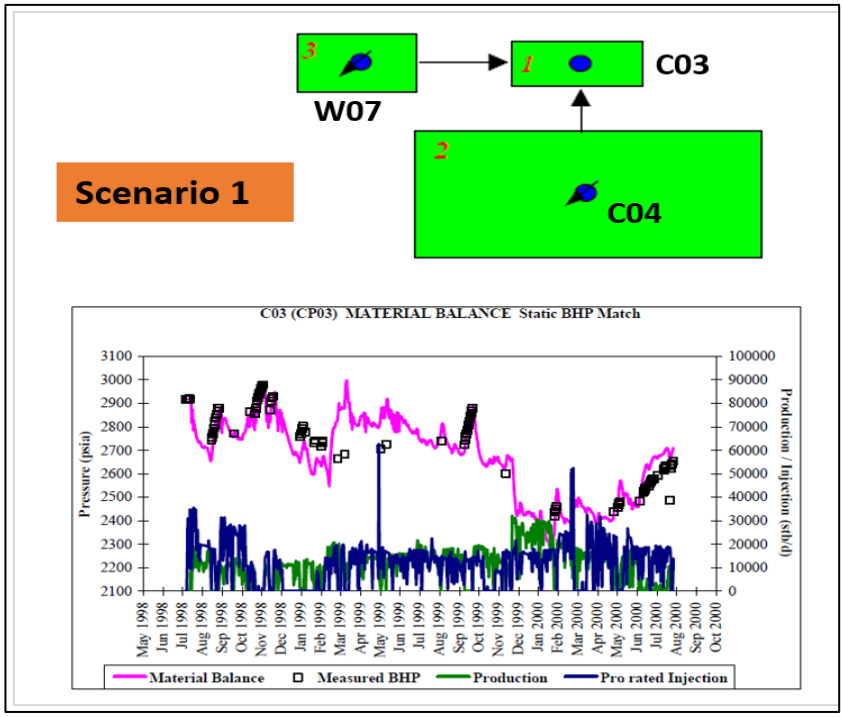

Figure 5-2 *Field layout and interpreted compartmentation of Schiehallion. The wells marked by green lines are producers and those marked by blue dots are injectors. Different colours indicate compartments and the dark blue lines are the tank boundaries. Two scenarios that matched equally well with well production observation (Dobbyn and Marsh, 2001).*

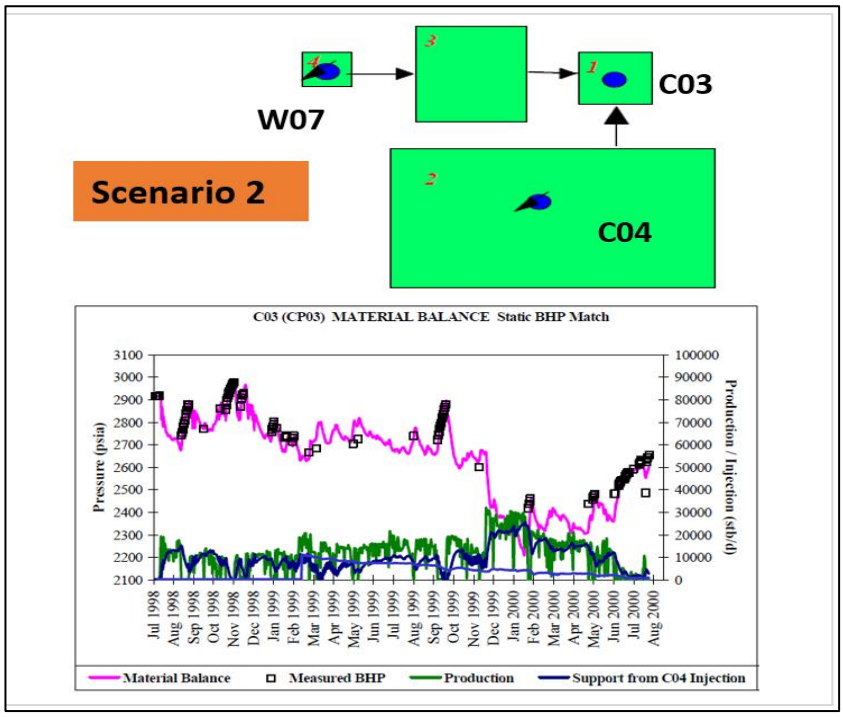

Figure 5-2 *(duplicate) Field layout and interpreted compartmentation of Schiehallion. The wells marked by green lines are producers and those marked by blue dots are injectors. Different colours indicate compartments and the dark blue lines are the tank boundaries. Two scenarios that matched equally well with well production observation (Dobbyn and Marsh, 2001).*

5.1.2 Building material balance model in the late field life

In the late life of Schiehallion, the reservoir management focus has shifted to managing sweep efficiency and controlling water cut (Govan et al., 2006). Optimising the water-injection distribution through available wells is the main considered approach, which requires a good understanding of reservoir connectivity and the supporting of injectors to producers. The evaluation of connectivity is always involved, as there are always new data available.

At this stage, the 3D simulation model has been built and more 4D surveys have been obtained. Seismic history matching is processed by integrating simulated well production profiles and modelled 4D seismic response (see Figure 3-1). As explained in Chapter 4, hundreds of geobodies have been interpreted and embedded in the Schiehallion 3D model. Such fine geobodies can be grouped and merged to form the ‘tanks’ and the associated STOIIP of each tank can be easily calculated from the 3D grids. Thus, at this present stage, the building of the MTM becomes easier than in the early life, when the tank boundaries and STOIIP data had to be estimated indirectly.

On the other hand, as a drawback, these complex simulation models are slowing down the SHM workflow; thus, this motivates the idea of applying the MTM, which used to be an effective and efficient tool. However, in the previous study the MTM could only reproduce the well production simulation results without the seismic results. Therefore, a new approach needs to be designed to integrate the MTM and 4D seismic in the SHM workflow.

5.1.3 Integration of 4D seismic and tank model: a new way

As mentioned above, if the 3D flow simulation model is replaced by the MTM, then a sim2seis model is needed to produce the seismic simulation results, based on the outputs of the MTM. Unlike the outputs of a 3D model, which are grid-based maps, the MTM can only provide the averaged pressure and fluid volume change of each tank. As introduced in Chapter 4, the conventional sim2seis model is performing a grid based calculation: from impedance calculation to modelling of seismic wiggles. Thus it cannot be used with the MTM. However, the linear superposition seismic proxy model can work without a grid-based model. The inputs are changes of pressure and saturation which can be in the format of 3D volume, 2D map or 0D tank, and the output, 4D seismic, can also be in 3D volume, 2D map or 0D tank format.

This dimensionless property of sim2seis proxy is well-matched with the tank model: the outputs of the multiple-tank model are pressure changes and fluid volume changes which can be directly used by the sim2seis proxy as model inputs. Subsequently, each tank would be assigned with one 4D change response. If the observed seismic is also upscaled to ‘tank’ scale (each tank has one averaged 4D response), then the history matching can be carried out between simulation and observation. Considering that the well production simulated by the tank model could be compared directly with observation, the combination of ‘MTM + seismic proxy’ can provide all the simulation results which are needed to perform SHM.

In this way, compared with the situation in the early life of Schiehallion, the 4D seismic data can be used in a more quantitative way to be integrated with well production data. Having introduced ‘seismic proxy’ in Chapter 3 and ‘areal model + seismic’ in Chapter 4, the combination of ‘MTM + seismic proxy’ is the final workflow for a proxy model based SHM that I have developed in this thesis.

5.2 Methodology

The material balance model was introduced in Chapter 2. In most applications of this method, the whole reservoir will be regarded as one tank, in which fluid properties and pressures are averaged over the entire reservoir. Variations in many properties, for instance, a change in porosity as a function of depth, cannot be handled adequately. The degree to which the results of a material balance calculation are invalidated depends on the magnitude of such variations: if these properties have high variation over the entire reservoir laterally or vertically, then, regarding the whole as one tank might not produce reliable results. Additionally, although the average fluid volume is easy to calculate from the tank model, it is difficult to infer how the fluid is distributed: for instance, whether the remaining oil is spread more or less evenly over the entire reservoir, or is concentrated in some localised areas.

In order to reduce the ambiguities resulting from regarding the entire reservoir as a tank, a Multiple Tank Model (MTM) is introduced in this chapter. By subdividing the reservoir into multiple tanks, the heterogeneity of the property distributions could be represented to a higher degree. Additionally, in order to describe the working mechanism of the MTM, three sub-models are introduced independently: 1) a single tank model, 2) a well model and 3) a tank communication model. Details of each model are given in the following sections.

5.2.1 Single tank model

The single tank model, as its name would suggest, describes the relationship between fluid volume changes and pressure change after a production period occurred in one single tank. This relationship is calculated on the basis of four assumptions:

Pressure: inside each tank the pressure is assumed as constant throughout the tank at a particular time. According to production engineering knowledge, there should be large pressure gradients between producers and injectors. Therefore, the injectors and producers should be assigned to different tanks to avoid averaging clearly distinct pressure regions in one single tank.

Temperature: the reservoir is considered as isothermal during production or injection, unless major external temperatures are imposed through, for example, thermal recovery processes and, in some cases, large cold water injection schemes. In this study the reservoir temperatures are assumed as constant during production.

Production rate: The production rates are assumed as constant ratios of fluid volume changes to the production period lengths. The historical injection or production rate data have been embedded in the 3D model and will be used in this tank model. By multiplying the rate by the length of time of the period, I can calculate the fluid volume change of the single tank in each time step.

Representative PVT data: In the 3D model, each cell has its pore compressibility coefficient values, and the fluid volume factors are also assigned to each cell according to the saturation of water, oil and gas. In the tank model, such PVT properties of each single tank are also assumed as the average (arithmetic mean) of the property values of all the cells inside each tank.

Based on these assumptions, a general material balance equation was given by Ahmed, 2006 (Equation 5.1) for a single tank which has three-phase fluid volume changes (Figure 5-3).

$$B_w(W_e - W_p) + (G - G_{pc})B_g - GB_{gi} + \frac{(C_f + C_w S_{wc})\Delta P N B_{oi}}{(1 - S_{wc})} = NB_{oi} - ((N - N_p)B_o + (NR_{si} - (N - N_p)R_s - G_p)B_g) \quad (5.1)$$

The physical meaning of each term in the equation is:

1) $B_w(W_e - W_p)$: net water volume change;

2) $(G - G_{pc})B_g - GB_{gi}$: gas cap volume change;

3) $\frac{(C_f + C_w S_{wc})\Delta P N B_{oi}}{(1 - S_{wc})}$: pore volume change;

4) NB_{oi}: original oil volume;

5) $(N - N_p)B_o$: oil volume at current pressure;

6) $(NR_{si} - (N - N_p)R_s - G_p)B_g$: free solution gas volume change;

A detailed nomenclature is given in Table 5-1. In this table I also present how these parameters were obtained or calculated when I built the tank model based on the 3D model.

Table 5-1 *Nomenclature of Equation 5.1 and corresponding industry and SI (International System of Units) units. The last column lists how the parameter values were obtained or calculated.*

Symbols	Meaning	Industry units	SI units	Data source
B_{gi}	Initial gas formation volume factor	bbl/SCF	M^3/SCM	3D model PVT input
B_g	Gas formation volume factor	bbl/SCF	M^3/SCM	Function of pressure, given by the 3D model
B_{oi}	Initial oil formation volume factor	bbl/STB	M^3/STM^3	3D model PVT input
B_o	Oil formation volume factor	bbl/STB	M^3/STM^3	Function of pressure , given by the 3D model
B_t	Total formation volume factor	bbl/STB	M^3/STM^3	3D model PVT input
B_w	Water formation volume factor	bbl/STB	M^3/STM^3	3D model PVT input (constant)
C_f	Pore compressibility	vol/vol/psi	vol/vol/MPa	3D model PVT input
C_w	Water compressibility	vol/vol/psi	vol/vol/MPa	3D model PVT input
G	Initial gas cap volume	SCF	SCM	Calculation from 3D model
G_p	Cumulative gas produced	SCF	SCM	Well history data
G_{pc}	Cumulative gas cap produced	SCF	SCM	Calculation from 3D model
N	Stock tank oil initially in place	STB	STM^3	Calculation from 3D model
N_p	Cumulative tank oil produced	STB	STM^3	Well history data
ΔP	Change of average reservoir pressure	psi	MPa	To be determined
R_{si}	Initial solution gas/oil ratio	SCF/STB	SCM/STM^3	Calculation from 3D model
R_s	solution gas/oil ratio	SCF/STB	SCM/STM^3	Function of pressure, given by the 3D model
S_{wc}	Average connate water saturation	fraction	fraction	Calculation from 3D model
W_e	Cumulative water influx	bbl or STB	M^3 or STM^3	To be determined
W_p	Cumulative water production	bbl or STB	M^3 or STM^3	Well history data

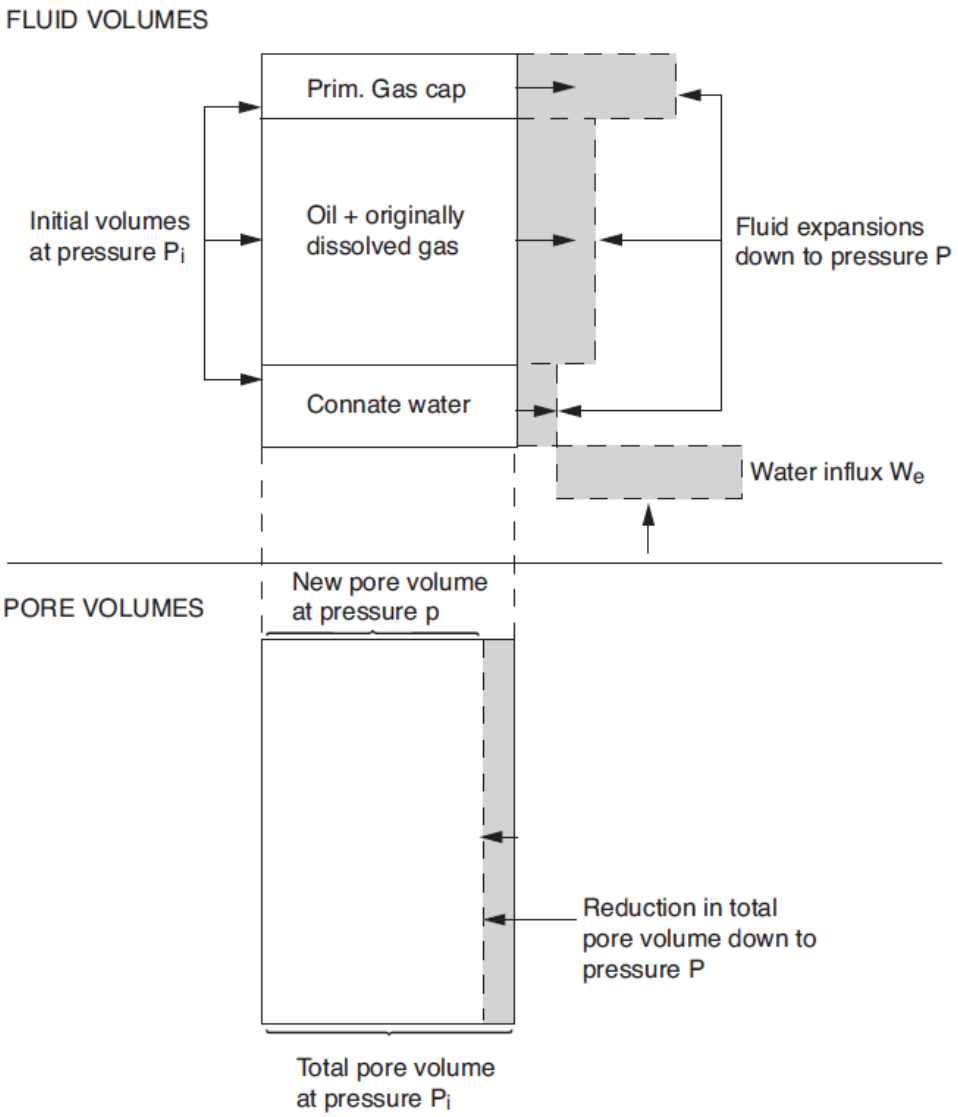

Figure 5-3 *Material balance by equating sub-surface expansion to fluid production (Reservoir Engineering Text Book, IPE, 2015).*

As illustrated in Table 5-1, all the parameter values can be calculated according to the 3D reference model except the pressure change (ΔP) and water influx (W_e). If there is no clear water influx from the outer aquifer, then, given the history of well injection or production data, the fluid volume changes could then be calculated, and then, according to Equation 5.1, the pressure change of each tank could be determined. Thus, this is the function of the single tank model: given the fluid volume changes, the model can simulate the tank pressure changes.

To summarise the single tank model, it consists of:

- Input: 3D reference model, well history rates (function of time), and known water influx.
- Output: average pressure of each tank (function of time).

5.2.2 Well model

Based on the single tank model, the average tank pressure could be linked with the well production or injection rates. In the real world, however, the average reservoir pressure can only be measured at the well shut-in time, thus only limited average reservoir data are available to carry out history matching. However, the well bottom hole pressure (BHP) data are more available for history matching. Therefore, a well model is built to connect the average tank pressure to the well bottom hole pressure (BHP).

According to the definition of the well productivity index (PI, Terry et al., 2013):

$$PI = \frac{q}{P - BHP} = \frac{2\pi Kh}{\mu \cdot \left(\ln(^{r_t}/_{r_w}) + S\right)} \tag{5.2}$$

where q is production rate, P is the reservoir average pressure, K indicates the average reservoir permeability, h is the reservoir thickness, μ is the fluid viscosity, $^{r_t}/_{r_w}$ is the ratio of effective reservoir (tank) radius and wellbore radius, and S is the skin factor.

In these parameters, q is the well production or injection rate which can be inputted from the 3D model history; K can be calculated based on empirical relationship with the mean porosity (arithmetic mean) over the cells enclosed by the tank boundaries. Similarly, average reservoir thickness h can be assigned to each tank. r_w and S can be directly obtained from well configurations in the simulation model. Only the effective tank radius, r_t, cannot be directly obtained. Because the tank boundaries are irregular polygons, I calculated its radius by this approximation (Figure 5-4, A):

$$r_t = 2\frac{S}{L} \tag{5.3}$$

This approximation was derived from the relationship between the radius, area and length of side of circles ($S = \pi r^2$ and $L = 2\pi r$). The tank polygons are drawn in the 3D model, thus its area and length of side could be calculated by counting the involved cells, and then the tank radius (r_t) could be calculated by Equation 5.3.

With the above analysis, in Equation 5.2, only average tank pressure P and BHP of the wells are flexible. Given the P (average tank pressure) as input, this well model can produce well BHP as output.

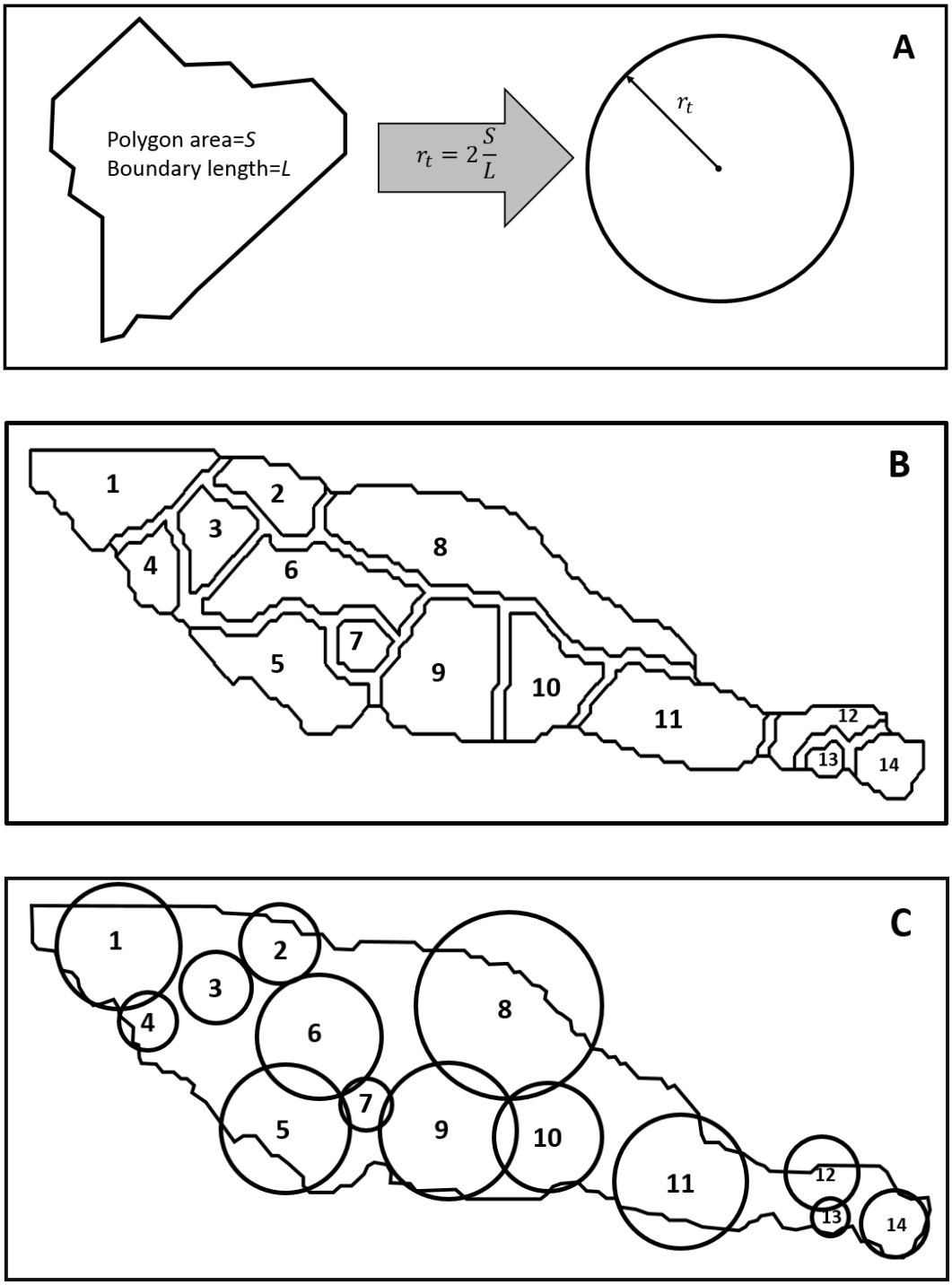

Figure 5-4 *A) Transforming from an irregular polygon to an effective circle whose radius is calculated by the Equation 5.3. B) Boundaries of one example MTM which has 14 tanks in total. C) The effective circles of all the 14 tanks: the centroid of an irregular polygon is determined by a 'Centroid Function' developed in Matlab, 2017; the radius of each circle is calculated by the Equation 5.3.*

5.2.3 Tank communication model

The strength of the MTM is its ability to represent the communication between regions (tanks) of the entire reservoir. Having obtained the single tank model and well model, the last stage to reach this goal is to build a function to control the communication (fluid and pressure transfer) between tanks. In the reservoir engineering domain, the control equation for fluid flow through a porous medium at core scale is Darcy's Law (Equation 5.4, Darcy, 1856):

$$q = \Delta P \cdot \frac{KA}{\mu L} \tag{5.4}$$

Darcy's law states that fluid flow rate is directly proportional to the pressure gradient between two places in the medium, the medium's permeability and its cross-section area; and is inversely proportional to the distance between them and fluid viscosity. The function of the tank communication model is to determine the fluid transfer between tanks under a certain pressure gradient, and I used the insights provided by Darcy's Law to build this model. In the tank communication model, the volume of fluid transferred between tanks is assumed as directly proportional to the pressure gradient between tanks, the average permeability and their contact area, and is inversely proportional to the distance between the centroid of two tanks and the fluid viscosity. This relationship will be constructed by an equation later in this section.

Before touching this equation, an important concept, 'active tank', first needs to be introduced. In previous sections, the single tank and the well model have been built to link the well production rate data with average tank pressure. Those tanks, which have fluid flow in or out, through an injector or producer, are defined as 'active tanks'. After simulating the pressure change caused by the fluid flowing in or out by the tank model, there will be pressure gradients between these active tanks and their neighbouring tanks. Therefore, under the pressure gradient there would be fluid flowing between active tanks and the neighbouring tanks; thus, these neighbouring tanks are activated. After this iteration the 'active tank' labels are assigned to a larger group of tanks (Figure 5-5). When the fluid transfer boundary reaches the reservoir border, all the tanks are marked as 'active tank' and this transferring process is stopped.

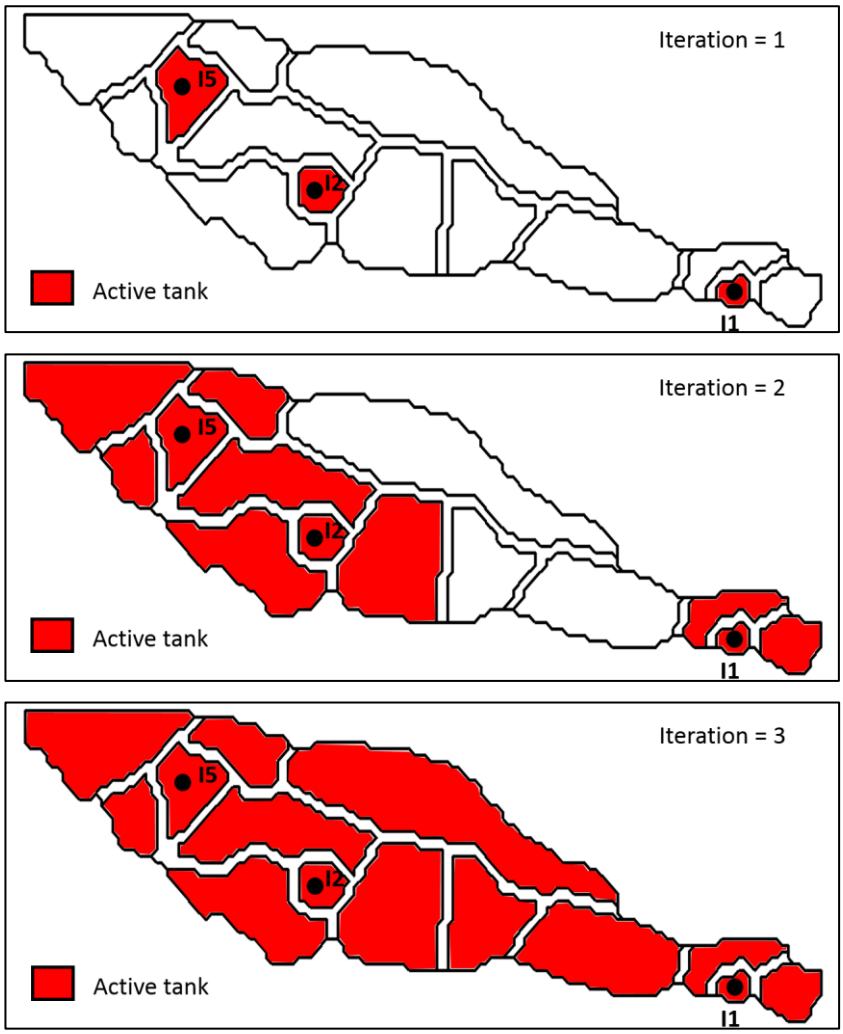

Figure 5-5 *Illustration of the expanding of the 'active tanks'. In iteration 1, only the tanks which have a connection to injectors or producers are activated. In iterations 2 and 3, the neighbouring tanks to the active tanks in the previous iteration are further activated. After these three iterations all tanks are activated.*

In the fluid transfer process described above, there is a key question about how to simulate the exact volume of fluids that would be transferred between an active tank and its neighbouring tanks. The tank communication model is designed to answer this question. As mentioned above, the insights to build this model were brought from Darcy's Law and I have constructed them into one equation set (Equation 5.5). As shown in Figure 5-6, given that the active tank has three neighbouring tanks, the next step is to determine how much of the volume change of fluids occurring in an active tank (ΔV_a) will be transferred to its neighbours (ΔV_{ai}) and how much will be reserved in the active tank after the transfer (ΔV_{aa}).

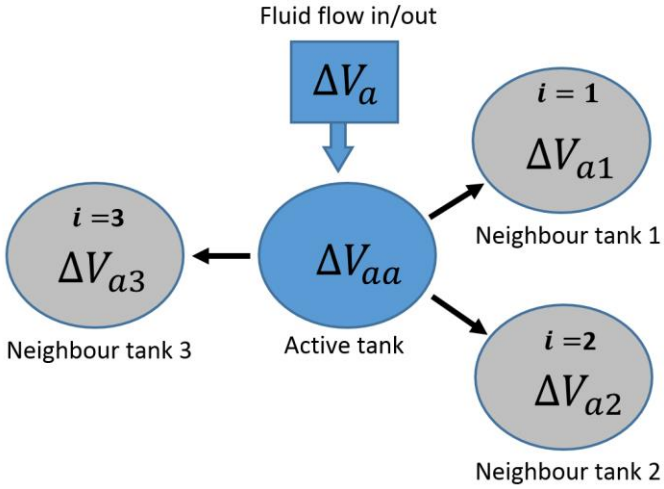

Figure 5-6 *Illustration of the fluid volume transfer between an active tank (in blue) with its three neighbouring tanks.*

Equation set 5.5 is transformed from Darcy's Law to simulate the fluid transfer between tanks. In this equation, the directly proportional and inversely proportional relationships are retained, as in Darcy's Law. The innovative details are: 1) the volume of fluid transferred from the active tank to its i^{th} neighbouring tank (ΔV_{ai}) is a proportion of the volume change that occurred within the active tank (ΔV_a). The proportion is determined by $[\Delta P_{ir} \cdot \left(\frac{KA}{\mu L}\right)_{ir} \cdot T_{ai}]$, in which the pressure gradient factor and the second factor are both 'relative'. I will explain later how to determine such relative parameters and why they are needed. 2) A third factor, T_{ai}, was included in the equation. This item describes the transmissibility between connected tanks; thus, the topological relationship of the tanks should be used later to determine how many pairs of connected tanks there are. As an advance notice, this item is what I will perturb during the SHM workflow.

$$\begin{cases} \Delta V_{ai} = [\Delta P_{ir} \cdot \left(\frac{KA}{\mu L}\right)_{ir} \cdot T_{ai}] \cdot \Delta V_a \\ \sum_i \Delta V_{ai} = \Delta V_a - \Delta V_{aa} = \left(1 - C_{res,a}\right) \cdot \Delta V_a \end{cases} \tag{5.5}$$

Besides the first equation of this set, there is a second one, which indicates that after the fluid is transferred to all the neighbouring tanks ($\sum_i \Delta V_{ai}$), there would be ΔV_{aa} volume of fluids reserved in the active tank. The reserved volume of fluid is also a proportion of the initial volume change which occurred in the active tank (ΔV_a) and this proportion is determined by the parameter $C_{res,a}$. This parameter is a function of the reservoir properties inside a tank (e.g. heterogeneity, average porosity or NTG) and the tank size; thus, each tank has its own $C_{res,a}$ value. Moreover, as an advanced notice, this set of

parameters will be determined in the model building stage, and will then be regarded as static parameters and kept constant during the SHM.

After the general introduction of the equation set, it has to be explained how to determine the parameters involved in the first equation. As mentioned before, the directly and inversely proportion relationships are retained in this equation as in Darcy's Law. However, unlike in Darcy's Law, the pressure gradient ΔP_{ir} is not the pressure difference between two tanks, but a relative pressure gradient which is defined by Equation 5.6.

$$\Delta P_{ir} = \frac{\Delta P_i - \min(\Delta P_j, j = 1{:}n)}{\max(\Delta P_j, j = 1{:}n) - \min(\Delta P_j, j = 1{:}n)} + 1 \tag{5.6}$$

where ΔP_i is the difference in pressure gradient between the active tank and its i^{th} neighbouring tank, and the active tank has n neighbouring tanks in total. Figure 5-7 presents an example to calculate the ΔP_{ir} of one active tank. In this case, the active tank has three neighbours and ΔP_i and ΔP_{ir} are listed in the table. It is observed that the relative pressure gradient has a value range of [1, 2], and a higher value indicates a steeper pressure gradient. Similarly, the second factor, $\left(\frac{KA}{\mu L}\right)_{ir}$, is also defined in the same way. For this factor, it needs to be mentioned here that the area between tanks, A, is calculated by multiplying the overlap boundary length with the reservoir thickness; the distance between tank centroids, L, is determined by measuring the distance between the tank centroids in the 3D model. The fluid viscosity, μ, is loaded from the PVT setting of the 3D model and the permeability, K, is the arithmetic mean of all the cells inside the tank.

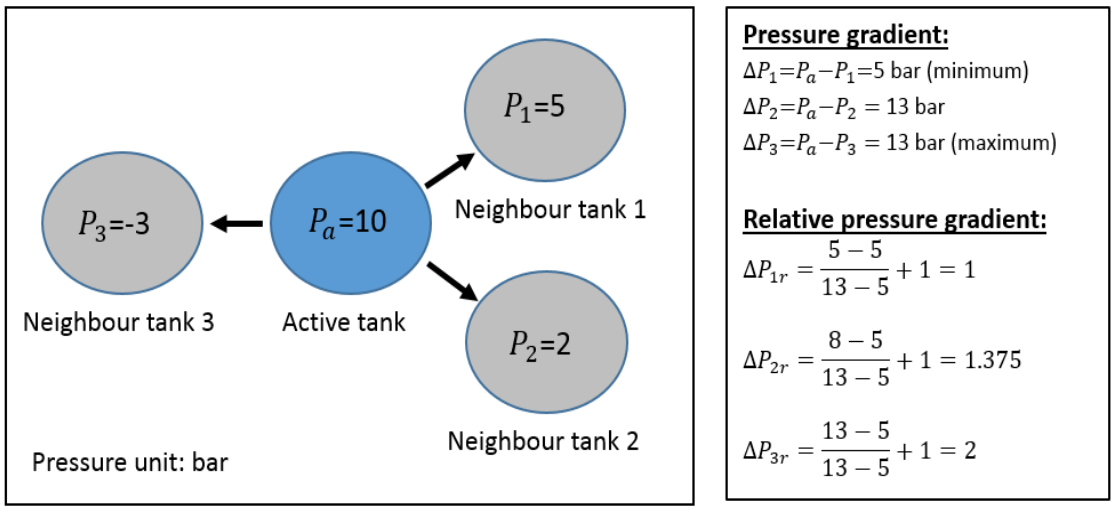

Figure 5-7 *Example of the calculation of the relative pressure gradient (ΔP_{ir}) using Equation 5.6.*

As a brief summary of this introduction to the tank communication model, it can be said that there are two sets of coefficients which need to be further determined in the Equation set 5.5: T_{ai} and $C_{res,a}$. T_{ai} is the transmissibility multiplier (in some papers referred to as the 'leakage factor') between tanks, which is flexible and has an effect on the transferred volume. $C_{res,a}$ indicates the proportion of ΔV_athat will be reserved in the active tank after fluid transfer and is a function of the static reservoir properties and tank size. The determination of these two coefficient sets is through a '3D model matching' procedure which will be explained in the next section.

Based on Equation 5.5, the communication of the active tank with its neighbours can be determined, and the neighbouring tanks will then be activated and this process will continue until the 'fluid transfer boundary' encounters the reservoir boundary. One interesting case is that one tank may be the neighbour of multiple active tanks. In this case, the active tanks will be ranked according to their pressure gradients, then the neighbouring tank with highest pressure gradient will be calculated first, followed by the tank with second highest pressure gradient and so on.

All the procedures mentioned above describe the fluid transferring at just one time step (from the tanks made active by an injector or producer, to the entire reservoir). However, the well BHP profile is a function of time; thus, the model will continue running until the last time step to model the well BHP changes with time. A general workflow for applying the MTM is listed as follows:

Step 1: time step=1, read ΔV_a from historic well injection and production data;

Step 2: determine the list of active tanks and corresponding ΔV_a;

Step 3: calculate the tank pressure change by using the single tank model;

Step 4: determine the pressure gradients between active tanks and their neighbouring tanks and rank them;

Step 5: calculate the transferred fluid volume for all active tanks by using the tank communication model;

Step 6: activate these neighbouring tanks, and calculate the neighbouring tanks' pressure change by using the single tank model;

Step 7: check if all tanks have been activated; if yes, continue step 8, otherwise repeat step 4;

Step 8: calculate BHP for all producers by using the well model at this time step;

Step 9: check if it is the last time step; if yes, finish; otherwise, repeat from step 1 for next time step.

In this section a theoretical MTM has been introduced. This model consists of three parts: single tank model, well model and tank communication model. The single tank model is designed to simulate the tank average pressure change with a certain fluid volume change. Material balance is the key to this model. The second model is to link the well bottom hole pressure (BHP) with the average tank pressure. With this model, the well BHP profile curves become available for simulation, and not only the shut-in pressure, as in the early usage of tank model on Schiehallion field. The third model, which is the key to the MTM, simulates the fluid transferring between tanks by preserving the directly and inversely proportional relationships from Darcy's Law and also introducing new features. The three models work together as an integrated 'multiple tank model' which is the second proxy I build for the reservoir fluid flow simulation model. As suggested in this introduction, the MTM should be built based on a known reference 3D model. Looking further ahead, after it has been built as an approximation of a reference 3D model, this MTM will be used in the SHM workflow instead of the 3D one.

When it comes to apply this model on a real world scenario, more questions come out, such as: how to build and configure the tanks with a reference 3D model? How to determine the embedded coefficients of tank communication model (T_{ai} and $C_{res,a}$)? What is the difference between the results of a conventional 3D model and this proxy? Exploration of all these questions will be conducted in the following sections.

5.3 Model building

5.3.1 Tank boundary and initial property distribution

The first and most important configuration data of the MTM are the tank boundaries and initial property distributions, both of which are derived from the 3D simulation model. These properties include the pressure and fluid saturations of each tank before production and are required parameters in the MTM. In order to determine these configuration data, a target reservoir region should be selected to build the MTM. As pointed out in section 5.2.1, the water influx from the outer aquifer is a main source of uncertainty. Thus, in order to simplify this study, I selected a part of Schiehallion segment 4 which has no clear water influx to build the MTM.

The target reservoir region is located in the east side of segment 4, north and south of this part the region is sealed by east-west structural faults. The seal from the east is provided by the pinch-out of the reservoir. In the middle of segment 4 there is a sealed fault which is considered to block the side-water supplement from the west. Vertically, the main reservoir T31 is considered to build the model, as there are no clear vertical communications between T31 and the reservoirs above or below it, because of the sealed shale layers. Therefore, this target region of segment 4 is relatively isolated from other parts of the reservoir and thus the uncertainty caused by water flux could be eliminated.

After selecting the region of the reservoir, the next step is to map the tank boundary. Initially, the 3D model was built based on the interpretation of static seismic. The sandbodies were mapped (Figure 5-8, top) and modelled as geobodies (labelled by eclipse keyword MULTNUM) in the 3D simulation model (Figure 5-8, middle). To map the boundary of each tank, such geobodies were grouped and merged to reduce the number of parameters involved in the model. In total there are 14 mapped tanks, as shown in Figure 5-8 (bottom).

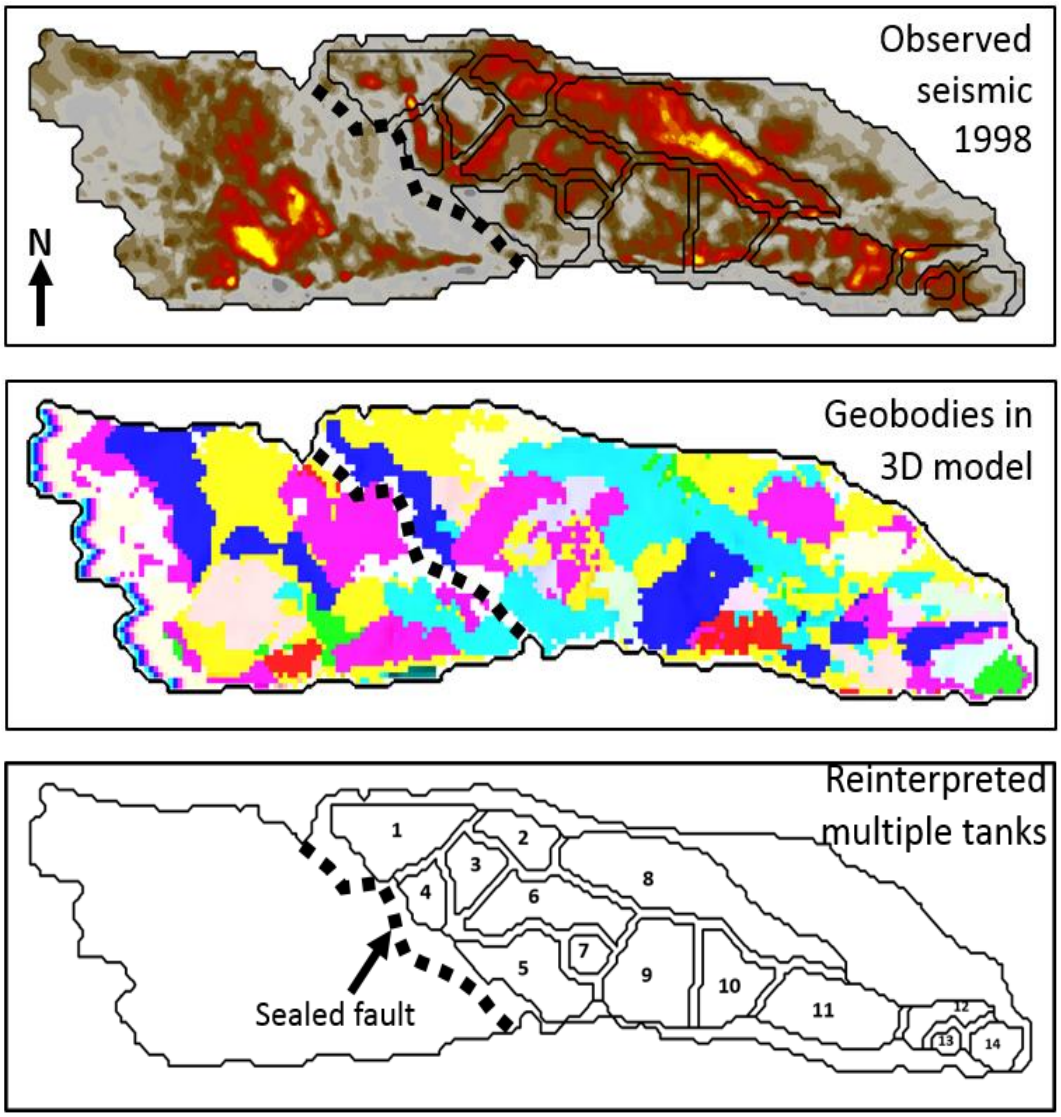

Figure 5-8 *Target part of Schiehallion segment 4 selected to build the MTM. The top figure has the observed seismic data as background, from which the sandbodies were interpreted. The middle figure presents the simulated sandbodies in the 3D simulation model. The bottom figure presents the locations of all 14 tanks simulated in this MTM.*

In terms of the properties for each tank, such as pressure, initial water, and oil or gas in place, I first generated pore volume weighted maps of these properties from a 3D simulation model, as I did in Chapter 4, then subdivided the map of the entire region into 14 tanks and calculated the arithmetic mean of these properties for each tank. This process could be regarded as a kind of 'upscaling', from 3D model cell scale to tank scale. Subsequently, in the application of the MTM, the fluid volume of each tank can be obtained by multiplying the tank pore volume and corresponding fluid saturation. All calculated configuration data are listed in Table 5-2 and the distributions of reservoir pressure and fluid saturation are plotted in Figure 5-9.

Table 5-2 *Configuration data of the MTM.*

Tank number	Pore volume /m^3	Initial pressure/bar	Initial gas saturation	Initial water saturation	Initial oil saturation
1	3692153.9	212.79	0.00	0.86	0.14
2	3452724.6	208.73	0.00	0.40	0.60
3	3138962.4	205.66	0.00	0.21	0.79
4	1015656.4	204.08	0.00	0.18	0.82
5	2915733.8	195.42	0.00	0.18	0.82
6	4823193.2	201.22	0.00	0.18	0.82
7	1587224.1	197.63	0.00	0.18	0.82
8	15677222.8	203.91	0.00	0.19	0.81
9	6067937.4	196.78	0.00	0.18	0.82
10	5322316.7	197.34	0.00	0.18	0.82
11	8632358.7	195.18	0.00	0.18	0.82
12	3419059.2	190.97	0.00	0.18	0.82
13	1346673.3	190.55	0.00	0.18	0.82
14	1231235.1	188.61	0.27	0.18	0.55

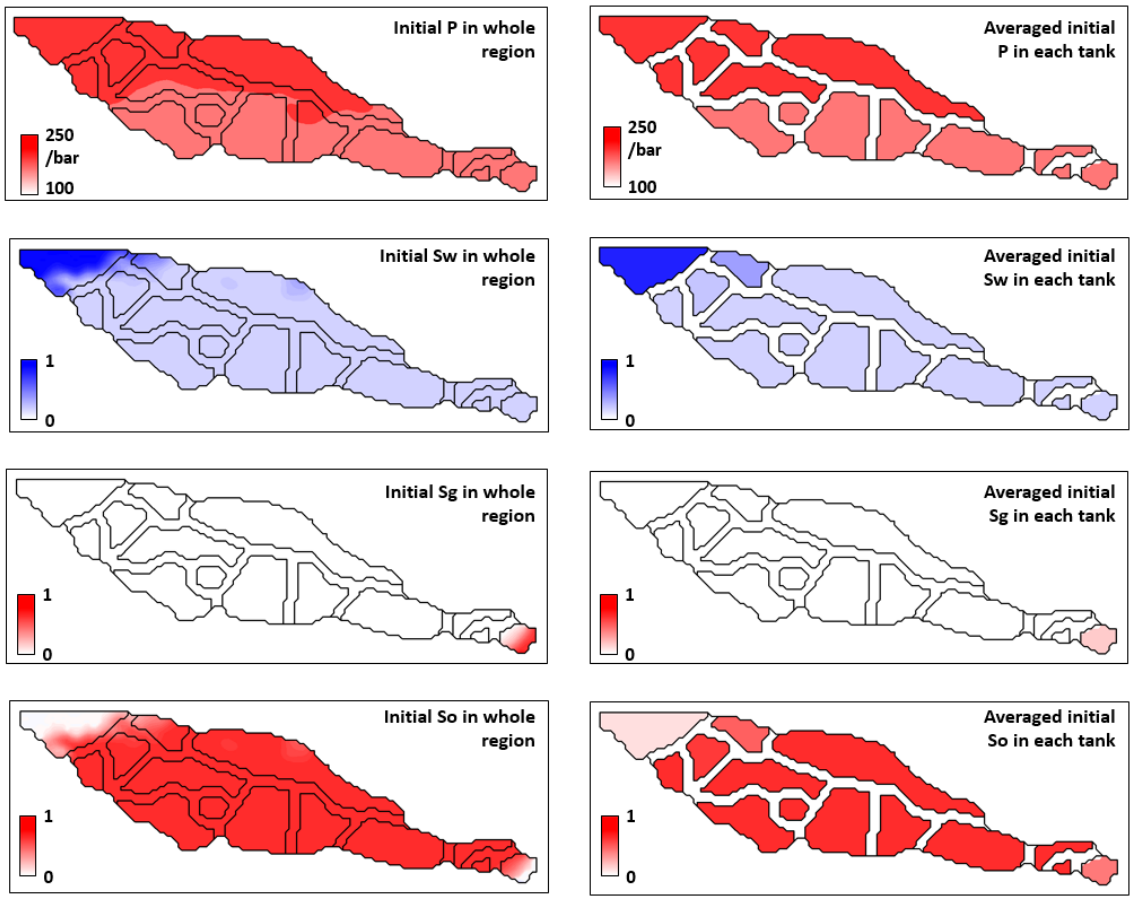

Figure 5-9 *Distribution of the initial pressure (P), water saturation (Sw), gas saturation (Sg) and oil saturation (So) in each tank before production. The left column is the mapped results of 3D simulation model, and the right column is the average (arithmetic mean) of the left column. This process (from left to right column) can be regarded as a model upscaling: from 3D model cell scale to tank scale.*

It can be observed from Figure 5-9 that after being upscaled from cell scale to tank scale, the distribution patterns of initial reservoir pressure and fluid saturations are preserved to a large degree. After defining these initial properties of each tank by averaging the cell-based values from the 3D simulation model, in the next section, I will determine the embedded parameters (T_{ai} and $C_{res,a}$) which are required in the tank communication model.

5.3.2 Model initialization

In section 5.2.3 where the tank communication model was introduced, it was explained that there are two sets of parameters which control the fluid transfer between tanks: T_{ai} and C_{res}. T_{ai} is the transmissibility multiplier between the active tank and its i^{th} neighbouring tank, and $C_{res,a}$ describes what proportion of the fluid volume change (flow in or out through an injector or producer) which occurred in the active tank would be finally retained after transferring to its neighbours. In this section, the model 'initialization' means determining these two parameter sets by matching the tank model outputs to 3D model outputs (3D model matching). Because the ultimate goal is to build a proxy for the reference 3D model, a better match between tank model and 3D model indicates a better approximation has been built. After this model initialization procedure, the MTM will then be used in the seismic history matching workflow which will be performed in Chapter 6.

Before introducing this '3D model matching' procedure, I have to firstly define the number of all the parameters. There are 14 tanks in the model (Figure 5-10), so the dimension of C_{res}, which controls the proportion of reserved fluid volume in each tank, is 14. The dimension of another parameter set, T_{ai}, has to be determined according to the topological relationship of the tanks, because this parameter describes the inter-tank property. Table 5-3 is designed to describe this spatial relationship between tanks: where 1 stands for the two tanks being connected and 0 means that they are not neighbours. For each '1', there should be a transmissibility multiplier T_{ij}, controlling the fluids transferring from the i^{th} tank to the j^{th} tank. For the purpose of simplification, one pair of connected tanks shares one T_{ij} value, which means $T_{ij} = T_{ji}$; thus, from the matrix point of view, this is a symmetrical matrix. From this table, the number of T_{ij}s which need to be defined is 24, so the total number of uncertain parameters (T_{ij} and C_{res}) is 38.

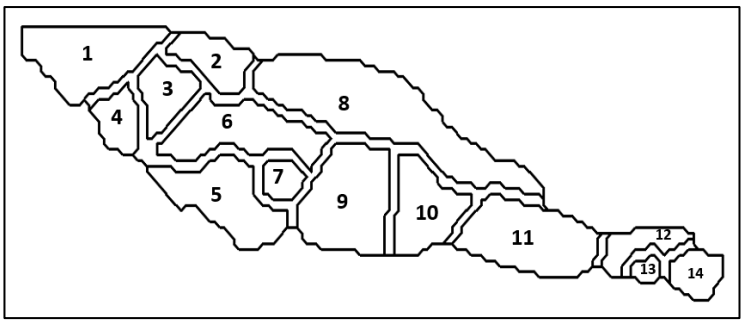

Figure 5-10 *Map of all the fourteen tanks located in the target region of the Schiehallion field. The topological relationship of the contiguity between tanks is presented in Table 5-3.*

Table 5-3 *Topological relationship of the contiguity between all the fourteen tanks.*

Tank index	1	2	3	4	5	6	7	8	9	10	11	12	13	14
1	-	1	1	1	0	0	0	0	0	0	0	0	0	0
2	1	-	1	0	0	1	0	1	0	0	0	0	0	0
3	1	1	-	1	0	1	0	0	0	0	0	0	0	0
4	1	0	1	-	0	0	0	0	0	0	0	0	0	0
5	0	0	0	0	-	1	1	0	1	0	0	0	0	0
6	0	1	1	0	1	-	1	1	1	0	0	0	0	0
7	0	0	0	0	1	1	-	0	1	0	0	0	0	0
8	0	1	0	0	0	1	0	-	1	1	1	0	0	0
9	0	0	0	0	1	1	1	1	-	1	0	0	0	0
10	0	0	0	0	0	0	0	1	1	-	1	0	0	0
11	0	0	0	0	0	0	0	1	0	1	-	1	0	0
12	0	0	0	0	0	0	0	0	0	0	1	-	1	1
13	0	0	0	0	0	0	0	0	0	0	0	1	-	1
14	0	0	0	0	0	0	0	0	0	0	0	1	1	-

0 unconnected 1 connected - same tank

After determining the parameter numbers, the next step is to match the outputs of the MTM with the 3D model. The well pressure profiles (BHP for 3 producers and 5 injectors) and distributions of pressure and saturation changes after production were selected as the model outputs to match, while the uncertain parameters to be perturbed are the 38 parameters. A PSO scheme was applied to find the optimal solutions, which are listed in Table 5-4. After obtaining these 38 parameters, then the MTM could be defined. The simulation results of the 'matched' MTM and the reference 3D simulation model are compared in Figures 5.11 and 5.12.

It is observed that for both the BHP data and dynamic property distributions, the proxy model results are well-matched with the 3D model. The well BHP curves simulated by the tank model respect the trend in the 3D model simulation results as an quantitatively effective approximation (Figure 5-11). The polarities of pressure and saturations changes simulated by two models are also comparable (Figure 5-12). However, this '3D model matching' is a data training procedure; even if one model can well match the training data, its overfitting condition has to be further analysed by testing data. In this case, the test data is another new set of the uncertain parameters, and the overfitting analysis is performed by applying this new parameter set on the 3D model and on the tank model individually, then comparing their simulation results on this new scenario. This analysis will be performed in a later section of this chapter. In this section, only the matching

quality is checked, to make sure that the MTM can produce similar outputs to the 3D simulation model.

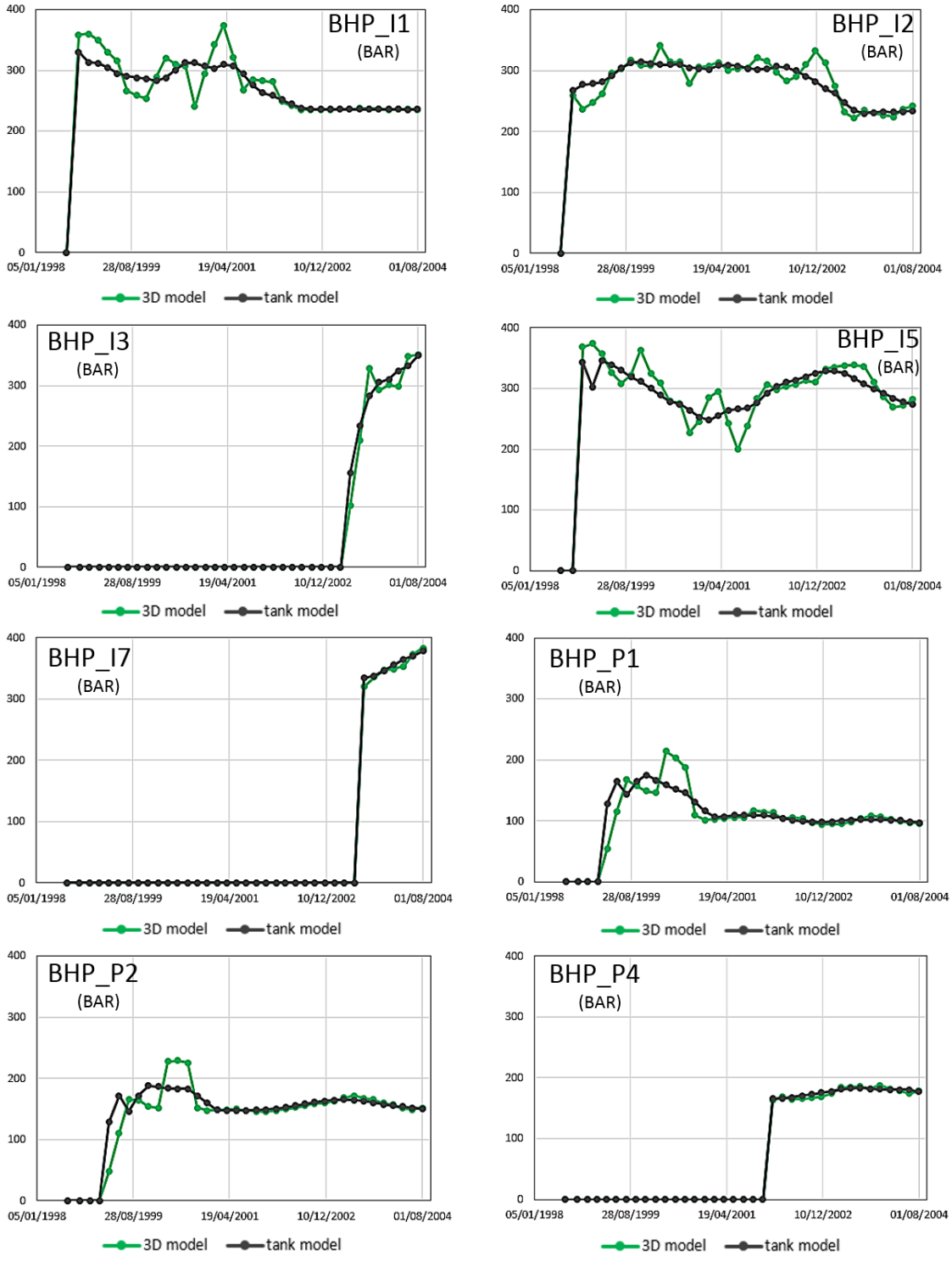

Figure 5-11 *The well bottom hole pressure (BHP) profiles simulated by the conventional 3D model (green line and markers) and by the matched MTM (black line and markers).*

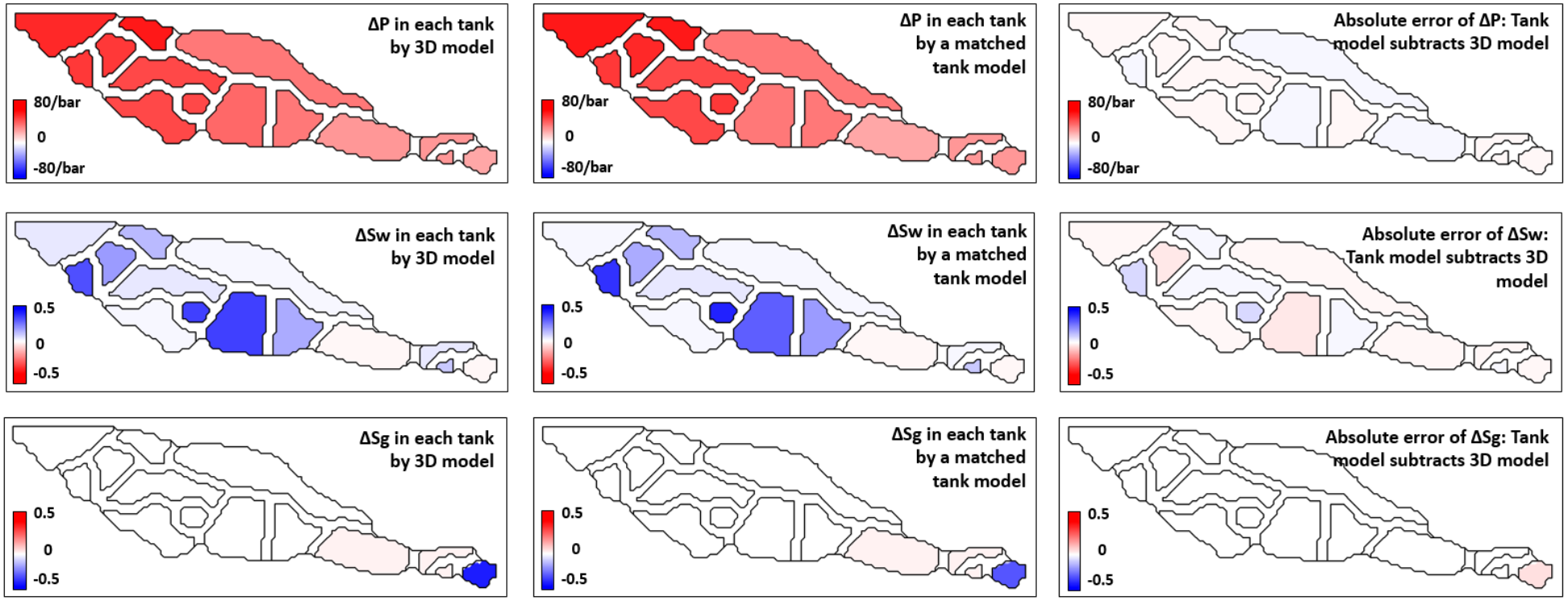

Figure 5-12 *Initialization results of the MTM: a comparison of the distribution of the pressure change (ΔP), water saturation change (ΔSw) and gas saturation change (ΔSg) simulated by the 3D model and the matched MTM. The left column shows the results of 3D simulation models (arithmetic mean value of each tank). The middle column shows the simulation result of MTM (matched to the left column) and the right column shows the error between the two columns ('map simulated by tank model'-'map simulated by 3D model').*

Table 5-4 *The values of parameter T_{ij} and C_{res} of the matched MTM.*

T_{ij}/C_{res}	1	2	3	4	5	6	7	8	9	10	11	12	13	14
1	0.204	0.138	0.192	0.205	0	0	0	0	0	0	0	0	0	0
2	0.138	0.192	0.143	0	0	0.118	0	0.108	0	0	0	0	0	0
3	0.192	0.143	0.164	0.060	0	0.109	0	0	0	0	0	0	0	0
4	0.205	0	0.060	0.179	0	0	0	0	0	0	0	0	0	0
5	0	0	0	0	0.248	0.165	0.154	0	0.049	0	0	0	0	0
6	0	0.118	0.109	0	0.165	0.185	0.050	0.059	0.035	0	0	0	0	0
7	0	0	0	0	0.154	0.050	0.106	0	0.093	0	0	0	0	0
8	0	0.108	0	0	0	0.059	0	0.272	0.084	0.188	0.055	0	0	0
9	0	0	0	0	0.049	0.035	0.093	0.084	0.236	0.152	0	0	0	0
10	0	0	0	0	0	0	0	0.188	0.152	0.304	0.148	0	0	0
11	0	0	0	0	0	0	0	0.055	0	0.148	0.268	0.279	0	0
12	0	0	0	0	0	0	0	0	0	0	0.279	0.226	0.254	0.081
13	0	0	0	0	0	0	0	0	0	0	0	0.254	0.185	0.181
14	0	0	0	0	0	0	0	0	0	0	0	0.081	0.181	0.192

T_{ij} C_{res}

In terms of the computing time, as there is a history matching procedure involved in the model initialization stage, the computing time is really case dependent. In this case, the total computing time is listed in Table 5-5 and compared with the 3D and 2D models:

Table 5-5 *A comparison of the computation cost of the 3D model, 2D model and tank model.*

	3D model	2D model	tank model
Dimension	$52 \times 14 \times 12$	$52 \times 14 \times 1$	14
Total number of grid cells (tanks)	8736	728	14
Computational cost of model building (s)	NA	300	54,600*
Computational cost of single run(s)	607	476	182

**: the computation cost of the history matching procedure involved in the model initialization stage.*

5.3.3 Coupling the MTM with sim2seis proxy

After the model initialization step, the MTM was set up and was found to be capable of producing similar results to those of the 3D simulation model. Having produced this fluid flow simulation proxy, the next step is to build the seismic proxy model so that the two proxy models can work together in the subsequent SHM workflow. The validation of the linear superposition seismic modelling proxy on the Schiehallion field was reported in Chapter 4. This section explains how a new version of the linear seismic proxy model was built by performing the same linear regression as in Chapter 4, but at tank scale. The arithmetic mean values of A_0, ΔP, ΔS_w, ΔS_g and ΔA of each tank were used to carry out the regression.

Based on the 3D fluid flow simulation model and sim2seis model, the volume weighted maps of A_0, ΔP, ΔS_w, ΔS_g and ΔA were plotted in the left column of Figure 5-13, and the arithmetic mean value of each tank was then calculated and plotted in the right column. By performing the linear regression, the three coefficients in Equation 5.7 could be determined, as shown in Table 5-6

$$\Delta A = \left(c_1 \cdot \Delta P + c_2 \cdot \Delta S_w + c_3 \cdot \Delta S_g\right) \cdot A_0 \tag{5.7}$$

Table 5-6 *Linear regression results of the three coefficients.*

c_1	c_2	c_3
-3.04	1542.31	-2224.58

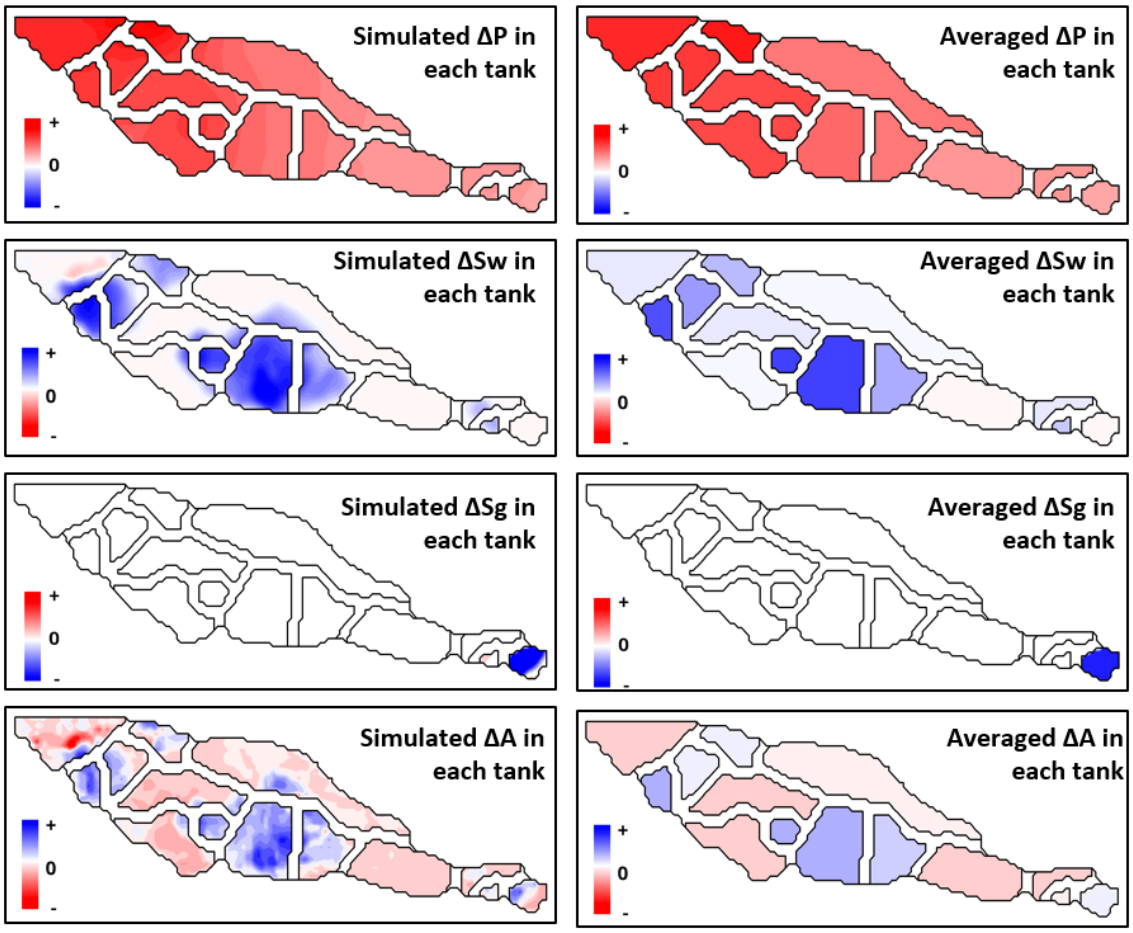

Figure 5-13 *Distribution of the pressure change (ΔP), water saturation change (ΔSw), gas saturation change (ΔSg) and 4D seismic (ΔA) in each tank after production. The left column is the results of the 3D simulation model; the right column shows the average (arithmetic mean) values of those on the left for each tank.*

The linear proxy model was then applied to generate proxy 4D seismic maps which are compared with sim2seis output in Figure 5-13. It is observed that the arithmetic mean 4D map based on the 3D model is qualitatively similar to the proxy model result, where the error level is clearly lower than the signal (Figure 5-14). From a more quantitative point of view, the correlation coefficient of the two maps was measured as r=0.95. Compared with r, another statistic, t, is more commonly used to quantify the significance of correlation relationships for small sample size (n<30) (Kremelberg, 2010). Considering there are only 14 data points (each tank has one output 4D seismic value) which is less than 30, I used t to quantify the significance of the correlation relationship. This statistic can be computed by the Equation 5.8 and more details about this statistic is given in the Appendix A.

$$t = \frac{r\sqrt{n-2}}{\sqrt{1-r^2}} \tag{5.8}$$

where *r* is the correlation coefficient and *n* is the number of data points. In this case, *t* is computed as 14.15. According to Table A.1 in Appendix A, the confidence is over 99% to determine that there is correlation between two data sets. It can also be observed from Figure 5-14 that the polarities of 4D seismic simulated by the sim2seis and proxy model are matched well, which is important for seismic interpretation. Further quality testing of the sequence of 'tank model + seismic proxy' will be carried out in a blind test in section 5.4.

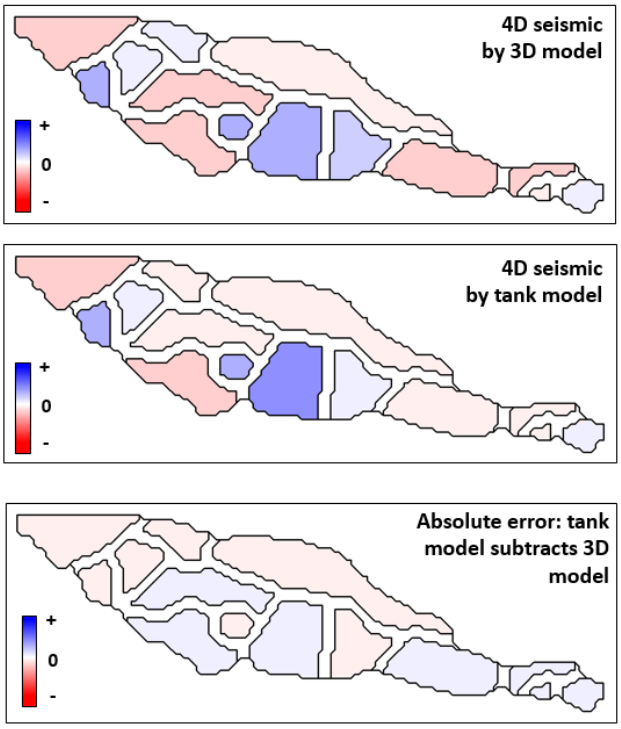

Figure 5-14 *Tank scale 4D seismic (ΔA) simulated by the 3D model (top, arithmetic mean of the initial 3D model results), MTM (middle) and the error between two maps ('map simulated by tank model'-'map simulated by 3D model').*

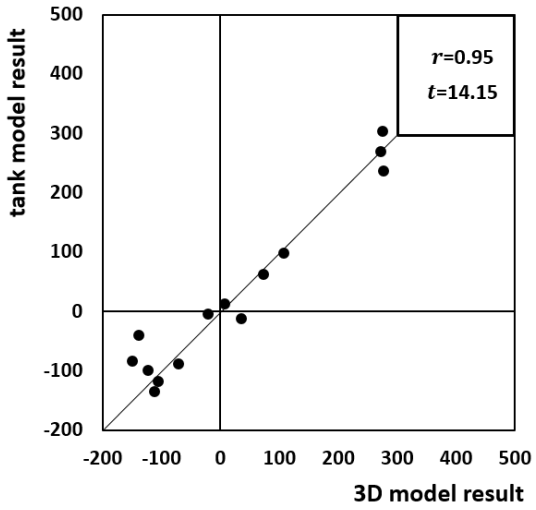

Figure 5-15 *Correlation coefficient (r) and t value between two sets of values: ΔA of each tank, simulated by 3D model and by the tank model, which are presented in the Figure 5-14.*

5.4 Blind test

In previous sections, the MTM and sim2seis proxy were built independently to simulate the well production (BHP profiles) and 4D seismic. As in Chapters 3 and 4, this sequence of proxy models needs to be qualified by a blind test. In this blind test, a reference 3D model is first used to obtain the 'synthetic history data', then an ensemble of 30 scenarios are created by applying the Latin Hypercube Sampling method (Iman, 2008). After running simulations by the conventional 3D model and the sim2seis model, the 4D seismic map of each scenario is plotted in Figure 5-18 to show the variance of these 30 scenarios.

For each scenario, the '3D model + seismic proxy' and 'tank model + seismic proxy' are run independently and their outputs are then matched with the 'synthetic history data'. Thus, for each scenario, two sets of Objective Function (O.F.) value will be measured by Equation 4.9: one is calculated based on the '3D model + seismic proxy' results and the other on 'tank model + seismic proxy' results. Following the procedure introduced in Chapter 4 (Equations 4.7, 4.8 and 4.9), the effect of ΔS_w, ΔS_g, ΔP and $\Delta Seis$ maps ($ERROR_{4\ maps}$) and BHP curves for 8 wells ($ERROR_{8\ curves}$) are integrated in the Objective Function, so that the production data (BHP curves) and seismic data (in map form) can be considered at the same time.

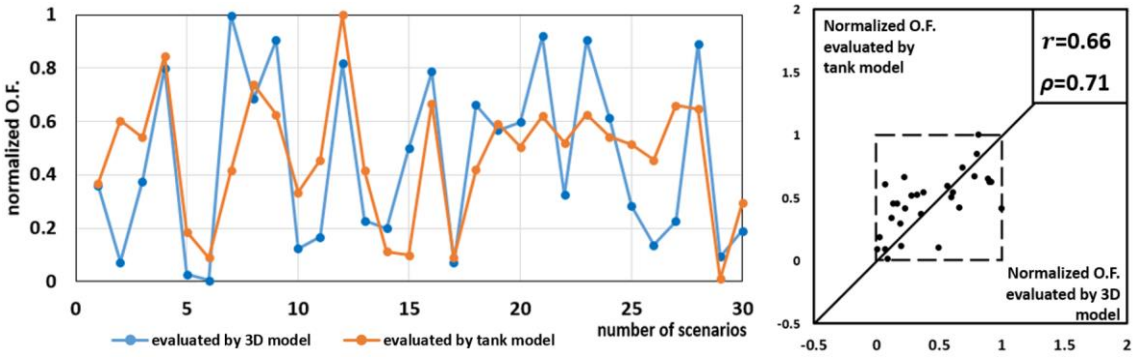

Figure 5-16 *Left: results of blind test, the objective function (misfit) evaluated by'3D model + seismic proxy' and by 'tank model + seismic proxy'; right: cross-plot of the two objective function value sets.*

Subsequently, the two sets of objective function values were normalized to [0, 1], and plotted in Figure 5-16 (left). The correlation coefficient was measured as r=0.66, Spearman's rank correlation coefficient, ρ=0.71 (Figure 5-16, right). r is below 0.7, indicating there was an insignificant correlation, however, ρ was above 0.7, which is an indicator of significant correlation between two data sets. However, as 0.7 is an arbitrary threshold by rule of thumb (Freedman, 2009), it is more informative to do a cross-

comparison with the previous blind test on the linear seismic proxy or 2D areal model proxy. The results of the blind tests were (r=0.81, ρ=0.83) for the linear seismic proxy, and (r=0.92, ρ=0.87) for the 2D areal proxy. Compared with these values, the MTM had worse performance in ranking the candidate models.

A possible reason would be that, in the case of seismic proxy or the 2D areal model, the uncertain parameters, which are randomly generated by the Latin Hypercube Sampling method, have same physical meaning as in the conventional or proxy model: the multipliers of transmissibility or permeability. However, in the case of the MTM, the same value of parameters (T_{ai}) has a totally different physical meaning in the 3D model and in the tank model. For example, if the transmissibility multiplier in the 3D model changes from 0.01 to 0.1, it may significantly increase the communication between two regions. If the same change happened in the tank model, the increase may not be as significant as in the 3D model, or can even make more dramatic changes. In brief, the parameter sensitivities are different in the 3D model and in tank models. In order to use it in the later section, I made a further test to validate this assumption. The set of uncertain parameter values, $M_{t,initial}$, was generated by the Latin Hypercube Sampling method, and was then assigned to the 3D model. However, for the MTM, the variance of the parameter values was first reduced by Equation 5.9, and one example is presented in the Figure 5-17. After the variance reduction, the set of the $M_{t,reduced}$ was assigned to the tank model. The blind test was conducted again over the 30 scenarios and the results were measured as (r=0.71, ρ=0.73), which was higher than the previous results. This comparison indicates that the parameter variance reduction helps to improve the performance of the tank model, thus it would be used in later SHM.

$$M_{t,reduced} = 10^{\log(M_{t,initial})/2} \tag{5.9}$$

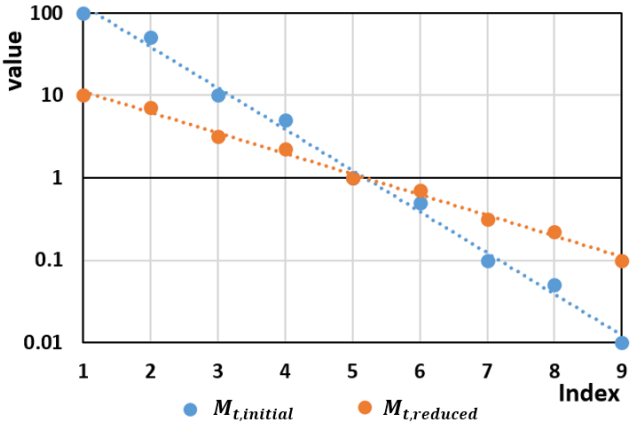

Index	$M_{t,initial}$	$M_{t,reduced}$
1	100	10
2	50	7.07
3	10	3.16
4	5	2.24
5	1	1
6	0.5	0.71
7	0.1	0.32
8	0.05	0.22
9	0.01	0.1

Figure 5-17 *Illustration of the variance reduction process by using Equation 5.9.*

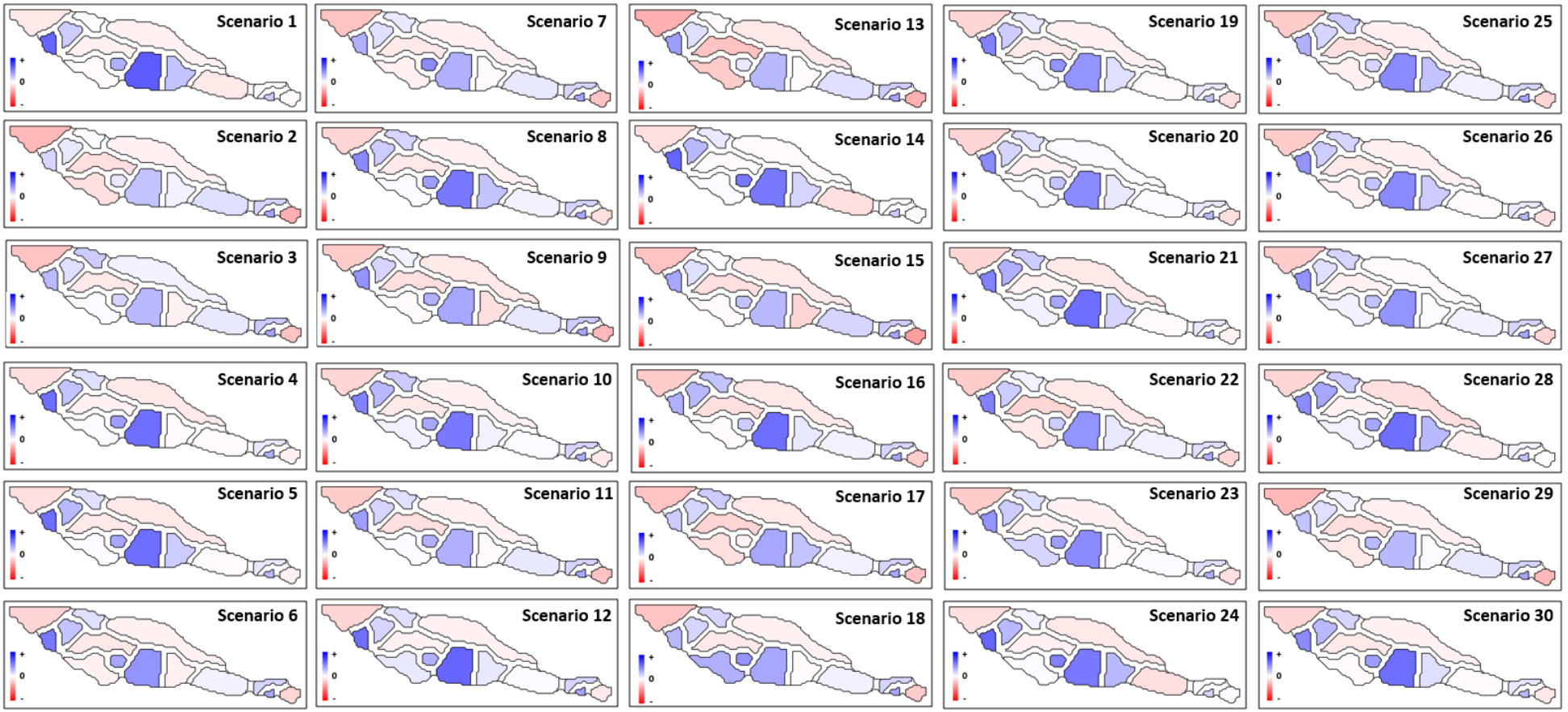

Figure 5-18 *4D seismic by the MTM over all of the 30 scenarios.*

5.5 Overfitting analysis

In section 5.3.2, when the tank model was initialized by matching a reference 3D model, there was a question on the overfitting of that matched model. I pointed out that a new parameter set should be generated to create a test model. Based on this test model, the simulation results of the tank model and 3D model are then compared, to check to what extent the tank model was over-fitted. The key procedure in this test is to assign 'same parameter' on the 3D model and on the tank model. From the previous section, we know that the sensitivity of the two models is different; thus I first randomly generate a set of transmissibility multipliers, $M_{t,initial}$ (Table 5-7). I applied this set of multipliers on the previous reference model, to generate a new 'test model'. A corresponding set of $M_{t,reduced}$ was calculated by Equation 5.9 and was applied on the tank model. Then, based on the new 'test model', the simulation results of the 3D model and proxy model are compared in Figure 5-19 and 5.20.

Table 5-7 *A set of multipliers ($M_{t,initial}$) that was used on the previous reference 3D simulation model, to generate a 'test model' to analyse the overfitting.*

multiplier	1	2	3	4	5	6	7	8	9	10	11	12	13	14
1	1.000	1.199	3.825	0.408	0	0	0	0	0	0	0	0	0	0
2	1.199	1.000	1.293	0	0	0.187	0	0.119	0	0	0	0	0	0
3	3.825	1.293	1.000	2.713	0	0.949	0	0	0	0	0	0	0	0
4	0.408	0	2.713	1.000	0	0.000	0	0	0	0	0	0	0	0
5	0	0	0	0	1.000	0.133	0.163	0	0.345	0	0	0	0	0
6	0	0.187	0.949	0	0.133	1.000	3.316	0.410	0.581	0	0	0	0	0
7	0	0	0	0	0.163	3.316	1.000	0	0.562	0	0	0	0	0
8	0	0.119	0	0	0	0.410	0	1.000	3.794	0.354	3.912	0	0	0
9	0	0	0	0	0.345	0.581	0.562	3.794	1.000	9.112	0	0	0	0
10	0	0	0	0	0	0	0	0.354	9.112	1.000	3.448	0	0	0
11	0	0	0	0	0	0	0	3.912	0	3.448	1.000	0.773	0	0
12	0	0	0	0	0	0	0	0	0	0	0.773	1.000	0.841	1.350
13	0	0	0	0	0	0	0	0	0	0	0	0.841	1.000	0.543
14	0	0	0	0	0	0	0	0	0	0	0	1.350	0.543	1.000

Multiplier of T_{ij} Multiplier of C_{res}

It is observed that in Figure 5-19, in the new test model, the BHP profiles simulated by the 3D model and tank model are still similar as in Figure 5-11 (the training model). In terms of the dynamic property maps, as shown in the Figure 5-20, the test model and training model (Figure 5-20, left column) have different 4D seismic polarity distribution, which help to confirm that the training data and testing data are diverse enough. It can also be noticed that, although the error level is clearly higher than in the Figure 5-12, ΔP,

ΔS_w and ΔS_g, still have similar polarities and patterns. Based on these analyses and comparisons, I qualitatively conclude that the tank model, which was built by matching the outputs with a reference 3D model, has not been over-fitted, it can still work well on new data set. The MTM driven SHM will be conducted in next chapter.

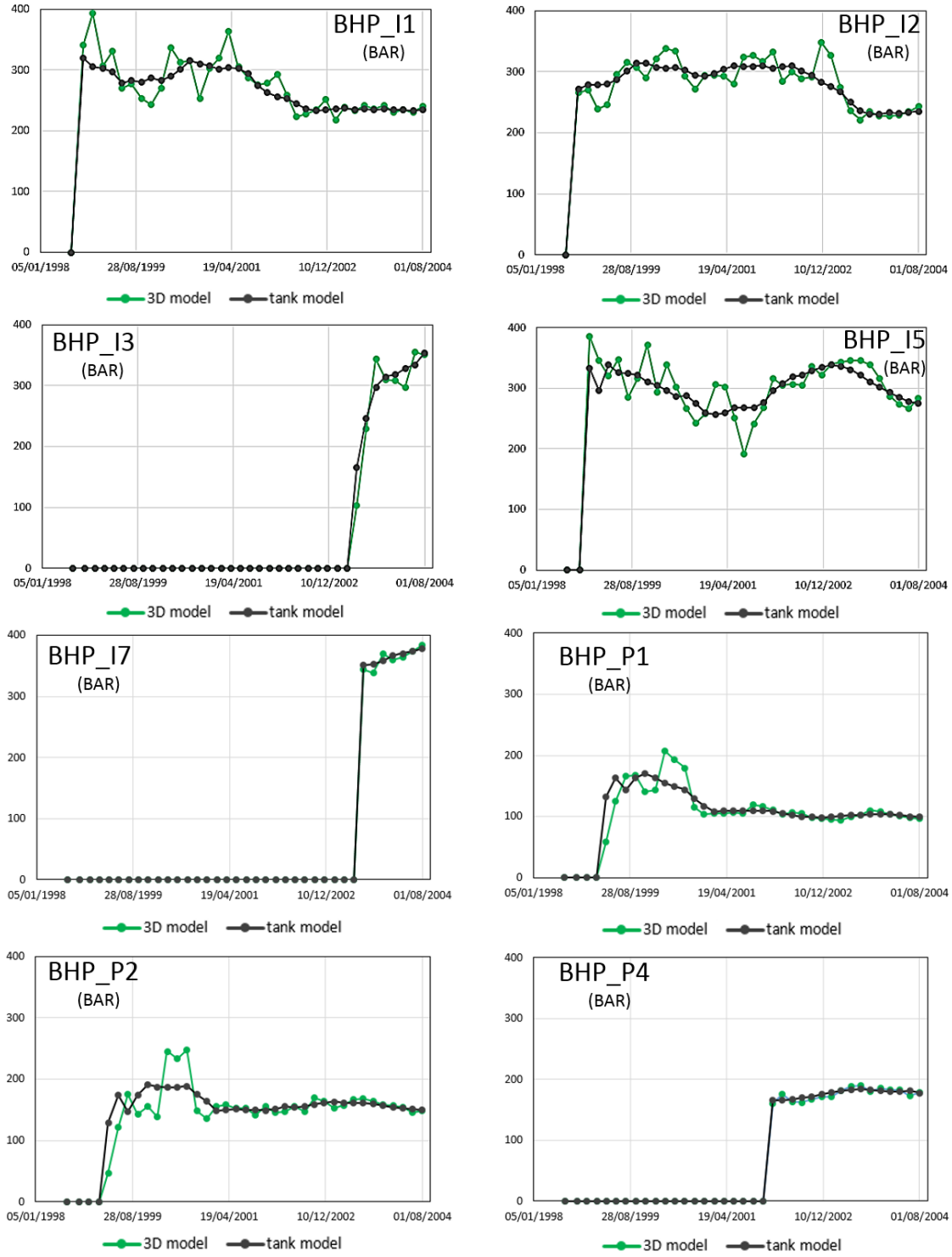

Figure 5-19 *The well bottom hole pressure (BHP) profiles for the testing model: simulated by the conventional 3D model (green line and markers) and by the matched MTM (black line and markers).*

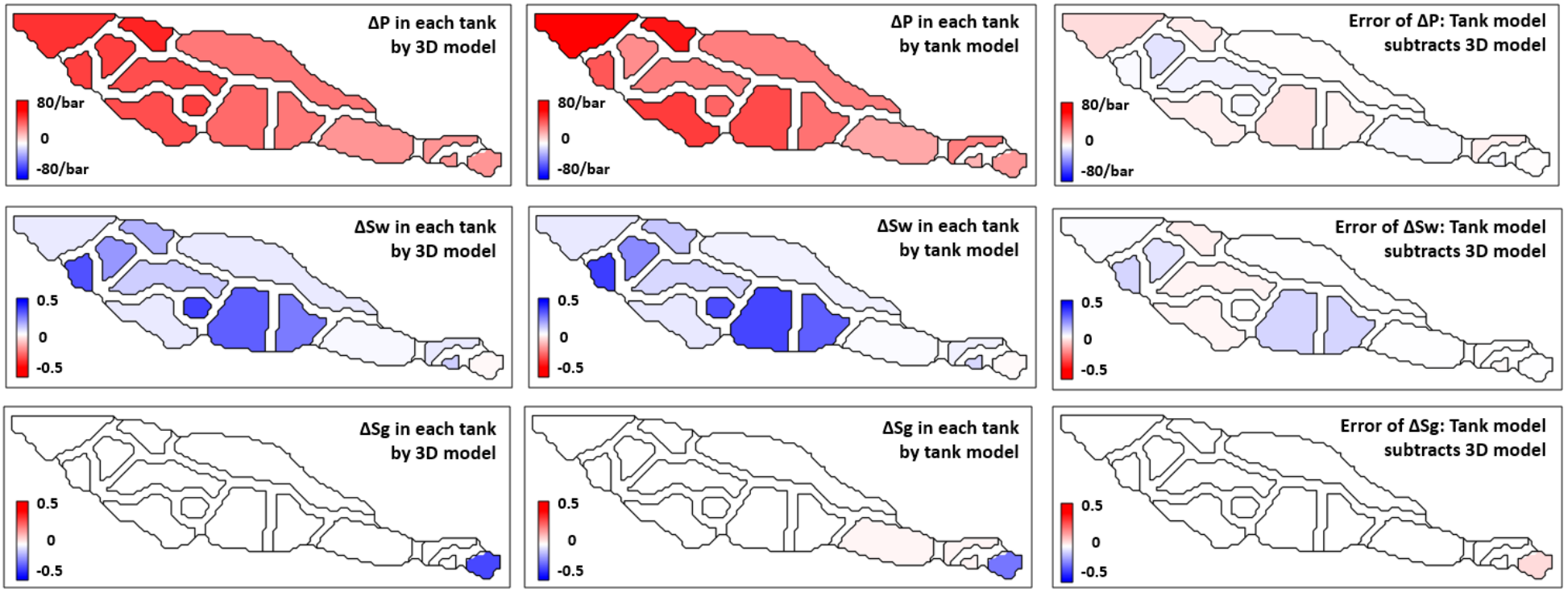

Figure 5-20 *Distribution of the pressure change (ΔP), water saturation change (ΔSw) and gas saturation change (ΔSg) for the testing model: simulated by 3D model (left column) and by tank model (middle column). The right column is the error between the left and the middle columns ('map simulated by tank model'- 'map simulated by 3D model').*

5.6 Summary

In this chapter it has been described how a MTM was developed as a proxy model for the initial 3D flow simulator. It is a further exploration of the material balance model use in the early life of the Schiehallion field, following the work of Dobbyn and Marsh, 2001. This proxy model worked in combination with the seismic modelling proxy and 'MTM+ seismic proxy', which is the main innovation point of this method. This exploration is driven by a philosophy that 4D seismic should be integrated with well production data in a more quantitative way, rather than by manual interpretation.

The proxy model can be regarded as an upscaling of the 3D simulation model from 3D grid-cell scale to 'tank' scale. The boundaries of tanks were determined by the geobodies which were interpreted from 3D seismic and have been embedded in the reference 3D simulation model. The configuration setting of each tank was also obtained from 3D simulation model data. Thus, this method can only work with an existing 3D model as reference, which is usually available for a mature field.

In this study, the tank model could reproduce similar results as the 3D model, but it was also observed that the model parameters are more sensitive than those in the 3D model. This fact would be a limitation of the MTM being applied in the SHM practice. Taking Schiehallion as a case scenario, the 2D areal proxy is more strongly recommended to work as a proxy model because it requires less effort to build and could generate more robust results than the tank model. Considering the ultimate goal of developing proxy methods is to simplify and speed up the conventional simulators, if the building of the proxy model itself is too complicated than we will lose the value of proxy. Additionally, this work is a tentative exploration of the material balance model; more refinements of the work could be added in the future and I will list these in the final chapter.

Chapter 6

Applying the proxy models in SHM

The seismic proxy, the areal model and the multiple tank model were introduced independently in Chapters 3 to 5, which also reported how they were tested in blind tests. The results indicated that the proxy models could produce similar results to the conventional simulation models. Considering the ultimate goal is to use these proxies in the SHM workflow, I conducted proxy assisted SHMs, which are reported in this chapter to present the application of the three proxy models in the SHM workflow. Firstly, a brief review is undertaken to summarise how the effect of 4D seismic on the HM was evaluated in previous research, and how the proxy models were applied in the HM workflow. Subsequently, a new method is described to evaluate the effect of 4D seismic and the proxy models in the SHM workflow. The chapter then describes how two tests were then conducted individually on the Norne and Schiehallion fields: the first one was to evaluate the effect of 4D seismic and to test the seismic proxy; the second one was to test the areal model and the multiple tank model. In these two tests, 4D seismic and three proxy models are evaluated by the new method, and the optimised combination of proxy models is recommended for Norne and Schiehallion fields.

6.1 Evaluating the 4D seismic in the SHM workflow

In Chapter 1, the role of 4D seismic in reservoir engineering and monitoring was introduced. For instance, the water flooding patterns could be mapped from the seismic response to help in locating new infilling wells. However, this is a qualitative application of 4D seismic which needs a great deal of manual work. In order to use the 4D data in a quantitative and more automatic way, 4D seismic has been successfully used, together with well production data, as the constraints in history matching workflow. Actually, the well production data, such as well production rate profiles, well pressure profiles and well testing data, are the most commonly used constraints for HM. This is not only because the well production data are available from the beginning of the field development, but these data are also directly linked with the key economic parameters for field development, such as oil production rate (Chierici, 2012).

These well production data are regarded as 'hard data' for history matching (Oliver et al., 2008); however, limited by the designed inter-well distance (which can be hundreds of metres onshore and thousands of metres offshore), well data can only provide very sparse and local information about what is happening underground. Therefore, if detailed information such as fluid front movement after a period of production is needed, the well data can offer only indirect interpretation results. Nevertheless, considering its high vertical resolution and direct representation of the productivity, well production data are still regarded as 'hard data' for history matching.

In Chapter 4, the resolution of seismic was analysed and it was demonstrated that the strength of seismic data is their lateral resolution; thus, they can offer the important spatial information which cannot be replaced by any other kinds of data. The application of 4D seismic in history matching workflow is named as SHM, which was introduced in Chapter 1. In this section, I carry out another survey on how the effect of 4D seismic in SHM has been evaluated in previous research. Skjervheim et al. (2007) used 4D in a synthetic SHM case where the true optimal solution was known. They found that by introducing 4D seismic, the history matching procedure led to a better matched permeability distribution solution (Skjervheim et al., 2007; Figure 6-1). Obidegwu used 4D in a real SHM case which had no predefined optimal solution (Obidegwu 2017; Figure 6-2). He found that by introducing the 4D as an extra constraint for HM, the optimal solution model could make better prediction than the matched model of WHM where only well production data were involved. Actually these are the two most common ways to demonstrate the value

of 4D seismic as an extra constraint in SHM: in the synthetic SHM case with a predefined optimal solution, comparing the solutions of SHM and WHM with the known optimal solution and in the real SHM case without a predefined solution, analysing the prediction accuracies of the models searched by the SHM and WHM.

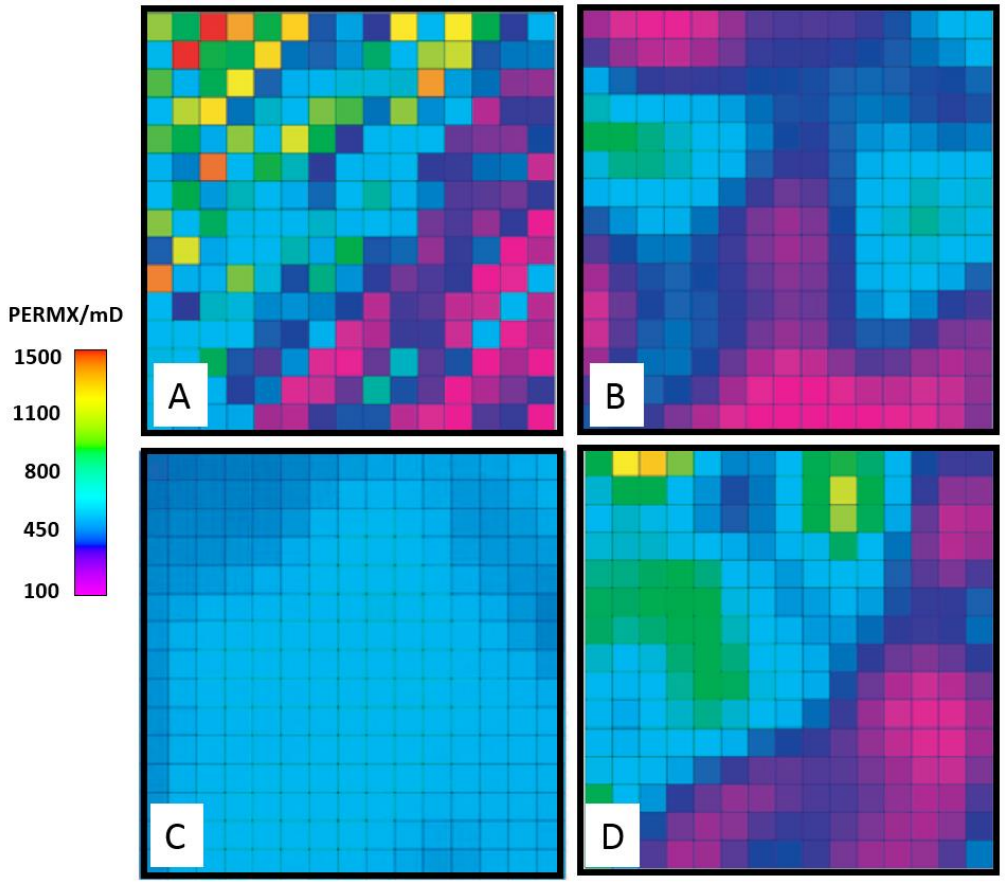

Figure 6-1 *A: the true permeability field of the synthetic history matching. B: the solution of seismic only history matching (SOHM). C: the solution of well only history matching (WOHM). D: the solution of seismic history matching (SHM) which considered both the well data and the seismic data. (Skjervheim et al., 2007)*

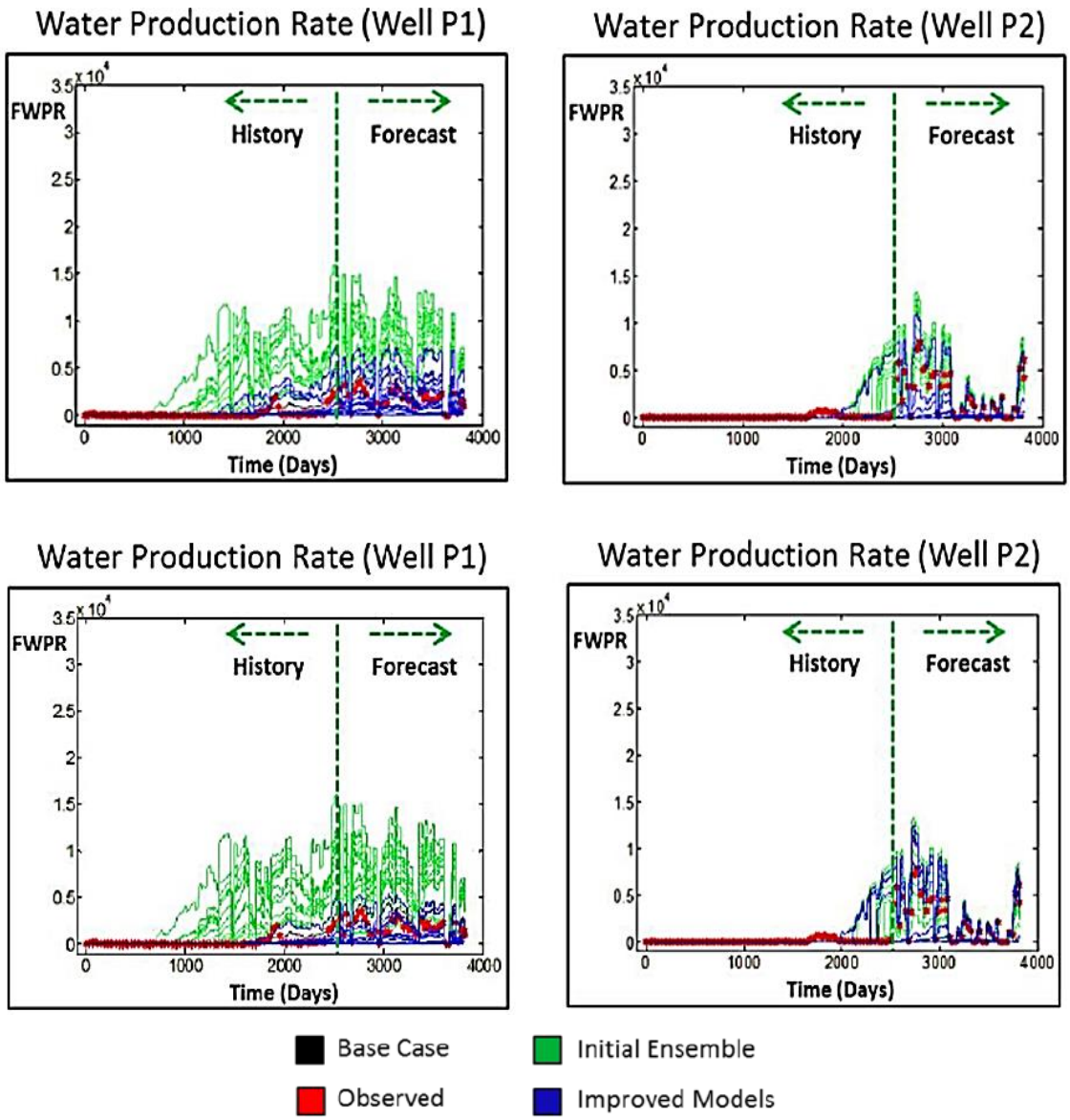

Figure 6-2 *Normalized production profiles for wells P1 (left column) and P2 (right column) highlighting the improved model responses (dark blue lines), after history matching to production data only (WOHM, top row) and to both well production and seismic data (SHM, bottom row). It was observed that the solution models of SHM had better forecasting ability than that of WOHM. (Obidegwu 2017)*

A third way could be thought to verify the value of 4D seismic in the real SHM case. Instead of comparing the history matching results of 'well production data only (WHM)' and 'well data plus seismic data (SHM)', a new workflow can use 4D seismic as the only constraint (seismic only history matching, SOHM: Figure 6-3); we can then check the performance to the well production. As no well production data are involved in the history matching, if we observe on the final history matched results that the well production match is improved, it means the 4D seismic data will work in synergy with the well production data in history matching. Therefore, the spatial information contained in 4D seismic can help to match the local well production data. In this way, one more value of 4D seismic can be credited.

In a later section of this chapter, I will report how I conducted a test on the Norne field following the SOHM workflow presented in Figure 6-3 to verify the extra value of 4D seismic data for the history matching procedure.

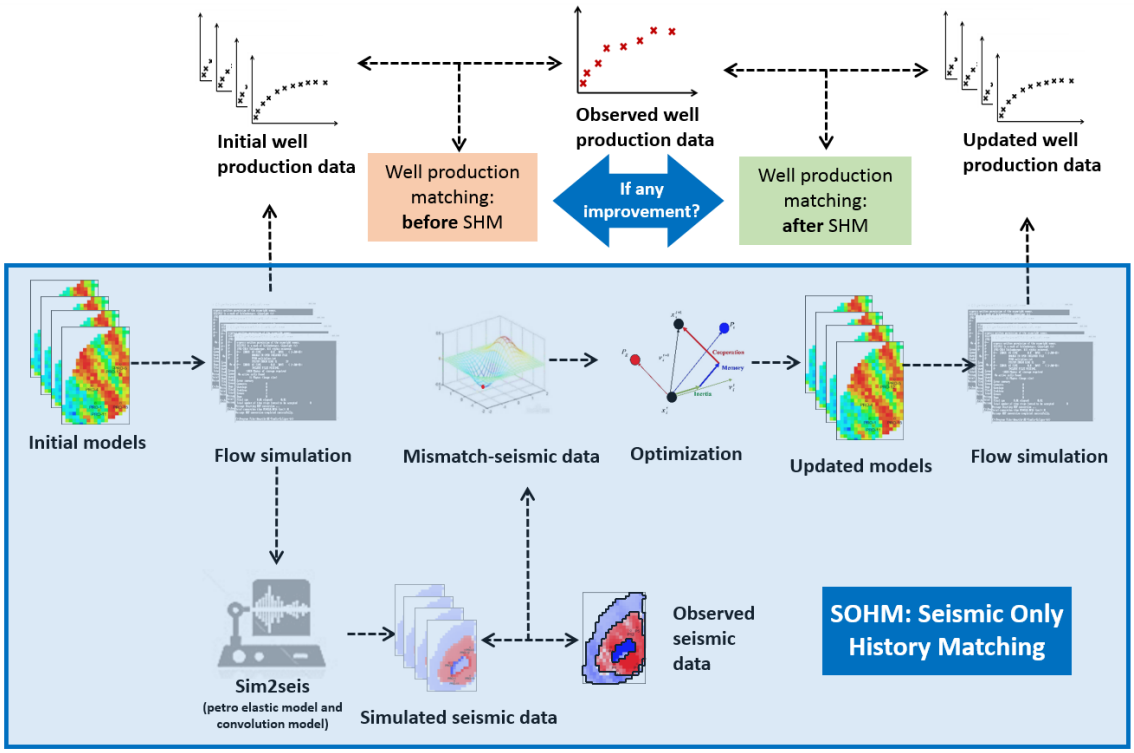

Figure 6-3 *Workflow of seismic only history matching (SOHM).*

6.2 Applying the proxy models in the SHM workflow

As well as the 4D seismic, the performance of proxy models in the SHM workflow should also be evaluated. Generally, there is a trade-off between model accuracy and speed; thus the value of proxy models should be evaluated from these two aspects. In former chapters, the approximation of proxy models with conventional simulation models was analysed in both qualitative and quantitative ways. Additionally, the blind tests were designed to check if the objective function evaluated by the proxy model could successfully sort the candidate models: if the sorting results are close to that of the conventional model, the proxy models are proved as successful approximations of the conventional model. The results of the previous chapters indicated that the proxy models could produce outputs approximate to those of the conventional models. Considering the ultimate goal is to apply these proxy models in the SHM workflow, I will first conduct a survey on how to evaluate the performance of the proxy model in the history matching workflow. The general literature review on the use of proxy models was presented in Chapter 2; here I limit my focus to how the proxy value was verified.

In a real WHM case without a predefined optimal solution, Cullick et al. (2006) trained a neural network as the proxy model, using uncertain parameters as model inputs and well production rates as outputs, then utilised the proxy to explore the search solution space and found an optimal solution (a set of model parameters). The conventional simulation model was then run with this set of parameters and it was observed that simulation results of the neural network model and the conventional simulator were very close (Figure 6-4); thus the optimal solution of proxy driven history matching was accepted as the final result.

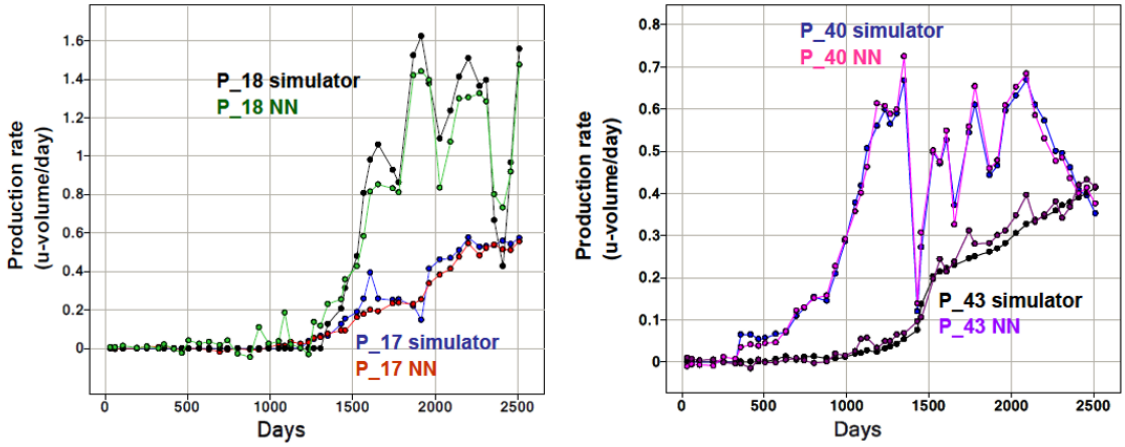

Figure 6-4 *Optimal solution of the conventional simulator driven history matching and proxy (Neural Network, NN) driven history matching. (Cullick et al., 2006.)*

In another WHM case, Zubarev et al. (2009) tested different proxy models such as polynomial regression models, multivariate kriging models, thin-plate spline models and artificial neural networks. For these models, the uncertain parameters are their input data, while the mismatch errors are used as the proxy output. They compared the optimal solution of the proxy assisted HM and the conventional HM (using the simulation model) and found that for many parameters (Figure 6-5, A, B and D), the two HMs could find similar results, but for some parameters (Figure 6-5, C) there was clear bias between the two solutions.

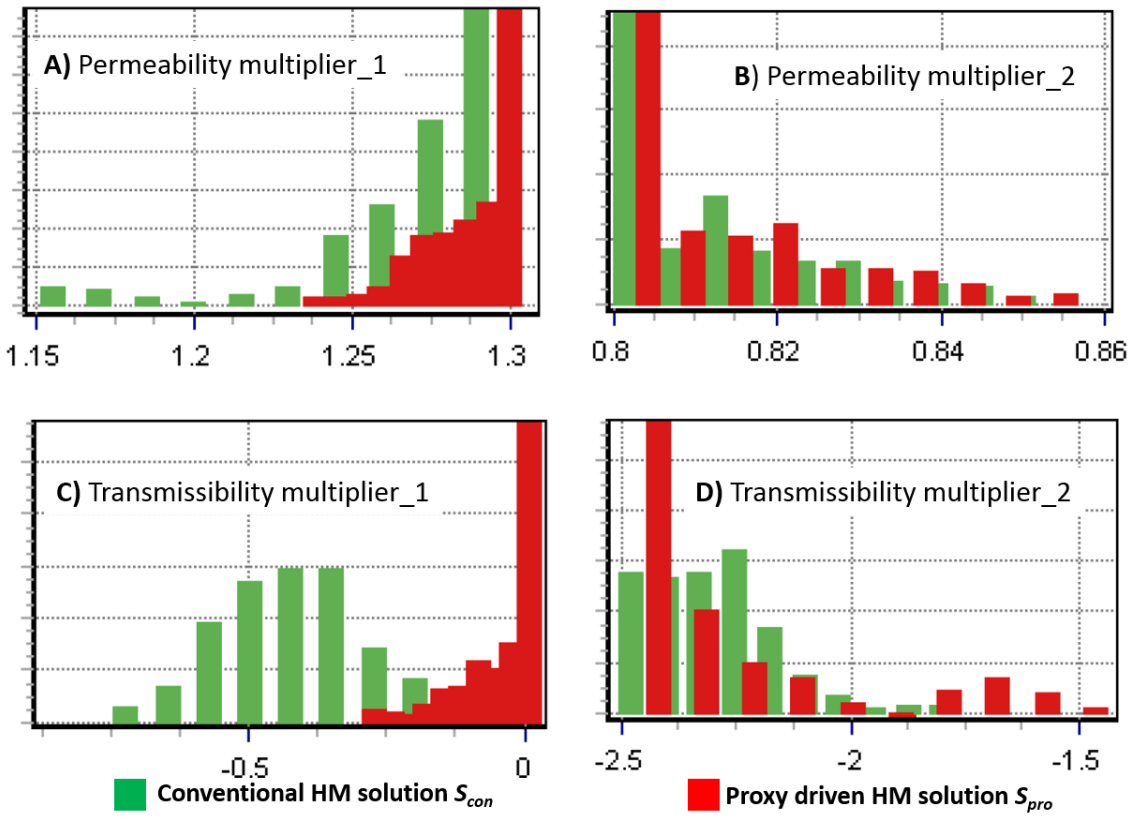

Figure 6-5 *Optimal solution (value distribution of the four selected parameters) of the conventional history matching (Scon) and proxy assisted history matching (Spro). (Zubarev et al., 2009.)*

In this case, clearly, the conventional solution (Scon) cannot be approximated by the proxy solution (Spro). However, the authors ran the conventional simulation model on the solution Spro and found that the mismatch value of this solution had also been reduced compared to the model pre-HM, but not as much as that of the Scon. Thus, in order to find the global optimal solution, the conventional model cannot be replaced by the proxy model. The value of introducing proxy models in this case is not as direct as in the previous case, as further work needs to be done to make a decision. For example, the conventional history matching could be relaunched based on the Spro; although this is

not the global optimal, it may shorten the search path (from the initial case to the final solution) of conventional model driven HM.

In my point view, the two validation procedures can be combined together: firstly, the solutions of the proxy driven and conventional model driven SHM are compared. If there is no significant bias, a decision could be made that the proxy model can be regarded as a good approximation for conventional models in history matching. In this case, the total computation cost will be obtained by summing up proxy model building and running time, then comparing the sum with the total cost of conventional ways.

On the other hand, if a significant bias between two solutions exists, then an extra step is needed: conducting a conventional history matching with the proxy solution as the new starting point. In this way, we can test the extent to which the proxy driven history matching solution could help the conventional SHM to converge. The computation cost of proxy-SHM and the following conventional SHM will be summed up and compared with the case in which only conventional simulators are involved. Figure 6-6 presents the whole workflow to verify the value of the proxy model in SHM.

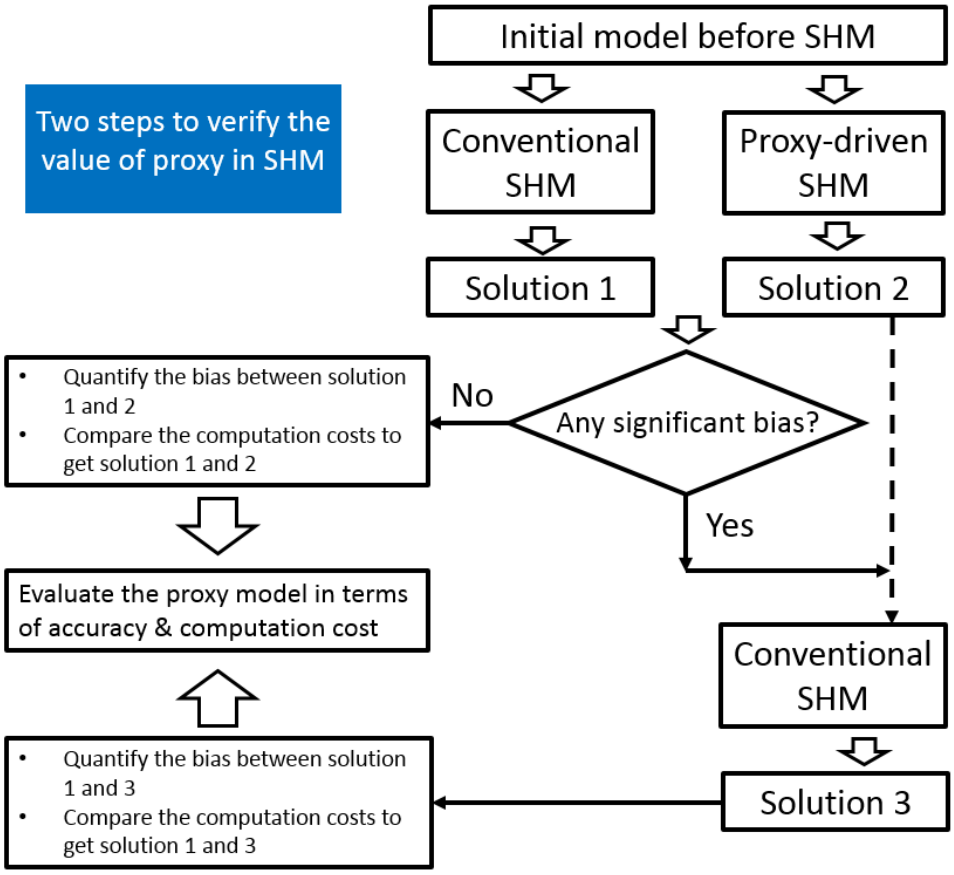

Figure 6-6 *Workflow of verifying the value of proxy model in the SHM workflow.*

6.3 Sim2seis proxy based SHM on Norne field

6.3.1 Parameterization

As mentioned in Chapter 3, one of the major uncertainties for Norne is the flow barriers and associated reservoir connectivity in the Ile and Tofte formations. Inspection of the initial simulation model also suggested that the connectivity should be reduced to match the water production data. I selected two main controls over the connectivity to be used as perturbed parameters for history matching: firstly, the transmissibility multipliers of local barriers and faults in the region of field to conduct history matching. Secondly, the vertical permeability multipliers of the simulation layers within the region. The ranges used for all the parameters are presented in Table 6-1.

These ranges were selected generally based on engineering judgement, so that the simulation model after history matching remains containing geological meaning and is consistent with the prior understanding of the field.

The upper limit of the barrier transmissibility multiplier is 10^0 and the lower limit is 10^{-4}, such that the barrier would be reduced and flow resistance would increase in history matching. The local barriers are relatively small in size; however, the two main faults in the region are too large to apply a single multiplier for the whole fault, which is the same case as the vertical permeability multiplier of the whole layer in the region. Therefore, the faults and horizontal layers were divided into parts and each was assigned with a multiplier. The upper limits are larger than 1, and the lower limits are 10^{-2} and 10^{-3} respectively. Hence, the partial sealed faults and discontinuous shale layers can be properly presented.

Table 6-1 *Uncertain parameters and value ranges.*

parameter	number	Power value range (10^x)
Barrier transmissibility multipliers (BTM)	5	[-4, 0]
Faults transmissibility multipliers (FTM)	10	[-2, 2]
Vertical permeability multipliers (VPM)	15	[-3, 3]

There were 30 parameters in total which were initially selected, then a one-at-a-time algorithm (Dehghan et al., 2012) was applied for sensitivity analysis to screen out the top 10 sensitive parameters (Figure 6-7 and Table 6-2) for the history matching exercise.

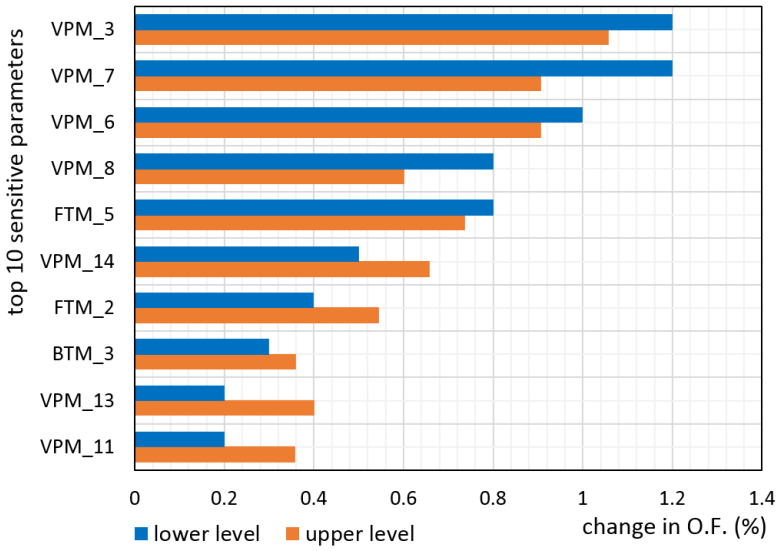

Figure 6-7 *Top ten sensitive parameters (transmissibility multipliers between geobodies) after the sensitivity analysis for the SOHM on Norne*

Table 6-2 *Selected sensitive parameters and value ranges*

Parameter	Number	Value range (10^x)
Barrier transmissibility multipliers (BTM)	1	[-4, 0]
Fault transmissibility multipliers (FTM)	2	[-2, 2]
Vertical permeability multipliers (VPM)	7	[-3, 3]

6.3.2 Objective function

As introduced in the first chapter, the objective function of seismic history matching is normally an integration of well production data and seismic data. However, my main purpose in conducting SHM in this chapter is to test the performance of a linear superposition seismic proxy model; therefore, a 'normalized square error' objective function (Equation 6.1) which consists only of the seismic data is used in the SHM.

$$O.F. = \frac{\sum(sim_i - obs_i)^2}{\sum(obs_i)^2} \times 100\% \tag{6.1}$$

where sim_i stands for the i^{th} cell of the simulated (by sim2seis or proxy) seismic map, and obs_i is the observed seismic at the corresponding cell.

6.3.3 Optimisation algorithm

The Particle Swarm Optimisation (PSO) algorithm was used in this history matching. It is a swarm intelligence technique originally introduced by Kennedy and Eberhart (1995). Subsequently, a substantial number of adaptations (Schutte et al., 2003, Brits et al., 2002, Blackwell et al., 2005) have been made to the basic algorithm. The variant I applied was developed by Engelbrecht et al., 2005.

This population-based approach is different from other population-based evolutionary methods, which use some form of evolutionary operators in order to move the population towards the global optimum (Holland, 1992). Here the "particles" which make up the population move in the search range with a velocity that is determined by a simple equation relating the experience of each individual particle and the population. In essence, each individual particle memorises the best position it has encountered and uses this together with the memory of the best position of its neighbours/population found thus far. Hence changes in the particle's trajectory from these influences are then made to its velocity in each iteration and this gives the particle direction in the search space. Position updates are then made from the new calculated velocity, which is illustrated in the following equation:

$$v_i^{t+1} = \omega \cdot v_i^t + c_1 \cdot rand_1 \cdot (P_i - x_i^t) + c_2 \cdot rand_2 \cdot (P_g - x_i^t) \tag{6.2}$$

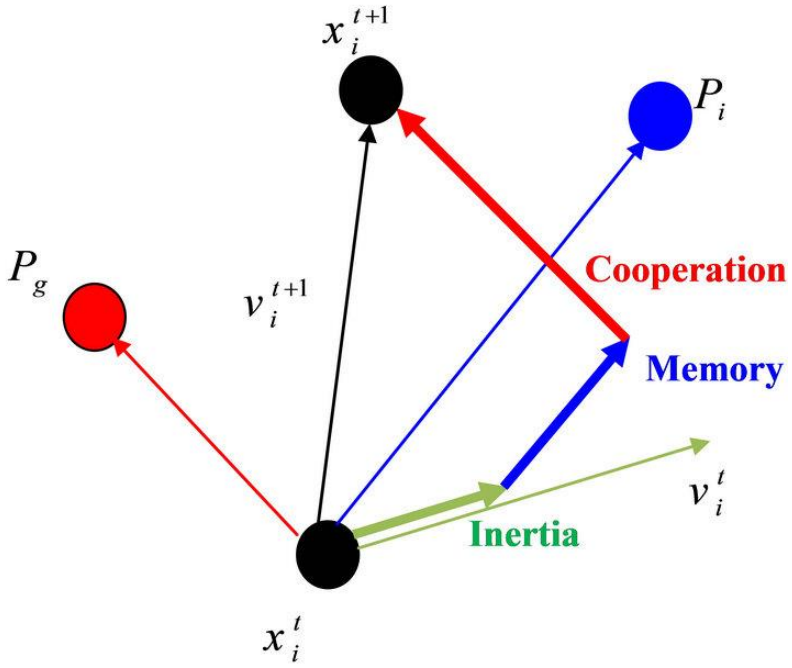

Figure 6-8 *Illustration of velocity and position updates in PSO algorithm.*

The velocity updating equation (Equation 6.2) has three major components. Figure 6-8 illustrates the updating mechanism which is as follows:

1) The first component, referred to as inertia, models the tendency of the particle to continue in the same direction it has been moving.

2) The second component, referred to as memory, is a linear attraction towards the best position ever found by the particle.

3) The third component, referred to as cooperation, is a linear attraction towards the best position found by the particle swarm.

The next issue that arises in the implementation is how to deal with particles that go out of the boundary range. Four boundary handling mechanisms can be employed: absorbing, reflecting, invisible and damping (Kathrada, 2009). In this work a reflecting strategy is applied, as depicted in Figure 6-9.

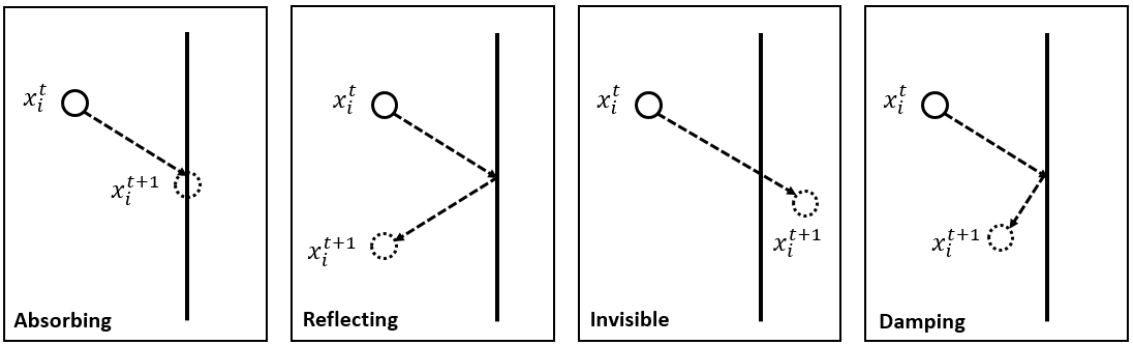

Figure 6-9 *Boundary handling mechanisms used in the PSO algorithm (Kathrada, 2009).*

In addition, the PSO is set up with 40 particles for 50 iterations, leading to a maximum of 2000 times of simulation model running and evaluation of the objective function. All of the configuration parameters of this algorithm are listed in Table 6-3.

Table 6-3 *Configuration of parameters for the PSO algorithm used in the SOHM on Norne.*

Parameters	Value
Dynamic inertial weight $\boldsymbol{\omega}$	0.4-0.9
Weights $\boldsymbol{c_{p\_best}}$	2
Weights $\boldsymbol{c_{g\_best}}$	2
Boundary condition	Reflecting strategy
Swarm size	40
Max iteration	50

6.3.4 Results

In this section, the results for a seismic only history matching (SOHM) conducted on Norne field are reported. Sim2seis and the fixed proxy work respectively as the seismic modelling part in the SHM loop (Figure 6-10), and the target of this part is to test the usage of a proxy model in history matching procedures by comparing the results of proxy driven SHM and sim2seis driven SHM.

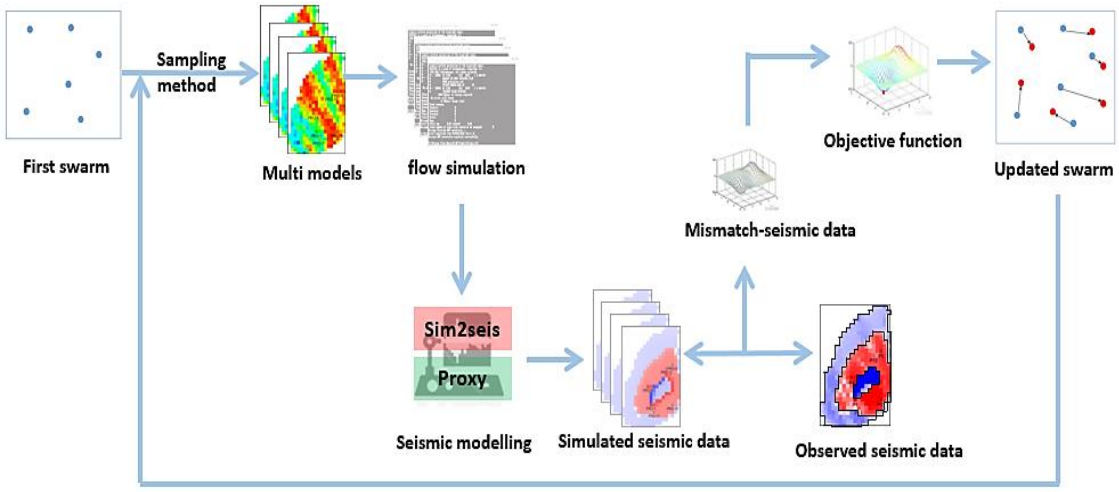

Figure 6-10 *The loop of SOHM where sim2seis and proxy can work independently as the seismic modelling module.*

Figure 6-11 plots the convergence of the objective function for the use of only the seismic data in the HM. The top is the sim2seis assisted SOHM and the bottom is the proxy assisted SOHM. The black bars denote the range of the objective function value of the ensemble and present the level of uncertainty inside the ensemble of simulation models: a shorter bar means a more similar model (or, a set of more concentrate parameter values). The mean value of the objective function of the ensemble is marked as black dots. After 40 iterations both schemes converged to the solution, thus the converging speed of two SOHM schemes were comparable. In terms of the specific parameter value, the two optimal solutions should be further compared.

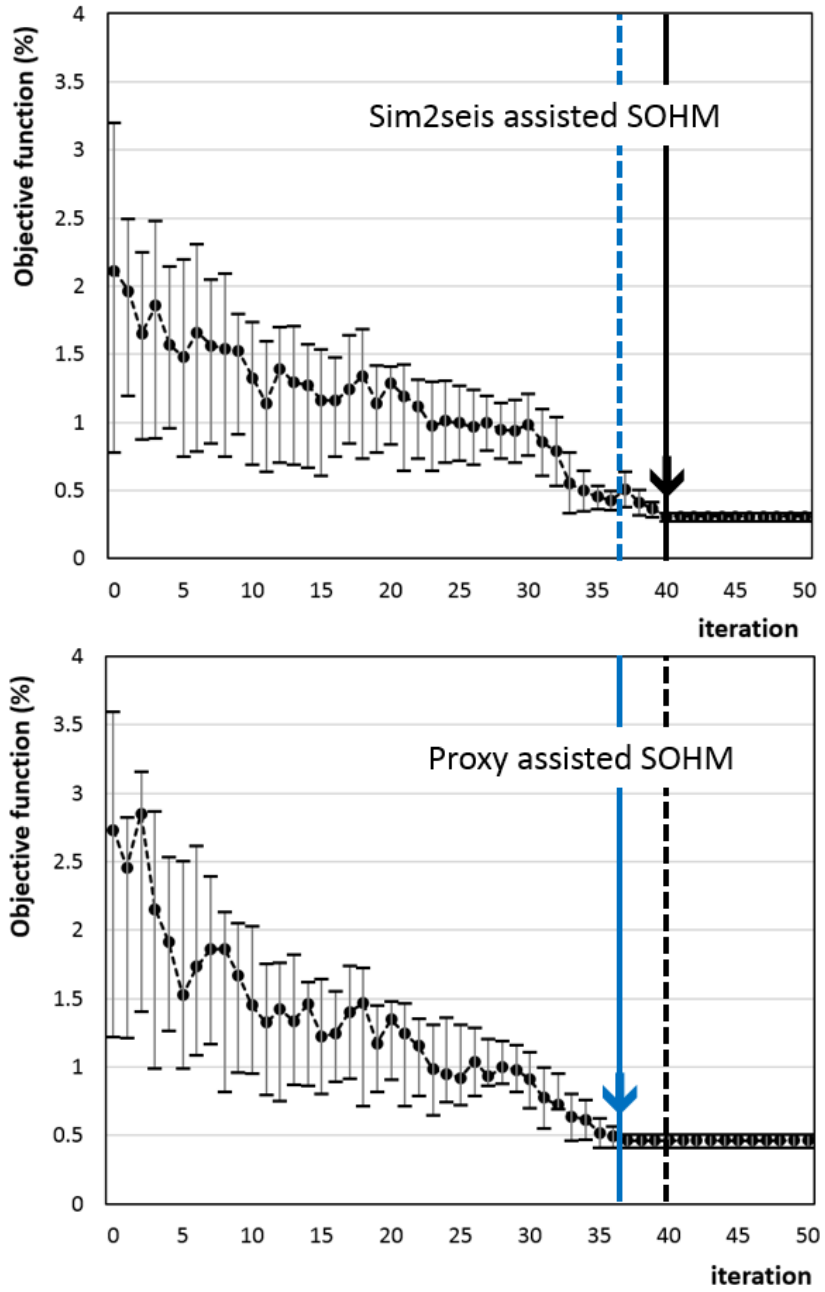

Figure 6-11 *Convergence of the objective function for seismic only history matching. Top: sim2seis assisted SOHM (black line); below: proxy assisted SOHM (blue line).*

The histograms of the selected converging parameters are displayed in Figure 6-12, in which it can be seen that the final parameters' distributions are similar with both the sim2seis driven and proxy model driven SHM. The results show that all of the three selected parameters have very close distributions after the two SOHM workflows, indicating that the proxy model worked as a good approximation of the sim2seis in this work.

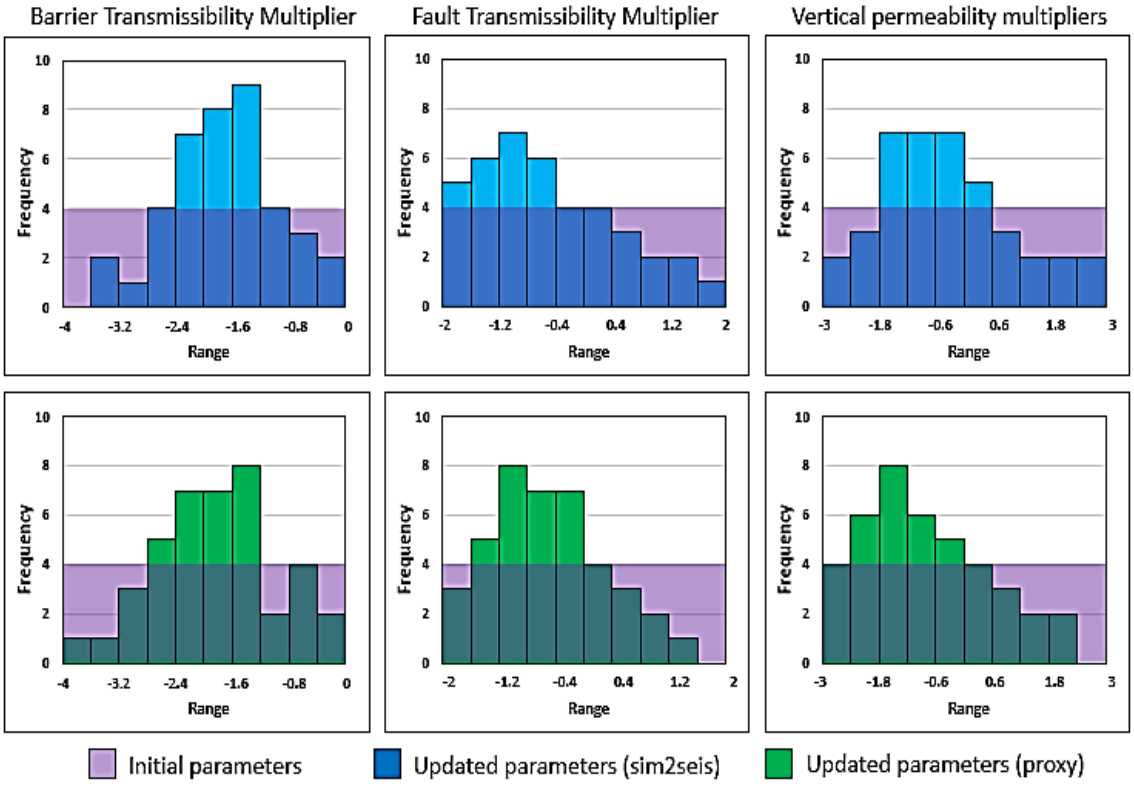

Figure 6-12 *Histogram of selected parameters before and after sim2seis driven SOHM (top) and proxy model driven SOHM (below).*

The solutions of both SHMs are plotted in Figure 6-13: the left map shows the observed seismic data and the top middle box is the seismic map which was simulated based on the initial simulation model; the bottom middle map was simulated by the proxy model before history matching. The solution of the sim2seis-derived SHM is plotted at the top right, while below is the proxy-assisted SHM solution. It is observed that in the solution maps of both SHMs, the hardening signal in the black box is stronger than the in map before SHM; this is caused by the perturbation of nearby fault transmissibility and vertical permeability multipliers, as shown in Figure 6-12.

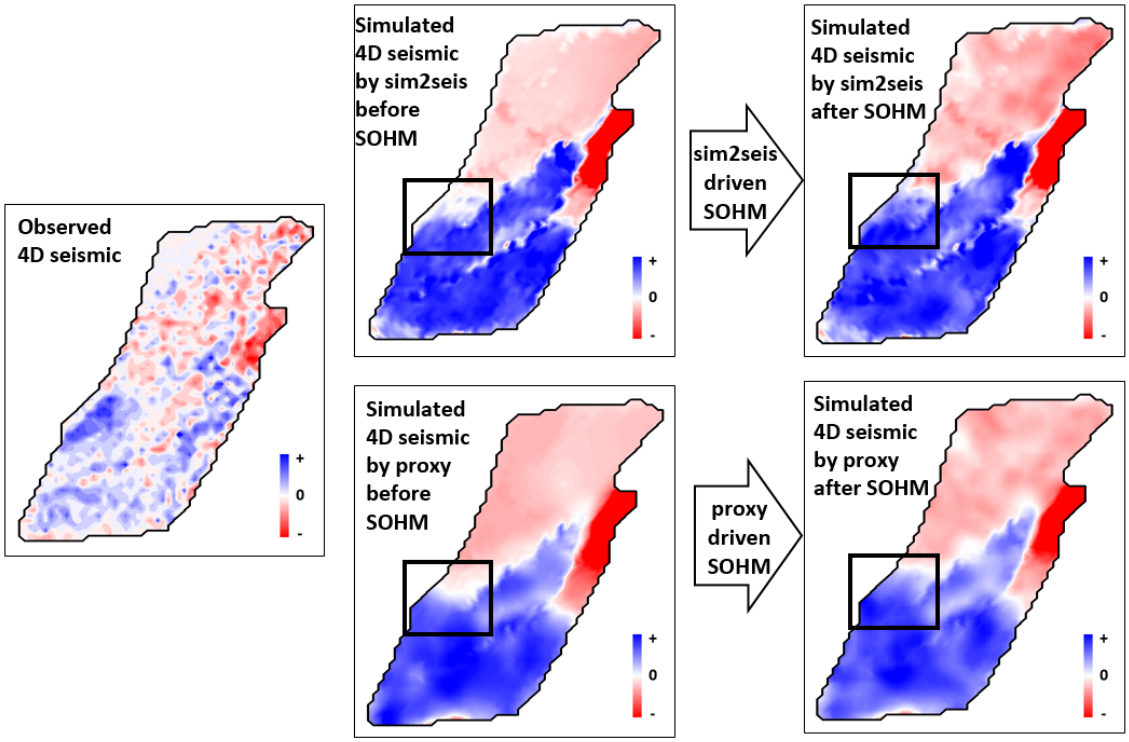

Figure 6-13 *Histogram of selected parameters before and after sim2seis driven SOHM (top) and proxy model driven SOHM (below row).*

Moreover, although the objective function of the two SHMs contains only seismic data (Equation 6.1), the matching of production data is also improved in both cases. The water cut data for a selected producer E-1H is plotted in Figure 6-14. It is observed that the initial simulation model over-simulated the water cut (WWCT) during the year 1997-2003. Regardless of using sim2seis or the proxy model, the water cut matching is improved significantly after SHM, which confirms that the information contained in the well production data are covered by the 4D seismic data, thus, the seismic only history matching procedure can help the well production data match.

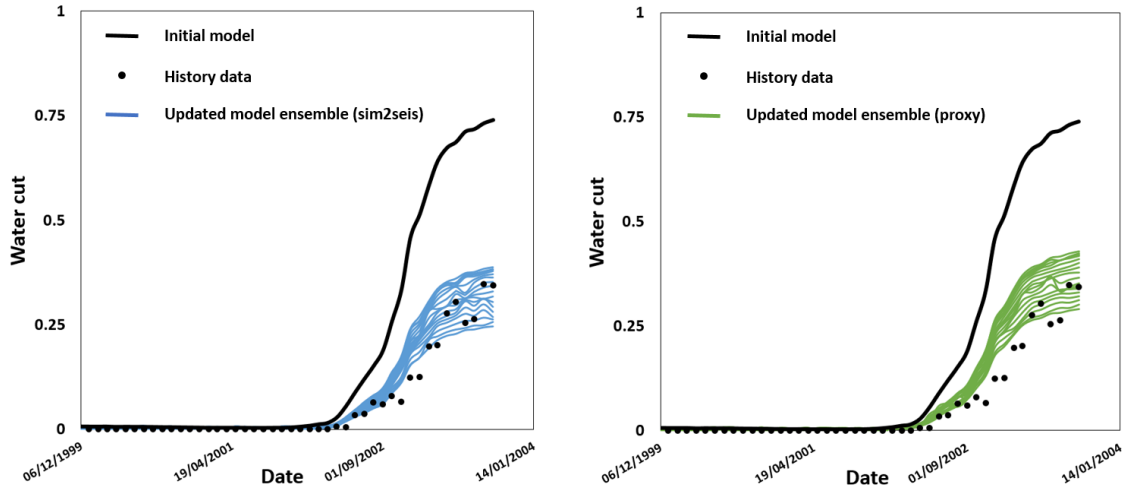

Figure 6-14 *Improvement of water cut matching of a producer E-1H after sim2seis driven SOHM (left) and proxy driven SOHM (right).*

In terms of the computation time, a single run of sim2seis (petro-elastic modelling, 1D convolution plus map extraction) on a standard computer workstation (Intel CPU i7-3770 @ 3.40GHz) with 8 processors takes approximately 800 seconds, while the proxy only needs couple of seconds (Table 6-4). In the SHM loop where fluid flow simulation is also included, the total computation cost can be reduced by 55% by using the proxy (Figure 6-15). As demonstrated in Figure 6-15, the conventional fluid flow simulation model was used in both SOHM workflows. In the next section, I will report the testing of two proxy models of fluid flow simulation in the SHM on Schiehallion field.

Table 6-4 *A comparison of the computation cost of the sim2seis and the proxy model: single iteration running time and the total cost of the SOHMs driven by these two models.*

	3D model + sim2seis	3D model + sim2seis proxy
Computational cost of models building (seconds)	0 [a]	5000 [b]
Computational cost of single iteration run (seconds)	1,450 [c]	660 [d]
Total computation cost of the SOHM (hours)	805.5 [e]	366.7 [f]

a: A reference 3D fluid flow simulation and sim2seis model are the start point of the whole work, thus there is no extra time consumed on building these two models.
b: The time needed for the linear regression of the sim2seis proxy.
c: Each iteration contains the running of the 3D flow simulation model and the sim2seis model.
d: Each iteration contains the running of the 3D flow simulation model and the sim2seis proxy model.
e: SOHM total computation cost=single '3D model + sim2seis' iteration running time × ensemble size (40) ×iteration (50).
f: SOHM total computation cost=single '3D model + sim2seis proxy' iteration running time × ensemble size (40) ×iteration (50).

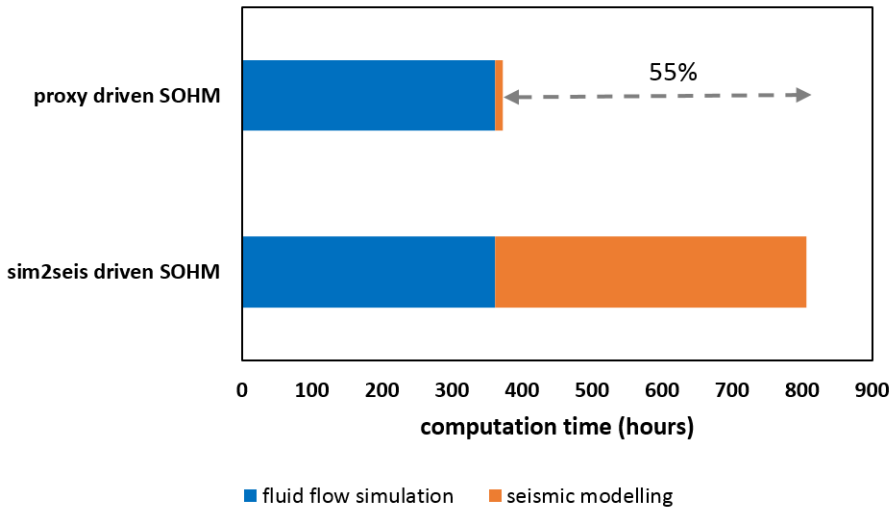

Figure 6-15 *Computation cost of sim2seis and proxy model: single model running time.*

6.4 Fluid flow proxy model based SHM on Schiehallion field

6.4.1 Parameterization

According to the reservoir geology and development history of Schiehallion field, which was described in Chapter 4, the connectivity between geobodies is the main uncertainty for the reservoir simulation. In the initial 3D simulation model which was built by the operator, the reservoir connectivity was controlled by the keyword MULTREGT (Eclipse manual, Schlumberger 2014), which stands for the transmissibility multipliers between two regions. As mentioned earlier, these regions are provided by the seismically-mapped geobodies, and the majority of these geobodies have localised "pancake" or channel-like shapes. In the initial 3D model, these geobodies were interpreted at fine scale (Figure 6-16, top) and the total number of multipliers between geobodies was over 200. However, in order to perform history matching efficiently, the total uncertain parameters should be reduced to a small number.

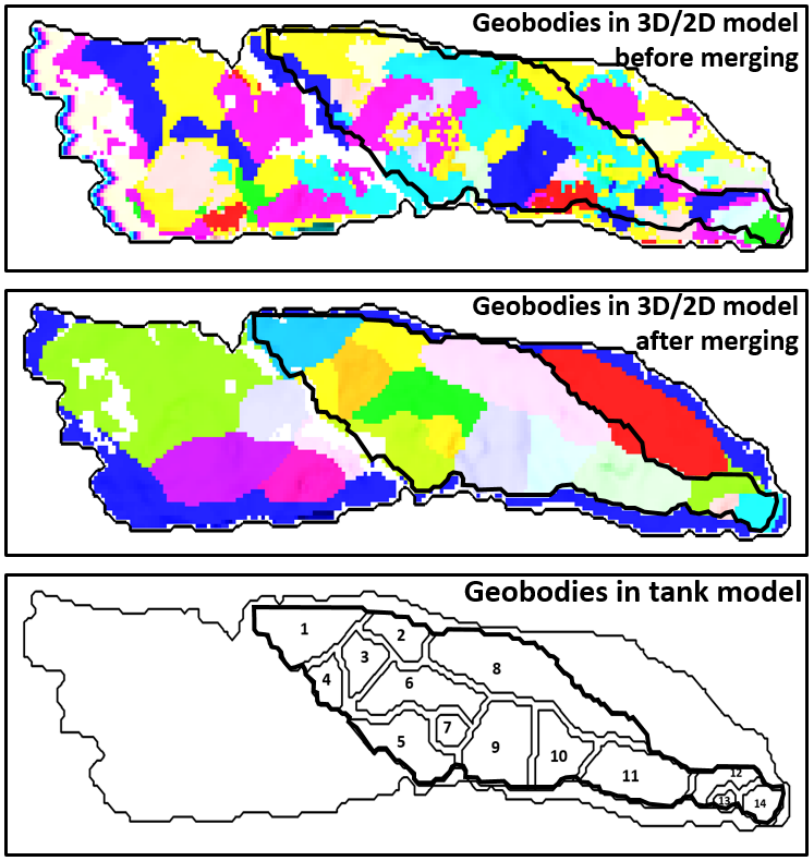

Figure 6-16 *The region of segment 4 to conduct SHM: in the 3D (and 2D) model before merging fine scale geobodies (top), after merging fine scale geobodies (middle) and the tank distribution in the multiple tank model (bottom).*

In my study, three procedures were applied to reduce the number of parameters: 1) region selection; 2) geobody merging and 3) sensitivity analysis. In considering the building of the tank model (see Chapter 5), only a part of the segment should be selected to build the multiple tank model (Figure 6-16, bottom). In order to compare the results of SHM driven by the 3D model, areal model and tank model respectively, the same region should be selected to carry out SHM in the 3D and areal models (Figure 6-16, middle). After determining the region in which to conduct SHM, the next step was to merge the neighbouring fine scale geobodies to reduce the total number of parameters. In addition, in order to have same parameterization on the three models, the geobodies in the 3D model and 2D model were merged according to the tank boundaries. It was calculated in Chapter 5 that the total number of T_{ij} is 24, and following the same sensitivity analysis method as in the previous section, the top 10 sensitive parameters (Figure 6-17) were screened out to perform the SHM. Thus, the total number of uncertain parameters was reduced (Table 6-5) and the three models had the same parameterization, making it possible to compare the results of SHM driven by the three models.

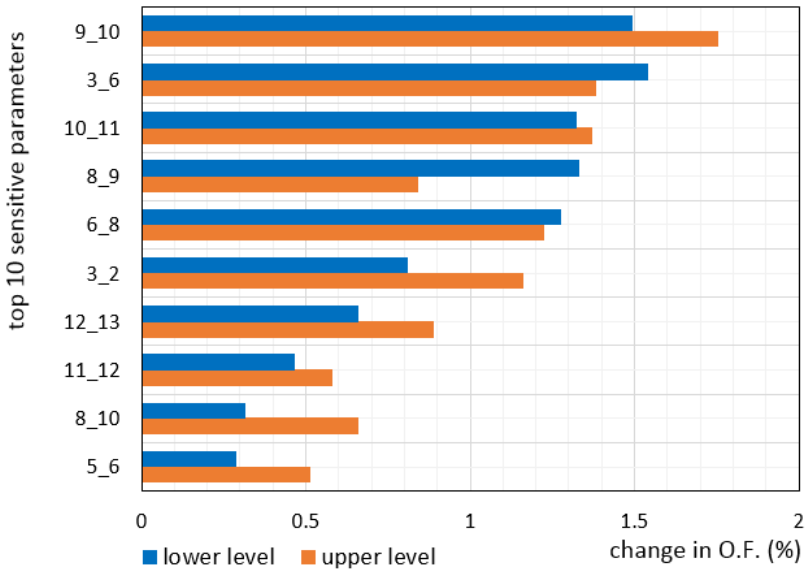

Figure 6-17 *Top ten sensitive parameters (transmissibility multipliers between geobodies) after the sensitivity analysis for the SHM on Schiehallion.*

Table 6-5 *Uncertain parameters used in the SHM on Schiehallion: parameter number and value range.*

	Parameter number: in 3D model	Parameter number: after geobody amalgamation	Parameter number: after sensitivity analysis	Parameter value range
Transmissibility multipliers between geobodies	156	24	10	[0.1, 10]

6.4.2 Objective function

The SHM conducted here involves the matching in two domain: seismic and well production. Thus the two mismatches should be included in the total objective function. Similarly, to the formulation in the earlier section, the 'normalised square error' is suitable for the mismatch of mapped seismic M_s; the 'normalised absolute error' is applied for BHP curves M_w. In order to combine the two sources of mismatch, two weights are also needed. In this case, I used the most common used weights (Obidegwu, 2017): W_s=0.5 and W_w=0.5.

$$\begin{cases} \mathrm{OF} = W_s \cdot M_s + W_w \cdot M_w \\ M_s = \frac{\sum(Sim_{s,i} - Obs_{s,i})^2}{\sum(Obs_{s,i})^2} \\ M_w = \frac{\sum|Sim_{w,i} - Obs_{w,i}|}{\sum|Obs_{w,i}|} \end{cases} \tag{6.3}$$

As explained in Chapter 4, there is a well-matched 3D simulation model with the observed data (Figure 4-11 and Figure 4-14). It has to be taken into account that the observed seismic and BHP data inescapably contain noise. In order to avoid the effect of such noise on the analysis of proxy performance, the simulation outputs of this history-matched 3D model will be regarded as the synthetic history. Thu the $Obs_{s,i}$ and $Obs_{w,i}$ in Equation 6.3 are simulation results of this history-matched 3D model.

6.4.3 PSO configuration

The Particle Swarm Optimisation (details in section 6.3.3) algorithm is applied in this study and the configuration parameters are listed in Table 6-6.

Table 6-6 *Configuration of parameters for the PSO algorithm used in the SHM on Schiehallion.*

Parameters	Value
Dynamic inertial weight $\boldsymbol{\omega}$	0.4-0.9
Weights $\boldsymbol{c_{p\_best}}$	2
Weights $\boldsymbol{c_{g\_best}}$	2
Boundary condition	Reflecting strategy
Swarm size	40
Max iteration	50

6.4.4 Results

After building the areal model (Chapter 4) and the tank model (Chapter 5), this section reports how I conducted three SHMs, independently driven by the 3D model, the areal model and the tank model. The performance of the two proxy models was tested through a comparison between the results of the proxy-driven SHMs (two treatment groups) and a conventional SHM (control group) where the 3D simulation model and sim2seis were applied (Figure 6-18).

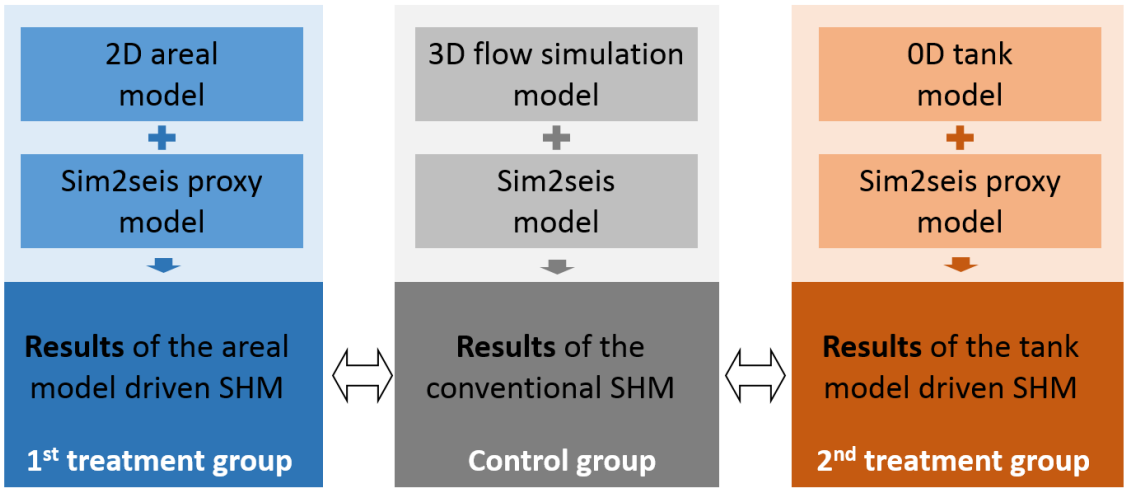

Figure 6-18 *Illustration of the three SHM workflows conducted in this section: the conventional SHM (middle column), which plays as the control group; the areal model driven SHM (left column, the first treatment group) and the tank model driven SHM (right column, the second treatment group).*

Based on the PSO optimisation algorithm, the convergence of the OF of the three SHMs are plotted in Figure 6-19. The results show that the three SHM schemes have close convergence speed: converging after 35 iterations. Thus, in terms of converging speed the two proxy model assisted SHMs and the conventional SHM are very close. If we look at the specific parameter values of their optimal solutions, the histograms of three selected parameters are presented in Figure 6-20. As mentioned earlier, this is a synthetic SHM of which the optimal solution is known: the value of the 10 multipliers are all equal to one. It is observed that all three SHM schemes successfully converged to the real optimal solution: their optimal values are all equal to one. However, although the distributions of parameter value obtained by the 3D model and the areal model (Figure 6-20, top and middle rows) both have clear unimodal distribution (the mean standard deviations σ=0.53 and 0.63), the tank model driven SHM results are less converged (mean standard deviations σ=2.7), compared to the top two rows.

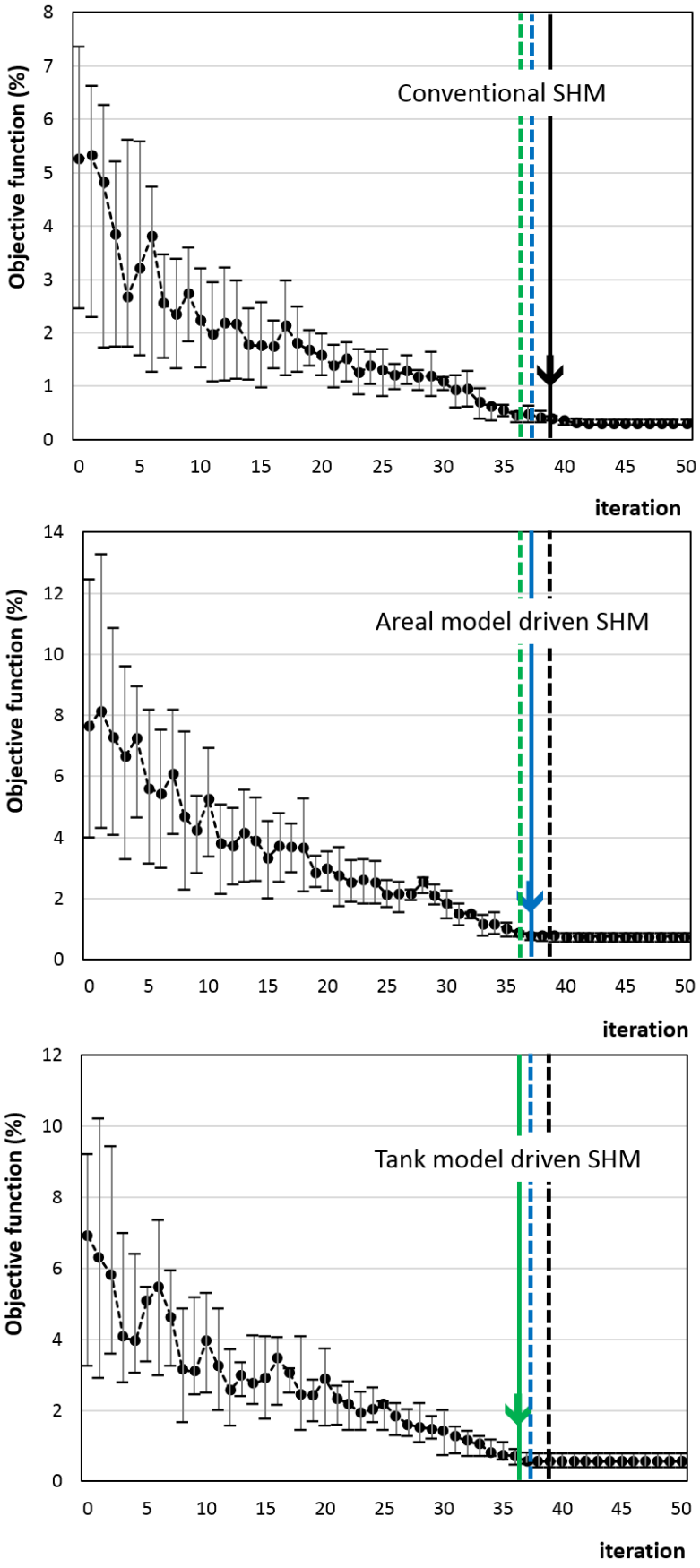

Figure 6-19 *Converging lines of the objective function for the seismic history matching. Top: the conventional SHM (black line); middle: the areal model driven SHM (blue line) and bottom: the tank model driven SHM (green line).*

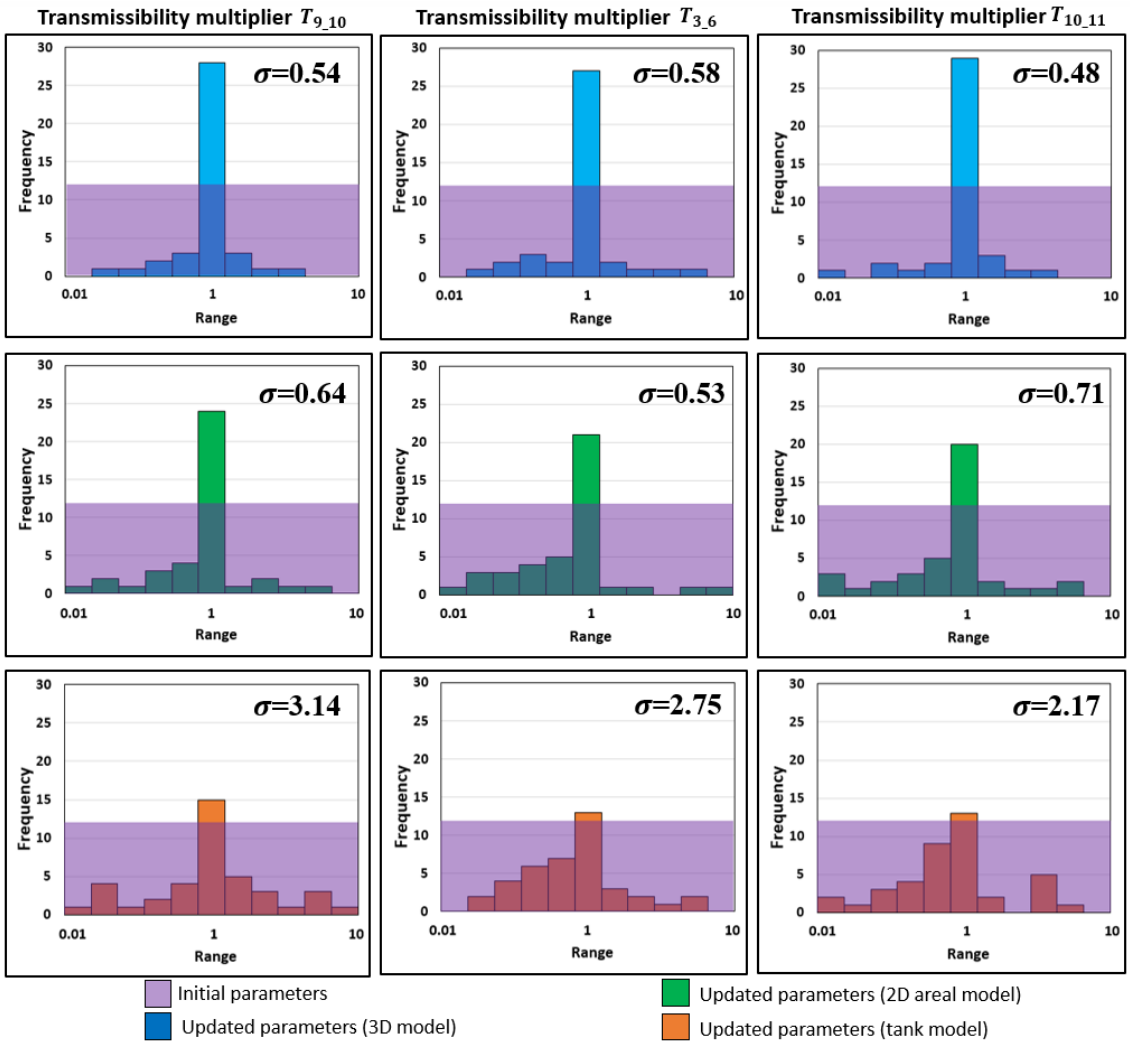

Figure 6-20 *Histogram of selected parameters before and after the conventional SHM (top), the areal model driven SHM (middle) and the tank model driven SHM (below).*

According to the workflow introduced in section 6.2 (Figure 6-6), the 2D areal model result and 3D model results are at similar magnitude (no significant bias), thus the solution of areal model driven SHM could be accepted as a good approximation of the solution of the conventional SHM. In order to establish the value of this proxy model, only the computation cost needs to be further considered (Table 6-7). However, the bias between results of the tank model driven SHM and the conventional SHM is clearly higher than that of the areal model; thus, a second stage of conventional SHM is needed, based on the solution of the tank model driven SHM (Figure 6-21). After this second stage of conventional SHM, the solution needs to be analysed (Figure 6-22) and the total computation cost of two-stage SHM will be summed up (Table 6-7).

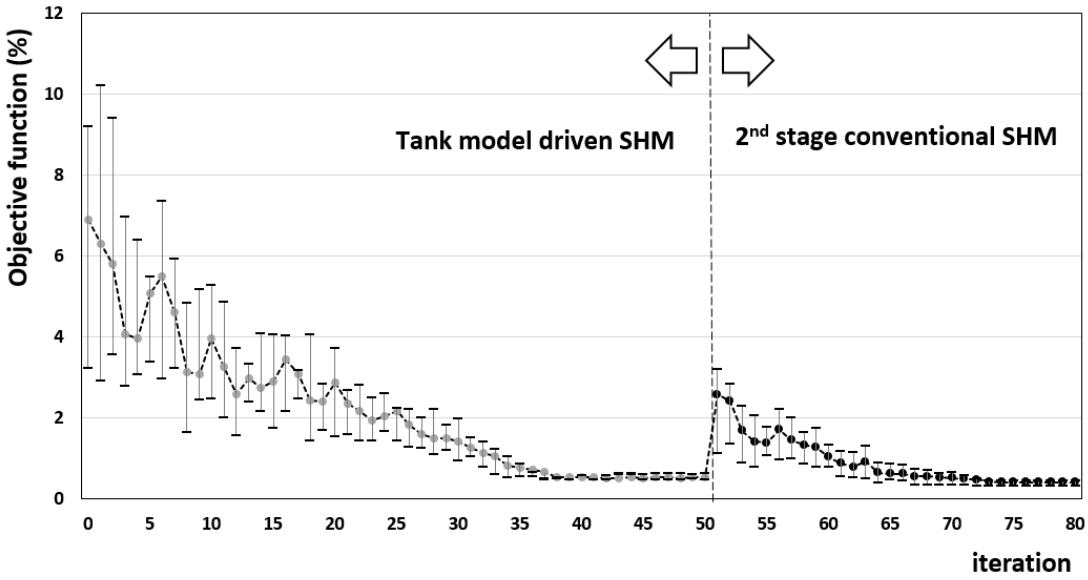

Figure 6-21 *Converging lines of the objective function for the tank model driven SHM and the second stage conventional SHM.*

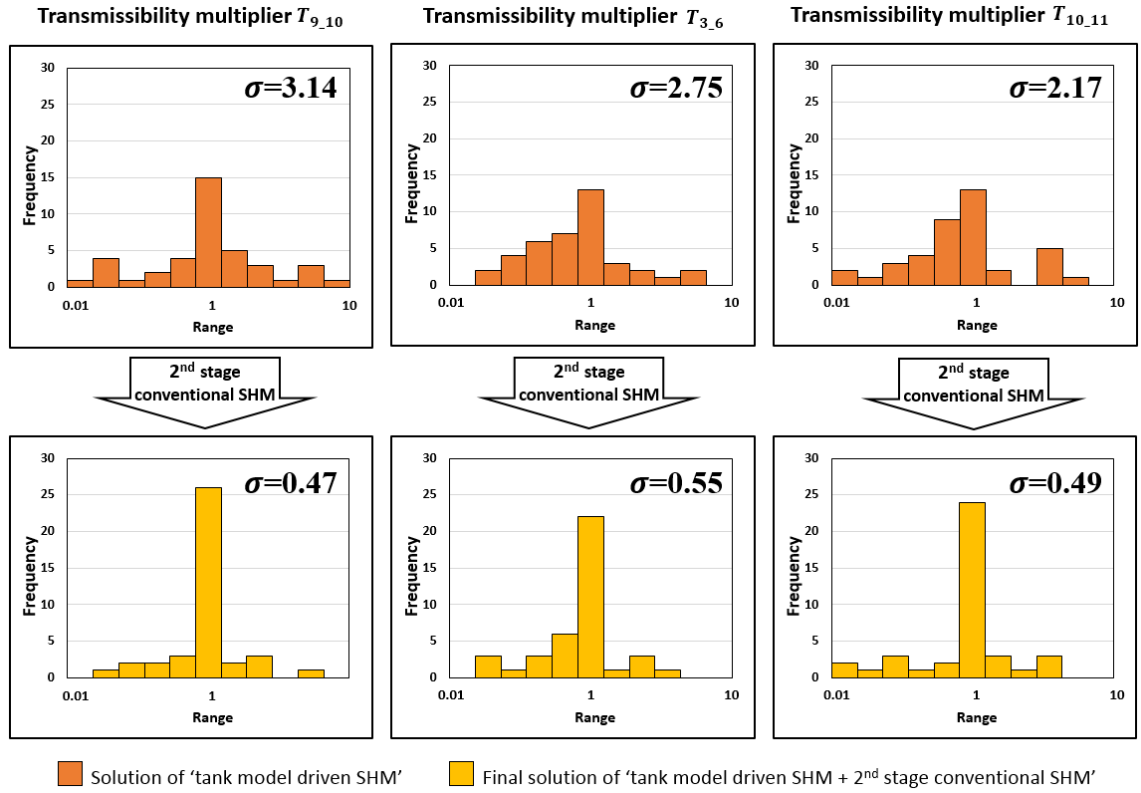

Figure 6-22 *Histogram of selected parameters after the tank model driven SHM (upper) and the second stage conventional SHM (below).*

Figure 6-21 presents the procedure of the 'tank model driven SHM + 2nd stage conventional SHM'. Based on the optimal solution obtained by the tank model driven SHM, the second stage conventional SHM firstly meet a jump in the objective function values. (That's because, the same ensemble of scenarios were evaluated by 3D model in the first stage, and by the 3D model in the second stage.) As the figure shows, the converging line found the final solution after the extra 30 iterations. The total number of needed iterations was 50 (tank model driven SHM) plus 30 (conventional SHM). These two solutions are plotted in Figure 6-22 in terms of the specific parameter values. It is observed that after the second conventional SHM, the final solution has smaller value of standard deviation (σ), which is close to both the conventional SHM solution and areal model driven SHM solution (Figure 6-22). Base on this observation, I draw the conclusion that the 'tank model driven SHM (50 iterations) + second stage conventional SHM (30 iterations)' workflow produced similar results to the conventional SHM (50 iterations) and areal model driven SHM (50 iterations). According to the workflow in Figure 6-2, apart from the solution accuracy, the other aspect which needs to be considered to establish the value of the proxy model is the computation cost. The total time consumption of each of the three workflows is listed in Table 6-7.

Table 6-7 *A comparison of the computation cost of the 3D model, 2D model and tank model: single iteration running time and the total cost of the SHMs driven by these models.*

	3D model + sim2seis	Areal model + sim2seis proxy	Tank model + sim2seis proxy
Computational cost of model building (s)	300 [a]	300 [b]	54600 [c]
Computational cost of single iteration run(s)	787	245	172
Total computation cost of the SHM (h)	437.2 [d]	136.1 [e]	373.1 [f]

a: A history matched 3D fluid flow simulation is the start point of the whole work, thus there is no extra time consumed on building the 3D fluid flow model; the time is needed by the linear regression procedure to build a linear sim2seis proxy.

b: The 'areal model building' procedure contains the vertical upscaling of the fluid flow model and the linear regression of the sim2seis proxy.

c: The building of the tank model contains two main parts:1) the initial configuration data transformed from 3D model to tank model (Table 5-1 and section 5.3.1); 2) model initialization (section 5.3.2).

d: 3D model driven conventional SHM total computation cost=single 3D model and sim2seis model running time × ensemble size (40) ×iteration (50).

e: Areal model driven SHM total computation cost=single areal model and sim2seis proxy model running time × ensemble size (40) ×iteration (50).

f: Tank model driven SHM total computation cost=single tank model and sim2seis proxy model running time × ensemble size (40) ×iteration (50) + single 3D model and sim2seis model running time × ensemble size (40) ×iteration (30).

These results show that, if we use the conventional SHM as the reference, the areal model driven SHM and tank model driven SHM (two stages) can both produce close results with lower computation cost. However, although the tank model has the lowest single model running time, it needs a second stage to converge to the final solution, this makes the workflow very complex and incurs extra computation cost. Thus, considering the workflow complexity and computation cost, the areal model is recommended to carry out SHM in this case. By applying the areal model, the computation cost of conventional SHM can be reduced by 70% (Figure 6-23). However, it has to be pointed out that this improvement percentage is case dependent; if a longer production history was used in the SHM, then this value could be higher. More details will be explained in the next chapter.

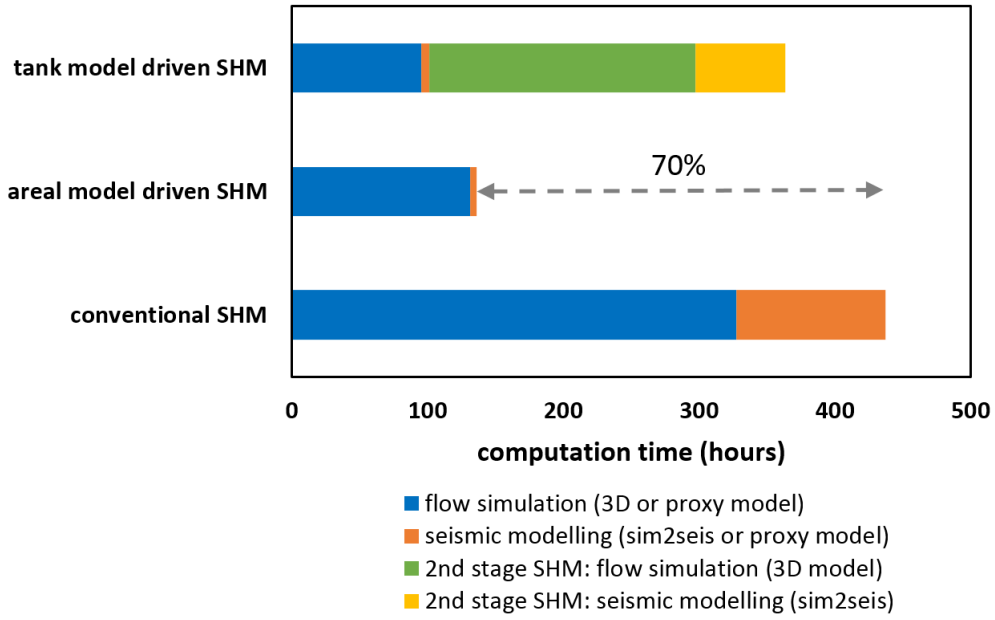

Figure 6-23 *Computation cost of the conventional SHM, the areal model driven SHM and the tank model driven SHM.*

6.5 Summary

In this chapter, the value of 4D seismic and the three proxy models which have been developed in previous chapters were explored in the SHM workflow. The first test, conducted on the Norne field, confirmed that the spatial information contained in the 4D seismic can help to match the sparsely located well BHP data. The results of this SOHM workflow also indicated that the linear superposition sim2seis proxy is a good approximation of the conventional sim2seis model. Both SOHM workflows, driven by the proxy model or the conventional sim2seis model, led to close solutions. The second test, conducted on Schiehallion field, was designed to establish the value of the two proxy models of fluid flow simulation. It was observed that using the areal model could lead to SHM results comparable with those of conventional simulator driven SHM, but with a time saving of 70%. However, the tank model was found to be oversimplified, because the tank model driven SHM results had higher bias compared with the reference conventional SHM results. According to the evaluation method I developed in the previous section of this chapter, a second stage conventional SHM was conducted based on the tank model driven SHM solution. The final solution of this 'tank model driven SHM + conventional SHM' workflow was close to the reference case, but the total computation cost was not reduced as much as in the case of areal model driven SHM. Thus in this case, the areal model is considered a better simplification of the 3D model for the Schiehallion field.

It has to be pointed out that the evaluation of proxy models is case-dependent: it cannot be known before running any simulation. The goal of this chapter is not to make any solid judgement that 4D seismic is always valuable in any case or that the tank model is never recommended. If we have longer production history then the performance of a tank model may surpass the areal model. The objectives of this chapter were to 1) design a new method to evaluate the 4D seismic data and proxy models in the SHM workflow; and 2) test the three proxy models which have been built in previous chapters. Two tests were conducted on Norne and Schiehallion field, and the results and conclusions were aimed to achieve these objectives. Potential ways to refine the evaluation method and enhance the three proxy models, will be discussed in the next chapter.

Chapter 7

Conclusions, limitations and recommendations

This chapter summarizes all the work that has been done in this thesis, presents the main conclusions and then provides recommendations for future work, which could enhance the efficiency and effectiveness of the method. The key objective of this thesis, which is the feasibility of applying a proxy model in the SHM workflow, is examined and the perceived limitations are used as a basis to prescribe future recommendations.

7.1 Conclusions

Using 4D seismic in reservoir engineering and management quantitatively is a rewarding but challenging job. SHM is such a procedure, in which the 4D seismic data and well production data are integrated to calibrate the reservoir simulation model. The objectives of this thesis were to explore potential proxy models to tackle certain challenges associated with SHM, such as the speed, the multi-domain challenge and communication barriers between experts in different fields. The proxy was built as a simplification of the two forward simulators used in the SHM workflow. In Chapter 2, the two simulators were first reviewed, followed by a review of different kinds of proxy models used in literature. Subsequently, three proxy models were built and validated, as described in the following three chapters.

The first proxy model was built for the sim2seis model. Chapter 3 presented the building and validation of this linear superposition proxy model, which belongs to the 'response surface model' type. The inputs of the proxy model are the pressure and saturation changes simulated by the fluid flow simulation model and the output is the 4D seismic. The main assumption behind this proxy is that the 4D seismic response could be simplified as a linear superposition of the effects of 4D pressure and water and gas saturations. One scenario was firstly launched by sim2seis and the simulation results were used the training data. The linear equation containing three coefficients was used as the proxy function and the least-square method was applied in the linear regression to obtain the coefficients. The model was then applied on new scenarios and the proxy results and sim2seis results were compared both qualitatively and quantitatively. A blind test was set up to test the capability of the proxy model in model ranking, using the same objective function as that used in the SHM. This is a 'quasi-SHM' because no optimisation algorithm was involved; thus both the sim2seis model and proxy model were applied to evaluate the same group of thirty scenarios. The results indicated that the linear superposition proxy model can produce outputs close to those of the conventional sim2seis model. This chapter only presented the building and validation of the proxy model; the further application of the proxy model in the SHM workflow was described in Chapter 6.

As described in Chapter 4, an areal model was developed for the Schiehallion field as a proxy for the 3D flow simulator used in SHM. This belongs to the 'reduced order model' type, which is vertically upscaled from the 3D model to speed up the simulation and keep

enough simulation accuracy. The geology of thin reservoirs and nature of seismic resolutions are the main motivations of this method. The areal model has been tested through comparison of visualizations and upscaling the error quantification. Qualitatively and quantitatively, the areal model has been proven to be a good simplification of the initial 3D model, with lower computation cost. The areal mode was then tested in a blind test and it was observed that the 3D model and areal model worked almost equally in ranking the candidate models. In this chapter, the sim3seis proxy that was described in Chapter 3 was coupled with the areal model; therefore, the two forward simulators used in the SHM workflow could be circumvented.

In Chapter 5, this 2D areal model described in Chapter 4 is further 'upscaled' to a 0D multiple tank model (MTM), with material balance as a key control. This MTM is the second model built in this thesis as a proxy for the reservoir fluid flow simulator. It is a 'reduced physics' type proxy, which can also work together with the seismic modelling proxy. The combination of 'MTM + seismic proxy' is the main innovation point of this method. This combination was compared with the '3D model + seismic proxy' workflow, following a similar workflow to that used in Chapter 4: from model building, to qualitative comparison to blind test and robustness analysis. The main observation is that, for the Schiehallion field, the 'MTM + seismic proxy' was also able to reproduce similar results to the '3D mode + seismic proxy'. However, considering the model's accuracy, complexity and computational cost, this proxy was not found to be as powerful as the 2D areal model on the Schiehallion field.

Chapters 3 to 5 explained how three proxy models of three types were built, validated and blind tested, all based on the comparison between the proxy model and conventional simulator. As the ultimate goal is to use these proxies in the SHM workflow, proxy-assisted SHMs were reported in Chapter 6 to present the application of the three proxy models in the SHM workflow. Firstly, a new method was described to evaluate the effect of 4D seismic and the proxy models in the SHM workflow. Two tests were then conducted individually on the Norne and Schiehallion fields: the first one was to evaluate the effect of 4D seismic and to test the seismic proxy; the second one was to test the areal model and the multiple tank model. The first test, conducted on the Norne field, confirmed that the spatial information contained in the 4D seismic can help to match the sparsely located well BHP data. The results of this SOHM workflow also indicated that the linear superposition sim2seis proxy is a good approximation of the conventional sim2seis model. Both SOHM workflows, driven by the proxy model or the conventional sim2seis

model, led to close solutions. The second test, conducted on the Schiehallion field, was designed to establish the value of the two proxy models of fluid flow simulation. It was observed that using the areal model could lead to SHM results comparable with those of conventional simulator driven-SHM, but with a time saving of 70%. However, the tank model was found to be oversimplified, because the tank model driven SHM results had higher bias compared with the reference conventional SHM results. A second stage conventional SHM was conducted based on the tank model driven SHM (first stage) solution. The final solution of this 'tank model driven SHM + conventional SHM' workflow was close to the reference case, but the total computation cost was not reduced as much as in the case of areal model driven SHM. Thus, for the Schiehallion field, the areal model is considered a better simplification of the 3D flow simulation model.

Returning to the initial driving force of developing the proxy model, three challenges of SHM were considered: speed, the multi-domain challenge and communication barriers between different fields. Having explored the three potential proxy models and used them in SHM, it could be concluded that:

1) The three proxy models developed in this research could speed up the SHM workflow by simplifying the conventional simulation models.

2) By using a combination of proxy models, such as 'areal model + sim2seis proxy', the fluid flow simulation outputs ($\Delta P, \Delta S_w \; and \; \Delta S_g$) can be directly linked with the seismic amplitude domain ($\Delta Seis$). Thus, only a couple of runs of the petro-elastic model and convolutional modelling procedure are needed to train the model, then in later SHM iterations the time consuming seismic modelling process can be bypassed.

3) Compared with the conventional simulators, the sim2seis proxy and 3D fluid flow simulator, the proxy model method contains fewer parameters, which are much easier to interpret, based on which the reservoir engineers and geophysicists can better understand both of the models involved in the SHM.

7.2 Limitations and recommendations for Future Research

7.2.1 Sim2seis proxy

1) In this thesis, only the first order linear polynomial was applied as the response surface proxy model, in which the three parameters (ΔP, ΔS_w and ΔS_g) are assumed as independent. This model was proved useful for Schiehallion and Norne fields, however, to utilise this proxy model in other reservoirs, a second order or higher order polynomial models might be better option. In higher order response surface model, the interaction between parameters can be presented. For instance, there are three cross terms ($\Delta P \Delta S_w$, $\Delta P \Delta S_g$ and $\Delta S_w \Delta S_g$) in the quadratic polynomial which can present the interactions between different effects. Thus, a higher order polynomial equation might make a more predictive approximation for a new field.

2) The proxy model built in Chapter 3 was regressed and used for the whole region. However, the controlling parameter for modelling the 4D seismic may vary over the whole region. For example, in some areas without any gas saturation change, the response surface model could be simplified by a two-item equation, containing only pressure and water saturation. Therefore, the whole region could be divided into sub-regions and for each of them, a distinct proxy model can be built.

3) The another assumption behind the linear superposition model is that the model coefficients were assumed as constant during the production history. To be more predictive, the model should be updated over the whole time period. In the future work, a recommendation is to build proxy models for different stages of the development history. For instance, before and after the gas exsolution, the proxy equation could be updated.

7.2.2 Areal model

1) The field which was used to test the model, Schiehallion, is a unique thin reservoir and thus can be simplified as one areal model. To generalise this method to other thicker reservoirs, such as Norne, where many vertical flow barriers exist inside the reservoir, the field cannot be regarded as one single layer. In this more general case, the ‘multilayer model’ might be applicable, which consists of a set of areal models. In future research, the multilayer model should be validated to generalise this method. One of the challenges of building the multilayer model could be analysing and understanding the vertical

connectivity between reservoir layers. An integration of well production data with 4D seismic data (Yin 2016) can work as a useful tool to do this analysis prior to building the proxy model.

2) In this thesis, the areal model was upscaled from the initial 3D model by using the vertical averaging method and in the XY-refined areal model, the model downscaling was implemented by a single refinement method, from 1×1 to 2×2, and there was no local refinement. Although the XY-refined model was not proved to bring much benefit in accuracy but needed more computation, a locally-refined areal model may improve the model's accuracy with low extra computing cost. The locally refined model could be built and tested for the case where local reservoir heterogeneity research is needed.

3) The areal model built in this thesis was upscaled from the 3D model: all the reservoir properties were vertical averages of the reference 3D model. In another way, these 2D properties can also be interpreted from mapped seismic. For instance, the NTG distribution map can also be interpreted from the 3D or 4D seismic maps. In this way, the 2D areal model is not only a simplification of the 3D model, but a brand new way of integrating the 4D seismic data to build the model.

7.2.3 Multiple tank model

1) The first step of building the multiple tank model is to interpret the tank boundaries from the seismic map. This is a manual task, thus the interpreted results are not unique, and a better set of tank boundaries may improve the performance of the tank model. Therefore, the sensitivity of the tank boundaries on the model evaluation should be further tested and different scenarios of tank boundary mapping should be compared to select the closest approximation of the 3D model. This option would benefit the fields which have high level of heterogeneity and apply more complexed production strategies.

2) In the work described in Chapter 5, the seismic proxy model was applied on the whole reservoir, which means all the 14 tanks shared the same set of coefficients of the seismic proxy model. However, as analysed in section 7.2.1, the whole reservoir can be divided into different regions, then a sim2seis proxy model built for each of the regions. For the multiple tank model, if a different sim2seis model can be built for each tank, the tank model may then work as better simplification of the 3D model. This procedure obviously

require high computation cost, thus the trade-off of speed and accuracy needs to be analyses further.

3) The transmissibility multipliers embedded in the multiple tank model are different to that in the 3D model. The transformation between these two sets was explored in Chapter 5 and a reduced-exponent function (Equation 5.9) was applied. Other linear functions could be further tested to reduce the variance of parameter values. As mentioned in the Chapter 2, such 'response surface models' are suitable to deal with such kind of black-box problem. Based on the new transforming function, the 3D model outputs and tank model outputs may be compared effectively and the performance of the tank model as an approximation of the 3D model would be further enhanced.

7.2.4 Depth Averaged Maps and Volumetric

In this work, map-based 4D seismic data were used in the SHM workflows. The map-based approach as opposed to a volumetric approach has been widely used due to its simplicity, and the feature of its seismic resolution. This approach is acceptable for fairly thin reservoirs that are below tuning thickness; however, reservoirs with great thickness might result in specious maps of seismic data and simulation model outputs. For such thick reservoirs, the potential to extract information from every grid cell in the vertical direction exists, as this will help in nullifying the smoothening effect of averaging to create maps, especially in a case where both water sweep in the lower cells and gas presence in the upper cells exist. Reservoir heterogeneity might also be better defined and preserved. The volumetric seismic should be considered in future research on thick reservoirs.

7.2.5 Objective Function

In this work, the objective function of production data for SHM is 'normalized absolute error' and the objective function of seismic data is 'normalized squared error'; both are commonly used in the literature. In recent research (Nobakht 2015), objective functions of seismic maps have been developed, by using Hamming distance, Hausdorff distance and the mutual Information and current measurement metric (Chassagne et al., 2016), which are considered as misfit metrics for comparing the observed 4D seismic data and the simulation model output. Thus, in future research, new versions of the objective

function should be developed and perhaps extended to other available metrics, such that the production data misfit and the seismic data misfit will be similar and of the same order.

7.2.6 Different optimisation methods

Different optimisation methods could be studied to figure out an optimal optimisation integrated with the proxy model to speed up the SHM process. In this study, Particle Swarm Optimisation (PSO) has been selected, due to its simple structure, easy implementation and smaller number of controlling parameters. However, the application and comparison of different optimisation methods, such as EnKF (Oliver and Chen, 2011) or evolutionary algorithms (Aranha et al. 2015), coupled with the proxy model could also be investigated, as these have the benefit in analysing the model uncertainty. Additionally, some algorithms have been developed for the distributed computing purpose (Yadav et al., 2005; Guo et al., 2016), which should also be researched to speed up the SHM workflow.

7.3 Final Remarks

The aim of the research output of this thesis was to explore the possibility of applying proxy methods to tackle the challenges associated with the SHM workflow. In the literature, the proxy method has been widely used in reservoir history matching processes where only well production data were involved. Going further in the SHM domain, an extra 4D seismic simulator should be introduced coupled with the fluid flow simulator. The outputs of the flow simulators have to be used as the inputs of the sim2seis model. Therefore, the proxy models for misfit of production data error are not suitable any more, as only the proxy for model outputs are available in this case. This is the unique feature of proxy models which should be considered carefully in the SHM. Three kinds of proxy model were tried in this study; however, the focus was not to compare them but to find the potential proxies which can work in sequence in the SHM. This research work has a background of applying the 4D seismic efficiently in a quantitative way, of which the driving force is to integrate the well production data and 4D seismic data in the reservoir model calibration. Even though some progress has been made in this work, I am fully aware of the fact that this is only the top of the iceberg. However, my hope is that this research will play some role towards quantifying the exact size, shape and location of the iceberg.

Appendix A The critical values for *t*-distributions

The critical values for *t*-distributions is provided by Table A.1. Here, *df* means the degree of freedom of data samples. In statistics, the *p*-value is practically used to measure the probability that the computed correlation is just a likely chance occurrence or due to the data errors (Bhattacharya and Habtzghi, 2002). The upper-tail *p*-value is selected for well2seis, as only positive correlations are preserved in the technique. Figure B.1 explains how the Table B.1 can be used to find the t critical value corresponding to a certainty upper tail *p*-value. The brown coloured area on the Figure B.1 represents the p-value, indicating the probability of an observed result assuming that there is no correlation (the null hypothesis is true). Once the *p*-value is selected (most commonly 0.05 or 0.01 is preferred), the t critical value can be read from the provided table.

Table A.1 *Table of t-distribution critical values (modified from Pardoe (2006)).*

df	Probability of extremes (statistical *p*-value)								
	0.10	0.05	0.025	0.02	0.01	0.005	0.0025	0.001	0.0005
1	3.078	6.314	12.71	15.89	31.82	63.66	127.3	318.3	636.6
2	1.886	2.92	4.303	4.849	6.965	9.925	14.09	22.33	31.6
3	1.638	2.353	3.182	3.482	4.541	5.841	7.453	10.21	12.92
4	1.533	2.132	2.776	2.999	3.747	4.604	5.598	7.173	8.61
5	1.476	2.015	2.571	2.757	3.365	4.032	4.773	5.893	6.869
6	1.44	1.943	2.447	2.612	3.143	3.707	4.317	5.208	5.959
7	1.415	1.895	2.365	2.517	2.998	3.499	4.029	4.785	5.408
8	1.397	1.86	2.306	2.449	2.896	3.355	3.833	4.501	5.041
9	1.383	1.833	2.262	2.398	2.821	3.25	3.69	4.297	4.781
10	1.372	1.812	2.228	2.359	2.764	3.169	3.581	4.144	4.587
11	1.363	1.796	2.201	2.328	2.718	3.106	3.497	4.025	4.437
12	1.356	1.782	2.179	2.303	2.681	3.055	3.428	3.93	4.318
13	1.35	1.771	2.16	2.282	2.65	3.012	3.372	3.852	4.221
14	1.345	1.761	2.145	2.264	2.624	2.977	3.326	3.787	4.14
15	1.341	1.753	2.131	2.249	2.602	2.947	3.286	3.733	4.073
20	1.325	1.725	2.086	2.197	2.528	2.845	3.153	3.552	3.85
30	1.31	1.697	2.042	2.147	2.457	2.75	3.03	3.385	3.646
40	1.303	1.684	2.021	2.123	2.423	2.704	2.971	3.307	3.551
50	1.299	1.676	2.009	2.109	2.403	2.678	2.937	3.261	3.496
100	1.29	1.66	1.984	2.081	2.364	2.626	2.871	3.174	3.39
	90%	95%	97.50%	98%	99%	99.50%	99.75%	99.90%	99.95%
	Level of confidence								

Appendix B Publications

A fast-track simulator to seismic proxy for quantitative 4D seismic analysis

Colin MacBeth, Chong Geng, and Romain Chassagne, Heriot-Watt University*

Summary

We propose a stable and accurate proxy for generating maps of 4D seismic attributes using only the original baseline seismic data and fluid-flow simulation predictions. The approach provides a fast track procedure for generating 4D seismic data from the simulator. It has particular use in quantitative 4D seismic analysis, and specifically for incorporating time-lapse seismic data into the history-matching loop where many seismic modeling iterations are required. The method circumvents the petro-elastic model with its associated uncertainties and also the need to choose a seismic full-wave or convolutional modeling solution. Despite the relative simplicity of the proxy, it is found not to bias the choice of optimal solution for the history match. Application to synthetic datasets based on a two North Sea fields indicates that the proxy can remain accurate to within a mean error of 5%.

Introduction

In reservoir management, integration of the dynamic well data into the reservoir model is achieved via history matching, the process of calibrating the model to make it reproduce the historical well behavior. The more static and dynamic data the simulation model is consistent with, the more reliable will be the model forecasts of future performance. An increasingly popular type of dynamic data that can be used for history matching is time-lapse (4D) seismic data (for example: Gosselin et al. 2001, Stephen and MacBeth 2006, Roggero et al. 2007). 4D seismic data has a better areal coverage of the reservoir than 1D well data, and is thus potentially useful as a further constraint. However, unlike well data, where the simulation model predictions can be compared with the production activity, time-lapse seismic data are not directly comparable with the output of fluid flow simulation.

From a practical perspective, simulator to seismic modeling is one of the most difficult and potentially erroneous tasks facing a reservoir engineer engaged in a seismic history matching (SHM) project. It requires selection and calibration of a petro-elastic model (PEM) (Alvarez and MacBeth 2014), building of a seismic geo-model of impedances, followed by seismic wave propagation modeling (Figure 1(a)). Finally, the key geological events for the reservoir must be identified and picked on the synthetic data and the requisite attributes evaluated. Unfortunately, in this process there is no straightforward way of avoiding the petro-elastic modeling or seismic modeling route. Indeed, if the comparison is performed by firstly inverting the seismic to pressure and saturation changes, then the PEM is still involved (Landrø 2001, MacBeth et al. 2006). Furthermore, if the intermediate domain of seismic impedances is used, the PEM must convert the simulator output to impedances (Stephen and MacBeth 2006). For this latter choice, although seismic modeling is avoided, one must still convert the seismic into an impedance volume using a suitable rock physics model. Thus, the simulator to seismic modeling step still affords a considerable bottleneck to making full use of seismic data in the final quantitative update of a simulation model. It significantly increases the difficulty of undertaking an SHM that requires fast model runs and the computation of seismic data at each iteration. The seismic modeling steps are both time-consuming, carry considerable uncertainty due mainly to the stress sensitivity component (MacBeth 2004; Furre et al. 2008), and require extensive calibration which is non-trivial (Amini 2014).

In an attempt to circumvent the difficulties outlined above, this current work implements a proxy (or response surface) for the PEM plus seismic modeling steps of the calculation (Figure 1(b)). This approach speeds up the workflow considerably and allows a reservoir engineer with no prior knowledge of seismic data or modeling to gain immediate access to 4D seismic data as a matching tool.

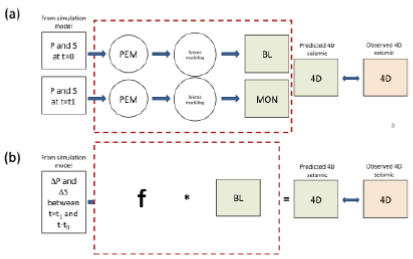

Figure 1 (a) Schematic illustrating the workflow required for modeling 4D seismic data for the purposes of comparing with the observed data. The processes in the red box are those for which a proxy is to be sought. (b) The proxy solution from this work, where the function *f* is at most a quadratic in terms of pressure and saturation change.

Development of the proxy

The objective of this work is to provide a quick and robust prediction of the seismic data from the pressure, water and gas saturation changes output from fluid-flow simulation. To do this we limit ourselves to only mapped seismic attributes, where the attribute has been evaluated with respect to a clear, stable and interpretable seismic horizon such as the top of the producing reservoir clearly identified in the seismic volume. The use of mapped seismic quantities is justifiable as many of the reservoirs we have interpreted are generally thinner than a fraction of a seismic wavelength, and the seismic response provides an adequate average of the fluid saturation and pressure for the entire producing depth interval. Maps for time-lapse seismic analysis are created by differencing the monitor and the baseline survey maps. The challenge is to calculate the time-lapse seismic map from depth-averaged pressure and saturation changes obtained via fluid-flow simulation.

Figure 2 shows observed maps of the root mean square amplitude of the top reservoir event for a North Sea clastic field (Obidegwu et al. 2015). Maps for the baseline (pre-production) survey and several subsequent monitor surveys are displayed. For reference purposes, Figure 3 gives an identical sequence of maps, but all are now derived from full synthetic seismic computation from a known simulation model using a well-log calibrated petroelastic model (see Amini 2014 for details). Inspection of the sequence for both observed and synthetic data indicates that both baseline and monitor images look visually similar. This is what we might expect, as the baseline response reflects the geological imprint of the reservoir's depositional architecture together with the initial fluid saturations and pressure. The monitors represent the same geology but with the fluid component and pressure perturbed due to well production and recovery. Key to our understanding is that these saturation and pressure signals only modify the seismic amplitudes in the regions bounded by reservoir, and thus the regions defined by the initial amplitude distribution. Of course, there are examples of saturation or pressure related time-lapse signals present outside the initially defined reservoir boundaries (Kloostermann et al. 2003), but these are generally not common and would be known prior to our analysis. A reservoir-related amplitude on the baseline seismic data will thus either brighten or dim in response to fluid saturation or pressure changes, but non-reservoir related amplitudes do not – assuming no geomechanical effects. A strong reservoir amplitude, consistent with a thick high porosity and low net-to-gross sand, also gives a strong time-lapse seismic response in response to production activities. The reverse is true for a lower quality reservoir sand. Obviously there is a limit this process - if the acquisition survey for the monitor seismic data does not adequately match the pre-production baseline survey, then non-repeatability noise will dominate.

To capture the above remarks, let $A_0(x,y)$ represent the seismic response at the pre-production baseline time and ΔR the effect of subsequent fluid saturation and pressure changes in the reservoir. Analysis of modeling and data suggests that the time-lapse seismic map $\Delta A(x,y)$ can be constructed as the product

$$\Delta A(x,y) = f(\Delta R, G).A_0(x,y) \tag{1}$$

where f is a function of the production-related changes and the geology, G, which depends on the petroelastic and seismic modeling. By involving the observed pre-production baseline survey in the time-lapse seismic calculation, we account for known (or unknown) lateral variations of the static reservoir properties such as thickness, porosity and net-to-gross, as well as destructive and constructive wavelet interference effects such as tuning in the 3D dataset. An additional benefit is that ΔA is already calculated in the attribute 'currency' of the seismic data. The form of the proxy function f can be considered from analogy with successful proxy (or response surface) modeling elsewhere (He et al. 2015). In our case, as we are dealing with relatively small changes, one obvious form for $f(\Delta R, G)$ can be obtained by a second order Taylor's series (see also MacBeth et al. 2006)

$$\Delta A = (a_1\Delta P + a_2\Delta S_w + a_3\Delta S_g + a_4\Delta P^2 + a_5\Delta S_w^2 + a_6\Delta S_g + a_7\Delta P\Delta S_w + a_8\Delta P\Delta S_g + a_9\Delta S_w\Delta S_g).A_0. \tag{2}$$

The relationship in (2) amplifies or diminishes the baseline seismic response according to the depth-averaged pressure ΔP and saturation (ΔS_w, ΔS_g) changes obtained from simulator predictions (they already obey material balance, and so too will the 4D seismic data), to yield the mapped time-lapse response ΔA. The coefficients a_i: i=1,9 are derivatives of the seismic attribute with respect to the individual pressure and saturation changes. The coefficients are functions of the reservoir geology, rock properties and fluid properties. As the bulk of the variability is supplied by the baseline amplitude the weighting coefficients a_i can be assumed fixed across the reservoir.

This approach is valid in practice provided the seismic survey configurations are reasonably repeatable, and that additional wave interferences are not induced by the time-lapse differencing procedure (i.e. 4D tuning). For the latter, it is helpful that differences of attribute maps are utilized rather than maps of the raw difference volume as these are more robust to time-shift effects, particularly for attributes calculated within a window such as the RMS (root mean

square) or sum of negative amplitudes. An additional benefit of the generalized framework in (2) is that any particular seismic attribute such as impedance, RMS amplitude, instantaneous frequency, time-shift etc., will work in practice for ΔA. Finally, although the 'proxy' relationship in (2) is partially empirical in origin, and thus seems to be less physically justifiable than a full-fledged petro-elastic model and full-wave propagation, the utility of the dynamic part of this equation has been established in past inversion studies (for example, Alvarez and MacBeth 2014). It should be noted that in the literature some debate has arisen as to whether only the linear terms in (2) should be preserved (Falahat et al. 2013). The quadratic form does appear necessary in some cases if gas is present, with perhaps the necessity of an exponential behavior in some reservoirs (Floricich et al. 2006). At a practical level, the linear version of this proxy is found to be useful for the purposes of directly inverting to pressure and saturation changes (Landrø 2001, MacBeth et al., 2006, Falahat et al., 2013). The accuracy and robustness of these proxy forms for modeling and history matching purposes will be tested in the next section.

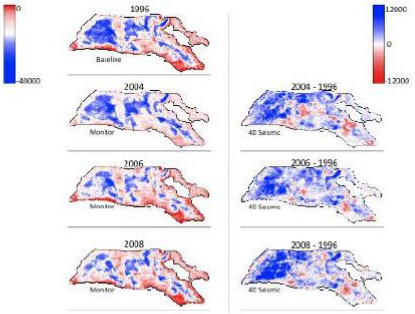

Figure 2 Comparison between the observed mapped seismic amplitudes for multiple 3D seismic surveys (left); and the corresponding mapped 4D seismic responses (right). The 1996 survey is the pre-production baseline, and all others are the monitors. The seismic attribute evaluated is the normalised RMS amplitude in a time gate of +/- 15ms either side of the picked horizon for the top of the producing reservoir interval for this North Sea field A.

Application to seismic history matching

The key to using (2) effectively in modeling as part of history matching is the rapid evaluation of the a_i coefficients without recourse to the time-consuming

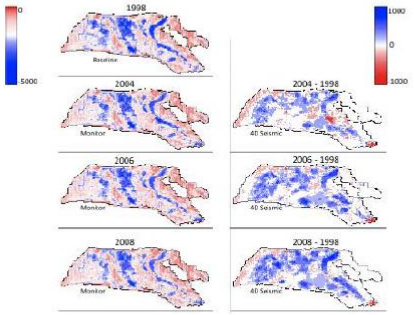

Figure 3 As in Figure 2, but for the synthetic data calculated using the full simulator to seismic modeling of Amini (2014).

calibration and modeling steps that we are trying to avoid. For any given simulation model run (and thus output pressures and saturations), the coefficients are determined by matching the righthandside of (2) to the observed time-lapse seismic data on the lefthandside. As there are only, at maximum, nine coefficients for the proxy and typically thousands of data points, this matching procedure is over-determined and can be achieved by multiple linear regression. An important feature of the matching algorithm, to ensure robustness and accuracy, is the introduction of physical constraints or inequality rules to the coefficients. This is necessary, as the relative magnitudes of the individual terms do behave according to predictable physical laws. For example, if impedance is the measured attribute, then a reservoir pressure decrease ($\Delta P < 0$) leads to a reservoir hardening or increase in ΔA. The coefficient a_1 must therefore be negative for the solution to remain physical. Similar scenarios also arise with the other coefficients, giving $a_1 < 0$, $a_2 > 0$ and $a_3 < 0$. Figure 4 shows the result of this procedure for the multiple-monitor synthetic data in Figure 3 from a North Sea field. The overall pattern of the mapped response is captured well, and the proxy is observed to fit to within a mean error of a few percent. Variations between the linear and the quadratic application are seen to be slight: 3.2% error versus 4.5% respectively. The coefficients for ΔP, ΔS_w and ΔS_g do not vary significantly when moving from the linear to quadratic form of the proxy (a_1=-0.6MPa^{-1}, a_2=101.5, a_3=-230.6) -> (a_1=-0.5MPa^{-1}, a_2=124.6, a_3=-208.0), and the cross-terms are reasonably small (a_4, a_5, $a_6 < \max(a_1,a_2,a_3)$), suggesting that in this reservoir and for these fluid mechanisms a linear form may be appropriate.

For seismic history matching the most important question is whether the multi-linear regression could compensate for a

bad model choice with equally bad predictions, and can influence the choice of the optimum and thus bias the selection of the best models. To test the impact of our approach on the ability of the SHM procedure in finding the correct optimal solution, synthetic tests are performed on reservoir models from two different North Sea field datasets A and B. The flow in Field A is governed by stratigraphy and for Field B it is governed by structure. In both tests, a full simulator to seismic modeling (sim2seis) has been performed with an extensively calibrated petroelastic model as a reference. A proxy model is created that matches the chosen reservoir model and its predictions to the reference case seismic data. Next, an ensemble of model scenarios are generated by stochastic variation of the controlling parameters (fault or geobody transmissibility multipliers and vertical permeability). For each model in the ensemble, the L2 norm objective function is determined for the difference between the reference 4D seismic response and the proxy response, and also between the reference case and the full simulator to seismic modeling. The results for thirty additional realizations for Field A and B are shown in Figure 5. Two tests are performed: in the first, the original a_i coefficients are fixed after one iteration; in the second the coefficients are re-evaluated after every iteration. Importantly, the behavior in the solution space for the objective function appears to well defined by the proxy, both in fixed and adaptive mode, and in good agreement with the full seismic modeling.

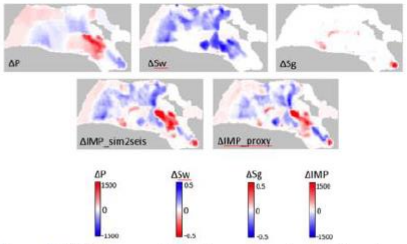

Figure 4 Field A comparison of pressure and saturation change output from the simulator with changes of impedance calculated with the full calibrated petroelastic model and the proposed proxy.

Discussion and conclusions

We have developed a fast-track seismic modeling procedure that helps to simplify seismic history matching and avoids the need for a petro-elastic model or full seismic modeling. The procedure relies on a data-driven relationship between the 4D seismic data and the reservoir dynamic properties. The procedure has been tested in a full seismic history matching workflow for two North Sea

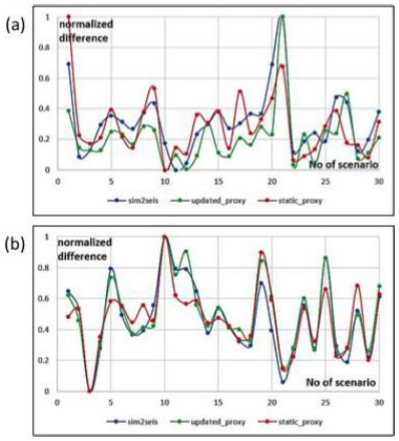

Figure 5 Misfits between predicted sim2seis solutions for thirty realizations of the simulation model and a pre-selected reference model. Blue line – full sim2seis calculation; Green line – adaptive proxy result; Red line – fixed proxy result. Results are for: (a) Field A; and (b) Field B.

fields and found to work well. The optimal SHM solution can still be found using the proxy, and solution space appears to have a similar character to that defined by full modeling. Whilst a perfect fit is not of course completely possible with a proxy, as the relationship between the depth-averaged pressure and saturation changes and the seismic data is in reality quite complex, it does appear that by working with mapped seismic attributes the response simplifies to the level where a good practical comparison is possible. The approximate result appears good enough to run a comprehensive seismic history matching, without recourse to the petroelastic model or seismic modeling tools that may not be readily available by an asset team engineer.

Acknowledgements

We thank the sponsors of the Edinburgh Time Lapse Project, Phase V and VI, for their support (BG, BP, Chevron, CGG, ConocoPhillips, ENI, ExxonMobil, Hess, Ikon Science, Landmark, Maersk, Nexen, Norsar, OMV, Petoro, Petrobras, RSI, Shell, Statoil, Suncor, Taqa, TGS, and Total). Ilya Fursov and Dennis Obidegwu of HWU are thanked for contributing to the development of this work.

EDITED REFERENCES

Note: This reference list is a copyedited version of the reference list submitted by the author. Reference lists for the 2016 SEG Technical Program Expanded Abstracts have been copyedited so that references provided with the online metadata for each paper will achieve a high degree of linking to cited sources that appear on the Web.

REFERENCES

Alvarez, E., and C. MacBeth, 2014, An insightful parametrization for the flatlander's interpretation of time-lapsed seismic data: Geophysical Prospecting, **62**, 75–96, http://dx.doi.org/10.1111/1365-2478.12071.

Amini, H., 2014, A pragmatic approach to simulator to seismic modelling for 4D seismic interpretation: Ph.D. thesis, Heriot-Watt University.

Falahat, R., A. Shams, and C. MacBeth, 2013, Adaptive scaling for an enhanced dynamic interpretation of 4D seismic data: Geophysical Prospecting, **61**, 231–247, http://dx.doi.org/10.1111/1365-2478.12005.

Furre, A.-K., M. Andersen, A. S. Moen, and R. K. Tønnessen, 2009, Deriving effects of pressure depletion on elastic framework moduli from sonic logs: Geophysical Prospecting, **57**, 427–437, http://dx.doi.org/10.1111/j.1365-2478.2008.00744.x.

Floricich, M., C. MacBeth, J. Stammeijer, R. Staples, A. Evans, and C. Dijksman, 2006, A new technique for pressure — Saturation separation from time-lapse seismic — Schiehallion case study: 68th Annual International Conference and Exhibition, EAGE, Extended Abstracts, http://dx.doi.org/10.3997/2214-4609.201402389.

Gosselin, O., S. van den Berg, and A. Cominelli, 2001, Integrated history-matching of production and 4D seismic data: Presented at the SPE Annual Technical Conference and Exhibition, SPE, SPE-71599-MS.

He, J., J. Xie, X.-H. Wen, and W. Chen, 2015, Improved proxy for history matching using proxy-for-data approach and reduced order modeling: Presented at the SPE Western Regional Meeting, SPE, http://dx.doi.org/10.2118/174055-MS.

Kloosterman, H., R. Kelly, J. Stammeijer, M. Hartung, J. van Waarde, and C. Chajecki, 2003, Successful application of time-lapse seismic data in Shell Expros Gannet Fields, Central North Sea, UKCS: Petroleum Geoscience, **9**, 25–34, http://dx.doi.org/10.1144/1354-079302-513.

Landrø, M., 2001, Discrimination between pressure and fluid saturation changes from time-lapse seismic data: Geophysics, **66**, 836–844, http://dx.doi.org/10.1190/1.1444973.

MacBeth, C., 2004, A classification for the pressure sensitivity properties of a sandstone rockframe: Geophysics, **69**, 497–510, http://dx.doi.org/10.1190/1.1707070.

MacBeth, C., M. Floricich, and J. Soldo, 2006, Going quantitative with 4D seismic analysis: Geophysical Prospecting, **54**, 303–317, http://dx.doi.org/10.1111/j.1365-2478.2006.00536.x.

Meadows, M. A., 2001, Enhancements to Landro's method for separating time-lapse pressure and saturation changes: 71st Annual International Meeting, SEG, Expanded Abstracts, 1652–1655.

Obidegwu, D., R. Chassagne, and C. MacBeth, 2015, Seismic assisted history matching using binary image matching: Presented at the SPE, Europec, http://dx.doi.org/10.2118/174310-MS.

Roggero, F., D. Y. Ding, P. Berthet, O. Lerat, J. Cap, and P.-E. Schreiber, 2007, Matching of production history and 4D seismic data — Application to the Girassol Field, Offshore Angola: Presented at the SPE Annual Technical Conference and Exhibition, SPE, SPE-109929-MS.

Stephen, K. D., J. Soldo, C. MacBeth, and M. A. Christie, 2006, Multiple model seismic and production history matching — A case study: SPE Journal, **11**, 418–430, http://dx.doi.org/10.2118/94173-PA.

Introduction

From a practical perspective, simulator to seismic modelling is one of the most difficult and potentially erroneous tasks facing a reservoir engineer engaged in a seismic history matching (SHM) project (Alvarez and MacBeth 2014). It requires selection and calibration of a petro-elastic model (PEM), building of a seismic geo-model of impedances, followed by seismic wave propagation modelling (Roggero et al. 2007). Finally, the key geological events for the reservoir must be identified and picked on the synthetic data and the requisite attributes evaluated. The simulator to seismic modelling workflow still presents a considerable bottleneck to making full use of seismic data in the final quantitative update of a simulation model. In particular, the PEM and seismic modelling steps are time-consuming, carry considerable uncertainty due mainly to the stress sensitivity component (MacBeth 2004; Furre et al. 2008), and require extensive calibration which is non-trivial (Amini 2014). In an attempt to circumvent the difficulties outlined above, this current work implements a proxy for these latter two steps of the calculation. This approach speeds up the workflow considerably and allows a reservoir engineer with no prior knowledge of seismic data or modelling to gain immediate access to 4D seismic data as a matching tool, with no associated loss of accuracy.

The seismic modelling proxy

We aim to provide a quick and robust prediction of the 4D seismic data from the pressure, water and gas saturation changes output from the fluid-flow simulator. To do this we limit ourselves to only mapped seismic attributes, where the attribute has been evaluated with respect to a stable and interpretable seismic horizon such as the top of the producing reservoir clearly identified in the seismic volume. The use of mapped seismic quantities is justifiable as many of the reservoirs we have interpreted are generally thinner than a fraction of a seismic wavelength, and the seismic response provides an average of the fluid saturation and pressure for the entire producing depth interval. Maps for time-lapse seismic analysis are created by differencing the individual monitor and the baseline survey maps. The challenge is to calculate this time-lapse seismic map from the depth-averaged pressure and saturation changes obtained via the fluid-flow simulation.

Our formulation is derived from the empirical observation of multiple monitor surveys across many North Sea fields (see for example Floricich et al. 2016). Inspection of the sequences for an extensive range of both observed and synthetic data indicates that both baseline and monitor images are visually similar. This is what we might expect, as the baseline response reflects the geological imprint of the reservoir's depositional architecture together with the initial fluid saturations and pressure. The monitors represent the same geology but with the fluid component and pressure perturbed due to well production and recovery. Key to our understanding is that these saturation and pressure signals only modify the seismic amplitudes in the regions bounded by reservoir, and thus the regions defined by the initial amplitude distribution. If $A_0(x,y)$ represents the seismic response at the pre-production baseline time and ΔR the effect of subsequent fluid saturation and pressure changes in the reservoir, the time-lapse seismic map $\Delta A(x,y)$ can be constructed

$$\Delta A(x,y) = f(\Delta R, G).A_0(x,y) \quad (1)$$

where f is a function of the production-related changes and the geology, G, which depends on the petroelastic and seismic modelling. By involving the observed pre-production baseline survey in the time-lapse seismic calculation, we account for known (or unknown) lateral variations of the static reservoir properties such as thickness, porosity and net-to-gross, as well as destructive and constructive wavelet interference effects such as tuning in the 3D dataset. An additional benefit is that ΔA is already calculated in the attribute 'currency' of the seismic data. The form of the proxy function

f can be considered from analogy with successful proxy modelling elsewhere (He et al. 2015). In our case, as we are dealing with relatively small changes, one obvious form for $f(\Delta R, G)$ is a quadratic in pressure and saturation changes (MacBeth et al. 2006). The relationship amplifies or diminishes the baseline seismic response according to the depth-averaged pressure ΔP and saturation (ΔS_w, ΔS_g) changes obtained from simulator predictions (they already obey material balance, and so too will the 4D seismic data), to yield the mapped time-lapse response ΔA. The accuracy and robustness of the proxy for history matching purposes is tested in the next section.

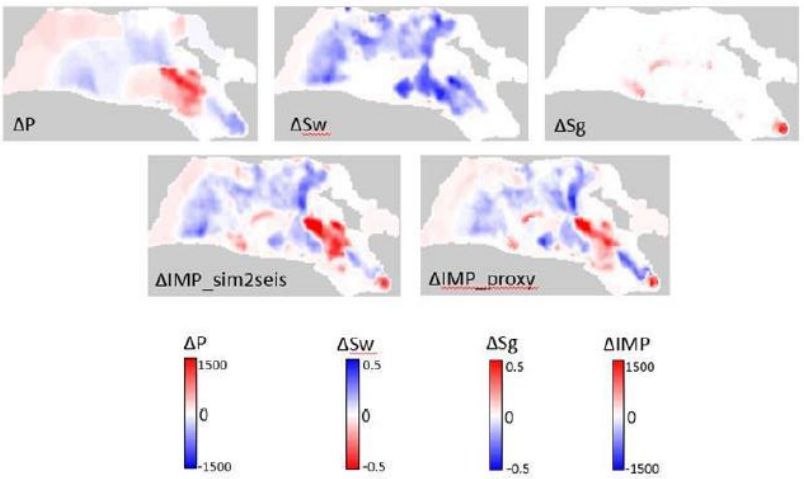

Figure 1 *Comparison of pressure and saturation change output from the simulator with changes of impedance calculated using a calibrated petroelastic model and the proposed proxy.*

Seismic history matching using the proxy

The key to using (1) effectively in modelling as part of history matching is the rapid evaluation of the proxy coefficients without recourse to the time-consuming calibration and modelling steps that we are trying to avoid. For any given simulation model run (and thus output pressures and saturations), the coefficients are determined by least squares regression to the observed time-lapse seismic data. As there are only, at maximum, nine coefficients for the proxy and typically thousands of data points, this matching procedure is over-determined and quite satisfactory. Despite being overdetermined, an important feature of the matching algorithm, to ensure robustness and accuracy, is the introduction of physical constraints or inequality rules to the coefficients. This is necessary, as the relative magnitudes of the individual terms should behave according to predictable physical laws (Alvarez and MacBeth 2016). Figure 1 shows the result of this procedure for a North Sea field. The overall pattern of the mapped response is captured well, and the proxy is observed to fit to within a mean error of a few percent. Variations between the quadratic and the linear proxy are also seen to be slight in this case: 3.2% error versus 4.5% respectively.

For seismic history matching the most important question is whether the multi-linear regression could compensate for a bad model choice with equally bad simulation predictions, and can influence estimation of the optimum and thus bias the selection of the best models. To test the impact of our

approach on the performance of the SHM procedure, synthetic tests are initially performed on the reservoir model for our North Sea field dataset. A full simulator to seismic modelling (sim2seis) is performed with an extensively calibrated petroelastic model as a reference. A proxy model is created that matches the chosen reservoir model and its predictions to the reference case seismic data. Next, an ensemble of model scenarios are generated by stochastic variation of the controlling parameters (fault, geobody transmissibility multipliers and vertical permeability). For each model in the ensemble, the L2 norm objective function is used to assess the difference between the reference 4D seismic response and the proxy response, and also between the reference case and the full simulator to seismic modelling. Patricle swarm optimization is utlised in the updating strategy for the pool of solutions. The results for thirty realisations are shown in Figure 2. Two tests are performed: in the first, the original proxy coefficients are fixed after one iteration; in the second the coefficients are re-evaluated after every iteration. Importantly, the behaviour in the solution space for the objective function appears to well defined by the proxy, both in fixed and adaptive mode, and in good agreement with the full seismic modelling. Figure 3 shows that the solution space near to and including the optimal point for parameter selection may not be distorted by the use of the proxy.

Discussion and conclusions

We have developed a fast-track seismic modelling procedure that helps to simplify seismic history matching and avoids the need for a petro-elastic model or full seismic modelling. The procedure relies on a data-driven relationship between the 4D seismic data and the reservoir dynamic properties. The procedure has been tested in a full seismic history matching workflow for several North Sea

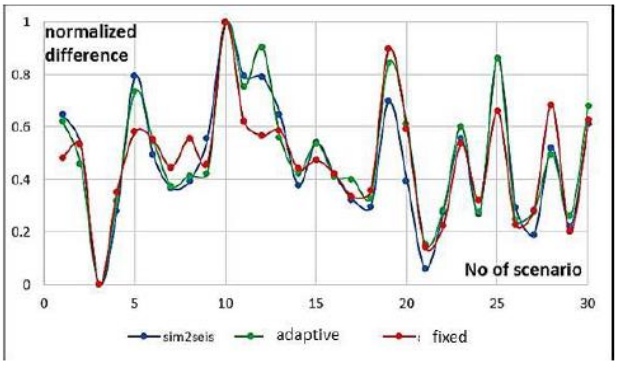

Figure 2 *Normalised misfits between predicted sim2seis solutions for thirty realisations of the simulation model and a pre-selected reference model. Blue line – full sim2seis calculation; Green line – adaptive proxy result; Red line – fixed proxy result.*

fields and found to work well. The optimal SHM solution can still be found using the proxy, and solution space appears to have a similar character to that defined by full modelling. Whilst a perfect fit is not of course completely possible with a proxy, as the relationship between the depth-averaged pressure and saturation changes and the seismic data is in reality quite complex, it does appear that by working with mapped seismic attributes the response simplifies to the level where a good practical comparison is possible. The approximate result appears good enough to run a comprehensive seismic history matching, without recourse to the petroelastic model or seismic modelling tools that may not be readily available by an asset team engineer.

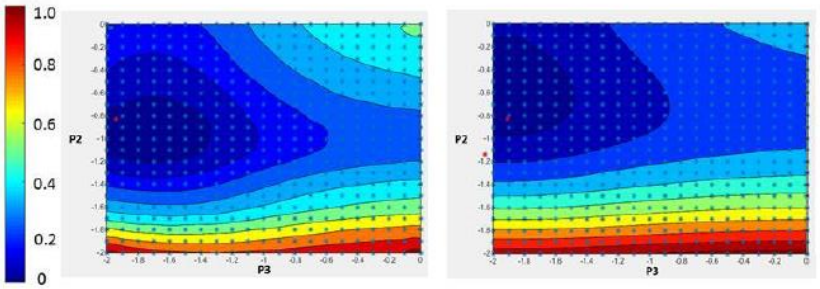

Figure 3 Misfit surfaces for two parameters (P2 and P3) in our history match. (a) surface using sim2seis procedure; (b) surface using the fixed proxy. The red dot indicates the true solution.

Acknowledgements

We thank the sponsors of the Edinburgh Time Lapse Project, Phase V and VI, for their support (BG, BP, Chevron, CGG, ConocoPhillips, ENI, ExxonMobil, Hess, Ikon Science, Landmark, Maersk, Nexen, Norsar, OMV, Petoro, Petrobras, RSI, Shell, Statoil, Suncor, Taqa, TGS, and Total). Ilya Fursov and Dennis Obidegwu of HWU are thanked for contributing to the development of this work.

References

Alvarez, E., and MacBeth, C. [2014] An insightful parametrization for the flatlander's interpretation of time-lapsed seismic data: Geophysical Prospecting, **62**, 75-96.

Amini, H. [2014] A pragmatic approach to simulator to seismic modelling for 4D seismic interpretation: PhD thesis, Heriot-Watt University.

Furre, A-K., Andersen, M. Moen A.S. and Tønnessen, R.K. [2008] Deriving effects of pressure depletion on elastic framework moduli from sonic logs: Geophysical Prospecting, **57**, 427–437.

Floricich, M., MacBeth, C. Stammeijer, J. Staples, R. Evans A. and Dijksman, C. [2006] A new technique for pressure - saturation separation from time-lapse seismic - Schiehallion case study: 68th Conference and Exhibition, EAGE, Extended Abstracts, DOI: 10.3997/2214-4609.201402389

He, J., Xie, J. Wen X-H. and Chen, W. [2015] Improved proxy for history matching using proxy-for-data approach and reduced order modelling: SPE Journal, doi:10.2118/174055-MS.

MacBeth, C. [2004] A classification for the pressure sensitivity properties of a sandstone rockframe: Geophysics, **69**, 497-510.

MacBeth, C., Floricich M. and Soldo, J. [2006] Going quantitative with 4D seismic analysis: Geophysical Prospecting, **54**, 303-317.

Roggero, F., Ding, D.Y., Berthet, P., Lerat, O., Cap J. and Schreiber, P-E. [2007] Matching of Production History and 4D Seismic Data - Application to the Girassol Field, Offshore Angola: SPE Annual Technical Conference and Exhibition, SPE-109929-MS.

SPE-185822-MS

Seismic History Matching Using a Fast-Track Simulator to Seismic Proxy

Chong Geng, Colin MacBeth, and Romain ChassagneHeriot Watt University

Abstract

In this paper we propose a proxy model based seismic history matching (SHM), and apply it to time-lapse (4D) seismic data from a Norwegian Sea field. A stable proxy model is developed for generating 4D seismic attributes by using only the original baseline seismic data and dynamic pressure and saturation predictions from reservoir flow simulation. This method (MacBeth et al., 2016) circumvents the petro-elastic modelling with its associated uncertainties and also the need to choose a seismic full-wave or convolutional modelling solution, which are used in conventional simulator to seismic (sim2seis) modelling. The method is tested on an offshore field case study from the Norwegian Sea.

In this study we firstly perform a check on the validity and accuracy of the proxy approach following the methodology of (Falahat et al. 2013) as a guide. The results confirm linear superposition between the pressure and saturation effects controlling the seismic data. Next a quasi-history matching is set up - here simulation model realisations are selected by random assignation of the key parameters to define a walk through solution space. After this, both the sim2seis and proxy modelling approach are compared for each realisation against a known reference case. The results show a mean seismic error of lower than 5%, which indicates the possibility to utilise a fixed proxy to model the 4D seismic. Finally, the full seismic history matching loop is implemented, where the sim2seis and the proxy-driven SHM are launched to find the optimal solution for our field. A particle swarm optimization (PSO) algorithm is applied as the optimisation tool, and only seismic data are used in the objective function. In both cases the algorithm converged after 30 iterations, and the optimal solutions of the two schemes are comparable. It is observed that the full sim2seis and proxy-driven SHMs are only marginally different, implying that solution space is similar in both cases. We also observe that in either case, matching to seismic data only can improve the production match. A unique feature of this study is the application of a seismic modelling proxy in the SHM scheme. Despite its relative simplicity, the approach is found not to bias the optimal solution of the more conventional SHM where the full physics of seismic modelling is applied. Meanwhile, this approach can save over 60% of the total computing time compared with the normal procedure, and this helps significantly to achieve a rapid and effective seismic history matching and better define uncertainty with a larger number of realisations.

Introduction

History matching is a common used practice which continuously assess the simulation model's performance against the historical data to decrease the uncertainty of the model and then improve the forecast reliability.

The more constraints a history matching scheme includes, the less uncertain will its outputs be (Landa and Roland, 1997, Wang and Kovscek, 2002, Katterbauer et al., 2015). Compared with the well production historical data (oil/gas/water rate, bottom hole pressure) which has been mainly used for history matching, time-lapse seismic (or 4D seismic) has a better areal coverage of the reservoir, and is thus potential useful as a further constraint (Oliver and Yan, 2011, Katterbauer et al., 2015, Stephen et al., 2014, Tolstukhin et al., 2012). Combining 1D well production data as high resolution vertical constraint and 4D seismic data as spatial constraint, seismic history matching (SHM) has been proven to provide more reliable model realisations in past decades (Huang et al., 1998, Gosselin, et al., Jin et al., 2011, Yin et al., 2016).

However, unlike simulated production prediction which can be directly compared with observation, the 4D seismic is not a direct output of fluid flow simulation (Amini 2014). Bringing the simulation and the seismic into a same domain is referred as closing the loop (Figure 1), and simulator to seismic (sim2seis) modelling is indispensable for this procedure. It requires calibration of a petro-elastic model to obtain impedance, building of a geo-model of impedance and seismic wave propagation modelling. This process is multidisciplinary, case dependent, contains high uncertainty and can be the most difficult task facing a reservoir engineer engaged in SHM (MacBeth et al., 2016, Santos et al., 2016).

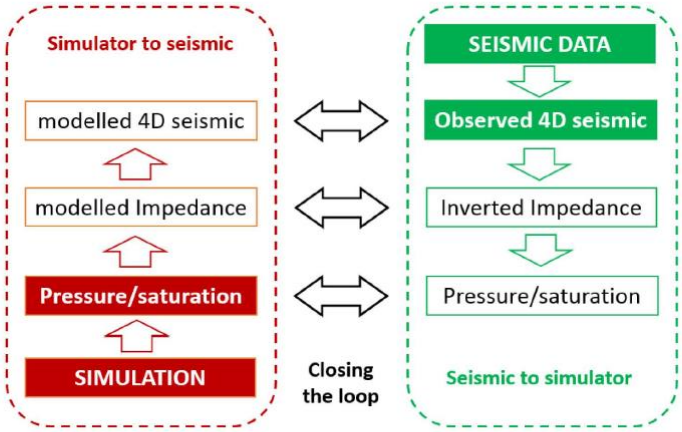

Figure 1—Different domains of closing the loop between the simulation model and the seismic data.

Figure 1 illustrates the different domain of comparison between seismic and simulation. Specifically, if the comparison is performed in the seismic domain, hence the petro-elastic modelling and seismic modelling will be applied to generate the simulated 4Dseismic data. A main drawback of this forward modelling procedure is to be able to deal with the associated uncertainty in the model parameters. It could be a huge challenge for the cases where a reliable petro-elastic model is hard to build. Moreover, forward modelling requires intensive computation which can be unaffordable for large size models. Examples of SHM in seismic domain can be given by Davolio (2011) on a Gulf of Mexico turbidite reservoir, and Rwechungura (2012) on a Norwegian Sea turbidite reservoir.

In another way, if bringing the seismic into saturation/pressure domain to bypass forward modelling in SHM, the petro-elastic model is still necessary and the inversion is a non-unique procedure. The literature examples of SHM in simulation domain are often conducted on a synthetic model (Landa et al., 1997, Davolio et al., 2011), and the non-uniqueness is usually treated inappropriately, or not treated at all (Jin et al., 2011, Osdal, 2012).

Furthermore, the intermediate domain of seismic impedance can also be used to compare simulation and real data. This approach appears to be the most popular choice in SHM literatures (Gosselin et al., 2003, Reiso et al., 2005, Roggero et al., 2007, Emerick et al., 2007), however, it has the disadvantages of the previous two: although the seismic modelling can be avoided, an extra suitable rock physics model should be applied to convert the seismic into impedance (Fursov 2015, MacBeth, et al 2016).

All the above approaches cannot totally avoid the petro-elastic modelling or seismic modelling route and all carry considerable uncertainty, increasing the difficulty of undertaking a rapid and effective SHM. In attempt to circumvent the abovementioned challenges, a proxy model based SHM approach is proposed in this paper. Despite its relative simplicity, the approach is found to perform equally as the conventional SHM where the physics of seismic modelling is applied. Above all, it speeds up the SHM workflow considerably and allows a reservoir engineer to gain immediate access to the SHM.

Methodology

4D seismic is created by differencing the monitor seismic survey from the baseline survey, in theory it can be 3D cube or 2D maps. Considering the relatively lower vertical resolution, in literature it is more likely to use mapped seismic attributes (Brown 2014, Obidegwu et al. 2015, Rwechungura, 2012), where the attribute has been evaluated with respect to a clear, stable and interpretable seismic horizon such as the top of the producing reservoir that has been clearly identified in the seismic volume. For thin sheet-like reservoirs which are generally thinner than a fraction of a seismic wavelength, the top/bottom reservoir horizons can be used as the window to generalise seismic map (Obidegwu 2016); for thick reservoirs or ones containing major shale layers, multiple maps can be generated for each formation separately (Yin 2016). In this paper we limit our research to mapped 4D seismic, and the role of our proxy model is to calculate the time-lapse seismic maps from the depth-averaged pressure and saturation maps, which have been obtained from reservoir flow simulation.

Figure 2 (a) shows observed maps of the root mean square (RMS) amplitude of the top reservoir event for a North Sea clastic field (MacBeth 2016). Figure 2 (b) gives an identical sequence of maps, but all are derived from sim2seis using a well-log calibrated petro-elastic model (see Amini and MacBeth (2010) for details of the modelling). Both observed and synthetic data indicates that baseline and monitor images look visually similar. This is because the baseline map reflects the geological imprint of the reservoir's depositional architecture, together with the initial fluid saturations and pressure. The monitors represent the same geology but with the fluid saturation and pressure changed due to well production and injection (MacBeth 2016). These saturation and pressure signals only modify the seismic amplitudes in the regions bounded by reservoir, and thus the regions defined by the initial amplitude distribution (a similar concept is described by Shams and MacBeth 2008 or Lin 2011).

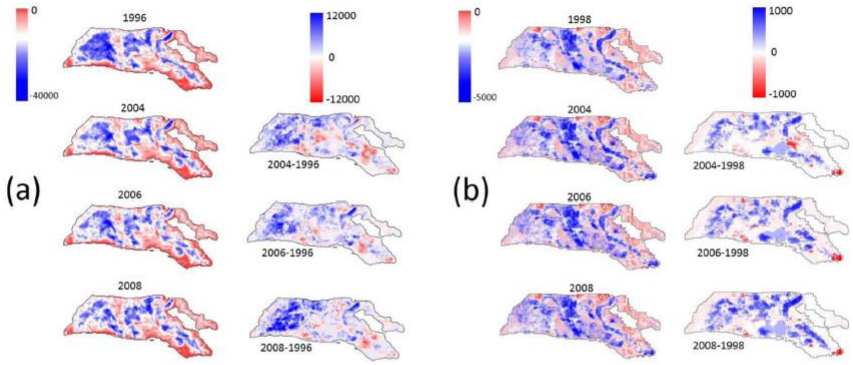

Figure 2—(a) Comparison between the observed mapped seismic amplitudes for multiple 3D seismic surveys (left); and the corresponding mapped 4D seismic responses (right); (b) Comparison between the simulated mapped seismic amplitudes for multiple 3D seismic surveys (left); and the corresponding mapped 4D seismic responses (right).

Analysis of above modelling and data suggests that the time-lapse seismic map $\Delta A(x, y)$ can be constructed as the product

$$\Delta A(x,y) = f(\Delta R, G) * A_0 \quad (1)$$

Where A_0 (x, y) represents the seismic response (any particular seismic attribute such as impedance, RMS amplitude, instantaneous frequency, time-shift etc.) at the pre-production baseline time and $\Delta R(x, y)$ represents the effect of subsequent fluid saturation and pressure changes in the reservoir. f is a function of the production-related changes and the geology, G, which depends on the petro-elastic and seismic modelling. By involving the baseline map $A_0(x, y)$ in the 4D seismic calculation, we account for variations of the static reservoir properties such as thickness, porosity and net-to-gross etc.. Although the 'proxy' relationship in (1) is empirical in origin, the utility of the dynamic part of this equation has been established in past inversion studies (for example, Alvarez and MacBeth 2014).

In our case, as we are dealing with relatively small changes, one obvious form for $f(\Delta R, G)$ can be obtained by a linear polynomial (Falahat et al. 2013)

$$\Delta A(x,y) = (a_1\Delta P + a_2\Delta S_w + a_3\Delta S_g) * A_0 \quad (2)$$

The relationship in (2) amplifies or diminishes the baseline seismic response according to the depth-averaged pressure ΔP and water and gas saturation changes (ΔS_w, ΔS_g) obtained from fluid flow simulator, to yield the mapped time-lapse response ΔA. The coefficients a_i with i = 1:3 are derivatives of the seismic attribute with respect to the individual pressure and saturation changes. The coefficients are functions of the reservoir geology, rock properties and fluid properties. As the main reservoir variability is supplied by the baseline amplitude, the weighting coefficients a_i can be assumed fixed across the reservoir (Falahat et al., 2013).

This equation is valid in practice provided the seismic survey configurations are reasonably repeatable (Fursov, 2015), and it should be noted that in the literature some debate has arisen as to whether the polynomial in (2) should be expanded as a quadratic (MacBeth et al. 2006). Arguments in favour of quadratic terms for pressure and saturation change have been provided by Meadows (2001), Cole et al. (2001) and Meadows and Lumley (2002). At a practical level, the linear version of this proxy is found to be useful for the purposes of directly inverting to pressure and saturation changes (Landro 2001, Falahat et al., 2013;

Floricich et al., 2006; MacBeth et al., 2006), thus in this study we applied the linear version, the accuracy and robustness of this proxy for history matching purposes will be tested in the next section.

Application

The methodology described in laste section is tested on a Norwegian Sea field. This is a rotated fault block field (Figure 3), and block C, D, E contain over 97% of the initial oil in place. In vertical, most of the hydrocarbon is stored in Ile and Tofte sand formations. Therefore the 4D RMS seismic map (Figure 3) of Ile formation in block E and D is used as the objective for SHM. In this formation, there is a set of carbonate layers which are partially sealing and have variable lateral extensions. These layers, together with some local faults and barriers, influence the flow in the reservoir and lead to high uncertainty in the simulation model. Thus the multipliers of faults transmissibility, vertical permeability and local barriers transsimissibility are applied as the uncertain parameters for the following history matching.

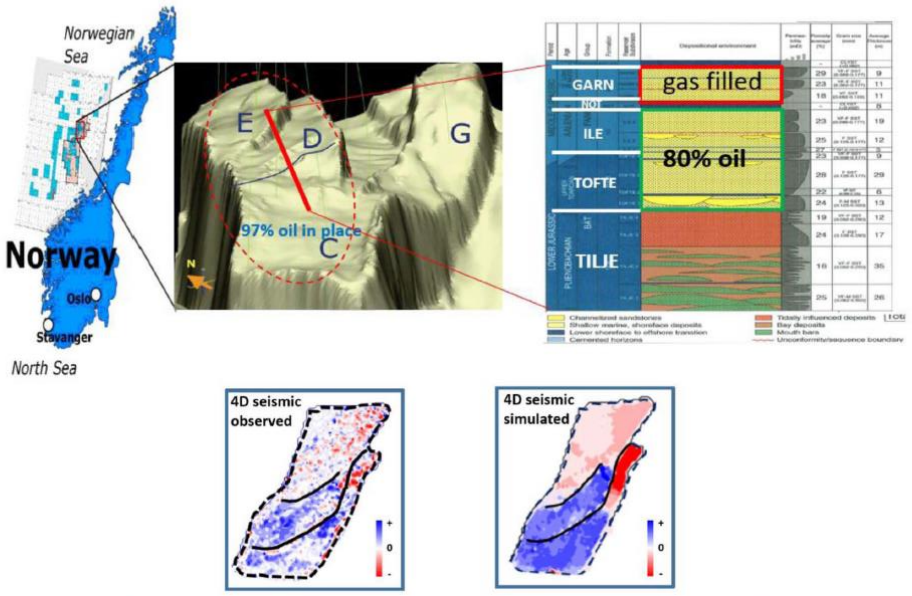

Figure 3—location (top left), horizontal view (top middle), and vertical view (top right) of the Norwegian Sea field; bottom: observed and simulated 4D seismic of Ile formation at block E and D

The initial simulation model is history matched using well production data, the field oil and gas production rate were perfectly matched, but the water cut was oversimulated (Figure 4). The the improvement of water cut matching is the target of the following SHM. In terms of seismic, four databases were available (2001, 2003, 2004 and 2006), the first two shots, 2001 and 2003, will be utilized in the following SHM workflow as the gap between simulation and observation developed from this period.

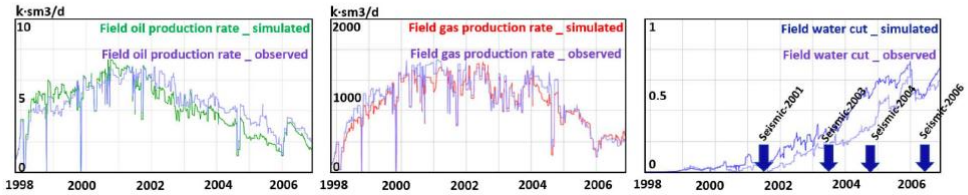

Figure 4—simulation vs observation of the initial simulation model (production history matched)

As mentioned in last section, before conducting SHM, a linearity evaluation of the proxy model (equation 2) need to be done first. The purpose of this process is to evaluate the accuracy and robustness of the linear proxy, in other words, to check the linear relationship between modelled 4D seismic and simulated pressure and saturation changes. Afterwards, a quasi-history matching (without optimization) is designed in order to test the numerical stability of the coefficients in equation (2): because the SHM workflow cannot afford the computational cost of running full sim2seis to update these coefficents for each model, a fixed set of coefficents is essential. Only if these coefficents does not vary too drasticaly, then a fixed proxy equation can be applied for further history matching use.

Linearity evaluation

The main assumption behind the equation (2) is that modelled seismic response might be decomposed into effects of P/S (pressure/saturation) changes linearly. Although it is a data-driven assumption with limited physical basics, it has been proved in literature (Falahat, 2013, Fursov, 2015) to be successful on synthetic or real field data. However, considering the complexity of the seismic attribute, reservoir geometry and other considerations, this proxy (equation 2) would have different performance based on specific cases. Therefore, before the further use of this proxy in SHM, we set up this linearity evaluation to confirm whether it is suitable for our case.

Following Falahat's method (2013), we use the initial simulation model and sim2seis to conduct this study. We first run the flow simulation, afterwards the pressure, water and gas saturation changes in Ile formation during 2001-2003 are made into maps using pore volume weighted algorithm (Figure 5.a). The sim2seis (Amini, 2014) are then applied to model the independent 4D seismic signatures (2003-2001) of these three variables (Figure 5.b), three independent seismic signatureare then summed up as the mixed 4D seismic. Meanwhile, we utilise sim2seis to model the real 4D seismic, taking all three variables into consideration.

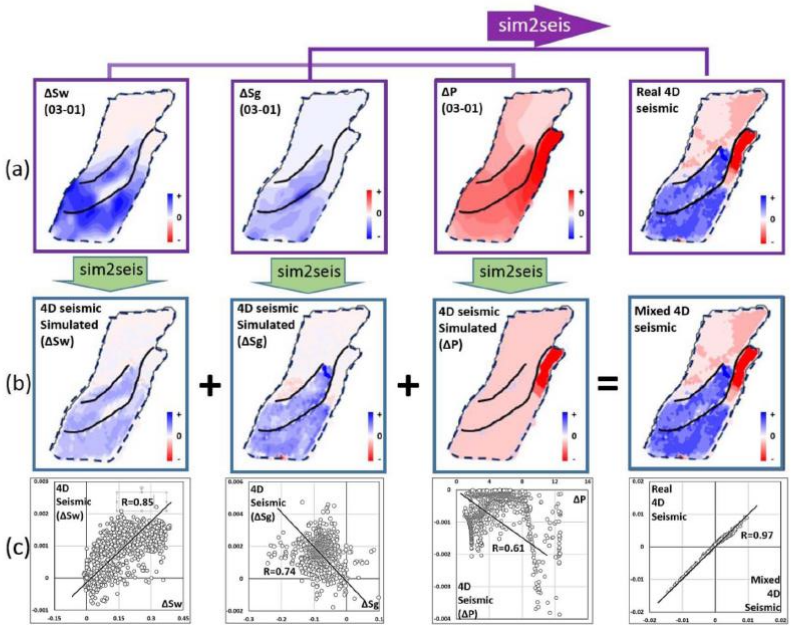

Figure 5—(a) From left to right: water saturation, gas saturation and pressure changes of Ile formation during 2001 and 2003 from initial simulation model, rightmost: real 4D seismic modelled by sim2seis; (b) Modelled 4D seismic signatures considering independent variables above, rightmost: modelled seismic considering all three variables; (c) From left to right: crossplot of above P/S variables and corresponding independent 4D seismic signatures, rightmost: crossplot of real and mixed 4D seismic.

We then make two test: 1) the mixed and real 4D seimic maps are compared and cross-plotted (Figure 5.c, rightmost). The correlation coefficient (R) =0.92, indicates that the real 4D seismic signature can be regarded as a mixture of independent effects of P/S changes. 2) The 4D seismic responses corresponding to each change are cross-plotted against the three independent variables suggested above (Figure 5.c, three on the left), the P/S is observed to show the strongest linear correlation with the seismic data. The results here suggest that modelled seismic can be approximated by linearly scaled P/S variables in this case.

Quasi-history matching

The coefficents in equation (2) are calculated by linear regression: (ΔS_w, ΔS_g, ΔP) come from the flow simulation outputs and (ΔA, A_0) are the seismic. According to Falahat's analytic calculation, the coefficents of a proxy model are related to the static properties such as porosity, thickness and NTG of the reservoir (these properties are presented by the products of (a_1, a_2, a_3) and A_0 in our equation (2)). Thus if the static parameters of the simulation model are updated during history matching, these coefficents will result in change of the perturbation. As mentioned above, a fixed proxy with a fixed set of coefficients is necessary for an efficient history matching loop, therefore we need to quantify the variance of the coefficents for a certain SHM.

We set up a quasi-history matching procedure to achieve the above purpose. Firstly the uncertain parameters of SHM and their value ranges were determined. Then a one-at-a-time algorithm (Dehghan, et al., 2012) is applied for sensitivity analysis to screen out the top 10 sensitive parameters (Table 1).

Afterwards 30 points are randomly selected from the 10-dimension search space, each represents a possible scenario during SHM. Our quasi-history matching is finally conducted on these 30 scenarios.

Table 1—sensitive parameters and value ranges

parameter	number	value range (10^x)
Barrier transmissibility multipliers	1	[-4, 0]
Faults transmissibility multipliers	2	[-2, 2]
Vertical permeability multipliers	7	[-3, 3]

$$O.F. = \frac{\sum(sim_i - obs_i)^2}{\sum(obs_i)^2} \times 100\% \quad (3)$$

An objective function of SHM is defined as equation (3). sim_i stands for the i-th cell of simulated (by sim2seis or proxy) seismic map, and obs_i is the observed seismic at the corresponding cell. Because this study focuses on seismic proxy, only seismic mismatch is counted in the function.

The initial simulation model is launched to obtain dynamic outputs like ΔS_w, ΔS_g and ΔP. Based on that the seismic data (ΔA, A_0) is then modelled by sim2seis and will be used as a reference (synthetic history data) for quasi history matching. With the data (ΔS_w, ΔS_g, ΔP, ΔA, Δ_0), a linear regression of equation (2) leads to the first set of coefficents is referred to as the "fixed proxy". Analogously, all the 30 scenarios are launched and each will have an individual set of coefficents and we name them "adaptive proxies". For the 30 scenarios, we then apply both fixed and adaptive proxy on each to obtain the modelled proxy seismic. The misfit value between reference and modelled (sim2seis, fixed and adaptive proxy) seismic of each scenario is then calculated (Figure 6). The top plot gives a visual comparasion, and correlation coefficent between sim2seis and the two proxies (Figure 6.b 6.c) indicates the results of proxy and full sim2seis are very close. The crossplot Figure 6.d shows that the fixed proxy performs as well as the adaptive one in this study, thus it is effective to use the fixed proxy in our later SHM workflow.

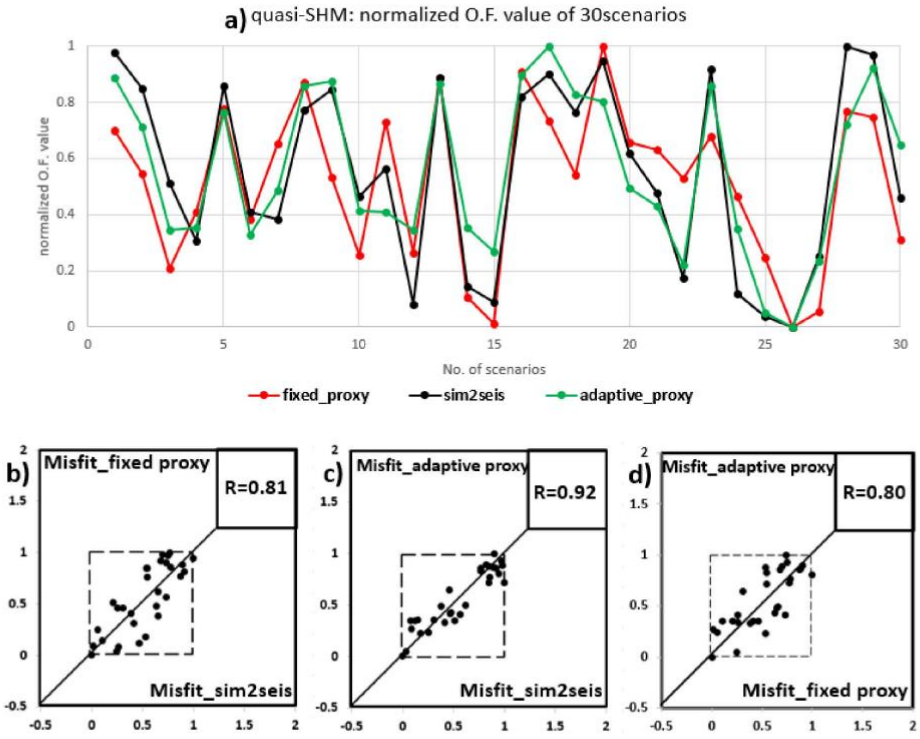

Figure 6—a) result of quasi-SHM, three set of normalized objective function values; b) crossplot of sim2seis and fixed proxy; c) crossplot of sim2seis and adaptive proxy; d) crossplot of adaptive and fixed proxy

Seismic history matching

Following the above two steps, a seismic history matching is eventually conducted. As mentioned earlier, the uncertain parameters and their value ranges are screened by a sensitivity analysis (Dehghan, et al., 2012), and the same objective function (equation 3) is applied for this SHM loop. The optimization algorithm is an ensemble based Particle Swarm Optimization (PSO, Omran, et al., 2005) and the configuration parameters are listed in Table 2.

Table 2—configuration parameters of PSO algorithm

parameters	value
Dynamic inertial weight ω	0.4-0.9
Weights c_p_best	2
Weights c_g_best	2
Boundary condition	reflecting strategy
Swarm size	10
Max iteration	30

The first iteration contains 10 randomly selected scenarios the specific values are plotted in Figure 8a. Then sim2seis and the fixed proxy work respectively as the seismic modelling part in the SHM loop (Figure 7). After 30 iterations, both SHM loops converge to a certain resolution (Figure 8.b, 8.c). The grey dashed broken lines mark the maximum and minimum value for each parameter of the last swarm, as the window is quite narrow we take the mean value of the window as a reference for the two optimal resolutions. In Figure 8d the two optimal solutions are plotted by a black line which stands for the initial simulation model. The solution of the full sim2seis and proxy-driven SHMs are only marginally different (only tiny difference around well P1) and it is similar from the comparison of 4D seismic maps (Figure 9). In both cases, compared with the initial model, the optimal solutions show lower value of transmissibility/permeability multipliers, which means after SHM, the flow resistance inside the region increases.

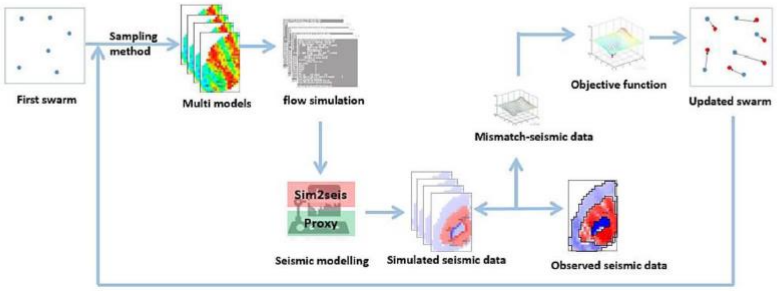

Figure 7—the loop of SHM where sim2seis and proxy can work as seismic modelling part

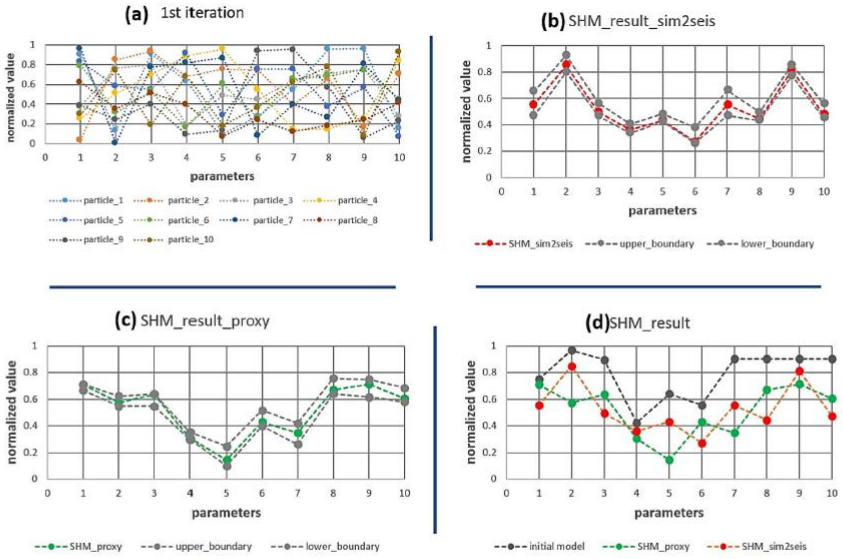

Figure 8—a): the first iteration of PSO: each dashed line stands for a simulation model and the dots indicate the value of each parameter; b), c): optimal solution of sim2seis and proxy driven SHM. The grey dashed lines mark the maximum and minimum value for each parameter of the last swarm, red and green lines stand for the optimal solution; d): comparison of SHMs optimal solutions and the initial model

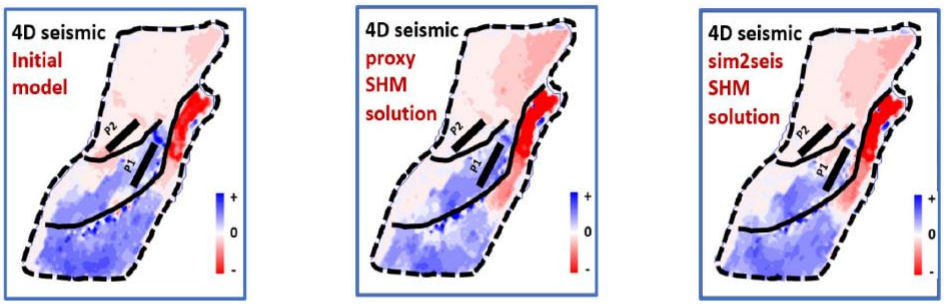

Figure 9—left 4D (03-01) seismic map of IIe formation in block E and D of the initial simulation model; middle: from the optimal solution of proxy driven SHM, right: sim2seis optimal SHM solution

Furthermore, we compare the production matching improvement of two SHMs, of which the objective function only contains seismic mismatch. As introduced at the beginning of this part, the main mismatch of the initial model is water cut. Hence we selected two main producers in the region, well P1 and P2, to check the improvement of the production match (Figure 10).

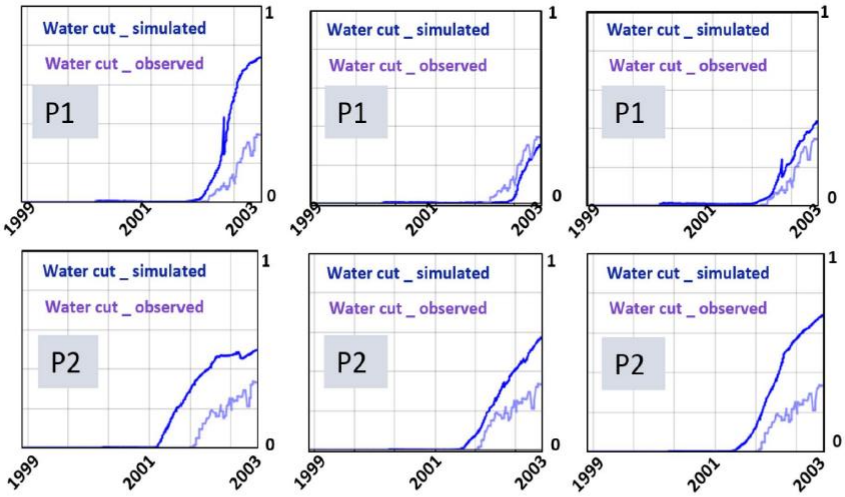

Figure 10—left side: the well water cut data and modelled seismic (by sim2seis) of the initial model; the middle column corresponds to the optimal solution of fixed proxy-driven SHM and the right side is from the sim2seis-driven SHM optimal solution.

In the initial case, well water cut for the two wells was over-simulated. Water breakthrough time (WBT) of P1 was well matched but cumulative water production (CWP) was over simulated. For well P2, the simulated WBT was 6 months before the observation and CWP was also over-simulated. In the optimal model of sim2seis SHM, the improvement of well P1is clear. For P2, the CWP became worse, but the WBT was improved by 50%. In the case of proxy solution, the match of two wells were both clearly improved.

In terms of the computation time, a single run of sim2seis (petro-elastic modelling, 1D convolution plus maps extraction) takes roughly 850 seconds while the proxy only needs couple of seconds. In the SHM loop where fluid flow simulation is also included, the speed could be improved by 60% by using the proxy.

Conclusion

We have developed a proxy seismic modeling procedure that helps to simplify seismic history matching and avoids the need for a petro-elastic model or full seismic modeling. This method relies on a data-driven relationship between the 4D seismic data and the reservoir dynamic properties. It has been studied in three ways from different perspectives, firstly we verified the linearity hypothesis, then we performed a quasi-SHM and finally we integrated this proxy into a complete SHM, applied on a Norwegian Sea field. The results, conclusions and further recommendations can be drawn from this study:

1. The linear relationship between 4D seismic map and 4D pressure and saturation maps is firstly confirmed following Falahat's method, and the results of quasi-history matching indicates the possibility to utilise a fixed proxy to model the 4D seismic. At the last stage, sim2seis and proxy-driven SHMs lead to comparable optimal solutions. Even with little perturbation, the proxy method performed well in the SHM workflow as a replacement of costly sim2seis modelling.
2. In either SHM case (sim2seis or proxy-driven), matching to seismic data can simultaneously improve the production match, this proves that the spatial information contained in seismic can be a further constraint for history matching in combination with production data.
3. For further recommendations, mapped based seismic is a precondition of this procedure which can be a potential limitation for other cases. In addition, the application conditions such as the field geostructure, seismic attributes selection need to be explored exhaustively.

Acknowledgements

We thank the sponsors of the Edinburgh Time Lapse Project, Phase V and VI, for their support (BG, BP, Chevron, CGG, ConocoPhillips, ENI, ExxonMobil, Hess, Ikon Science, Landmark, Maersk, Nexen, Norsar, OMV, Petoro, Petrobras, RSI, Shell, Statoil, Suncor, Taqa, TGS, and Total). Ilya Fursov and Dennis Obidegwu of HWU are thanked for contributing to the development of this work.

Reference

Amini, H. 2014. A pragmatic approach to simulator-to-seismic modelling for 4D seismic interpretation. PhD thesis, Heriot-Watt University.

Davolio, A., Maschio, C., Schiozer, D.J. 2011. Incorporating 4D Seismic Attributes into History Matching Process through an Inversion Scheme, SPE-142946.

Dehghan Monfared, A., Helalizadeh, A., and Parvizi H. 2012. Automatic history matching using the integration of response surface modeling with a genetic algorithm. *Petroleum science and technology* **30.4** (2012): 360–374.

Emerick, A.A., Moraes, R.J., Rodrigues, J.R.P. 2007. History Matching 4D Seismic Data with Efficient Gradient Based Methods, SPE-107179.

Falahat R., Shams A., Macbeth C. 2013. Adaptive scaling for an enhanced dynamic interpretation of 4D seismic data. *Geophysical Prospecting*, **61**(s1):231–247.

Fursov, I. 2015. Quantitative application of 4D seismic data for updating thin-reservoir models. PhD thesis, Heriot-Watt University.

Gosselin, O., Aanonsen, S.I., Aavatsmark, I., Cominelli, A., Gonard, R., Kolasinski, M., Ferdinandi, F., Kovacic, L., Neylon, K. 2003. History matching Using Time-lapse Seismic, SPE-84464.

Huang, X., Meister, L., Workman, R. 1998. Improving production history matching using time - lapse seismic data. *Leading Edge*, **17**(10), 1430–1433.

Jin, L., Alpak, F.O., Hoek, P., Pirmez, C., Fehintola, T., Tendo, F., Olaniyan, E.E. 2011. A Comparison of Stochastic Data-Integration Algorithms for the Joint History Matching of Production and Time-Lapse Seismic Data, SPE-146418.

Katterbauer, K., Arango, S., Sun, S., & Hoteit, I. 2015. Multi-data reservoir history matching for enhanced reservoir forecasting and uncertainty quantification. *Journal of Petroleum Science & Engineering*, **128**, 160–176.

Landa, J. L., Horne, R. N. 1997. A procedure to integrate well test data, reservoir performance history and 4-d seismic information into a reservoir description. *Oil Field*, 99–114.

MacBeth, C., Geng, C., and Chassagne, R. 2016. A fast-track simulator to seismic proxy for quantitative 4D seismic analysis. SEG Technical Program Expanded Abstracts. *Society of Exploration Geophysicists*, 5537–5541.

Oliver, D. S., Chen, Y. 2011. Recent progress on reservoir history matching: a review. *Computational Geosciences*, **15**(1), 185–221.

Omran, M., Andries Petrus Engelbrecht, and A. Salman. 2005. Particle swarm optimization method for image clustering. *International Journal of Pattern Recognition and Artificial Intelligence 19.03* (**2005**): 297–321.

Omran, M., Engelbrecht, A. P., and Salman, A. 2005. Particle swarm optimization method for image clustering. *International Journal of Pattern Recognition & Artificial Intelligence*, **19**(3), 297–321.

Osdal, B. 2012. Mapping the fluid front and pressure buildup using 4d data on norne field. *Leading Edge*, **25**(9), 1134–1141.

Reiso, E., Haver, M. C., and Aga, M. 2005. Integrated workflow for quantitative use of time-lapse seismic data in history matching: A North Sea field case.

Roggero, F., Lerat, O., Ding, D. Y., and Berthet, P. 2012. History matching of production and 4d seismic data: application to the girassol field, offshore Angola. *Oil & Gas Science & Technology*, **67**(2), 237–262.

Rwechungurai, R., Bhark, E. W., Miljeteig, O. T., Suman, A., Kourounis, D., and Foss, B. A. 2012. Results of the First Norne Field Case on History Matching and Recovery Optimization Using Production and 4D Seismic Data. *Spe Technical Conference and Exhibition*.

Santos, J.M.C., Davolio, A., and Macbeth, C. 2016. 4D Seismic Interpretation of the Norne Field-A Semi-quantitative Approach." *78th EAGE Conference and Exhibition 2016*.

Stephen, Karl D., and Kazemi, A. 2015. Improved normalization of time - lapse seismic data using normalized root mean square repeatability data to improve automatic production and seismic history matching in the nelson field. *Geophysical Prospecting*, **62**(5), 1009–1027.

Tolstukhin, E., Lyngnes, B., and Sudan, H. H. 2012. Ekofisk 4d seismic - seismic history matching workflow. *Society of Petroleum Engineers*.

Wang, Y., and Kovscek, A. R. 2002. A streamline approach for ranking reservoir models that incorporates production history. *SPE Annual Technical Conference and Exhibition. Society of Petroleum Engineers*.

Yin, Z. 2016. Enhancement of dynamic reservoir interpretation using the well2seis technique. PhD thesis, Heriot-Watt University.

Yin, Z., Macbeth, C., Chassagne, R., and Vazquez, O. 2016. Evaluation of inter-well connectivity using well fluctuations and 4d seismic data. *Journal of Petroleum Science & Engineering*, **145**, 533–547.

References

Aanonsen, S.I., Nævdal, G., Oliver, D.S., Reynolds, A.C. and Vallès, B., 2009. The ensemble Kalman filter in reservoir engineering--a review. Spe Journal, 14(03), pp.393-412.

Al-Kasim, F.T., Synøve, T., Jakobsen, K.A., Tang, Y. and Jalali, Y., 2002, January. Remotely controlled in-situ gas lift on the Norne subsea field. In SPE Annual technical conference and exhibition. Society of Petroleum Engineers.

Alsos, T., Sørensen, H. and Huang, Y., 2013. 4D seismic as a powerful IOR tool in the Norne area–from mature fields to fast track projects. In SPE Workshop on Arctic Norway.

Altan, S., Zhu, X., Dillon, G., McArdle, J., Walker, C., Parr, R.S. and Westwater, P., 2001, January. Schiehallion 4D: From time-lapse repeatability study to reservoir monitoring. In 2001 SEG Annual Meeting. Society of Exploration Geophysicists.

Alvarez, E. and MacBeth, C., 2012, June. Constraining the Petro-elastic Model with a Flatlander's Interpretation of the 4D Signal. In 74th EAGE Conference and Exhibition incorporating EUROPEC 2012.

Alvarez, E. and MacBeth, C., 2014. An insightful parametrization for the flatlander's interpretation of time-lapsed seismic data. Geophysical Prospecting, 62(1), pp.75-96.

Amini, H., 2014. A pragmatic approach to simulator-to-seismic modelling for 4D seismic interpretation (Doctoral dissertation, Heriot-Watt University).

Amini, H., MacBeth, C. and Shams, A., 2011, May. Calibration of simulator to seismic modeling for quantitative 4D seismic interpretation. In 73rd EAGE Conference and Exhibition incorporating SPE EUROPEC 2011.

Amudo, C., Graf, T., Harris, N.R., Dandekar, R., Amor, F.B. and May, R.S., 2008, December. Experimental design and response surface models as a basis for stochastic history match-a Niger delta experience. In IPTC 2008: International Petroleum Technology Conference.

Andersen, T., Zachariassen, E., Otterlei, C., Hatland, K. and Liestolt, F., 2006. Method for conditioning the reservoir model on 3D and 4D elastic inversion data applied to a fluvial reservoir in the North Sea. SPE, 100190, p.6.

Anterion, F., Eymard, R. and Karcher, B., 1989, January. Use of parameter gradients for reservoir history matching. In SPE Symposium on Reservoir Simulation. Society of Petroleum Engineers.

Aranha, C., Tanabe, R., Chassagne, R. and Fukunaga, A., 2015, May. Optimization of oil reservoir models using tuned evolutionary algorithms and adaptive differential

evolution. In Evolutionary Computation (CEC), 2015 IEEE Congress on (pp. 877-884). IEEE.

Archer, J.S. and Wall, C.G., 1986. Petroleum engineering; principles and practise: Graham and Trotman Ltd. London, 362p.

Artus, V., Durlofsky, L.J., Onwunalu, J. and Aziz, K., 2006. Optimisation of nonconventional wells under uncertainty using statistical proxies. Computational Geosciences, 10(4), pp.389-404.

Arwini, S. and Stephen, K.D., 2010, January. A New Method to Improve Convergence Rates with Seismic History Matching. In SPE EUROPEC/EAGE Annual Conference and Exhibition. Society of Petroleum Engineers.

Azad, A. and Chalaturnyk, R.J., 2010. A mathematical improvement to SAGD using geomechanical modelling. Journal of Canadian Petroleum Technology, 49(10), pp.53-64.

Aziz, K. and Settari, A., 1979. Petroleum reservoir simulation. Chapman & Hall.

Badley, M.E., 1985. Practical seismic interpretation, www.osti.gov.

Bai, Z., Dewilde, P.M. and Freund, R.W., 2005. Reduced-order modeling. Handbook of numerical analysis, 13, pp.825-895.

Batycky, R.P., Blunt, M.J. and Thiele, M.R., 1997. A 3D field-scale streamline-based reservoir simulator. SPE Reservoir Engineering, 12(04), pp.246-254.

Batzle, M. and Wang, Z., 1992. Seismic properties of pore fluids. Geophysics, 57(11), pp.1396-1408.

Bi, Z., Oliver, D.S. and Reynolds, A.C., 1999, January. Conditioning 3D stochastic channels to pressure data. In SPE Annual Technical Conference and Exhibition. Society of Petroleum Engineers.

Blackwell, T.M., 2005. Particle swarms and population diversity. Soft Computing, 9(11), pp.793-802.

Box, G.E. and Wilson, K.B., 1992. On the experimental attainment of optimum conditions. In Breakthroughs in statistics (pp. 270-310). Springer, New York, NY.

Briceño, Angel E., 2017. Calibration and use of petroelastic model for 4D seismic interpretation (Doctoral dissertation, Heriot-Watt University).

Brits, R., Engelbrecht, A.P. and Van den Bergh, F., 2002, November. A niching particle swarm optimiser. In Proceedings of the 4th Asia-Pacific conference on simulated evolution and learning (Vol. 2, pp. 692-696). Singapore: Orchid Country Club.

Brown, A.R., 2011. Interpretation of three-dimensional seismic data. Society of Exploration Geophysicists and American Association of Petroleum Geologists.

Buchert, T., Melott, A.L. and Weiss, A.G., 1993. Testing higher-order lagrangian perturbation theory against numerical simulations-1. pancake models. arXiv preprint astro-ph/9309056.

Bui-Thanh, T., Damodaran, M. and Willcox, K.E., 2004. Aerodynamic data reconstruction and inverse design using proper orthogonal decomposition. AIAA journal, 42(8), pp.1505-1516.

Cai, L. and White, R.E., 2009. Reduction of model order based on proper orthogonal decomposition for lithium-ion battery simulations. Journal of The Electrochemical Society, 156(3), pp.A154-A161.

Cardoso, M.A., Durlofsky, L.J. and Sarma, P., 2009. Development and application of reduced-order modeling procedures for subsurface flow simulation. International journal for numerical methods in engineering, 77(9), pp.1322-1350.

Carter, J.N. and Ballester, P.J., 2004, August. A real parameter genetic algorithm for cluster identification in history matching. In ECMOR IX-9th European conference on the mathematics of oil recovery.

Chappelear, J.E. and Hirasaki, G.J., 1976. A model of oil-water coning for two-dimensional, areal reservoir simulation. Society of Petroleum Engineers Journal, 16(02), pp.65-72.

Chassagne, R., Obidegwu, D., Dambrine, J. and MacBeth, C., 2016. Binary 4D seismic history matching, a metric study. Computers & Geosciences, 96, pp.159-172.

Chatterjee, S. and Hadi, A.S., 1986. Influential observations, high leverage points, and outliers in linear regression. Statistical Science, pp.379-393.

Chen, W.H., Gavalas, G.R., Seinfeld, J.H. and Wasserman, M.L., 1974. A new algorithm for automatic history matching. Society of Petroleum Engineers Journal, 14(6), pp.593-608.

Chen, Y. and Oliver, D.S., 2014. History matching of the Norne full-field model with an iterative ensemble smoother. SPE Reservoir Evaluation & Engineering, 17(02), pp.244-256.

Chen, Y., 2005. Upscaling and subgrid modeling of flow and transport in heterogeneous reservoirs (Doctoral dissertation, Stanford University).

Chierici, G.L., 2012. Principles of petroleum reservoir engineering (Vol. 2). Springer Science & Business Media.

Chopra, S., Castagna, J. and Portniaguine, O., 2006. Seismic resolution and thin-bed reflectivity inversion. CSEG recorder, 31(1), pp.19-25.

Christie, M., MacBeth, C. and Subbey, S., 2002. Multiple history-matched models for Teal South. The Leading Edge, 21(3), pp.286-289.

Christie, M.A. and Blunt, M.J., 2001, January. Tenth SPE comparative solution project: A comparison of upscaling techniques. In SPE Reservoir Simulation Symposium. Society of Petroleum Engineers.

Clayton, J.L., Spencer, C.W., Koncz, I. and Szalay, A., 1990. Origin and migration of hydrocarbon gases and carbon dioxide, Bekes Basin, southeastern Hungary. Organic Geochemistry, 15(3), pp.233-247.

CMG Manual, Computer Modelling Group Ltd., 2017, https://www.cmgl.ca/general-release-2017.

Coats, K.H., Dempsey, J.R. and Henderson, J.H., 1970. A new technique for determining reservoir description from field performance data. Society of Petroleum Engineers Journal, 10(01), pp.66-74.

Cole, S., Lumley, D., Meadows, M. and Tura, A., 2002, January. Pressure and saturation inversion of 4D seismic data by rock physics forward modeling. In 2002 SEG Annual Meeting. Society of Exploration Geophysicists.

Cottrell, C.W., 1983. The Application of Curvilinear Coordinate Systems To Predict the Behavior of Pattern Waterfloods in the Lekhwair Oil Field, Oman. Journal of Petroleum Technology, 35(07), pp.1-385.

Cullick, A.S., Johnson, W.D. and Shi, G., 2006, January. Improved and more rapid history matching with a nonlinear proxy and global optimisation. In SPE Annual Technical Conference and Exhibition. Society of Petroleum Engineers.

Dadashpour, M., Landrø, M. and Kleppe, J., 2007. Nonlinear inversion for estimating reservoir parameters from time-lapse seismic data. Journal of Geophysics and Engineering, 5(1), p.54.

Daniel, W.W., 1978. Applied nonparametric statistics. Houghton Mifflin.

Darcy, H., 1856. The public fountains of the city of Dijon. Victor Dalmont, Paris, France.

Datta-Gupta, A. and King, M.J., 2007. Streamline simulation: theory and practice (Vol. 11). Richardson: Society of Petroleum Engineers.

Davolio, A., Maschio, C. and Schiozer, D.J., 2011, January. Incorporating 4D Seismic Attributes Into History Matching Process Through An Inversion Scheme. In SPE EUROPEC/EAGE Annual Conference and Exhibition. Society of Petroleum Engineers.

DesBrisay, C.L., Gray, J.W. and Spivak, A., 1975. Miscible flood performance of the Intisar" D" field, Libyan Arab Republic. Journal of Petroleum Technology, 27(08), pp.935-943.

Dobbyn, A. and Marsh, M., 2001, January. Material balance: A powerful tool for understanding the early performance of the Schiehallion Field. In Offshore Europe. Society of Petroleum Engineers.

Dong, Y. and Oliver, D.S., 2005. Quantitative use of 4D seismic data for reservoir description. SPE Journal, 10(01), pp.91-99.

Dong, Y. and Oliver, D.S., 2008, January. Reservoir simulation model updates via automatic history matching with integration of seismic impedance change and production data. In International Petroleum Technology Conference. International Petroleum Technology Conference.

Dong, Y., Gu, Y. and Oliver, D.S., 2006. Sequential assimilation of 4D seismic data for reservoir description using the ensemble Kalman filter. Journal of Petroleum Science and Engineering, 53(1-2), pp.83-99.

Dougherty, E.L. and Khairkhah, D., 1975, January. History matching of gas simulation models using optimal control theory. In SPE California Regional Meeting. Society of Petroleum Engineers.

Durlofsky, L.J., 2005, June. Upscaling and gridding of fine scale geological models for flow simulation. In 8th International Forum on Reservoir Simulation Iles Borromees, Stresa, Italy (Vol. 2024).

Eberhart, R. and Kennedy, J., 1995, October. A new optimiser using particle swarm theory. In Micro Machine and Human Science, 1995. MHS'95., Proceedings of the Sixth International Symposium on (pp. 39-43). IEEE.

Eclipse Manual, Schumberger, 2017, https://www.software.slb.com/software-news/software-top-news/eclipse-2017-1.

Elde, R.M., Haaland, A.N., Ro, H.E., Ystad, B. and Zachariassen, E., 2000, January. Troll West-Reservoir Monitoring by 4D Seismic. In SPE European Petroleum Conference. Society of Petroleum Engineers.

Eldred, M.E., Orangi, A., Al-Emadi, A.A., Ahmad, A., O'Reilly, T.J. and Barghouti, N., 2014, April. Reservoir simulations in a high performance cloud computing environment. In SPE Intelligent Energy Conference & Exhibition. Society of Petroleum Engineers.

Emerick, A.A. and Reynolds, A.C., 2013. Ensemble smoother with multiple data assimilation. Computers & Geosciences, 55, pp.3-15.

Emerick, A.A., Moraes, R.J., Rodrigues, J.R.P. 2007. History Matching 4D Seismic Data with Efficient Gradient Based Methods, SPE-107179.

Erbas, D. and Christie, M.A., 2007, January. Effect of sampling strategies on prediction uncertainty estimation. In SPE Reservoir Simulation Symposium. Society of Petroleum Engineers.

Ertekin, T., Abou-Kassem, J. and King, G., 2001. Basic practical reservoir simulation. SPE Textbook Series, 7.

Evensen, G., 2003. The ensemble Kalman filter: Theoretical formulation and practical implementation. Ocean dynamics, 53(4), pp.343-367.

Fahimuddin, A., Aanonsen, S.I. and Skjervheim, J.A., 2010, January. Ensemble based 4D seismic history matching: Integration of different levels and types of seismic data. In SPE EUROPEC/EAGE Annual Conference and Exhibition. Society of Petroleum Engineers.

Falahat R., Shams A., MacBeth C. 2013. Adaptive scaling for an enhanced dynamic interpretation of 4D seismic data. Geophysical Prospecting, 61(s1):231-247.

Falcone, G., Gosselin, O., Maire, F., Marrauld, J. and Zhakupov, M., 2004, January. Petroelastic modelling as key element of 4D history matching: A field example. In SPE Annual Technical Conference and Exhibition. Society of Petroleum Engineers.

Fanchi, J.R., 2005. Principles of applied reservoir simulation. Elsevier.

Fasanino, G., Molinard, J.E., de Marsily, G. and Pelce, V., 1986, January. Inverse modeling in gas reservoirs. In SPE Annual Technical Conference and Exhibition. Society of Petroleum Engineers.

Fetkovich, M.J., Ebbs Jr, D.J. and Voelker, J.J., 1994. Multiwell, Multilayer Model To Evaluate Infill-Drilling Potential in the Oklahoma Hugoton Field. SPE Reservoir Engineering, 9(03), pp.162-168.

Floricich, M., MacBeth, C., Stammeijer, J., Staples, R., Evans, A. and Dijksman, N., 2006. Determination of a seismic and engineering consistent petro-elastic model for time-lapse seismic studies: Application to the Schiehallion Field. In SEG Technical Program Expanded Abstracts 2006 (pp. 3205-3209). Society of Exploration Geophysicists.

Forrester, A.I. and Keane, A.J., 2009. Recent advances in surrogate-based optimisation. Progress in Aerospace Sciences, 45(1-3), pp.50-79.

Freedman, D.A., 2009. Statistical models: theory and practice. Cambridge University Press.

Freitag, L., Ernst, A., Unger, M., Kovitz, K. and Marquette, C.H., 2007. A proposed classification system of central airway stenosis. European Respiratory Journal, 30(1), pp.7-12.

Fursov, I., 2015. Quantitative application of 4D seismic data for updating thin-reservoir models (Doctoral dissertation, Heriot-Watt University).

Güyagüler, B., Horne, R.N., Rogers, L. and Rosenzweig, J.J., 2002. Optimisation of well placement in a Gulf of Mexico waterflooding project. SPE Reservoir Evaluation & Engineering, 5(03), pp.229-236.

Gainski, M., MacGregor, A.G., Freeman, P.J. and Nieuwland, H.F., 2010. Turbidite reservoir compartmentalization and well targeting with 4D seismic and production data: Schiehallion Field, UK. Geological Society, London, Special Publications, 347(1), pp.89-102.

Gassmann, F., 1951, Über die elastizität poröser medien: Vierteljahrss-chrift der Naturforschenden Gesellschaft Zurich 95, 1-23. (English translation from http://sepwww.stanford.edu/sep/berryman/PS/gassmann.pdf)

Gavalas, G.R., Shah, P.C. and Seinfeld, J.H., 1976. Reservoir history matching by Bayesian estimation. Society of Petroleum Engineers Journal, 16(06), pp.337-350.

Geng, C., MacBeth, C. and Chassagne, R., 2017, June. Seismic History Matching Using a Fast-Track Simulator to Seismic Proxy. In SPE Europec featured at 79th EAGE Conference and Exhibition. Society of Petroleum Engineers.

Gervais C.V., Roggero, F., Feraille, M.D., Ravalec-Dupin, L. and Seiler, A., 2010, January. Joint history matching of production and 4D-seismic related data for a North Sea field case. In SPE Annual Technical Conference and Exhibition. Society of Petroleum Engineers.

Goldberg, D.E., 1989. Genetic Alogorithms in Search. Optimisation & Machine Learning.

Gosselin, O., Aanonsen, S.I., Aavatsmark, I., Cominelli, A., Gonard, R., Kolasinski, M., Ferdinandi, F., Kovacic, L., Neylon, K. 2003. History matching Using Time-lapse Seismic, SPE-84464.

Gosselin, O., van den Berg, S. and Cominelli, A., 2001, January. Integrated history-matching of production and 4D seismic data. In SPE Annual Technical Conference and Exhibition. Society of Petroleum Engineers.

Govan, A.H., Primmer, T., Douglas, C.C., Moodie, N., Davies, M. and Nieuwland, F., 2005, January. Reservoir management in a deepwater subsea field–the Schiehallion experience. In Offshore Europe. Society of Petroleum Engineers.

Gunst, R.F., 1996. Response surface methodology: process and product optimisation using designed experiments.

Guo, Z., Chen, C., Gao, G., Cao, R., Li, R. and Liu, C., 2017. EUR Assessment of Unconventional Assets Using Machine Learning and Distributed Computing Techniques. Unconventional Resources Technology Conference (URTEC).

Hajizadeh, Y., 2010, January. Ants can do history matching. In SPE Annual Technical Conference and Exhibition. Society of Petroleum Engineers.

Hajizadeh, Y., Christie, M.A. and Demyanov, V., 2009, January. Ant Colony Optimisation Algorithm for History Matching. In EUROPEC/EAGE Conference and Exhibition. Society of Petroleum Engineers.

Hanneing, A. and Paton, G., 2012, February. Understanding thin beds using 3D seismic analysis workflows, attributes: new views on seismic imaging—their use in exploration and production. In 31st Annual GCSSEPM Foundation Bob F. Perkins Research Conference (Vol. 1, pp. 322-341).

Harris, P.E. and Henry, B., 1998, January. Time-lapse processing: a North Sea case study. In 1998 SEG Annual Meeting. Society of Exploration Geophysicists.

Hatchell, P.J., Kawar, R.S. and Savitski, A.A., 2005, June. Integrating 4D seismic, geomechanics and reservoir simulation in the Valhall oil field. In 67th EAGE Conference & Exhibition. In SPE Reservoir Simulation Symposium. Society of Petroleum Engineers.

Haugen, V.E.J., Natvik, L.J., Evensen, G., Berg, A.M., Flornes, K.M. and Naevdal, G., 2006, January. History matching using the ensemble Kalman filter on a North Sea field case. In SPE Annual Technical Conference and Exhibition. Society of Petroleum Engineers.

Haverl, M.C., Aga, M. and Reiso, E., 2005, June. Integrated Workflow for Quantitative Use of Time-Lapse Seismic Data in History Matching–A North Sea Field Case (SPE94453). In 67th EAGE Conference & Exhibition.

He, J., Xie, J., Sarma, P., Wen, X.H., Chen, W.H. and Kamath, J., 2016. Proxy-based work flow for a priori evaluation of data-acquisition programs. SPE Journal, 21(04), pp.1-400.

He, J., 2013. Reduced-order modeling for oil-water and compositional systems, with application to data assimilation and production optimisation (Doctoral dissertation, Stanford University).

He, Q., 2016. Investigating Continuously Updated History Matching Using Smart Proxy (Surrogate Reservoir Model). West Virginia University.

Hirasaki, G.J., 1975. Sensitivity coefficients for history matching oil displacement processes. Society of Petroleum Engineers Journal, 15(01), pp.39-49.

Huang, X., Meister, L. and Workman, R., 1997, January. Reservoir characterization by integration of time-lapse seismic and production data. In SPE Annual Technical Conference and Exhibition. Society of Petroleum Engineers.

Huang, Y., Alsos, T., Sørensen, H.M. and Tian, S., 2013. Proving the value of 4D seismic data in the late-life field–Case study of the Norne main field. First Break, 31(9), pp.57-67.

Hunt, J.L. and Rester, S., 2003, January. Multilayer reservoir model enables more complete reservoir characterization during underbalanced drilling. In IADC/SPE Underbalanced Technology Conference and Exhibition. Society of Petroleum Engineers.

Idogun, I., Jeboda, O., Charles, D. and Ufomadu, H., 2015, August. Material Balance Modeling and Performance Prediction of a Multi-Tank Reservoir. In SPE Nigeria Annual International Conference and Exhibition. Society of Petroleum Engineers.

Iman, R.L., 2008. Latin hypercube sampling. Encyclopedia of quantitative risk analysis and assessment.

Islam, M.R., Hossain, M.E., Mousavizadegan, S.H., Mustafiz, S. and Abou-Kassem, J.H., 2016. Advanced Petroleum Reservoir Simulation: Towards Developing Reservoir Emulators. John Wiley & Sons.

Jacks, H.H., Smith, O.J. and Mattax, C.C., 1973. The modeling of a three-dimensional reservoir with a two-dimensional reservoir simulator-the use of dynamic pseudo functions. Society of Petroleum Engineers Journal, 13(03), pp.175-185.

Jacquard, P., 1965. Permeability distribution from field pressure data. Society of Petroleum Engineers Journal, 5(04), pp.281-294.

Jahns, H.O., 1966. A rapid method for obtaining a two-dimensional reservoir description from well pressure response data. Society of Petroleum Engineers Journal, 6(04), pp.315-327.

Jawwad Ahmed, S., Recham, R., Nozari, A., Bughio, S., Schulze-Riegert, R. and Ben Salem, R., 2013, March. Uncertainty Quantification Workflow for Mature Oil Fields: Combining Experimental Design Techniques and Different Response Surface Models. In SPE Middle East Oil and Gas Show and Conference. Society of Petroleum Engineers.

Jin, L., Alpak, F.O., Hoek, P., Pirmez, C., Fehintola, T., Tendo, F., Olaniyan, E.E. 2011. A Comparison of Stochastic Data-Integration Algorithms for the Joint History Matching of Production and Time-Lapse Seismic Data, SPE-146418.

Johnston, D.H., 2013. Practical applications of time-lapse seismic data. Society of Exploration Geophysicists.

Kathrada, M., 2009. Uncertainty evaluation of reservoir simulation models using particle swarms and hierarchical clustering (Doctoral dissertation, Heriot-Watt University).

Kowalewski, E., Rueslåtten, I., Steen, K.H., Bødtker, G. and Torsæter, O., 2006. Microbial improved oil recovery-bacterial induced wettability and interfacial tension effects on oil production. Journal of Petroleum science and Engineering, 52(1-4), pp.275-286.

Kremelberg, D., 2010. Practical statistics: A quick and easy guide to IBM® SPSS® Statistics, STATA, and other statistical software. SAGE publications.

Kruger, W.D., 1961. Determining areal permeability distribution by calculations. Journal of Petroleum Technology, 13(07), pp.691-696.

Landa, J., Meadows, M., Thacher, C., Waddle, R. and Williams, N., 2015, September. Map-Based Estimation of Reservoir Pressure and Saturation from 4D Seismic with a Data-Driven Procedure. In SPE Annual Technical Conference and Exhibition. Society of Petroleum Engineers.

Landa, J.L. and Horne, R.N., 1997, January. A procedure to integrate well test data, reservoir performance history and 4-D seismic information into a reservoir description. In SPE Annual Technical Conference and Exhibition. Society of Petroleum Engineers.

Landrø, M., 2001. Discrimination between pressure and fluid saturation changes from time-lapse seismic data. Geophysics, 66(3), pp.836-844.

LeBlanc, J.L. and Caudle, B.H., 1971. A streamline model for secondary recovery. Society of Petroleum Engineers Journal, 11(01), pp.7-12.

Leeuwenburgh, O., Brouwer, J. and Trani, M., 2011. Ensemble-based conditioning of reservoir models to seismic data. Computational Geosciences, 15(2), pp.359-378.

Leung, J.Y.W. and Shi, J., 2013, June. Physics-based proxy for vapex process modeling in heterogeneous reservoirs. In SPE Heavy Oil Conference-Canada. Society of Petroleum Engineers.

Li, R., Reynolds, A.C. and Oliver, D.S., 2001, January. History matching of three-phase flow production data. In SPE reservoir simulation symposium. Society of Petroleum Engineers.

Liberge, E., Benaouicha, M. and Hamdouni, A., 2007. Proper orthogonal decomposition investigation in fluid structure interaction. European Journal of Computational Mechanics/Revue Européenne de Mécanique Numérique, 16(3-4), pp.401-418.

Lie, K.A. and Mallison, B.T., 2013. Mathematical models for oil reservoir simulation. Encyclopedia of Applied and Computational Mathematics, pp.1-8.

Lumley, D.E., 2001. Time-lapse seismic reservoir monitoring. Geophysics, 66(1), pp.50-53.

Lumley, D.E., Nunns, A.G., Delorme, G., Adeogba, A.A. and Bee, M.F., 1999. Meren Field, Nigeria: A 4D seismic case study. In SEG Technical Program Expanded Abstracts 1999 (pp. 1628-1631). Society of Exploration Geophysicists.

Luo, X., Bhakta, T., Jakobsen, M. and Nævdal, G., 2016, August. An Ensemble 4D Seismic History Matching Framework with Wavelet Multiresolution Analysis-A 3D Benchmark Case Study. In ECMOR XV-15th European Conference on the Mathematics of Oil Recovery.

Lygren, M., Lindeberg, E., Bergmo, P., Dahl, G.V., Halvorsen, K.Å., Randen, T. and Sønneland, L., 2002. History matching of CO2 flow models using seismic modeling and time-lapse data. In SEG Technical Program Expanded Abstracts 2002 (pp. 1677-1680). Society of Exploration Geophysicists.

MacBeth, C., 2004. A classification for the pressure-sensitivity properties of a sandstone rock frame. Geophysics, 69(2), pp.497-510.

MacBeth, C., Geng, C. and Chassagne, R., 2016, January. A fast-track simulator to seismic proxy for quantitative 4D seismic analysis. In 2016 SEG International Exposition and Annual Meeting. Society of Exploration Geophysicists.

Marsh, J.M., Whitcombe, D.N., Raikes, S.A., Parr, R.S. and Nash, T., 2003. BP's increasing systematic use of time-lapse seismic technology. Petroleum Geoscience, 9(1), pp.7-13.

Martin, K. and MacDonald, C., 2010. Schiehallion Field: applying a geobody modelling approach to piece together a complex turbidite reservoir. In 7th European Production & Development Conference, Aberdeen, UK.

Mattax, C.C. and Dalton, R.L., 1990. Reservoir Simulation (includes associated papers 21606 and 21620). Journal of Petroleum Technology, 42(06), pp.692-695.

Mavko, G., Mukerji, T. and Dvorkin, J., 2009. The rock physics handbook: Tools for seismic analysis of porous media. Cambridge university press.

Meadows, M.A., 2001. Enhancements to landro's method for separating time-lapse pressure and saturation changes. In SEG Technical Program Expanded Abstracts 2001 (pp. 1652-1655). Society of Exploration Geophysicists.

Mezghani, M., Fornel, A., Langlais, V. and Lucet, N., 2004, January. History matching and quantitative use of 4D seismic data for an improved reservoir characterization.

In SPE Annual Technical Conference and Exhibition. Society of Petroleum Engineers.

Miller, R.T. and Rogers, W.L., 1973, January. Performance of oil wells in bottom water drive reservoirs. In Fall Meeting of the Society of Petroleum Engineers of AIME. Society of Petroleum Engineers.

Mohaghegh, S.D. and Abdulla, F.A.S., 2014, October. Production Management Decision Analysis Using AI-Based Proxy Modeling of Reservoir Simulations–A Look-Back Case Study. In SPE Annual Technical Conference and Exhibition. Society of Petroleum Engineers.

Mohamed, L., Christie, M.A., Demyanov, V., Robert, E. and Kachuma, D., 2010, January. Application of particle swarms for history matching in the Brugge reservoir. In SPE Annual Technical Conference and Exhibition. Society of Petroleum Engineers.

Molokwu, V.C. and Onyekonwu, M.O., 2017, July. Multi-Tank Material Balance Analysis in Heterogeneous Oil Reservoirs. In Nigeria Annual International Conference and Exhibition. Society of Petroleum Engineers.

Mustafiz, S. and Islam, M.R., 2008. State-of-the-art petroleum reservoir simulation. Petroleum Science and Technology, 26(10-11), pp.1303-1329.

Obidegwu, D., 2016. Seismic history matching using binary images (Doctoral dissertation, Heriot-Watt University).

Obidegwu, D., Chassagne, R. and MacBeth, C., 2015, June. Seismic assisted history matching using binary image matching. In EUROPEC 2015. Society of Petroleum Engineers.

Obidegwu, D., Chassagne, R. and MacBeth, C., 2017. Seismic assisted history matching using binary maps. Journal of Natural Gas Science and Engineering, 42, pp.69-84.

Oliver, D.S., Reynolds, A.C. and Liu, N., 2008. Inverse theory for petroleum reservoir characterization and history matching. Cambridge University Press.

Oliver, D.S. and Chen, Y., 2011. Recent progress on reservoir history matching: a review. Computational Geosciences, 15(1), pp.185-221.

Omofoma, V., 2017. The quantification of pressure and saturation changes in clastic reservoirs using 4d seismic data (Doctoral dissertation, Heriot-Watt University).

Onwunalu, J., 2006. Optimisation of nonconventional well placement using genetic algorithms and statistical proxy. MS report, Stanford University.

Osdal, B. 2012. Mapping the fluid front and pressure buildup using 4d data on norne field. Leading Edge, 25(9), 1134-1141.

Pan, Y. and Horne, R.N., 1998, January. Improved methods for multivariate optimisation of field development scheduling and well placement design. In SPE Annual Technical Conference and Exhibition. Society of Petroleum Engineers.

Pannett, S., Slager, S., Stone, G. and Dekker, S., 2004, January. Constraining a Complex Gas-Water Dynamic Model Using 4D Seismic. In SPE Annual Technical Conference and Exhibition. Society of Petroleum Engineers.

Parr, R.S., Marsh, M. and Griffin, T., 2000, January. Interpretation and integration of 4-D results into reservoir management, Schiehallion Field, UKCS. In 2000 SEG Annual Meeting. Society of Exploration Geophysicists.

Pletcher, J.L., 2000, January. Improvements to reservoir material balance methods. In SPE Annual Technical Conference and Exhibition. Society of Petroleum Engineers.

Puryear, C.I. and Castagna, J.P., 2008. Layer-thickness determination and stratigraphic interpretation using spectral inversion: Theory and application. Geophysics, 73(2), pp.R37-R48.

Reservoir Engineering Text Book, 2015, Institute of Petroleum, Heriot Watt University.

Roggero, F., Ding, D.Y., Berthet, P., Lerat, O., Cap, J. and Schreiber, P.E., 2007. Matching of Production History and 4D Seismic Data--Application to the Girassol Field, Offshore Angola. In SPE Annual Technical Conference and Exhibition. Society of Petroleum Engineers.

Roggero, F., Lerat, O., Ding, D. Y., and Berthet, P. 2012. History matching of production and 4d seismic data: application to the girassol field, offshore Angola. Oil & Gas Science & Technology, 67(2), 237-262.

Romero, C.E., Carter, J.N., Zimmerman, R.W. and Gringarten, A.C., 2000, January. Improved reservoir characterization through evolutionary computation. In SPE Annual Technical Conference and Exhibition. Society of Petroleum Engineers.

Rotondi, M., Nicotra, G., Godi, A., Contento, F.M., Blunt, M.J. and Christie, M., 2006, January. Hydrocarbon production forecast and uncertainty quantification: A field application. In SPE Annual Technical Conference and Exhibition. Society of Petroleum Engineers.

Rukavishnikov, V., 2015. Updating the simulation model using dynamic clusters extracted from 4d seismic data (Doctoral dissertation, Heriot-Watt University).

Rwechungura, R.W., Dadashpour, M. and Kleppe, J., 2011, January. Application of Particle Swarm Optimisation for Parameter Estimation Integrating Production and Time Lapse Seismic Data. In Offshore Europe. Society of Petroleum Engineers.

Sacks, J., Schiller, S.B. and Welch, W.J., 1989. Designs for computer experiments. Technometrics, 31(1), pp.41-47.

Sampaio, T.P., Ferreira Filho, V.J.M. and Neto, A.D.S., 2009, January. An application of feed forward neural network as nonlinear proxies for use during the history matching phase. In Latin American and Caribbean Petroleum Engineering Conference. Society of Petroleum Engineers.

Santos, J.M.C.D., 2017. Semi-quantitative 4D seismic interpretation integrated with reservoir simulation: application to the Norne field. (Master thesis, University of Campinas).

Schilthuis, R.J., 1936. Active oil and reservoir energy. Transactions of the AIME, 118(01), pp.33-52.

Schutte, J.F., Fregly, B.J., Haftka, R.T. and George, A.D., 2003. A parallel particle swarm optimiser. florida univ gainesville mechanical and aerospace engineering.

Sedighi D.F. and Stephen, K., 2010. Faster convergence in seismic history matching by dividing and conquering the unknowns. SPE Journal, 15(04), pp.1-077.

Sedighi D.F. and Stephen, K.D., 2009, January. Faster Convergence in Seismic History Matching by Efficient Parameter Searching. In EUROPEC/EAGE Conference and Exhibition. Society of Petroleum Engineers.

Selle, O.M., Springer, M., Auflem, I.H., Chen, P., Matheson, R., Mebratu, A.A. and Glasbergen, G., 2008, January. Gelled scale inhibitor treatment for improved placement in long horizontal wells at norne and heidrun fields. In SPE International Symposium and Exhibition on Formation Damage Control. Society of Petroleum Engineers.

Selvi, V. and Umarani, D.R., 2010. Comparative analysis of ant colony and particle swarm optimization techniques. International Journal of Computer Applications (0975–8887), 5(4).

Shahkarami, A., Mohaghegh, S., Gholami, V., Haghighat, A. and Moreno, D., 2014. Modeling pressure and saturation distribution in a CO2 storage project using a Surrogate Reservoir Model (SRM). Greenhouse Gases: Science and Technology, 4(3), pp.289-315.

Sheriff, R.E., 1980. Seismic Stratigraphy, published by International Human Resources Development Corporation. Boston, Massachusetts, pp.85-116.

Shi, Y. and Eberhart, R.C., 2001. Fuzzy adaptive particle swarm optimisation. In Evolutionary Computation, 2001. Proceedings of the 2001 Congress on (Vol. 1, pp. 101-106). IEEE.

Shirer, J.A., Ainsworth, W.J. and White, R.W., 1974, January. Selection of a Waterflood Pattern for the Jay-Little Escambia Creek Fields. In Fall Meeting of the Society of Petroleum Engineers of AIME. Society of Petroleum Engineers.

Skjervheim, J.A., Evensen, G., Aanonsen, S.I., Ruud, B.O. and Johansen, T.A., 2007. Incorporating 4D seismic data in reservoir simulation models using ensemble Kalman filter. SPE journal, 12(03), pp.282-292.

Slotte, P.A. and Smorgrav, E., 2008, January. Response surface methodology approach for history matching and uncertainty assessment of reservoir simulation models. In Europec/EAGE Conference and Exhibition. Society of Petroleum Engineers.

Smith, G.C. and Gidlow, P.M., 1987. Weighted stacking for rock property estimation and detection of gas. Geophysical Prospecting, 35(9), pp.993-1014.

Soldo, J., 2005. Quantitative Integration of Time-Lapse Seismic Data (Doctoral dissertation, Heriot-Watt University).

Souza, R.M., Machado, A.F., Munerato, F.P. and Schiozer, D.J., 2010, January. Iterative History Matching Technique for Estimating Reservoir Parameters from Seismic Data. In SPE EUROPEC/EAGE Annual Conference and Exhibition. Society of Petroleum Engineers.

Souza, R.M., Schiozer, D.J. and dos Santos, M.S., 2011, January. Petro-Elastic Parameters Effects on History Matching Procedures. In SPE EUROPEC/EAGE Annual Conference and Exhibition. Society of Petroleum Engineers.

Statoil, 2001. PL128 Norne Field Reservoir Management Plan.

Statoil, 2006. Annual reservoir development plans Norne Field.

Steffensen, I. and Karstadt, P.I., 1996. Norne field development-fast track from discovery to production. Journal of Petroleum Technology, 48(04), pp.296-339.

Stephen, K.D. and Arwini, S., 2010, September. Improving Stochastic Inversion Methods in History Matching Using Proxy Models. In ECMOR XII-12th European Conference on the Mathematics of Oil Recovery.

Stephen, K.D., Shams, A. and MacBeth, C., 2009. Faster seismic history matching in a United Kingdom continental shelf reservoir. SPE Reservoir Evaluation & Engineering, 12(04), pp.586-594.

Stephen, K.D., Soldo, J., Macbeth, C. and Christie, M.A., 2006. Multiple model seismic and production history matching: A case study. SPE Journal, 11(04), pp.418-430.

Subbey, S., Christie, M. and Sambridge, M., 2004. Prediction under uncertainty in reservoir modeling. Journal of Petroleum Science and Engineering, 44(1-2), pp.143-153.

Terry, R.E., Rogers, J.B. and Craft, B.C., 2013. Applied petroleum reservoir engineering. Pearson Education.

Thenon, A., Gervais, V. and Le Ravalec, M., 2016. Multi-fidelity meta-modeling for reservoir engineering-application to history matching. Computational Geosciences, 20(6), pp.1231-1250.

Thiele, M.R., 2001. Streamline simulation. In proceedings of the sixth international forum on reservoir simulation.

Tolstukhin, E., Lyngnes, B. and Sudan, H.H., 2012, January. Ekofisk 4D seismic-seismic history matching workflow. In SPE Europec/EAGE Annual Conference. Society of Petroleum Engineers.

Van Gestel, J.P., Best, K.D., Barkved, O.I. and Kommedal, J.H., 2011. Integration of the life of field seismic data with the reservoir model at the Valhall Field. Geophysical Prospecting, 59(4), pp.673-681.

Van Leeuwen, P.J., 1999. Comment on "Data assimilation using an ensemble Kalman filter technique". Monthly Weather Review, 127(6), pp.1374-1377.

Vanegas, J.W.P., Deutsch, C.V. and Cunha, L.B., 2008, January. Uncertainty assessment of SAGD performance using a proxy model based on Butler's theory. In SPE Annual Technical Conference and Exhibition. Society of Petroleum Engineers.

Vasconcellos Soares, R., 2017, October. Use of an Iterative Ensemble Smoother Methodology in a History Matching and Uncertainties Assessment Process. In SPE Annual Technical Conference and Exhibition. Society of Petroleum Engineers.

Vauthrin, R., Bird, B., Will, R., Eastwood, J. and Johnston, D., 1999, January. Improvements in 4D legacy data quality and repeatability through reprocessing, Lena Field. In Society of Exploration Geophysicists Annual Meeting, Houston.

Vermeulen, P.T.M., Te Stroet, C.B.M. and Heemink, A.W., 2006. Model inversion of transient nonlinear groundwater flow models using model reduction. Water resources research, 42(9).

Waggoner, J.R., Cominelli, A. and Seymour, R.H., 2002, January. Improved reservoir modeling with time-lapse seismic in a Gulf of Mexico gas condensate reservoir. In Spe Annual Technical Conference and Exhibition. Society of Petroleum Engineers.

Walker, G.J. and Lane, H.S., 2007, January. Assessing the accuracy of history-match predictions and the impact of time-lapse seismic data: A case study for the Harding reservoir.

Wang, H. and Marongiu-Porcu, M., 2015. Impact of shale-gas apparent permeability on production: combined effects of non-darcy flow/gas-slippage, desorption, and geomechanics. SPE Reservoir Evaluation & Engineering, 18(04), pp.495-507.

Wang, Z., 2000. The Gassmann equation revisited: Comparing laboratory data with Gassmann's predictions. Seismic and acoustic velocities in reservoir rocks, 3, pp.8-23.

Wantawin, M., Yu, W., Dachanuwattana, S. and Sepehrnoori, K., 2017. An Iterative Response-Surface Methodology by Use of High-Degree-Polynomial Proxy Models for Integrated History Matching and Probabilistic Forecasting Applied to Shale-Gas Reservoirs. SPE Journal.

Wasserman, M.L., Emanuel, A.S. and Seinfeld, J.H., 1975. Practical applications of optimal-control theory to history-matching multiphase simulator models. Society of Petroleum Engineers Journal, 15(04), pp.347-355.

Watkins, A.J. and Parish, R.G., 1992, January. Computational aids to reservoir history matching. In Petroleum Computer Conference. Society of Petroleum Engineers.

Watson, A.T., Seinfeld, J.H., Gavalas, G.R. and Woo, P.T., 1980. History matching in two-phase petroleum reservoirs. Society of Petroleum Engineers Journal, 20(06), pp.521-532.

Widess, M.B., 1973. How thin is a thin bed? Geophysics, 38(6), pp.1176-1180.

Willmott, C.J. and Matsuura, K., 2005. Advantages of the mean absolute error (MAE) over the root mean square error (RMSE) in assessing average model performance. Climate research, 30(1), pp.79-82.

Wilson, A., 2016. Project Tests High-Performance Cloud Computing for Reservoir Simulations. Journal of Petroleum Technology, 68(07), pp.57-58.

Wilson, K. and Durlofsky, L.J., 2012, January. Computational optimisation of shale resource development using reduced-physics surrogate models. In SPE Western Regional Meeting. Society of Petroleum Engineers.

Wolpert, D.H. and Macready, W.G., 1997. No free lunch theorems for optimisation. IEEE transactions on evolutionary computation, 1(1), pp.67-82.

Wong, M., 2017. Pressure and saturation estimation from prm time-lapse seismic data for a compacting reservoir (Doctoral dissertation, Heriot-Watt University).

Yadav, S., Srinivasan, S., Bryant, S.L. and Barrera, A., 2005, January. History matching using probabilistic approach in a distributed computing environment. In SPE Reservoir Simulation Symposium. Society of Petroleum Engineers.

Yang, Y., Davidson, J.E., Fenter, D.J., Ozen, O. and Boyett, B.A., 2009, January. Reservoir development modeling using full physics and proxy simulations. In International Petroleum Technology Conference. International Petroleum Technology Conference.

Yeten, B., Castellini, A., Guyaguler, B. and Chen, W.H., 2005, January. A comparison study on experimental design and response surface methodologies. In SPE Reservoir Simulation Symposium. Society of Petroleum Engineers.

Yin, Z., 2016. Enhancement of dynamic reservoir interpretation using the well2seis technique (Doctoral dissertation, Heriot-Watt University).

Zangl, G. and Hermann, R., 2004, January. Waterflood Pattern Optimisation Using Genetic Algorithms with Multi-tank Material Balance. In SPE Annual Technical Conference and Exhibition. Society of Petroleum Engineers.

Zhang, Y. and Oliver, D.S., 2009, January. History matching using a hierarchical stochastic model with the ensemble Kalman filter: a field case study. In SPE Reservoir Simulation Symposium. Society of Petroleum Engineers.

Zubarev, D.I., 2009, January. Pros and cons of applying proxy-models as a substitute for full reservoir simulations. In SPE Annual Technical Conference and Exhibition. Society of Petroleum Engineers.